MICRO-SCALE REACTION MOTOR STUDIES OF PROPELLANT SYSTEMS INVOLVING CONCENTRATED HYDROGEN PEROXIDE

by

ARTHUR SPRAGENS COLLINS
B.S., University of Kentucky
1942

SUBMITTED IN PARTIAL FULFILLMENT
OF THE REQUIREMENTS FOR
THE DEGREE OF DOCTOR OF SCIENCE
at the
MASSACHUSETTS INSTITUTE OF TECHNOLOGY
1948

Signature of Author_____
Dept. of Chemical Engineering. Sept. 3, 1948

Certified by_____
Thesis Supervisor

_____
Chairman, Dept. Comm. on Graduate Students

Cambridge, Mass.
September 3, 1948

Professor J. S. Newell
Secretary of the Faculty
Mass. Institute of Technology
Cambridge, Massachusetts

Dear Professor Newell:

I take great pleasure in submitting herewith a thesis entitled "Micro-scale Reaction Motor Studi[illegible] of Propellant Systems involving Concentrated Hydrogen Peroxide," in partial fulfillment of the requirements for the degree of Doctor of Science in Chemical Engineering.

Respectfully yours,

Arthur S. Collins

ACKNOWLEDGMENT

The author wishes to express his sincere thanks and appreciation to Professor H. C. Hottel for his many helpful suggestions which were applied to all parts of the work involved in this thesis. His aid in defining the exact objectives and scope of the work and in furnishing its guidance was especially vital. Thanks are due to Dean T. K. Sherwood for originally suggesting the problem and to Professors C. N. Satterfield, G. C. Williams and F. G. Keyes for their timely suggestions and criticisms.

The financial support of the Naval Bureau of Ordnance and the Office of Naval Research is gratefully acknowledged.

In addition, the author is deeply indebted to Saul Wolf and Reed Fulton for their aid in carrying out the experimental program of study, to M. W. Raymond for designing much of the equipment used, to H. A. Passler and Charles Gallagher for constructing equipment, to John Brean and Richard Wentink for their aid with the mechanical drawings, and to all other members of DIC Project 6552 who spent their time and effort in behalf of the work presented in this thesis.

TABLE OF CONTENTS

TABLE OF CONTENTS (Cont'd)

LIST OF APPENDICES

LIST OF FIGURES

LIST OF TABLES

OBJECT

The broad general objective of the investigation of which this is a part has been a study of the nature of the combustion reaction of concentrated hydrogen peroxide and various self-igniting fuels, and an examination of the factors affecting the smoothness of this combustion. As a part of the program it was desired to measure the actual performance of these propellant systems in a small reaction motor. A large part of the present investigation has, therefore, been spent in developing the experimental technique of operating a small rocket motor and in devising methods of making performance calculations in such a way as to arrive at significant test results despite large energy losses associated with micro-scale rocketry. A second major aim of the thesis was to improve the reliability of these results sufficiently to make the operation of a small reaction motor test stand at least a satisfactory method of evaluating the practical potentialities of chemical propellant systems if not also the logical starting point in the serious design of a large power plant.

ABSTRACT

One of the most striking developments of the last world war was the intensification of activity in the field of jet propulsion. And one of the newest and most interesting developments in this field was the advent of concentrated hydrogen peroxide as a possible oxidizer component in chemical propellant systems. It was due to the interest in this new oxidizer that the present work was begun. The original object of the work was to investigate the reaction of concentrated peroxide with various fuels, especially self-igniting fuels, and to compare the experimental performance and the reliability and suitability for practical operation of several of these propellant systems.

In planning the experimental program for such an investigation, it was decided that operation of a very tiny thrust motor or reaction motor would provide the most suitable method of testing the hydrogen peroxide-fuel systems. In fact, the small scale of operation was dictated by the high cost and short supply of the propellants to be used and by the potential hazard in handling or storing such chemicals in any quantity. It was recognized that achievement of significant quantitative results on a reaction motor of a thrust size as small as 10 pounds might constitute a challenging

problem. Accordingly, the investigation and evaluation of the operation of a micro-rocket motor as an experimental technique was made a second major objective of the present work. In fact this objective might be considered more important than the original purpose, because if such a micro-rocket technique could be shown to be really successful, large savings might be effected in the cost of research and development programs in which it was subsequently adopted and used.

For the most part, the apparatus and equipment used in the present study assumed the form of the micro-counterpart of the large scale equipment customarily used in testing conventional sized thrust motors. Two major exceptions to this rule were the injectors and the feed system. Most of the injectors used wereof the simple orifice type with orifice diameters of about 0.04" which is in the range of sizes normally used. However, a single pair of these orifices mixing a single stream of fuel with a single stream of oxidant comprised the complete injector in the micro-rocket motors whereas several or even several hundred pairs of orifices usually operate in a similar large test motor. The feed system employed with the micro-rocket test stands was decidedly unique in the field of reaction motor testing being designed to give positive displacement flow

and therefore truly constant flow rates which were completely independent of and unaffected by pressure variations within the reaction motor.

Two self-igniting fuel components were tested with concentrated hydrogen peroxide in the present study. They were an 85% aqueous solution of hydrazine hydrate containing a few grams of iron and copper salts as catalyst (1.07 g/liter of $Na_2Fe(CN)_5NO \cdot 2H_2O$, 0.47 g/liter of CuCN and 0.39 g/liter KCN being used for normal or 1 x catalyst), and Naphferrol which is methyl alcohol containing 200 grams of ferrous β-naphthalene sulfonate trihydrate per liter. Extensive tests were made with each of these fuel-peroxide combinations on both the stationary stand and the thrust stand. On both stands measurements were made of the flow rates of each propellant, combustion chamber pressure and feed pressures and the throat diameter of the nozzle. In addition, on the thrust stand measurements were made of the thrust and the average rate of heat loss for combustion chamber and nozzle under equilibrium conditions. And on the stationary stand (as well as on the thrust stand in a few cases), a time record of the instantaneous combustion chamber pressure through a representative part of the run was generally taken by means of the General Motors capacitance type pressure indicator and associated equipment.

The relative roughness or smoothness of combustion was judged not only by the percentage fluctuation in the mean chamber pressure as noted from the G.M. gauge record but also by comparing the sound and appearance of the exhaust jets. The ratio of experimental chamber pressure actually obtained to that theoretically obtainable for complete combustion under the same conditions ($100 \times \frac{P_{c\ exp}}{P_{c\ theor}}$) was selected as the simple and practical criterion of combustion efficiency to be used. Overall performance was judged by comparing the experimental value of specific impulse (ratio of thrust to total mass flow rateof propellant) with the value theoretically calculated for a perfect motor operating with complete combustion but over the same expansion ratio as the experimental motor. Both of these comparisons were made with and without corrections for measured heat loss to indicate the extent of the effect which is exerted on these results by the heat losses of a small reaction motor.

Based on the rather limited experience of the present study, it appears that the performance obtained in a 10 lb thrust motor closely approximates that commonly obtained in large scale reaction motors which provide approximately equal residence times of the reactants in the combustion chamber. For example, with the stoichiometric mixture of 85% $N_2H_4 \cdot H_2O$ and 90% hydrogen peroxide, the

performance of micro-rocket motors with combustion chambers of various sizes (corrected for the effects of measured heat losses) is given below:

$\frac{P_{c\ exp}}{P_{c\ theor}} \times 100$	$L^* = \frac{\text{Comb. Chamber Vol}}{\text{Nozzle Thrust Area}}$ inches
85	20
90	100
95	150

It appears that heat losses on 10 lb. thrust motors with L* values of 100 inches or less should amount to only about 10% of the total energy available and that the net effect of the amount of heat loss on any of common performance parameters should amount to only about 5%. Consequently, a simplified analysis of the effect of heat loss upon the performance is completely satisfactory and the necessary correction calculations to the micro-rocket results can be made with ease. It also appears that, with a good system of injection, the smoothness, steadiness and consistency of the combustion operation and the reproducibility of results therefrom is almost as good in the present case as would be expected on a large scale test stand. This is probably due to the use of the special positive displacement feed system since the constancy of the flow rates thus obtained probably outweighs the disadvantage of using an injector composed of

only a single orifice for each propellant.

In spite of the promising nature of the above results, it still appears that an exceedingly large amount of experience would be required in micro-scale operations as well as in large scale operations with the same propellant systems and types of injection methods in order to establish the relationships needed to design large scale injectors and combustion chambers from micro-scale operational data. However, as the results of this thesis show, the micro-rocket technique is of utility for comparing the experimental performance and operating suitability of propellant systems under given conditions and for obtaining preliminary evaluation of certain types of equipment. In addition, it is the only method of experimentally testing those propellant systems which are in short supply.

The more specific results of the present study indicate that the hydrazine hydrate-peroxide system is superior to the Naphferrol-peroxide combination in nearly all respects. For example, the hydrazine hydrate combination was found to ignite more reliably , burn more smoothly and operate more consistently, and its combustion efficiency was so much higher that the specific impulse obtained at the stoichiometric mixture ratio in a given motor ($L^* = 150$ inches) with a given injector amounted to 185 lbs-sec/lb compared to 170 lbs-sec/lb

for the Naphferrol system while the corresponding theoretical values of the specific impulse are approximately 210 lbs-sec/lb for the Hyd.Hyd. System and 220 for the Naphferrol system.

The efficiency of combustion and smoothness of combustion were both found to be affected by the method of injection and the size of the combustion chamber, as well as by the chemical nature of the reactants and the amount of a given ignition catalyst which was used. The combustion efficiency was also affected by the fuel to oxidant mixture ratio but no study was made of the effect of this variable on smoothness of combustion. Nozzle design was not studied in much detail but it appeared that use of divergence angles of less than 20° was ineffectual since the gain in directional thrust tended to be more than offset by the increase in frictional losses.

The generalized thermodynamic charts devised by Satterfield, Hottel and Williams were used as a basis for most of the calculations in the present thesis with great simplification of the procedures involved thus being effected. These charts present the more important thermodynamic functions of high temperature combustion gas mixtures (at equilibrium down to a temperature of 1600°K) in a generalized correlation which comprises all systems composed of C, H, O and N. Specific impulse can be calculated by a graphical procedure using only these generalized charts. However, in order to determine the

theoretical chamber pressure, use of the theoretical equations was found to be necessary in making the actual calculation although the values of the thermodynamic properties of the equilibrium gas mixture could still be obtained from the generalized charts. Consequently, studies were made of calculation methods based on theoretical equations for both chamber pressure and specific impulse. The chief uncertainty in the use of these equations was found to lie in the type of average values of molal specific heat $MW(\partial H/\partial T)_p$ which should be used. A simplified theoretical analysis was made based on the use of a linear relationship between molal specific heat and temperature. Trial calculations were then made on representative systems using the type of average mold heat capacities thus evolved in the theoretical equations. The theoretical quantities calculated in this way were compared with these obtained by a rigorous procedure on Mollier Type diagrams and the maximum deviation in the results was noted. In this way it was estimated that the equation type methods of calculation based on the generalized thermodynamic charts and the simple types of average molal specific heats or the graphical calculation techniques on the charts alone were probably accurate within 2% for any system and within 1% for the relatively low temperature systems experimentally studied in this thesis.

The error due to the assumption of a linear relation between molal specific heat and temperature was estimated to be negligible in the calculation of chamber pressure and less than 1% in the calculation of specific impulse.

INTRODUCTION

One of the most striking developments resulting from the last world conflict has been the rapid growth of the field of jet propulsion. One phase of this development was the introduction of highly concentrated 80-90% hydrogen peroxide into the picture by the Germans. Since the cessation of hostilities in Europe, production of this material has been initiated both in England and in this country, and is now being carried out on a fairly large scale. A better understanding of its chemical nature has gradually been acquired and it has come to be regarded as a fundamentally stable substance, quite contrary to the opinion which originally prevailed.

The interest in concentrated hydrogen peroxide as a ready source of power has increased concurrently with the improvements in our methods of producting and handling it, and with our gain in knowledge of its properties. The spectacular German accomplishments in the use of H_2O_2 in operations of the past war considerably enhanced this interest. However, since their accomplishments were achieved under the stress of extreme emergency, the background of fundamental research is necessarily limited. Moreover, the results of this work which are available are somewhat confused due to the destruction which existed at war's end. Accordingly, a fairly widespread program has now been initiated in this country to

determine systematically some of the more basic properties and characteristics of concentrated H_2O_2, with the intention of facilitating a rapid evaluation of its suitability for any specific purpose in the future. At the same time, a considerable effort is being expended on the engineering and development of actual power plants involving hydrogen peroxide. Owing to the extremely complex nature of most reactions of peroxide under conditions of practical operation, a partially empirical approach will probably continue to be necessary to the solution of many problems.

Present Field of Concentration

One of the most interesting German uses of peroxide was as an oxidant for various "hypergolic" or self-igniting fuels. This development received their closest attention and evidently showed considerable promise. This property of self-ignition greatly simplifies operational use since igniters are unnecessary and intermittent use of the power plant is extremely easy to achieve.

It was principally in this field of "hypergolic" or self-igniting peroxide-fuel combinations that the present work was undertaken. The original object of the work was to make a general study of the combustion characteristics of these self-igniting systems, with emphasis on determining the causes of smooth or rough burning. However, in conjunction with this study, a quantitative evaluation of the power output of the various fuel-peroxide systems was also intended.

A small reaction motor was chosen as the most suitable experimental tool for making such a study. This choice was based upon the simplicity of operation of the rocket, the ease of measuring its performance directly on a reaction stand, the practical relation to the field of jet propulsion where concentrated peroxide would be most certain of being used to advantage, and the widespread use of this method of testing propellants which would make possible the comparison of results by other investigators on similar systems.

The work reported in this thesis was initiated in February 1946. It constituted a small portion of a comprehensive program of study of hydrogen peroxide at M.I.T. which included work on catalytic decomposition, determination of stability and other basic physical and chemical properties, thermal decomposition, and direct reaction with fuels. The present work is a part of this last phase.

Pioneering Work in Jet Propulsion

Since most of the previous work on concentrated peroxide has been carried out in connection with jet propulsive mechanisms and the primary interest in this work is still directed along those lines, a short review of the earlier work in this general field will be given, followed by a summary of the more pertinent experiments in which concentrated peroxide was used as one of the propellants.

Rockets have been known for an exceedingly long time and the jet propulsion principle was undoubtedly employed long before it was completely understood by many of those

using it. The oxidizing material is included in the rocket fuel load, and the rocket consequently can operate successfully in any type of atmosphere or in a vacuum.

The liquid-fuel rocket is a relatively modern modification of the fairly ancient but simpler solid-fuel type, having taken form sometime in the present century. Many of the pioneers in the rocket field foresaw the advantages of liquid fuel rockets for long-range missiles early in the present century. This advantage was not generally recognized, however, until the fantastic potentialities of long-range rocket propulsion were so vividly delineated by some practical developments of the past world war, notably the German V-2 weapon.

Most deserving of mention among the pre-World War II 20th century liquid-rocket pioneers are the following: Esnault-Pelterie (14) of France, Alexander Rinin (33) of Russia, E. Sanger (35) of Austria, H. Oberth (30) of Roumania, and R. H. Goddard (15) in America. All of these men not only carried out experimental work, but left comprehensive records of their work, as well as treatises on ideas and developments of far-reaching import. A description of the work of these men is included in A. Ananoff's (3) survey of reaction propulsion, which outlines the progress in the field during this early period of liquid rocket development. The interest inspired by the work of these individuals led to the formation of rocket research societies in several countries, including Germany and the United States. Reports on the work of members

of the American Rocket Society are generally given in their official periodical (2). In addition, Buckingham (12), Africano (1), Vogelpohl (42), Malina (25), Rogge (34), Hausenstein (17) and Stemmer (40) are among those publishing work in the field of rocket propulsion. These groups furnished the background of experimentation which made possible the recent accelerated advances in the field.

Wartime Developments

The widespread effort in the field which has been expended in the past few years resulted in several rather spectacular applications of rockets for military purposes, including the following:

The German V-1 robot buzz bomb was operated by intermittent firing of a gasoline-air motor with an appropriate valving cycle to take in air, inject fuel, fire, and eject hot gases rearward. Both the V-1 and its American counterpart the JB-2 (experimental) were launched by means of a slotted gun-tube using concentrated peroxide with calcium permanganate catalyst as a source of compressed gas.

Jet-assisted take-off units for aircraft were employed both here and in Germany. These usually consisted of rocket motors operating on solid fuels or liquid fuel combinations such as acid-aniline, or peroxide and catalysts or fuels. The German rocket-powered airplane, Me-163, employed a reaction motor using a self-igniting fuel combination of peroxide with a mixture of hydrazine hydrate and methanol. Much experimental work was done both in America and in Germany on liquid fuel-

oxidant systems for generating gases for torpedo and submarine propulsion. The most promising of these in Germany used hydrogen peroxide with hydrazine hydrate and decalin for a fuel. In this country a non self-igniting cycle using 48% hydrogen peroxide with catalyst (permanganate) and 92.5% ethyl alcohol was employed.

The largest rocket missile yet used operationally was the German V-2, propelled by a 55,000-pound thrust motor operating on liquid oxygen and an ethyl alcohol-water mixture. Catalytic decomposition of hydrogen peroxide furnished the power for the turbine-driven fuel pumps in this device. [Sherwood and Gardner (C-8) give a critical survey of these developments, and Mrs. Murray (C-19) has abstracted many of the available reports on German peroxide developments.]

The chief research centers for liquid-rocket and guided-missile research in Germany were the Luftfahrtforschungsanst near Brunswick where Lutz, Noeggerath and Edse (C-3) were employed, the Electromekanische Werke at Peenemunde where the V-2 was developed, the firm of Hellmuth Walter at Kiel where the Me-163 was developed and where underwater propulsion systems were studied, the Bavarian Motor Works where Nitric Acid Systems were of chief interest. In addition, Firms of Schmidding, Henschel, and Messerschmitt all did miscellaneous development and research work. In this country most of the liquid rocket work was carried out at California Institute of Technology, Reaction Motors, Inc., of Dover, Del., Engineering Research Laboratory at Annapolis, Md., and in several Naval Ordnance

laboratories. In addition, liquid fuel-oxidant systems for underwater propulsion were studied at the Massachusetts Institute of Technology and at the Naval Torpedo Station in Newport, R. I. Chemical Warfare Service carried out the work on the JB-2 launcher.

Since the close of hostilities, a more systematic and general research program has been initiated to fill in the voids left by the hasty investigations which were usually necessary during war time. The large amount of fundamental work now being carried out in the laboratories of industrial firms as well as universities and other institutions on the chemistry of combustion reactions and hydrodynamic and aerodynamic theory should result in a broader understanding of jet-propulsion power plants, making future developments easier and quicker to achieve.

When the work of this thesis was begun, very little of the recent work in this field had been published. During the course of the present work, however, much of this recent research has appeared in the form of restricted or classified reports, although very little of it has yet been made available in the open literature.

German Research

The only large amount of work on self-igniting fuel-oxidant systems included in the war effort of this country was done in connection with nitric acid systems. All of the known background work on self-igniting fuels for concentrated hydrogen peroxide as well as a large amount of study of other spontaneous-

ly igniting systems was carried out in Germany. The reports on this huge amount of German experience in the field have not been reduced to a completely clear picture as yet. Among the original German reports which are available and the American and British intelligence and survey reports, there are many obscure and conflicting points yet to be straightened out. Most of these reports cannot be used as reference material here because of their classified nature. The following overall picture of the use and philosophy of self-igniting propellants in Germany is generally accepted however.

Apparently the German leaders decided to concentrate a large part of their effort upon the problem of simplifying the operation of rockets since the possibility of discovering new propellants with appreciably greater effectiveness than those now known seemed remote. The most promising scheme for simplification proved to be the use of their so-called "Hypergols" or propellants which ignite upon mixing. They tested many combinations but developed only a few satisfactory ones. [redacted]

It seems definite even from the briefest review of the German work that hydrazine was the most reactive toward peroxide of all the fuels which they tested. Because of its scarcity, however, it was always diluted for operational use, most often with methyl alcohol. With 0.6-0.8 grams of copper per liter, usually as potassium cupro cyanide ($K_3Cu(CN)_4$) as catalyst, this mixture seems to have made a very satisfactory self-igniting fuel. The chief difficulty was in obtaining a stable solution

or suspension of the catalyst. Experimentally, the addition of iron salts, eg., sodium nitroprusside, was found to improve this storage stability. However, this combined catalyst never got into actual use.

The exact mechanism of the reaction which results in the initiation of flame when a self-igniting fuel and its oxidant are mixed is not known. In general, there is a liquid reaction which generates the heat necessary to raise the reactants above their flash point, with the burning probably beginning in the vapor just above the liquid surface or around the surface of a partially atomized drop of the fuel-oxidant mixture. The ignition-delay time seems to offer a short period in which a rapid and complete mixing, if it could be accomplished, would be very successful in promoting a rapid attainment of reasonable completeness in the subsequent combustion reaction.

No actual test-stand performance data on reaction motors using H_2O_2 systems are reported in the German work which is available to the author. However, it is evident that they used approximately the same parameters for judging rocket performance that have been customarily used in this country. These parameters include specific impulse Isp; specific fuel consumption w_{sp}; effective exhaust velocity, C_{eff}; the nozzle thrust coefficient, C_F; the characteristic exhaust velocity, C*; and the characteristic chamber length, L*. All of these are discussed in the section on THERMODYNAMIC ANALYSIS OF ROCKET PER-

FORMANCE, in pages 56 to 61.

The combustion chambers of the German rocket motors appear to have been designed along lines similar to those conventionally used in this country. In small-scale motors, the combustion chamber usually consisted of a cylindrical section followed by the approach section or converging section of the nozzle. However, in large-scale motors such as the V-2 rocket, the combustion chamber becomes nearly spherical consisting mainly of the converging section of the nozzle.

[redacted]

Requirements of Present Program

In planning the present program of study, several unique features required consideration. Because of their special nature, the fuels which had been found to be self-igniting with peroxide had all proved to be scarce and expensive. The probability was that any new fuels which might be developed for use with peroxide would also be rare and difficult to obtain in large quantities. In order to make possible an experimental evaluation of such compounds, it was necessary to limit the scale of operation as much as possible. In addition, the need for safety in operation within the Institute buildings and the desirability of minimizing numbers of operating personnel both dictated the use of a small (or "micro-size") reaction motor.

For these reasons a reaction motor capable of producing approximately 10 lbs. thrust was chosen for the experimental work. It thus appeared that the present study was being undertaken not only in a relatively unexplored pro-

pellent field, but also through the use of an experimental technique which represented a considerable modification of that conventionally used in the static testing of jet motors. The smallest size motor on which quantitative performance could be found reported in the literature was a 25-lb. thrust model and even here thrust measurements were not made. Quantitative testing is usually carried out on a thrust scale of at least 500 lbs. On motors of this size, heat losses usually amount to no more than about one percent of the total energy convertible into the energy of the exhaust jet. However, in the present case preliminary calculations indicated that heat losses might account for an appreciable fraction of the available energy. Accordingly, it appeared that it would be necessary to measure heat losses on the micro-size thrust motor in order to obtain quantitative results of significance.

In this connection there would be the associated problem of developing a method of correcting experimental or theoretical performance figures for these measured heat losses. It was hoped that simple methods of making these calculations as well as the general theoretical performance calculations could be developed. The Satterfield (36) charts of Generalized Thermodynamic Properties for combustion gases composed of the elements C,H,O, and N were being developed at the time as an aid in simplifying combustion calculations. These charts seemed promising as a means of handling general calculations of rocket

performance as well as some of the special problems of the micro-rocket analysis. At any rate the present study was planned to include an exploration of general calculation methods with the emphasis on use of the generalized technique of Satterfield and with the objective of developing the simplest possible methods of analysis consistent with the requirements of reasonable accuracy.

Complete Objectives

It was intended, therefore, that the present thesis should make the following contributions to the general field:

1. Investigate the nature of the combustion reactions of concentrated peroxide and self-igniting fuels as encountered in rocket chambers.

2. Determine quantitative performance data on these propellant systems, and study the factors influencing performance.

3. Develop a method of correcting performance data on a very small scale reaction motor to give it practical significance. This should be of great value in making studies of systems involving scarce or expensive propellants. Also, if fully developed, it might make possible great economies in time and expense of investigating any fuel system.

4. Develop a simple and satisfactory method of calculating the theoretical parameters of interest for the purpose of analyzing experimental performance data on any scale of operation.

THERMODYNAMIC ANALYSIS OF ROCKET PERFORMANCE

Calculations of the theoretical performance of propellant systems when used in operating reaction motors have been made by many investigators and for many different purposes. Such information may be desired in order to compare the maximum output which could be expected from different systems, or as a basis for design of a rocket type power plant, or for comparison with experimental results in order to determine actual operating efficiencies.

In spite of this wide-spread use of such calculations, the only truly rigorous procedure which has been widely used is very long and tedious and fairly complicated. It involves the trial-and-error solution of several simultaneous equations expressing (1) the relations between the partial pressures of the various chemical species and the thermodynamic equilibrium constants, (2) material balances, and (3) an energy balance in order to determine the conditions of equilibrium combustion. Following this, conditions at the exit of the nozzle are determined by imposing the condition of constant entropy for the expansion process. If equilibrium is assumed to be maintained throughout the nozzle passage, this calculation will also involve a trial-and-error solution of the exit gas composition using the equilibrium constants and material balances. In order to minimize the labor involved in making these calculations on rocket engines as well as similar calculations on other high-temperature combustion

systems, Satterfield has recently presented a generalized correlation of the essential thermodynamic properties of the combustion gases from those systems composed of the elements C, H, O, and N. This correlation is based on rigorous calculations of representative systems carried out in the usual manner and under representative conditions. However, this generalized technique makes possible the presentation of the pertinent properties of widely different systems by means of only a few charts which are quite simple to use.

Theoretical relationships for such commonly used rocket parameters as specific impulse or chamber pressure can be and have been derived by various authors in the field. These derivations are usually based on an extremely idealized analysis, however. In order to obtain expressions of sufficient simplicity for direct utility, certain assumptions, which are known to be inexact, are necessarily made. For example, the molecular weight and specific heat of the combustion gas mixture are both usually assumed constant during the expansion through the exhaust nozzle.

Certain calculations of rocket motor performance, where extreme accuracy is not required, are sometimes made using such equations in which average values are actually substituted for the specific heat and molecular weight which were assumed constant in the derivation. Because of the ease, convenience and flexibility of using such equations especially for widely varying conditions, this method of calculation has

been investigated in connection with the present work. An effort has been made to determine the kind of average values of these terms (primarily specific heat and molecular weight) which would be required in order to identify these simple theoretical equations with those derived by a theoretical analysis sufficiently rigorous to serve as a reliable basis for making really accurate calculations of theoretical performance.

Those propellant systems which are characterized by low combustion temperatures generally produce negligible amounts of dissociation products on reaction; hence, changes in molecular weight during the subsequent expansion process through the exhaust nozzle are insignificant. As will be seen later, there is a smaller variation in the "effective" specific heat of these systems also due to the absence of the heat of reaction effects on this effective c_p defined as $\left(\frac{\partial H}{\partial T}\right)_p$. Accordingly, the use of an average value for this term involves less chance for error in such a system.

In addition to the general shortcoming of the usual thermodynamic analysis of the rocket motor due to the assumption of constancy of molecular weight and specific heat, in the present case this simplified analysis was inadequate also because of its failure to consider heat losses. As noted previously, heat losses are of small consequence in rocket motors of conventional size; in the micro-motors of the present study they account for a significant if not a major portion of the total energy losses of the system. Therefore, a second major

modification of the usual thermodynamic analysis has been made to include the effects of heat losses in the theoretical relationships.

Derivation of Theoretical Equations

The usual simplified and idealized presentation which is available generally in the literature will be developed first. Following this review of the derivation of the usual relationships in their simplest form, the analysis will be extended to include the effects of heat loss and variable molecular weight and specific heat. By comparison of the expressions developed on these two different bases, an attempt will be made to estimate the kind of average values of specific heat and molecular weight which would be required in order to use the simpler expressions with assurance.

A. Usual Simplified Analysis

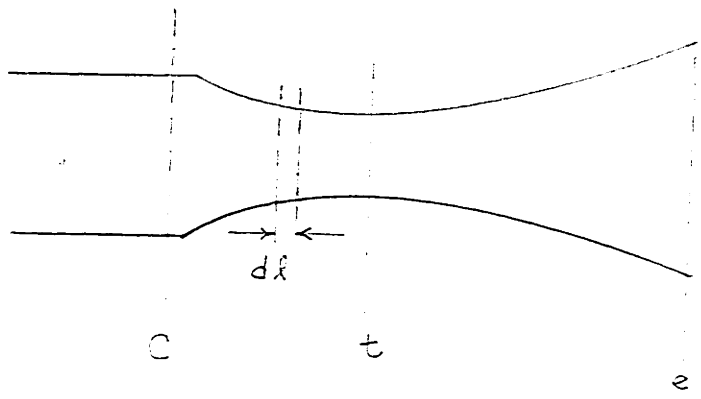

Consider the flow system through a converging-diverging nozzle such as pictured above from the initial conditions in the combustion chamber of a high pressure, low velocity gas stream which is being gradually expanded to lower pressure and accelerated as it flows through the nozzle passage. For simplification, this flow process will be considered unidimensional; this treatment implies that all the variables considered are uniform over any given cross section of the nozzle passage.

An energy balance over a small increment dl of the length of the nozzle yields, on the basis of a unit mass,

$$dH + \frac{udu}{g_o} = dQ \qquad (1)$$

where H is enthalpy per unit mass, u is its velocity, Q is the heat added, and g_o is a unit conversion factor. For the <u>adiabatic case</u> this becomes:

$$-\frac{udu}{g_o} = dH = c_p dT \qquad (2)$$

where c_p is the specific heat at constant pressure defined as $\left(\frac{\partial H}{\partial T}\right)_p$ and T is the temperature of the gas.

A balance between net force and change in momentum across this same section of the nozzle, dl, yields

$$-vdp + \frac{vdL}{A} = \frac{u\,du}{g_o} \qquad (3)$$

where v is specific volume, p is pressure, dL is wall friction

force in length dl, and A is cross-sectional area.

For the case of <u>reversible flow</u> this becomes:

$$-v\,d\not{p} = \frac{u\,du}{g_o} \tag{4}$$

Combining (2) and (4) gives:

$$-v\,d\not{p} = dH = c_p\,dT \tag{5}$$

The perfect gas law yields:

$$pv = \frac{RT}{MW} \tag{6}$$

where R is the universal gas constant, and MW is the molecular weight of the gas.

Substituting for v from (4) and (5) gives

$$-\frac{RT}{p\,MW}\,d\not{p} = c_p\,dT \tag{7}$$

Assuming no reaction as the gas flows through the nozzle and no change of $c_p \left[= \left(\frac{\partial H}{\partial T}\right)_p\right]$ with temperature, this can be integrated between any two points along the nozzle axis to give:

$$\frac{T_2}{T_1} = \left(\frac{P_2}{P_1}\right)^{\frac{\gamma-1}{\gamma}} \tag{8}$$

since $\gamma = \frac{c_p}{c_v}$ and $R = Mc_p - Mc_v$

Similarly equation (2) can be integrated under the same conditions between points 1 and 2 along the nozzle axis to give:

$$\frac{u_2^2}{2g_o} - \frac{u_1^2}{2g_o} = c_p (T_1 - T_2) \qquad (9)$$

If point 1 is made the entrance from the combustion chamber to the nozzle, u_1^2 can usually* be neglected. (Such was the case in the experimental work of this thesis where the combustion chamber cross-sectional area was at least ten times the nozzle throat area in every case). For this case, neglecting u_1^2, this becomes:

$$u_2^2 = 2g_o c_p (T_c - T_2) \qquad (10)$$

where subscript c refers to conditions in the combustion chamber or at the entrance to the exhaust nozzle, and (8) becomes:

$$\frac{T_2}{T_c} = \left(\frac{P_2}{P_c}\right)^{\frac{\gamma-1}{\gamma}} \qquad (11)$$

Equation (10) can also be written:

$$u_2^2 = 2g_o T_c \frac{R}{MW} \left(1 - \frac{T_2}{T_c}\right) \frac{\gamma}{\gamma-1} \qquad (12)$$

Substituting from (11) in (12) yields:

$$u_2^2 = \frac{2g_o RT}{MW} \left[1 - (P_2/P_c)^{\frac{\gamma-1}{\gamma}}\right] \frac{\gamma}{\gamma-1} \qquad (13)$$

Since specific impulse is defined as $I_{sp} = \frac{u_e}{g_o}$ (for the case

---

* At least one development exists, however, in which the relative chamber cross-section is too small for u_1^2 to be neglected.

of the perfectly designed nozzle where $P_e = P_{atm}$ and where the divergence angle is so small that all of the mass ejected can be considered to flow axially out of the exhaust nozzle), it can be expressed in terms of p's, T's, MW, and γ using equation (13) thus:

$$I_{sp} = \sqrt{\frac{2RT_c}{g_o MW}} \sqrt{\frac{\gamma}{\gamma-1}} \sqrt{1 - \left(\frac{P_e}{P_c}\right)^{\frac{\gamma-1}{\gamma}}} \qquad (14)$$

where subscript e refers to conditions at the nozzle exit, which is now the 2nd limit

Another useful relation is the continuity equation ~~where subscript e refers to conditions at the nozzle exit which is now the 2nd limit~~ for steady flow:

$$\dot{m} = \frac{A_1 u_1}{v_1} = \frac{A_2 u_2}{v_2} = \frac{A_c u_c}{v_c} = \frac{A_t u_t}{v_t}, \text{ etc.} \qquad (15)$$

where A is the cross-sectional area of the nozzle passage, $\dot{m}$ is the mass flow rate, or mass per unit of time (sec.) and subscript t refers to conditions at the nozzle throat.

From equation (11) and the perfect gas law,

$$\frac{v_2}{v_1} = \left(\frac{P_2}{P_1}\right)^{\frac{\gamma-1}{\gamma}-1} = \left(\frac{P_1}{P_2}\right)^{\frac{1}{\gamma}} \qquad (16)$$

Using this relation (as between chamber and point (2) in equation (15) gives:

$$\dot{m} = \frac{A_2 u_2}{v_c} \left(\frac{P_2}{P_c}\right)^{\frac{1}{\gamma}} \qquad (17)$$

Substituting from equation (13) for u_2 yields:

$$\dot{m} = \frac{A_2}{v_c} \left(\frac{P_2}{P_c}\right)^{\frac{1}{\gamma}} \left\{ \frac{2g_o RT_c}{MW} \left[1 - \left(\frac{P_2}{P_c}\right)^{\frac{\gamma-1}{\gamma}}\right] \frac{\gamma}{\gamma-1} \right\}^{\frac{1}{2}} \qquad (18)$$

Substituting for v_c from the perfect gas law expression,

$$v_c = \frac{RT_c}{MW\ P_c} \quad \text{gives:}$$

$$\dot{m} = \frac{P_c}{} A_2 \sqrt{\frac{2g_o MW}{RT_c}} \sqrt{\frac{\gamma}{\gamma-1}} \sqrt{\left(\frac{P_2}{P_c}\right)^{\frac{2}{\gamma}} - \left(\frac{P_2}{P_c}\right)^{\frac{\gamma+1}{1}}} \qquad (19)$$

Substituting for P_2/P_c from equation (8) converts this expression to:

$$\frac{\dot{m}}{A_2} = P_c \sqrt{\frac{2g\ MW}{RT_c}} \sqrt{\frac{\gamma}{\gamma-1}} \sqrt{\left(\frac{T_2}{T_c}\right)^{\frac{2}{\gamma-1}} - \left(\frac{T_2}{T_c}\right)^{\frac{\gamma+1}{\gamma-1}}} \qquad (20)$$

Since $\dot{m}$ is a constant, $\frac{\dot{m}}{A_2}$ will reach its maximum value when A_2 is a minimum; that is, at the throat of the nozzle when $A_2 = A_t$ = minimum. This information is sufficient to determine conditions at the throat. If the curve of $\dot{m}/A_2$ vs. T_2 contains no discontinuity at its maximum point, the derivative of $\frac{\dot{m}}{A_2}$ with respect to T_2 may be set equal to zero

$$\text{i.e.} \quad \frac{d\left(\frac{\dot{m}}{A_2}\right)}{d\ T_2} = 0 \ , \text{ and}$$

we find that $T_2 = T_t = T_c \left(\frac{2}{\gamma+1}\right)$

$$\text{or} \quad \frac{T_t}{T_c} = \frac{2}{\gamma+1} \qquad (21)$$

Equation (8) may then be used to determine p_c corresponding to T_t; unless P_t exceeds atmospheric pressure, setting the above derivative equal to zero was not permissible. Sub-

stituting from (22) into equation (20), we find:

$$\frac{\dot{m}}{A_t} = P_c \sqrt{\frac{2\, g_o MW}{RT_c}} \sqrt{\frac{\gamma}{\gamma-1}} \sqrt{\left(\frac{2}{\gamma+1}\right)^{\frac{2}{\gamma-1}} - \left(\frac{2}{\gamma+1}\right)^{\frac{\gamma+1}{\gamma-1}}} \qquad (22)$$

or

$$\frac{P_c}{} = \frac{\dot{m}}{A_t} \sqrt{\frac{RT_c}{2\, g_o\, MW}} \sqrt{\frac{\gamma-1}{\gamma}} \sqrt{\frac{1}{\left(\frac{2}{\gamma+1}\right)^{\frac{2}{\gamma-1}} - \left(\frac{2}{\gamma+1}\right)^{\frac{\gamma+1}{\gamma-1}}}} \qquad (23)$$

Equation (24) for P_c and equation (14) for I_{sp}, it is to be remembered, are both derived for the adiabatic, isentropic expansion of a perfect gas with no reaction and no change in c_p with temperature.

B. Analysis with Change of Molecular Weight and Specific Heat with Temperature

In the average rocket exhaust nozzle, the temperatures are sufficiently high and the pressures sufficiently low that perfect gas behavior is a fair approximation to the real gas behavior. Also, the expansion takes place so rapidly that the process is usually without appreciable heat loss. Isentropic restrictions are justified because of the resulting simplicity and because the actual performance can be compared with the ideal in this respect. However, the restrictions of no reaction and no change in c_p with temperature during the process are known to be in error. In propellant systems with high combustion temperatures, considerable dissociation takes place and considerable heat effects as well as small changes in molecular weight takes place

as these products reassociate during the expansion process. One of the major effects of these reassociation reactions is to change the slope of the enthalpy-temperature curve or the value of

$$c_p = \left(\frac{\partial H}{\partial T}\right)_p$$ at any point. In addition, of course, the heat capacities of the pure gaseous components are known to change with temperature.

In order to represent actual conditions more closely, these respections of no reaction and no change of heat capacity with temperature during the exapnsion process will be removed.

Instead, we will use a simplified relation for the manner in which c_p changes with temperature and assume that

$$c_p = \left(\frac{\partial H}{\partial T}\right)_p = a + bT \qquad (24)$$

where a and b are constants.

An expression of this type is fairly accurate for a pure gaseous molecular specie over a restricted temperature range and could be made to fit the curve of specific heat versus temperature very closely for any gas mixture in which there was no reaction. However, in a combustion gas mixture containing appreciable dissociation products, considerable reaction would occur during the expansion process, assuming that equilibrium were maintained. The amount of this reaction

as these products reassociate during the expansion process. One of the major effects of these reassociation reactions is to change the slope of the enthalpy-temperature curve or the value of

$$c_p = \left(\frac{\partial H}{\partial T}\right)_p$$ at any point. In addition, of course, the heat capacities of the pure gaseous components are known to change with temperature.

In order to represent actual conditions more closely, these respections of no reaction and no change of heat capacity with temperature during the exapnsion process will be removed.

Instead, we will use a simplified relation for the manner in which c_p changes with temperature and assume that

$$c_p = \left(\frac{\partial H}{\partial T}\right)_p = a + bT \qquad (24)$$

where a and b are constants.

An expression of this type is fairly accurate for a pure gaseous molecular specie over a restricted temperature range and could be made to fit the curve of specific heat versus temperature very closely for any gas mixture in which there was no reaction. However, in a combustion gas mixture containing appreciable dissociation products, considerable reaction would occur during the expansion process, assuming that equilibrium were maintained. The amount of this reaction

and the heat effects due to it are considerably greater at high temperatures but no appreciable reaction occurs below about 2200°K for any system composed of the elements C,H,O, and N. However, at these higher temperatures, the heat effects of these reassociation reactions contribute significantly to the "specific heat", defined as $(\partial H/\partial T)_p$, and as a result, the curve of effective specific heat versus temperature has significant curvature at temperatures above 2200°K. However, in the expansion process through the exhaust nozzle of a rocket motor, temperature changes slowly. In fact the change in temperature from chamber to nozzle throat is usually only about ten to twenty per cent while the total change in temperature from chamber to exhaust is generally considerably less than two fold. For this reason the above expression for c_p is a good approximation in most cases and entirely adequate in many situations. In fact, as will be shown later, due to compensating effects, the results of this analysis are adequate for nearly all systems.

The previous derivations for I_{sp} and P_c are now repeated with this new condition. Equation (5) then becomes

$$-v\,dp = dH = c_p\,dT = (a + bT)\,dT \qquad (5a)$$

or

$$-\frac{RT}{p\,mw}\,dp = (a+bT)\,dT \qquad (7a)$$

FIG. 1 APPARENT HEAT CAPACITY AND MOLECULAR WEIGHT AND PRODUCT OF TWO (MOLAL HEAT CAPACITY) AS A FUNCTION OF TEMPERATURE

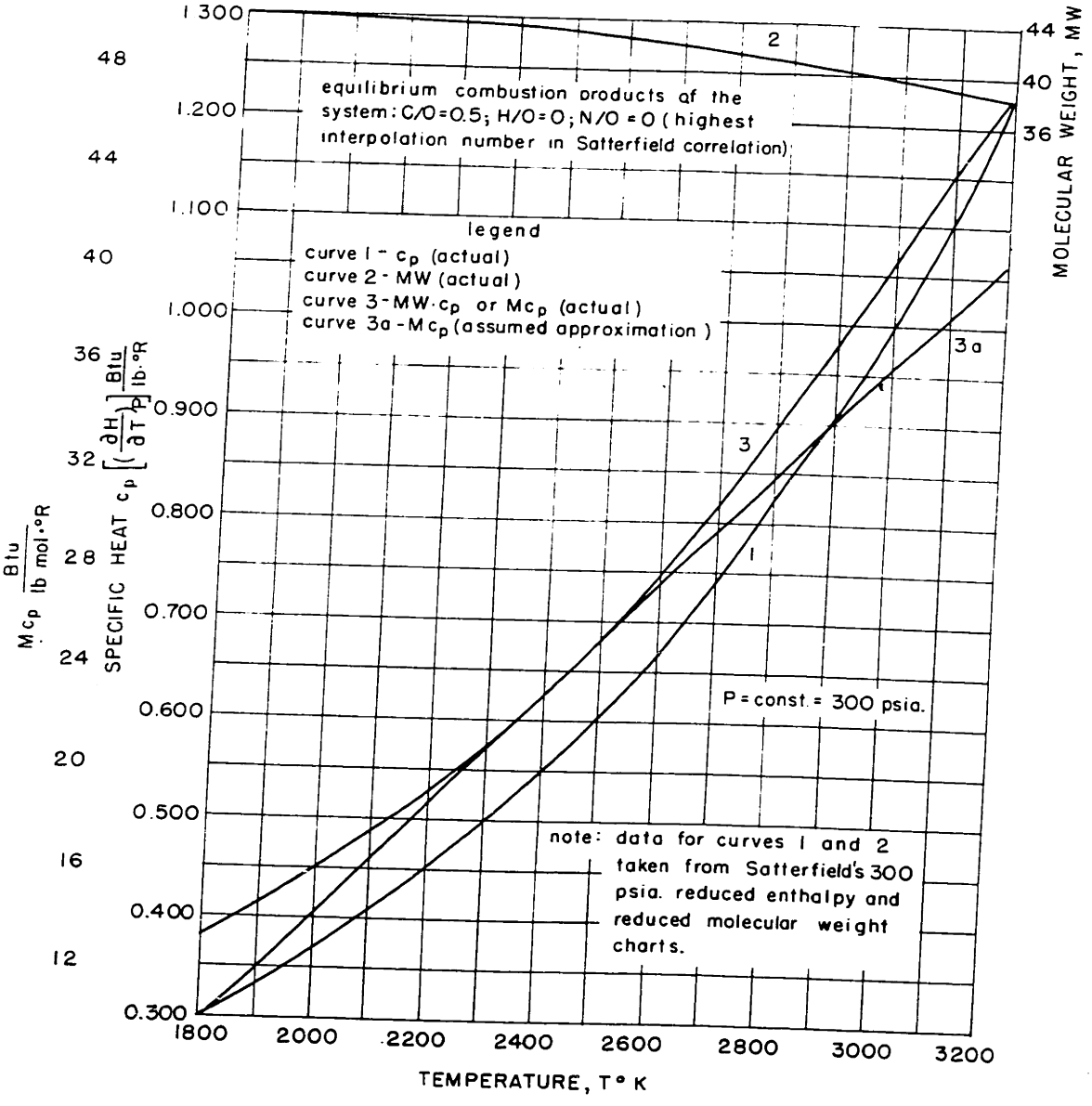

Integrating, we get

$$\frac{R}{MW_{AV}} \ln P_2/P_1 = a \ln T_2/T_1 + b(T_2 - T_1)$$

$$= \ln T_2/T_1 \left(a + b \frac{T_2 - T_1}{\ln T_2/T_1}\right)$$

$$= \ln T_2/T_1 \left(a + b\, T_{\log \text{mean}}\right)$$

$$\frac{R}{MW_{AV}} \ln P_2/P_1 = \ln T_2/T_1 \,[c_p]_{\text{at } T_{\log \text{mean}}} \qquad (25)$$

$$= c''_{p_{1-2}} \ln T_2/T_1$$

where MW_{Av} is the proper average for the integration as performed, and equal to $(\ln P_2/P_1) \Big/ \int_{P_1}^{P_2} dp/p\,MW$ and $c''_{p_{1-2}}$ is the specific heat $\left[\left(\frac{\partial H}{\partial T}\right)_p\right]$ at the logarithmic mean temperature between T_1 and T_2. In most cases the change in molecular weight is so small that an arithmetic average of the initial and final values can be used. However, to eliminate the uncertainty of the type of average required for MW, it can be included with c_p as the molal specific heat $\underline{M}c_p$. In fact, this product has been found to be more nearly linear with temperature than c_p for systems with large amounts of dissociation. This can be seen from Figure 1 which shows the variation of these quantities and of molecular weight with temperature at a constant pressure of 300 psia for the system represented by the element ratios C/O = 0.5, H/O = 0, N/O = 0, which is characterized by the most dissociation of any system composed of H, O, N, and C. Since the molecular weight curve of Figure 1 (curve (2)) has reverse curva-

ture to that of the specific heat curve (curve (1)), it follows that curve (3) for molal specific heat has less curvature than curve (1) for specific heat c_p. In the actual expansion through the exhaust nozzle of a rocket the temperature pressure decreases steadily. Therefore, the plot of specific heat (c_p) against temperature through the actual nozzle would have somewhat less curvature than in Figure 1.

The quantity $c''_{p_{1-2}}$ in equation (25) is the slope $\frac{(\partial H)}{(\partial T)_p}$ at the log mean temperature between T_1 and T_2. This slope $\frac{(\partial H)}{(\partial T)_p}$ changes only slightly with pressure since only that part of its value which is due to the dissociation reaction varies with pressure. (See Figure 2). Consequently, an arithmetic average of the two values $\frac{(\partial H)}{(\partial T)_p}$ at $T_{\log \text{ mean}}$ at p_1 and at p_2 can be taken. Equation (25) can also be written:

$$T_2/T_1 = \left(P_2/P_1\right)^{\frac{R}{MW_{AV} c''_{p_{1-2}}}} \quad \text{or} \quad T_2/T_1 = \left(\frac{P_2}{P_1}\right)^{R/Mc''_{p_{1-2}}} \tag{8b}$$

where $Mc''_{p_{1-2}}$ is the molal heat capacity at the log mean temperature between T_1 and T_2. This expression can also be written in terms of a pseudo-isentropic exponent or γ. However, this γ cannot now be defined as C_p/C_v since $Mc_p - Mc_v$ does not equal R for the case where reaction is occurring. However, if γ is defined as $= \frac{Mc_p}{Mc_p - R}$, then equation (8b) becomes:

$$T_2/T_1 = \left(P_2/P_1\right)^{\frac{\gamma''_{1-2} - 1}{\gamma''_{1-2}}} \tag{8a}$$

where γ''_{1-2} is evaluated at $T_{\text{log mean}}\Big]_1^2$ from $\dfrac{Mc''_{p_{1-2}}}{Mc''_{p_{1-2}} - R}$.

Also, equation (4) can be integrated using $c_p = a + bT$ as follows:

$$-\frac{u\,du}{g_o} = (a + bT)\,dT \tag{4a}$$

$$\frac{u_2^2 - u_1^2}{2g_o} = a(T_1 - T_2) + b\,\frac{(T_1^2 - T_2^2)}{2}$$

$$= (T_1 - T_2)\left(a + b\,\frac{T_1 + T_2}{2}\right)$$

$$= (T_1 - T_2)\left(a + b\,T_{\text{arith. mean}}\right)$$

$$\frac{u_2^2 - u_1^2}{2g_o} = (T_1 - T_2)\,c_p\Big]_{\text{at } T_{\text{arith. mean}}} = (T_1 - T_2)\,c'_{p_{1-2}} \tag{9a}$$

where $c'_{p\ 1-2}$ is the slope $\left(\dfrac{\partial H}{\partial T}\right)_p$ at the arithmetic mean temperature between T_1 and T_2. Here again, the average value at this temperature of two separate values at p_1 and at p_2 will also have to be taken.

If point 1 is again made, the entrance from the combustion chamber to the nozzle, u_1^2, can be neglected and equation (9a) becomes

$$u_2^2 = 2g_o\,c'_{p_{c-2}}\,(T_c - T_2) \tag{10a}$$

where $c'_{p_{c-2}} = \left(\dfrac{\partial H}{\partial T}\right)_p$ at arithmetic mean temperature$\Big]_c^2$

Equation (8a) becomes

$$T_2/T_c = (P_2/P_c)^{\frac{\gamma''_{c-2}-1}{\gamma''_{c-2}}} \qquad (11a)$$

Again assuming $\gamma = \frac{Mc_p}{Mc_p - R}$, equation (10a) can be written

$$u_2^2 = 2g_o T_c \frac{R}{\frac{Mc'_{p\,c-2}}{c'_{p\,c-2}}} \left(1 - \frac{T_2}{T_c}\right)\left(\frac{\gamma'_{c-2}}{\gamma'_{c-2}-1}\right) \qquad (12a)$$

where γ'_{c-2} is evaluated at T arithmetic mean $\Big]_c^2$ from $\frac{Mc'_{p\,c-2}}{Mc'_{p\,c-2} - R}$.

Thus, we have now introduced two types of average cp, Mcp, and γ. The arithmetic mean of each of these has and will be henceforth designated by a single prime, while the logarithmic mean of each has and will be designated by a double prime. The temperature limits over which the mean of each of these terms is evaluated has and will be henceforth designated by two subscripts which will correspond to those used for pressure, temperature and other point variables.

Substituting from equation (11a) into (12a)

$$u_2^2 = \frac{2g_o R T_c}{Mc'_{p\,c-2}/c'_{p\,c-2}} \left[1 - \left(P_2/P_c\right)^{\frac{\gamma''_{c-2}-1}{\gamma''_{c-2}}}\right] \frac{\gamma'_{c-2}}{\gamma'_{c-2}-1} \qquad (13a)$$

and specific impulse becomes by definition (taking point 2 in equation (13a) as the nozzle exit and assuming as before that $p_e = p_{atm}$):

$$I_{sp} = \sqrt{\frac{2RT_c}{g_o \frac{Mc'_{c-e}}{c'_{c-e}}}} \sqrt{\frac{\gamma'_{c-e}}{\gamma'_{c-e}-1}} \sqrt{1-\left(\frac{P_e}{P_c}\right)^{\frac{\gamma''_{c-e}-1}{\gamma''_{c-e}}}} \qquad (14a)$$

Using equation (8b) in equation (10a), an alternate equation to (13a) can be obtained,

$$u_2^2 = 2g_o T_c c'_{c-2} \left[1-\left(P_2/P_c\right)^{\frac{R}{MW_{AV} c''_{c-2}}}\right] \qquad (13b)$$

which does not contain the pseudo γ defined as $\gamma = \dfrac{Mc_p}{Mc_p - R}$.

In the same way, equation (14a) can assume the alternate form

$$I_{sp} = \sqrt{\frac{2T_c c'_{c-e}}{g_o}} \sqrt{1-\left(P_e/P_c\right)^{\frac{R}{MW_{AV} c''_{c-e}}}} \qquad (14b)$$

From equation (8b) and the perfect gas law:

$$\frac{MW_2 v_2}{MW_c v_c} = \left(\frac{P_2}{P_c}\right)^{\frac{R}{MW_{AV} c''_{c-2}}-1} = \left(\frac{P_2}{P_c}\right)^{\frac{R - MW_{AV} c''_{c-2}}{MW_{AV} c''_{c-2}}} \qquad (16b)$$

or in terms of pseudo γ'' $\left(\dfrac{MW_2 v_2}{MW_c v_c}\right)^{\gamma''_{c-2}} = P_c/P_2$ (16a)

Substituting from (16b) in the continuity equation [(15)],

$$\dot{m} = \frac{A_2 u_2 MW_2}{v_c MW_c} \left(\frac{P_2}{P_c}\right)^{\frac{R - MW_{AV} c''_{c-2}}{MW_{AV} c''_{c-2}}} \qquad (17b)$$

Using equation (13b) this becomes:

$$\dot{m} = \frac{A_2 MW_2}{v_c MW_c} \left(\frac{P_c}{P_2}\right)^{\frac{R-MW_{AV} c''_{c-2}}{MW_{AV} c''_{c-2}}} \left\{2g_o T_c c'_{c-2}\left[1-\left(\frac{P_2}{P_c}\right)^{\frac{R}{MW_{AV} c''_{c-2}}}\right]\right\}^{\frac{1}{2}} \qquad (18b)$$

using $v_c = \dfrac{RT_c}{MW_c P_c}$

$$\dot{m} = \frac{A_2 MW_2 P_c}{R}\sqrt{\frac{2g_o c'_{p_{c-2}}}{T_c}}\sqrt{\left(\frac{P_2}{P_c}\right)^{\frac{2MW_{AV}c''_{p_{c-2}}-2R}{MW_{AV}c''_{p_{c-2}}}}-\left(\frac{P_2}{P_c}\right)^{\frac{2MW_{AV}c''_{p_{c-2}}-R}{MW_{AV}c''_{p_{c-2}}}}} \quad (19b)$$

From equation (8b)

$$P_2/P_c = \left(T_2/T_c\right)^{\frac{MW_{AV}c''_{p_{c-2}}}{R}}$$

$$\therefore \dot{m} = \frac{A_2 MW_2 P_c}{R}\sqrt{\frac{2g_o c'_{p_{c-2}}}{T_c}}\sqrt{\left(\frac{T_2}{T_c}\right)^{\frac{2MW_{AV}c''_{p_{c-2}}-2R}{R}}-\left(\frac{T_2}{T_c}\right)^{\frac{2MW_{AV}c''_{p_{c-2}}-R}{R}}} \quad (20b)$$

In terms of pseudo γ's, equation (20b) would be written

$$\dot{m} = A_2 P_c\sqrt{\frac{2g_o MW_2^2}{RT_c}\frac{Mc_{p_{c-2}}}{c'_{p_{c-2}}}}\sqrt{\frac{\gamma'_{c-2}}{\gamma'_{c-2}-1}}\sqrt{\left(\frac{T_2}{T_c}\right)^{\frac{2}{\gamma''_{c-2}-1}}-\left(\frac{T_2}{T_c}\right)^{\frac{\gamma''_{c-2}+1}{\gamma''_{c-2}-1}}} \quad (20a)$$

In the first derivation, when c_p and γ were assumed constant, conditions at the throat (where $\dot{m}/A_2$ is a maximum) were represented by

$$\frac{T_t}{T_c} = \frac{2}{\gamma+1} \quad (21)$$

Now, if we assume an expression of the same form for the present case, we can say

$$\frac{T_t}{T_c} = \frac{2}{\gamma_d+1} \quad (21a)$$

where γ_d is the proper kind of average γ to make this true, - (see p. 45 for further discussion of it). Substituting from

equation (21a) in equation (20a) with point 2 now designated as the nozzle throat gives

$$\dot{m} = A_t P_c \sqrt{\frac{2g_o \overline{MW}_t^2}{RT_c} \frac{\gamma'_{c-t}}{\frac{mc_{p'c-t}}{c_{p'c-t}}}} \sqrt{\frac{\gamma'_{c-t}}{\gamma'_{c-t}-1}} \sqrt{\left(\frac{2}{\gamma_d+1}\right)^{\frac{2}{\gamma''_{c-t}-1}} - \left(\frac{2}{\gamma_d+1}\right)^{\frac{\gamma''_{c-t}+1}{\gamma''_{c-t}-1}}} \qquad (22a)$$

And substituting from (21a) and (8a) in (13a) with point 2 again designated as the nozzle throat gives:

$$u_t^2 = \frac{2g_o R T_c}{\frac{mc_{p'c-t}}{c_{p'c-t}}} \left[\frac{\gamma'_{c-t}}{\gamma'_{c-t}-1}\right] \left[\frac{\gamma_d - 1}{\gamma_d + 1}\right] \qquad (13c)$$

Velocity of Sound

From the continuity equation

$$\frac{\dot{m}}{A} = \frac{u}{v}$$

As before, the derivative of $\frac{\dot{m}}{A}$ with respect to either of the other variables is zero at the throat since $\frac{\dot{m}}{A}$ is a maximum at the throat.

$$\frac{d\left(\frac{\dot{m}}{A}\right)}{du} = \frac{1}{v} - \frac{u}{v^2}\frac{dv}{du} = 0$$

$$\therefore \frac{du}{u} = \frac{dv}{v} \qquad (26)$$

Substituting for $\frac{du}{u}$ from equation (4) into (26) gives:

$$-\frac{g_o v dp}{u^2} = \frac{dv}{v}$$

or $$u^2 = g_o v^2 \left(\frac{\partial p}{\partial v}\right)_s$$

since we have assumed adiabatic reversible flow.

$$\therefore u_t = \sqrt{-g_o v_t^2 \left(\frac{\partial p}{\partial v}\right)_s} \qquad (27)$$

which is identical with the expression for the velocity of sound in a gas. Therefore, the throat velocity in a converging-diverging nozzle will be the velocity of sound in the gas under throat conditions.

Using the adiabatic relation between p and v for a perfect but reacting gas mixture (equation 16a), together with the perfect gas law, equation (27) becomes

$$u_t = \sqrt{\gamma_t g_o \frac{RT_t}{MW_t} + \gamma_t g_o \frac{RT_t v_t}{MW_t^2}\left(\frac{\partial MW_t}{\partial v_t}\right)_s} \qquad (28)$$

Squaring both sides of (28) and substituting for T_t from equation (21a) gives

$$u_t^2 = \gamma_t g_o \frac{RT_c}{MW_t}\left(\frac{2}{\gamma_d+1}\right) + \gamma_t g_o \frac{RT_c v_t}{MW_t}\left(\frac{2}{\gamma_d+1}\right)\left(\frac{\partial MW_t}{\partial v_t}\right)_s \qquad (29)$$

Equating expressions (13c) and (29) for u_t^2,

$$\frac{\gamma'_{c-t}}{\gamma'_{c-t}-1}(\gamma_d-1)\frac{1}{Mc_{p'c-t}} = \frac{\gamma_t}{MW_t} + \frac{\gamma_t v_t}{MW_t^2}\left(\frac{\partial MW_t}{\partial v_t}\right)_s \qquad (30)$$

If the definition of pseudo γ'_{c-2} (or actually γ'_{c-t} when point 2 is taken as the nozzle throat) is changed from the arbitrary expression used in equation (12a), page 38, which was

$$\gamma'_{c-2} = \frac{Mc_{p'c-2}}{Mc_{p'c-2} - R}$$

to another arbitrary but equally permissible definitive expression,

$$\gamma'_{c-2} = \frac{MW_t \, c_{p'c-2}}{MW_t \, c_{p'c-2} - R} \qquad)$$

then the ratio $\frac{Mc_{p'}}{c_{p'}}$ in equations (12a), (13a), (13c), and (30) reduces to MW_t. With this new definition of γ'_{c-2} (or γ'_{c-t}), equation (22a) becomes

$$\dot{m} = A_t p_c \sqrt{\frac{2g_o MW_t}{RT_c}} \sqrt{\frac{\gamma'_{c-t}}{\gamma'_{c-t}-1}} \sqrt{\left(\frac{2}{\gamma_d+1}\right)^{\frac{2}{\gamma''_{c-t}-1}} - \left(\frac{2}{\gamma_d+1}\right)^{\frac{\gamma''_{c-t}+1}{\gamma''_{c-t}-1}}} \qquad (22c)$$

and equation (30) becomes

$$\frac{\gamma'_{c-t}}{\gamma'_{c-t}-1}(\gamma_d-1) = \gamma_t \left[1 + \frac{v_t}{MW_t}\left(\frac{\partial MW_t}{\partial v_t}\right)_s\right] \qquad (31)$$

If the gas mixture were not reacting, $\left(\frac{\partial MW_t}{\partial v_t}\right)_s$ would equal zero, and equation (31) then simplifies further to

$$\frac{\gamma'_{c-t}}{\gamma'_{c-t}-1}(\gamma_d-1) = \gamma_t \qquad (32)$$

The difference between equations (31) and (32) can be shown to be small for any system composed only of C,H,O and N

at any temperatures below 3200°K. by the following considerations. The term $-\frac{v_t}{MW_t}\left(\frac{\partial MW_t}{\partial v_t}\right)_s$ (dimensionless) will be greatest for that system represented by the element ratios C/O = 0.5, H/O = 0, and N/O = 0 for which a plot of the molecular weight versus temperature at a constant pressure of 300 psia has already been presented in Figure 1. For this system an approximate value of

$$-\left[\frac{\left(\partial MW_t\right)_{p=300}}{MW_t}\right]_{T=3150°K}$$

is given by $-\left(\frac{\left[\Delta MW_t\right]_{3100}^{3200}}{MW_t}\right)_{p=300}$. From Figure 1 this can be seen to be

$$\frac{38.9 - 38.1}{38.1} = \frac{0.8}{38.1} = 0.021.$$

The term $-\left[\frac{\left(\partial MW_t\right)_s}{MW_t}\right]_{T=3150°K}$ will be somewhat smaller than this because molecular weight changes slightly less rapidly during passage through an actual rocket nozzle (along a constant entropy path) due to the decrease in pressure and resultant tendency to shift equilibrium toward greater dissociation counterbalancing somewhat the decrease in dissociation due to decreasing temperatures. However, as a maximum figure the above value of 0.021 can be used in this approximate evaluation of the term $\frac{v_t}{MW_t}\left(\frac{\partial MW_t}{\partial v_t}\right)_s$. The second factor of this term, $\left[\frac{v_t}{\left(\partial v_t\right)_s}\right]_{T=3150}$ can be approximated similarly by $\left(\frac{v_t}{\Delta v_t\,]_{3100}^{3200}}\right)_s$. Using the perfect gas law, this can be evaluated very closely

for the case when P_1 = 300 psia and T_1 = 3200°K. Since γ'' will have a maximum value of 1.2 at this high temperature, from equation (8a), P_2 will be no more than 250 psia at T_2 = 3100°K. Values of molecular weight at 3200°K and 3100°K and 300 psia (taken from Figure 1) will closely approximate the true molecular weights. In this way, $\left(\frac{v_t}{\Delta v_t}\right)_s$ can be given the approximate value of $\frac{5.42}{6.18-5.42} = 7.13$. Therefore, the maximum value of the term $\left[+\frac{v_t}{MW_t}\left(\frac{\partial MW_t}{\partial v_t}\right)_s\right]_{T=3100}$ will be less than (0.021) (7.13) = 0.15.

For this case, equation (31) becomes

$$\frac{\gamma'_{c-t}}{\gamma'_{c-t}-1}(\gamma_d - 1) = 1.15\,\gamma_t \qquad (33)$$

Thus, the two extremes of equation (31) are represented by (32) and (33). Equations (32) and (33) can be solved for γ_d to yield the following expressions:

From (32)

$$\gamma_d = \gamma_t + \frac{\gamma'_{c-t} - \gamma_t}{\gamma'_{c-t}} \qquad (34)$$

From (33)

$$\gamma_d = 1.15\,\gamma_t + \frac{\gamma'_{c-t} - 1.15\,\gamma_t}{\gamma'_{c-t}} \qquad (35)$$

In either case then γ_d is seen to be some sort of weighted average of two types of pseudo γ, namely γ_t and γ'_{c-t}.

In either case, if γ'_{c-t} were equal to one, γ_d would be identical with γ'_{c-t} or also equal to one. (It is not actually possible in general for γ to assume a value of 1, although γ approaches a values of 1 as a limit as $\left(\frac{\partial H}{\partial T}\right)_p$ approaches ∞). At the other extreme (also actually impossible) if γ'_{c-t} were equal to 2, γ_d would be approximately the arithmetic average of γ_t and γ'_{c-t}. Using equation (34) imposition of this condition gives $\gamma_d = 0.5\,\gamma_t + 0.5\,\gamma'_{c-t}$ and using equation (35), the corresponding expression is $\gamma_d = 0.5\,\gamma'_{c-t} + 0.575\,\gamma_t$. In practice γ'_{c-t} assumes values between 1.1 and 1.2 in most cases. Using a value of 1.15 for γ'_{c-t}, in equation (34) makes $\gamma_d = 0.87\,\gamma'_{c-t} + 0.13\,\gamma_t$ whereas in equation (35) this makes $\gamma_d = 0.87\,\gamma'_{c-t} + 0.125\,\gamma_t$. Thus, the difference between the two cases is obviously too small to be significant and γ_d can be said to be a weighted average of γ'_{c-t} and γ_t consisting of about 87% γ'_{c-t} and 13% γ_t. In the usual case then, γ_d would be somewhat more heavily weighted toward γ_t than would be the case with γ''_{c-t} which is based on a log mean of the chamber and nozzle throat temperatures.

Thus, it would appear that based on this more rigorous analysis, the most useful expression for calculating theoretical chamber would be

$$\dot{m} = A_t p_c \sqrt{\frac{2 g_o M w_t}{R T_c}} \sqrt{\frac{\gamma'_{c-t}}{\gamma'_{c-t}-1}} \sqrt{\left(\frac{2}{\gamma_d+1}\right)^{\frac{2}{\gamma''_{c-t}-1}} - \left(\frac{2}{\gamma_d+1}\right)^{\frac{\gamma''_{c-t}+1}{\gamma''_{c-t}-1}}} \qquad (22c)$$

for which, it would be necessary to know $\dot{m}$, A_t MW_t, T_c, c'_p, Mc_p'', and c_{p_t}.

Similarly, the most useful expression for calculating theoretical specific impulse developed by this analysis seems to be

$$I_{sp} = \sqrt{\frac{2RT_c}{g_o \frac{Mc'_{p_{c-e}}}{c'_{p_{c-e}}}}} \sqrt{\frac{\gamma'_{c-e}}{\gamma'_{c-e}-1}} \sqrt{1-\left(\frac{p_e}{p_c}\right)^{\frac{\gamma''_{c-e}-1}{\gamma''_{c-e}}}} \qquad (14a)$$

for use of which it would be necessary to know T_c, $Mc'_{p_{c-e}}$, $c'_{p\ c-e}$, $Mc''_{p_{c-e}}$, and p_c and p_e. Examination of these two expressions (22c) and (14a) plus expression (34) or (35) for γ_d reveals that there are five different types of specific heat involved here - four kinds of average specific heat namely

$c'_{p_{c-t}}$, $c''_{p_{c-t}}$, $c'_{p_{c-e}}$, and $c''_{p_{c-e}}$

and one point value which is c_{p_t} (the specific heat at throat conditions.

The basis for this entire second analysis has been the assumption that specific heat, $c_p \left[\left(\frac{\partial H}{\partial T}\right)_p\right]$ would be linear with temperature. In order to test the validity of this assumption, let us consider once more that system in the group composed only of C,H,O, and N which is characterized by the greatest amount of dissociation and therefore the largest variation of Molecular weight and specific heat with temperature. It can be seen from Figure 1 that even for this system, c_p or Mc_p is linear with temperature over the short range from

chamber to throat which is usually about 300 - 400°K (e.g. from 3000°K to 2700°K). Therefore, the results of this analysis are applicable over this range and equation (22c) is strictly valid for calculating chamber pressure.

However, the total change of temperature over this range is so small that the difference between c_p' and c_p'' is negligible and therefore a single value of c_p such as c_p' can be determined and used for c_p' & c_p''. Also, the total variation in γ from γ_c to γ_t is relatively small (about 5% at most) and accordingly γ_d can also be taken as equal to $\gamma' = \gamma''$ without introducing errors of more than 1/2% in the worst case in the calculation of p_c by equation (22c).

In determining specific impulse from equation (14a), the complete range of temperature from T_c to T_e is encountered. It is seen from Figure 1 that specific heat is not strictly linear with temperature over this complete range, e.g., from 3100°K to 1800°K. If the value of specific heat at the arithmetic mean temperature were taken as the average over this range, it would correspond to a variation of Mc_p with temperature such as that given by the straight line tangent to the curve. This is seen to be somewhat lower than the correct curve of c_p against T especially at the ends. Therefore, equation (14a) is strictly valid only for a system with negligible dissociation. For the case of the curved line relation which exists for systems

with dissociation, c_p' evaluated at the arithmetic mean temperature and Mc_p'' evaluated at the log mean temperature are both somewhat too low and the γ's evaluated therefrom are correspondingly higher than the correct average values. Graphical integration (using the curve of Mc_p versus T in Figure 1) of $\int Mc_p dT$ yields an average value of Mc_p of about 26 compared to the value at the arithmetic average temperature of 24.1. These figures correspond to the following values of pseudo γ: $\bar{\gamma}$ (correct average) $= \frac{26}{24.01} = 1.082$, and

γ' (arithmetic mean temp.) $= \frac{24.1}{22.11} = 1.09$.

Since the system represented in Figure 1 is characterized by the most dissociation of any within the range of fuels consisting only of C,H,O and N, this error in the γ at arithmetic mean temperature (γ') should also be the maximum deviation from the correct average for this case. Presumably the γ at the log arithmic mean temperature (γ'') will also be in error by about the same amount from the correct average for that integration [performed in obtaining equation (25)]. Reference to figure 3 indicates that if both γ' and γ'' in equation (14a) were in error in the same direction by only 1%, the net error in the calculated specific impulse would be only about 0.5%. An accuracy of 1% can be maintained in the calculated specific impulse even with a common error in γ' and γ'' of 2%. It is felt that the above analysis leading to an evaluation of γ' from c_p' at the arithmetic mean temperature

FIGURE -2

$\sqrt{\frac{\gamma}{\gamma-1}}$ & $\sqrt{1-(\frac{P_e}{P_c})^{\frac{\gamma-1}{\gamma}}}$ & PRODUCT AS A FUNCTION OF γ FOR VARIOUS P_c

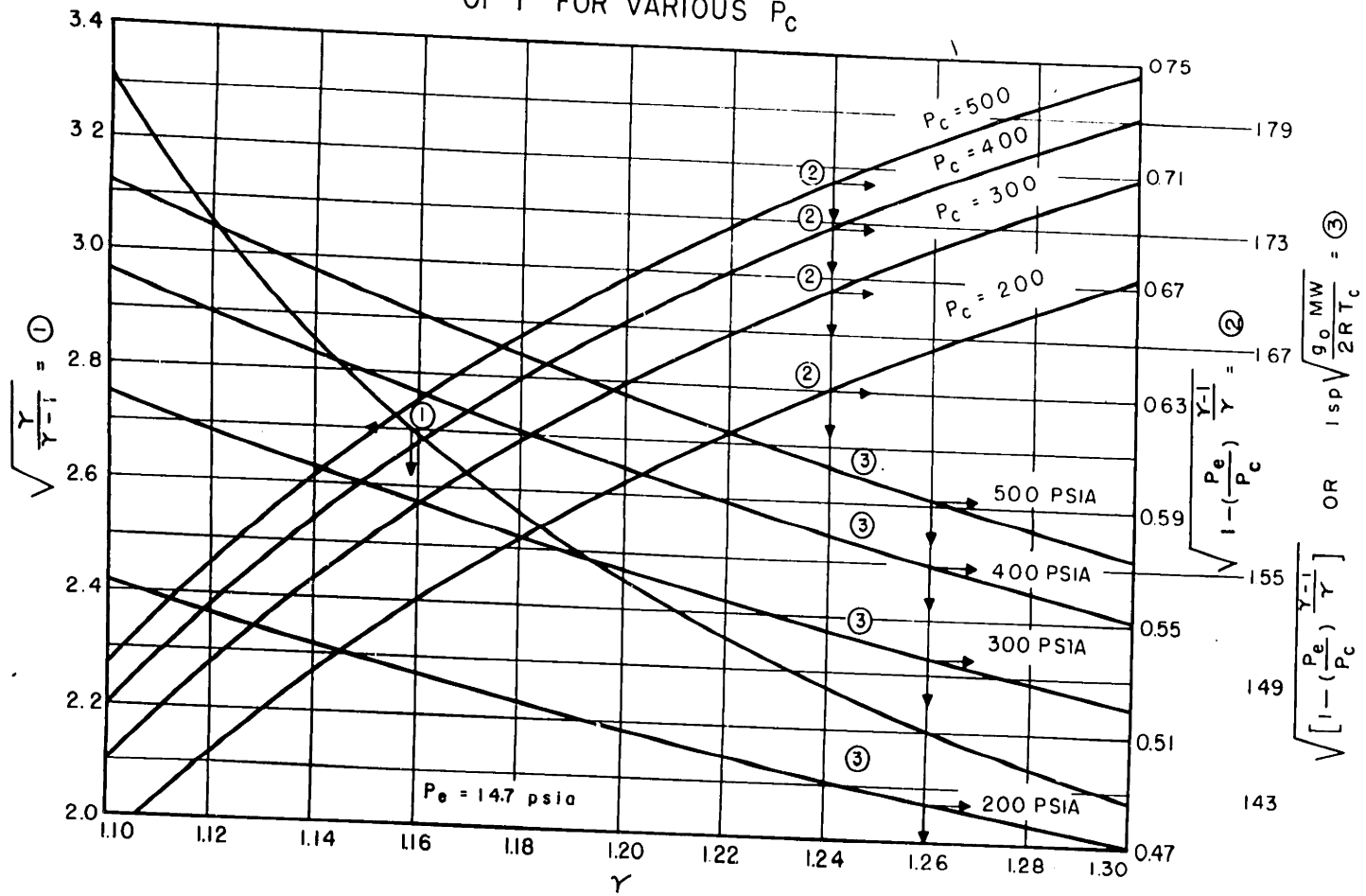

FIGURE 3 $\sqrt{\frac{\gamma}{\gamma-1}}$ & $\sqrt{\left(\frac{2}{\gamma+1}\right)^{\frac{2}{\gamma-1}} - \left(\frac{2}{\gamma+1}\right)^{\frac{\gamma+1}{\gamma-1}}}$ & RECIPROCAL OF PRODUCT AS A FUNCTION OF γ

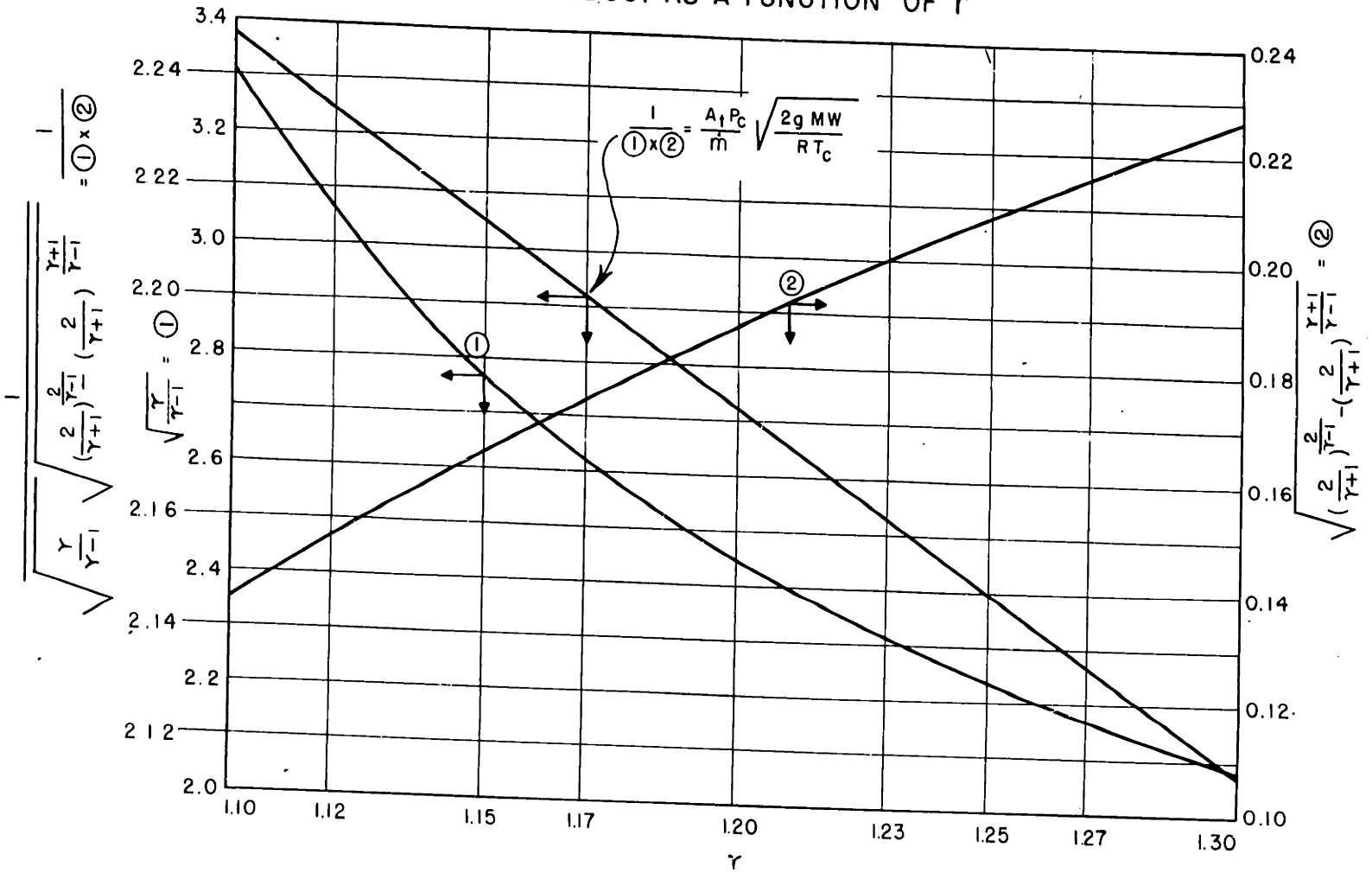

and an evaluation of γ'' from c_p'' at the log mean temperature will in all cases lead to values of well within this accuracy.

Figures 2 and 3 show how the various terms involving γ in equation (22c) and (14a) for p_c and I_{sp} respectively vary with γ and also how much less the product of each of these two terms in each case varies with γ due to the counterbalancing affect. This illustrates why a common error in the γ used in both terms of as much as 3% results in a net error in either P_c or I_{sp} of only about 1% in most cases.

In fact, as will be shown later, a single value of γ, preferably γ', can be used for both γ' and γ'' with less than 1% error even in equation (14a) for calculating specific impulse and even for a high temperature system provided dissociation is moderate. This approximation has been used in order to test its accuracy in the system red fuming nitric acid (6.5% NO_2) and aniline.

For any given case the exact values of each of these different kinds of average specific heat could be determined indirectly if an independent solution of the problem were already available, e.g., from a graphical method or other rigorous calculation. For example, the value designated as Mc_p'' could be determined from equation (8b) if all four values T_2, T_1, p_2, and p_1 were known and the value designated as c_p' could be determined from equation (10a) if u_2 or ΔH and T_c and T_2 were known. If the operating range of pressures is known, all of these quantitities can be determined readily with an accuracy of

1 or 2% from the Satterfield charts or even more accurately by the conventional bng-hand enthalpy and entropy balances. If these calculations were carried out for a sufficient number of representative systems, the proper kinds of average temperature to be used in order to determine the correct values of the various kinds of average specific heat could be ascertained. Lacking this complete body of knowledge, however, the present analysis has been applied and the arithmetic mean temperature has proven adequate, as will be shown, for the systems experimentally studied in this thesis.

C. Analysis with Heat Loss

Heat losses in the combustion chamber proper (prior to the entrance of the exhaust nozzle) are easily accounted for since their effect is merely to reduce the initial enthalpy of the combustion gases entering the nozzle. However, in order to correct accurately for heat loss along the nozzle passage, the exact distribution of the heat loss along the length of the nozzle must be known. Since this distribution was not measured or known exactly in the experiments of this thesis, no attempt was made to carry out such an exact theoretical analysis for this nozzle heat loss. Even if an analytical expression for heat loss in terms of nozzle geometry, which could be converted to be in terms of gas temperature, were known, the expressions resulting from integrations of equations (1) and (1) and (2) combined would probably be too complicated to be of much use.

Accordingly, the following approximate analysis of the effect of nozzle heat loss seems worthy of consideration and applicable to the present conditions.

It is obvious that if all of the heat lost in the nozzle or in the converging section of the nozzle were lost in the first infinitesimal length of the nozzle dl_1, then this nozzle heat loss would be exactly equivalent to that heat lost before the nozzle, i.e., in the combustion chamber proper. On the other hand if all of this nozzle heat loss occurred in the final infinitesimal length dl_2 of the nozzle or of the converging section of the nozzle (if that alone is being considered), then the heat loss would be almost completely ineffectual, since the expansion process under consideration would be essentially complete at that point. Assuming that the variation in the effect of nozzle heat loss is regular and continuous between these two extremes and that the nozzle heat loss is uniformly distributed over the nozzle or the nozzle section in question, then the average affect of this nozzle heat loss should be somewhere between these two extremes or approximately one half as great as the effect of the combustion chamber heat loss.

This is the method used to handle nozzle heat losses in the calculations of this thesis. For the equation type calculations of chamber pressure one half of the heat loss in the converging section of the nozzle was added to the combustion chamber heat loss and the total amount then

subtracted from the enthalpy of the unburned system to obtain the initial enthalpy of the gas entering the nozzle. With this pre-correction of the initial enthalpy to allow approximately for nozzle heat loss, the expansion process could then be treated as isentropic. The same method was used in calculating theoretical specific impulse except that one half of the heat loss in the entire nozzle was added to the combustion chamber heat loss and the total amount subtracted from the initial enthalpy under adiabatic conditions to obtain the initial enthalpy of the gas entering the nozzle which allows for all heat losses.

Since the nozzle heat losses experimentally measured in this thesis were never large enough to affect performance calculations by more than 4% and usually caused corrections of only about 2% or less, there is no possibility for large errors in spite of the crudeness of this method of analysis. The least accurate of the above assumptions is that the nozzle heat loss will be uniformly distributed over the entire process. It has been generally observed in actual experiments for example that heat transfer rates are much higher at the nozzle throat than at the entrance or exit to the nozzle. However, the lateral surface area for heat transfer per unit length is considerably greater at the entrance and exit than at the throat which tends to level out the heat loss per unit length.

The assumption of uniform heat loss probably implies

"with respect to temperature" in order for the above interpretation of the average effect of nozzle heat loss to hold. Since temperature changes nearly linearly with length of the nozzle, that is equivalent to requiring a nearly constant heat loss per unit length.

The easiest way to handle nozzle heat losses (especially if the distribution of the heat through the nozzle were known) is by means of an enthalpy- entropy diagram for the system. It has been found from calculations on this type of Mollier diagram that assuming all of the heat lost in the nozzle to be lost at a temperature midway between T_c and T_e produces about one half of the effect on the specific impulse of that produced when all of this heat is transferred at the nozzle entrance (essentially in the combustion chamber proper).

Usual Criteria of Rocket Motor Performance

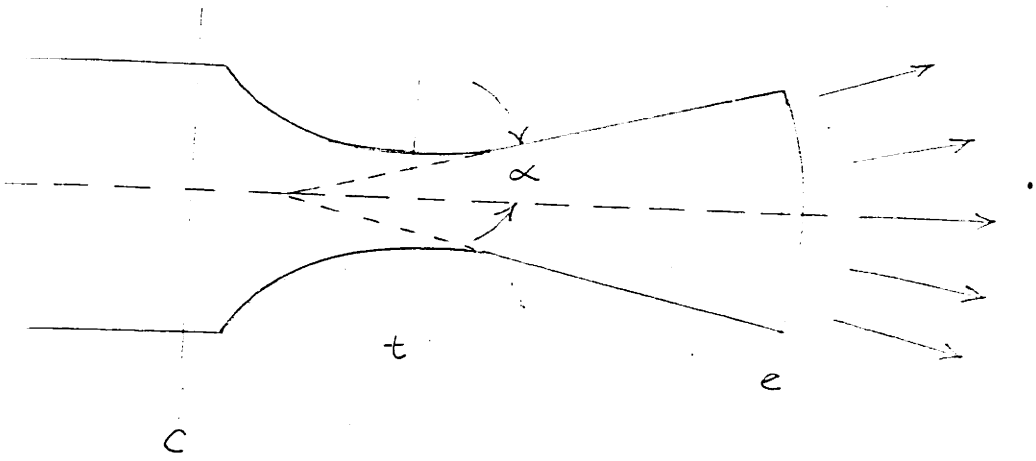

In a real exhaust nozzle, the angle of divergence is usually so large that the assumption of a plane pressure front is not longer justifiable. Assuming that the gas stream conforms to the shape of the nozzle passage with no separation from the walls, the existence of a spherical pressure front for the flowing gas is much more representative of true conditions. In this case the velocity of the gas stream will have a radial distribution perpendicular to this spherical surface of equal pressure. As a result, the final exhaust velocity of the

TABLE I

α, in $^{\circ}$	λ
0	1.0
5	0.998
10	0.99
20	0.97
30	0.934
37	0.90

Ref. F. J. Malina Jour. Franklin Inst., 230, p. 452, 1940

entire gas stream as it leaves the nozzle will not be solely in the axial direction.

Therefore, an expression for the average axial component of the exhaust velocity, called $\bar{u}_{e_x}$, is determined in terms of the exhaust velocity u_e and the half angle of divergence α, namely:

$$\bar{u}_{e_x} = 0.5\,(1+\cos\alpha)\,u_e = \lambda u_e \tag{36}$$

Values of λ as a function of α are given in Table 1. They show that a very wide angle of divergence can be used with small loss in impulse.

Using this information, the force balance across the exit plane of the exhaust nozzle can be written

$$F = \frac{\dot{m}\,\bar{u}_{ex}}{g_o} + (p_e - p_{atm})\,A_e \tag{37}$$

where F = thrust force.

Of course in a perfectly designed nozzle, p_e would be exactly equal to p_{atm} and the second term would be eliminated in equation (37). In this case, by definition:

$$I_{sp} = F/\dot{m} = \frac{\bar{u}_{ex}}{g_o} = \frac{\lambda u_e}{g_o} \tag{38}$$

Effective Exhaust Velocity

In experimental work, however, it is impossible to attain this perfect nozzle design, consistently at least. It has been found that best performance is obtained with design for an exhaust pressure which is equal to or greater than the atmospheric pressure because when the gases are expanded

to less than atomospheric pressure, a compression shock wave occurs inside the nozzle passage which greatly increases the irreversibility of the flow and the inefficiency of the nozzle. Accordingly, in experimental work with thrust motors, the nozzles are generally designed for slight under expansion so that the pressure term of equation (37) is present. While the maximum thrust for a given system expanding from a given chamber pressure is obtained when p_e is just equal to p_{atm}, the loss is negligible if p_e is within about 1 atmosphere of p_{atm}. Because of this fact, in experimental work, the term effective exhaust velocity, c, is usualy defined so that thrust force, F and specific impulse I_{sp} can still be expressed simply as

$$F = \frac{\dot{m} c}{g_o} \tag{39}$$

and

$$I_{sp} = c/g_o \tag{40}$$

where

$$c = \bar{u}_{ex} + \frac{g_o (p_e - p_{atm}) A_e}{\dot{m}} \tag{41}$$

Due to the difficulty in measuring p_e experimentally, $\bar{u}_{ex}$ is usually not determined. Thus the effective exhaust velocity is usually the only value of exhaust velocity which is determined experimentally.

Characteristic Velocity and Thrust Coefficient

This effective exhaust velocity c, like the specific impulse I_{sp}, is a measure of the overall performance of the rocket engine. It has been found to be helpful in

testing the performance of thrust motors to separate this overall performance figure into two parts as follows:

$$c = \frac{F g_o}{\dot{m}} = \frac{F p_c A_t g_o}{\dot{m} p_c A_t} = C_F C^* \tag{42}$$

These separate parameters c_F and c* are then defined as

$$C_F = \frac{F}{p_c A_t} \tag{43}$$
(dimensionless)

and

$$c^* = \frac{p_c A_t g_o}{\dot{m}} \tag{44}$$
(units of velocity)

The quantity c* is called the characteristic velocity and is taken to be a measure of the performance of the combustion chamber only. From its definition it is seen to be determined only by quantities related to the combustion chamber except for the dimensions of the nozzle throat.

The quantity c_F is called the thrust coefficient and is taken to be a measure of the performance of the exhaust nozzle only.

Theoretical expressions for the quantities, c* and c_F, can be obtained easily from the previously developed expressions for p_c and I_{sp}. Thus from equations (20b) and (21a)

$$\frac{p_c A_t}{\dot{m}} = \frac{R}{MW_t}\sqrt{\frac{T_c}{2 g_o c'_{p_{c-t}}}}\frac{1}{\sqrt{\left(\frac{2}{\gamma_d+1}\right)^{\frac{2MW_{av}c''_{p_{c-t}}-2R}{R}} - \left(\frac{2}{\gamma_d+1}\right)^{\frac{2MW_{av}c''_{p_{c-t}}-R}{R}}}} \tag{22b}$$

And by the definition of c* of equation (44)

$$c^* = \frac{R}{MW_t}\sqrt{\frac{g_o T_c}{2c'_{p_{c-t}}}}\frac{1}{\sqrt{\left(\frac{2}{\gamma_d+1}\right)^{\frac{2MW_{av}c''_{p_{c-t}}-2R}{R}} - \left(\frac{2}{\gamma_d+1}\right)^{\frac{2MW_{av}c''_{p_{c-t}}-R}{R}}}} \tag{45b}$$

or in terms of pseudo γ's

$$c^* = \sqrt{\frac{g_o R T_c}{2 MW_t}}\sqrt{\frac{\gamma'_{c-t}-1}{\gamma'_{c-t}}}\frac{1}{\sqrt{\left(\frac{2}{\gamma_d+1}\right)^{\frac{2}{\gamma''_{c-t}-1}} - \left(\frac{2}{\gamma_d+1}\right)^{\frac{\gamma''_{c-t}+1}{\gamma''_{c-t}-1}}}} \tag{45a}$$

And from equation (42) we can write

$$C_F = \frac{c}{c^*}$$

From equation (13b) since u_e (when $p_e = p_{atm}$ and all reactants are assumed to be discharged axially) is identical with the effective exhaust velocity

$$u_e = c = \sqrt{2 g_o T_c c'_{p\,c-e}} \sqrt{1 - \left(\frac{p_e}{p_c}\right)^{\frac{R}{MW_N c''_{p\,c-e}}}}$$

Then using this expression with equation (45b)

$$C_F = \frac{\sqrt{2 g_o T_c c'_{p\,c-e}} \sqrt{1 - \left(\frac{p_e}{p_c}\right)^{\frac{R}{MW_N c''_{p\,c-e}}}}}{\frac{R}{MW_t}\sqrt{\frac{2 g_o T_c}{2 c'_{p\,c-t}}}} \cdot \frac{1}{\sqrt{\left(\frac{2}{\gamma''_{c-t}+1}\right)^{\frac{2 MW_N c''_{p\,c-t} - 2R}{R}} - \left(\frac{2}{\gamma''_{c-t}+1}\right)^{\frac{2 MW_N c''_{p\,c-t} - R}{R}}}}$$

$$C_F = \frac{2 MW_t}{R}\sqrt{c'_{p\,c-t}\, c'_{p\,c-e}}\sqrt{1 - \left(\frac{p_e}{p_c}\right)^{\frac{R}{MW_N c''_{p\,c-e}}}}\sqrt{\left(\frac{2}{\gamma''_{c-t}+1}\right)^{\frac{2 MW_N c''_{p\,c-t} - 2R}{R}} - \left(\frac{2}{\gamma''_{c-t}+1}\right)^{\frac{2 MW_N c''_{p\,c-t} - R}{R}}}$$

Or in terms of pseudo γ's (46b)

$$C_F = \sqrt{\frac{MW_c}{MW_t}}\sqrt{\frac{\gamma'_{c-t}}{\gamma'_{c-t}-1}}\sqrt{\frac{\gamma'_{c-e}}{\gamma'_{c-e}-1}}\sqrt{1 - \left(\frac{p_e}{p_c}\right)^{\frac{\gamma''_{c-e}-1}{\gamma''_{c-e}}}}\sqrt{\left(\frac{2}{\gamma''_{c-t}+1}\right)^{\frac{2}{\gamma''_{c-t}-1}} - \left(\frac{2}{\gamma''_{c-t}+1}\right)^{\frac{\gamma''_{c-t}+1}{\gamma''_{c-t}-1}}}$$

where γ'_{c-e} is based on $MW_c\, c'_{p\,c-e}$
and γ'_{c-t} is based on $MW_t\, c'_{p\,c-t}$ (46a)

Therefore it can be seen that c^* and C_F could be determined also once the necessary quantities for the calculation of the theoretical chamber pressure and the theoretical specific impulse have been obtained since there are no additional quantities involved in these

expressions [(45) and (46)] which have not already appeared in equations (20) and (14) for chamber pressure and specific impulse respectively.

Specific Impulse and Specific Fule Consumption

The specific impulse I_{sp} is usually used as the criterion of overall rocket motor performance. From equation (40) above it can be seen to be essentially the same as the effective exhaust velocity, however. Instead of I_{sp} the quantity specific propellant consumption, w_{sp} is sometimes used. This is defined as the mass of propellants consumed per second per pound of thrust produced, or the mass of propellants consumed per unit of total impulse produced. Therefore,

$$w_{sp} = \frac{\dot{m} g_o}{F} = g_o / c$$

or the reciprocal of specific impulse.

Characteristic Length and Aspect Ratio

Two additional parameters are commonly used to describe the size and shape of the rocket motor combustion chamber. The first of these is L*, the characteristic length, which is defined as the ratio of the combustion chamber volume to the nozzle throat area. The volume of the converging section of the nozzle is generally added to the volume of the combustion chamber proper in calculating L*. As pointed out previously, for a given propellant system with a given degree of combustion completeness and operating at a given chamber pressure, L* is proportional to the average resident time of the reactants in the combustion chamber up to the nozzle throat.

The second of these parameters is the aspect ratio which is defined as the ratio of combustion chamber langth to combustion chamber diameter, L_c/D_c. Since most combustion chambers are cylindrical in shape, this is the only shape parameter commonly used.

Explanation of Performance Criteria Used in Analysis Results of This Thesis

The method of evaluating overall thrust motor performance in the present study has been to compare experimental specific impulse with the theoretically calculated value. As seen from equation (14a), specific impulse varies with the operating pressure ratio even for the same propellant system. Accordingly, all of the experimental results as well as the theoretical figures are corrected to the basis of operation between a chamber pressure of 300 psia and an exhaust pressure of 14.7 psia. In most runs these conditions were closely approximated; so these pressure corrections were not large in any case.

The parameters of c^* and c_F were used only to gain a preliminary estimate of the experimental performance figures on the combustion chamber and the exhaust nozzle respectively. Accurate calculations of the theoretical values of these quantities were not made. Such calculations would, of course, be necessary in order to analyze the performance accurately since c_F varies with the operating pressure range and properties of the working fluid while c^* varies with the

propellant system used. Both of these quantities have also been found to be a function of the combustion chamber design when the combustion chamber diameter is nearly as small as the nozzle throat diameter, i.e., in the nearly "throatless" or "tubular" motor. Thus, too much weight should not be given to the actual numerical values of these quantities but if they are used, performance should be judged by the comparison of their experimental and theoretical values.

In the present thesis combustion chamber performance was evaluated on the basis of comparing experimental chamber pressure with the theoretically calculated value. This is equivalent to comparing c* experimental with c* theoretical since c* is directly proportional to chamber pressure. The exhaust nozzle performance was evaluated by comparing the experimental specific impulse with the ϵ theoretical value calculated on the basis of a combustion efficiency equivalent to that experimentally obtained. Since actual combustion efficiencies were not determined, this equivalency is based upon attainment with a theoretical equilibrium gas mixture of the experimental chamber pressure assuming the same flow rate and nozzle design. In other words the chamber temperature theoretically necessary to produce the experimental chamber pressure is used to calculate the theoretical specific impulse still assuming gas composition to be that corresponding to equilibrium at the temperature and pressure in question.

This discrepancy between the theoretical and experimental working fluid is present in all calculations.

However, the difference in properties of the two gas mixtures is probably not great provided combustion efficiencies of 80% or more are obtained.

Both combustion chamber performance and overall motor performance were compared with and without corrections for heat losses. This was done in order to indicate the magnitude of the effects on performance of the measured heat losses.

Specific Methods of Calculation Used in the Present Study

The theoretical calculation of chamber pressure and specific impulse carried out in this thesis were made for the most part on the basis of the foregoing analysis and with the aid of the Satterfield Generalized Thermodynamic charts. The exact simplified procedures used under various conditions are described later in this section. Since most of these procedures involve minor approximations in either the underlying theory or the methods of evaluating the actual terms, the validity of each was tested for at least one representative case by comparison with a rigorous analysis based on the use of a Mollier Type diagram of the working fluid. These Mollier Type charts were enthalpy-entropy diagrams similar to those used for combustion power plant calculations by Hershey, Eberhard and Hottel (18) and by others. Such charts have been used for rocket calculations by Wagner in Germany (43), by Brinsmade (10) and Boll (7) and doubtless others in this country.

Basic Assumptions

Certain assumptions had to be made in all the theoretical calculations even including those which were performed in constructing the Mollier diagrams. However, these assumptions have all been extensively employed in the past in analyzing similar thermodynamic systems and consequently the reliability of each of them under comparable conditions is known. Most of them have been found to represent actual conditions very closely. They include the following:

a.) The combustion gases are assumed to follow the perfect gas behaviour represented by the expression $PV = nRT$ and, for the individual pure components of the gaseous mixture by the relation, $\left(\frac{\partial H}{\partial T}\right)_P = 0$.

b.) The enthalpy and entropy of a given gas mixture are assumed to be the sum of the enthalpy and entropy of the separate pure gaseous components each at its partial pressure in the mixture and at the temperature in question.

c.) The entropy, enthalpy and internal energy values are based upon the assignment of a value of zero to these functions for the products of complete combustion (CO_2, H_2O (g), O_2 and N_2) at 1 atmosphere of pressure and 0°K.

d.) The products of combustion of the reaction systems are assumed to attain and maintain complete chemical equilibrium at all temperatures above 1600°K. However, upon cooling below this temperature the

system is assumed to have remained at the chemical composition represented by the equilibrium conditions at 1600°K. In other words, down to a temperature of 1600°K, the rates of all the gaseous reactions are assumed to be fast enough to keep pace with the rapidly changing conditions of temperature and pressure as the gas expands through the exhaust nozzle or the work cycle. But, if the temperature of the expanding gases falls below 1600°K, the reaction rate is assumed to have become so slow that the gas composition was "frozen" at the equilibrium composition of 1600°K. While this single assumption cannot be expected to conform exactly to the true conditions of any and all work cycles, it is believed to represent the facts more closely in the average case than the assumption of maintenance of equilibrium at lower temperatures.

Experimental evidence for use of 1600°K as the "frozen equilibrium" temperature has been reported for the water gas reaction by Bone and Townsend (8), and by Bone, Newitt and Townsend (7). Since, at pressures of 14.7 psia or above, the water gas equilibrium is the only one in the C,H, O,N, system which undergoes a considerable shift with temperatures below 1600°K, this evidence is

valid for most rocket propellant systems. Mickley (C-18), however, reports evidence of a freezing temperature between 1800 - 2100°K for the combustion gases formed by burning ethanol in the oxygen produced by decomposing 48% peroxide, when these hot gases are quenched by mixing with the liquid water phase (at 500°K) which had previously been separated from the peroxide decomposition products.

e.) It is assumed that the distribution of energy of the gaseous molecules among the rotational, translational and vibrational energy states is that dictated by statistical equilibrium at the temperature and pressure in question. There is some indication that in very high velocity gas streams at extremely high temperatures the changes in vibrational energy states especially may lag changes in the temperature of the system, but no attempt is made here to consider such effects in the theoretical calculations.

f.) In all cases the exhaust nozzle is assumed to be of the correct design to expand the gas stream exactly to the atmospheric pressure of 14.7 psia at the exit plane of the nozzle. This is done in order to eliminate the pressure term in the expression for thrust or specific impulse. Also, the gas flow through the exhaust nozzle is assumed to be friction-

less and, therefore, the process is isentropic except when heat transfer is considered.

g.) The power required to pump the liquid reactants into the combustion chamber is not considered in the theoretical analysis of the systems.

h.) When the amount of catalyst in the chemical propellant system is less than one per cent of the total mass, it is not considered in any way in the analysis of the energy release from the system. The metallic elements in all the systems considered amount to much less than one per cent of the total mass of the system. Consequently, their contribution to the thrust and specific impulse of the fluid stream leaving the exhaust nozzle is neglected. Since these elements in most cases would leave the system as solids, probably as the solid oxides, it is doubtful if they would attain sufficient velocity during the expansion process to contribute materially to the thrust produced in most cases anyway.

The above assumptions are all compatible with or the same as those used by Satterfield in the construction of his charts of thermodynamic properties. In fact, as indicated before, these charts are either the basis for, or the source of the data used in most of the calculations made in connection with the present study.

Theoretical Chamber Pressure Calculations

Method 1 - Use of Equation (22c) Plus Satterfield's Correlations of Reduced Thermodynamic Data

The theoretical analysis previously carried out resulted in the expression of chamber pressure in the following form:

$$P_c = \frac{\dot{m}}{A_t}\sqrt{\frac{RT_c}{2g_o MW_t}}\sqrt{\frac{\gamma'_{c-t}-1}{\gamma'_{c-t}}}\sqrt{\frac{1}{\left(\frac{2}{\gamma_d+1}\right)^{\frac{2}{\gamma''_{c-t}-1}} - \left(\frac{2}{\gamma_d+1}\right)\frac{\gamma''_{c-t}+1}{\gamma''_{c-t}-1}}} \qquad (22c)$$

Case A - No Appreciable Dissociation

Any system with a maximum combustion chamber temperature of 2200°K or less can be handled quite simply. For a given mass flow rate and nozzle throat area the chamber pressure for such a system can be calculated from equation (22c) using only the 300 psia reduced enthalpy chart of Satterfield and the fictitious gas composition involved in the calculation of reduced enthalpy in connection with this chart. For these low temperature systems, the combustion temperature read from the 300 psia enthalpy chart will be close enough to the true temperature regardless of actual chamber pressure since dissociation is negligible. Due to the small amount of dissociation and absence of reaction in the gas stream MW_t can be taken as the molecular weight of the simplified or fictitious gas composition mixture and γ' can be evaluated from $\frac{MW_t c_p'}{MW_t c_p' - R}$ where the specific heat c_p' is the average value of c_p at the arithmetic mean temperature of the pure gaseous components weighted according to the fictitious mol fractions of each. For these

FIGURE 4 ENTHALPY (REDUCED) VS. TEMPERATURE AT VARIOUS PRESSURES FOR RED FUMING NITRIC ACID-ANILINE SYSTEM

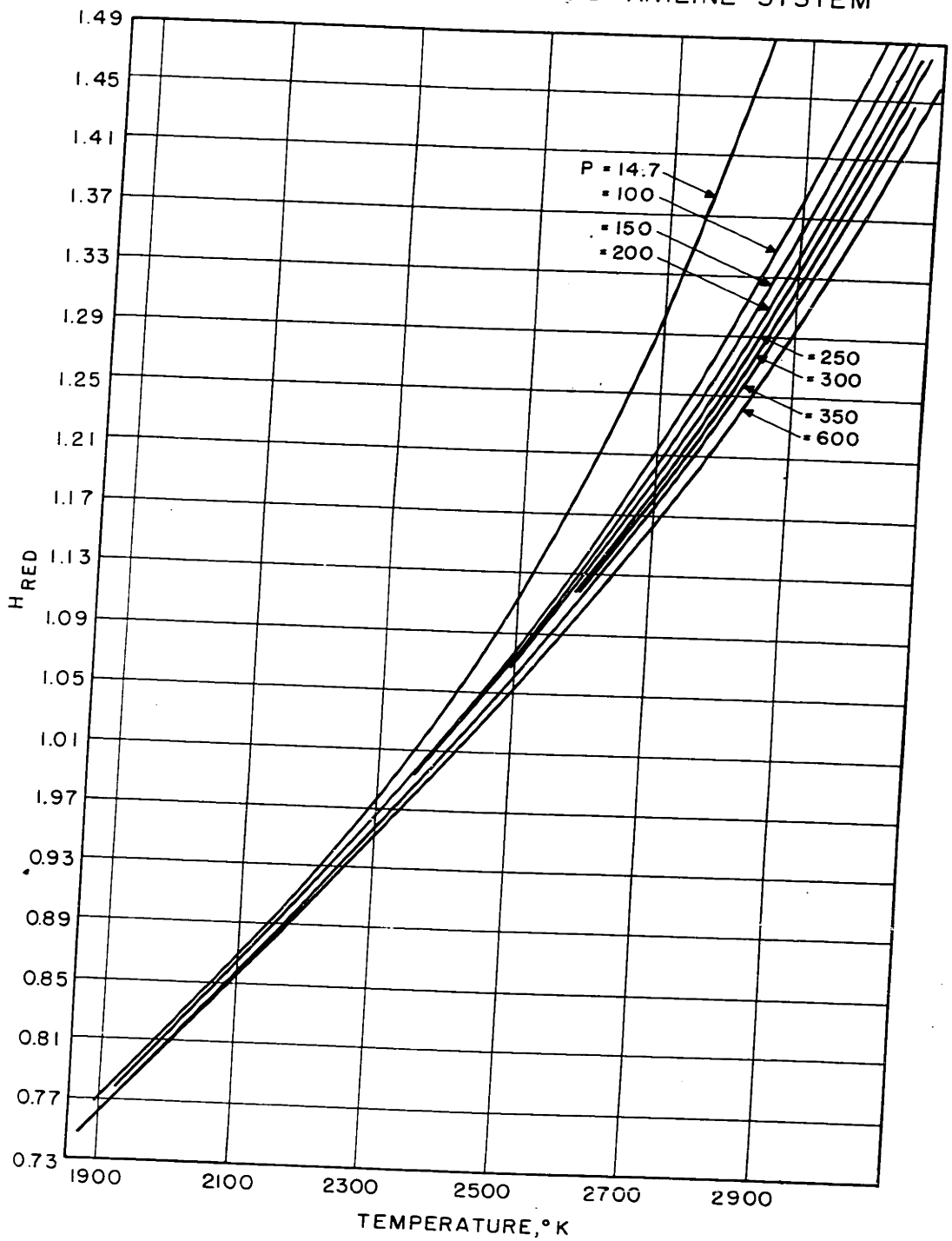

systems, γ'' and γ_d can be assumed identical with γ' with negligible error.

After T_c had been determined a short trial-and-error calculation between T_t and γ_d (γ') is necessary to fix T_t and γ. This is carried out using equation (21a) previously derived:

$$\frac{T_t}{T_c} = \frac{2}{\gamma_d + 1} \qquad (21a)$$

Case B - Appreciable Dissociation

Many systems with combustion temperatures above 2200°K are characterized by appreciable quantities of dissociation products in the equilibrium gas composition. Such highly dissociating systems are identified in the Satterfield correlation by high interpolation numbers. In order to calculate chamber pressure from equation (22c) for these systems with assurance of an accuracy within 1 or 2%, the effect of pressure upon the amount of dissociation in the equilibrium gas mixture must be considered. This is done by use of a chart of reduced enthalpy against temperature at several different pressures such as Figure 4. This chart can be obtained from the regular 14.7 psia and 300 psia reduced enthalpy charts plus the pressure interpolation chart of Satterfield. The procedure involved in construction of a chart such as Figure 4, is outlined in Appendix H.

In order to use a chart such as Figure 4, it is necessary to know the chamber pressure approximately before making the calculation. A trial-and-error calculation is usually not necessary, however, since an accuracy of at least

2% can be maintained if P_c can be estimated within no better than 20% beforehand. In most cases the pressure experimentally obtained would lie within 10 or 20% of P_c theoretical. If no experimental pressure is available and the approximate magnitude of the theoretical chamber pressure is not known, it can easily be estimated by making a single rough calculation of the value of $\dot{m}/A_t$ required to produce a given pressure (e.g. 300 psia) for the same system, and then assuming direct proportionality of $\dot{m}/A_t$ and P_c in order to estimate P_c for the case in question. For this preliminary rough calculation, the chamber temperature and molecular weight can be obtained at 300 psia from Satterfield's charts. The correct individual values of γ could also be evaluated from this generalized data but to save time a constant arbitrary value of γ of 1.20 can be used. It can be seen from Figure 3 that as long as the correct value of γ is between 1.10 and 1.30, the maximum error in the calculated P_c that will be produced by assigning γ, a value of 1.20 is less than 3%. Since we need a preliminary estimate of P_c of 10-20% accuracy, this is good enough.

The actual calculation of the correct theoretical chamber pressure (within 2%) is made using equation (22c). The value of T_c can be obtained from the pressure interpolation chart at the approximate value of P_c previously estiiated. The various values of γ can be obtained from the specific heat values taken as the slopes of the enthalpy-temperature curves $\frac{(\partial H)}{(\partial T)_p}$ on Figure 4 at the appropriate points. Again, a

short trial and error between T and γ (γ_d) is necessary to fix T_t and therefore determine the values of γ accurately. Again, γ' can be used in place of γ_d and γ'' also with less than 1% error. The values of MW_c, MW_t and MW_{AV} can be closely approximated from the reduced Molecular Weight plots of Satterfield. The method of approximating molecular weight at pressures between 300 psia and 14.7 psia is described in Appendix I and illustrated in the sample calculations of Appendix L.

Method 2 - Use of Mollier Type Diagram

This involves the use of a graphical procedure on the enthalpy-entropy diagram of the working fluid (assumed to be the equilibrium combustion gas mixture down to a temperature of 1600°K). The method of constructing these Mollier Type Diagrams is outlined in Appendix M.

The detailed steps in such a calculation are outlined in connection with a sample calculation in Appendix L. Sample calculations by means of Methods 1A and 1B are also given in Appendix L.

Theoretical Specific Impulse Calculations

Method 1 - Use of Equation (14a) Plus Satterfield's Correlations of Reduced Thermodynamic Data

The theoretical analysis previously carried out resulted in the expression of specific impulse in the form:

$$I_{sp} = \sqrt{\frac{2RT_c}{g_o \frac{M}{C_p'_{c-e}}}} \sqrt{\frac{\gamma'_{c-e}}{\gamma'_{c-e}-1}} \sqrt{1-\left(\frac{P_e}{P_c}\right)^{\frac{\gamma''_{c-e}-1}{\gamma''_{c-e}}}} \qquad (14a)$$

By defining $Mc_p{}'_{c-e}$ arbitrarily as $MW_c C_p{}'_{c-e}$, this can be written:

$$I_{sp} = \sqrt{\frac{2RT_c}{g_o MW_c}} \sqrt{\frac{\gamma'_{c-e}}{\gamma'_{c-e}-1}} \sqrt{1-\left(\frac{p_e}{p_c}\right)^{\frac{\gamma''_{c-e}-1}{\gamma''_{c-e}}}} \qquad (14c)$$

Case A - No Appreciable Dissociation

As with the calculation of chamber pressure, for systems with maximum temperatures of 2200°K or less, T_c can be obtained from the 300 psia reduced enthalpy chart regardless of actual chamber pressure. Also, MW_c can be obtained from the fictitious or simplified gas composition. If the operating pressure ratio is known (i.e., p_e and p_e), T_e and γ''_{c-e} can be obtained by trial and error using the equation $\frac{T_e}{T_c} = \left(\frac{p_e}{p_c}\right)^{\frac{\gamma''_{c-e}-1}{\gamma''_{c-e}}}$ (8a) which is equation (8a) previously derived. As in calculating the pressure P_c from equation (22c) for these systems, γ' may be used in place of γ'' with very little error. This γ' is determined by a procedure similar to that used in 1A for calculating chamber pressure from $\frac{MW_c C_p'}{MW_c C_p' - R}$ where c'_p is evaluated from the specific heats at the arithmetic mean temperature of the pure gaseous components of the fictitious gas mixture weighted according to their mol fractions.

Case B - Appreciable Dissociation

When dissociation is appreciable T_c is obtained from the pressure interpolation chart of reduced enthalpy against

temperature (such as Figure 4). The specific heat c_p' from which γ' is evaluated as $\frac{MW_c\, c_p'}{MW_c\, c_p' - R}$ is also obtained from this chart (Figure 4) as the slope $\left(\frac{\partial H}{\partial T}\right)_p$ at the arithmetic mean temperature. (The arithmetic average of the slopes at p_c and p_e are used.) The value of γ'' is similarly obtained from the average slope $\left(\frac{\partial H}{\partial T}\right)_p$ at the log mean temperature; an accuracy of better than 3% can be maintained in the calculated I_{sp} in the worst case even if γ' is used for γ'' here also.) Also, the molecular weights, MW_t, MW_c, and MW_{AV} can be evaluated from the Satterfield reduced molecular weight charts. Both the molecular weight terms MW_t and MW_{AV} are closely approximately in most cases by an arithmetic average of MW_c and MW_e.

Method 2 - Using only a Pressure-Interpolation Chart of Reduced Enthalpy versus Temperature (Such as Fig. 5.)

This method depends on finding the quantity $(H_c - H_e)$ for the expansion process in question and evaluating specific impulse from the expression

$$I_{sp} = \frac{u_e}{g_o} = \sqrt{\frac{2g_o(H_c - H_e)}{g_o^2}} = \sqrt{\frac{2(H_c - H_e)}{g_o}} \qquad (47)$$

which follows from integration of equation (2).

From the pressure interpolation chart (Figure 4) T_c is determined at P_c corresponding to H_c. Then using equation (8a) as in method 1B, T_e and γ''_{c-e} can be obtained

by trial and error if P_e is also know. Thus

$$\frac{T_e}{T_c} = \left(\frac{P_e}{P_c}\right)^{\frac{\gamma''_{c-e}-1}{\gamma''_{c-e}}} \qquad (8a)$$

where γ''_{c-e} is determined from Figure 4 as in Method 1B. From Figure 4, once T_e has been determined, H_e can be read at T_e and P_e and thus $H_c - H_e$ and I_{sp} determined.

Tests are made of this method later using both γ'' and γ' for γ in expression (8a).

Method 3 - Using only the Regular Reduced Enthalpy and Entropy Charts of Satterfield

This method also involves the determination of $H_c - H_e$ and evaluation of specific impulse from this enthalpy difference as in Method 2. Method 3 depends upon the use of the fact that for a frictionless, adiabatic expansion the final value of entropy at the exhaust conditions is the same as the initial value at combustion chamber conditions. S_c at H_c and P_c can be found by reading S_{300} and H_{300} from Satterfield's 300 psia reduced entropy chart and then correcting to convert to S_c and H_c can be made according to the perfect gas laws. Since S_e is equal to this S_c for an isentropic expansion, T_e and hence H_e can be evaluated from Satterfield's 14.7 psia charts of reduced entropy and reduced enthalpy.

Method 4 - Using the Mollier Type Diagram

The necessary entropy balance to determine T_e and H_e when T_c, H_c, and P_c and P_e are known is easily carried out on the enthalpy-entropy diagram. The details of this pro-

cedure are illustrated by the sample calculations of Appendix L.

Methods 1A, 1B, 2 and 3 are also illustrated by sample calculations of specific impulse from them in Appendix L.

Of the systems experimentally studied in this thesis only the stoichiometric mixture of Naphferrol and 90% Peroxide possessed a sufficiently high combustion temperature to require use of any of these methods of calculating chamber pressure or specific impulse except method 1A in each case. However, the Mollier type diagram (Method 2) was used in check calculations on the stoichiometric mixture of 85% Hydrazine-Hydrate and 90% Peroxide. Method 1B was used to calculate chamber pressure for the stoichiometric mixture of Naphferrol and Peroxide while Method 3 was used to calculate specific impulse of all the Naphferrol-Peroxide mixtures.

Method 1B for calculating chamber pressure was compared with method 2 using the Mollier type diagram for a high temperature system composed of red fuming Nitric Acid and Aniline while methods 1B and 2 for calculating specific impulse were checked against calculations by method 4 using the Mollier type diagram for this same system.

Basis for Comparison of the Experimental Results with the Results of the Theoretical Calculations - Theoretical calculations were made by one of the above methods over a range of variables sufficient to cover any involved in the experimental runs actually made on a given system, rather than for each individual experimental run. These theoretical results were then incorporated in general plots of chamber pressure and

FIGURE 5 THEORETICAL CHAMBER PRESSURE (ADIABATIC CASE) AS A FUNCTION OF MASS FLOW RATE

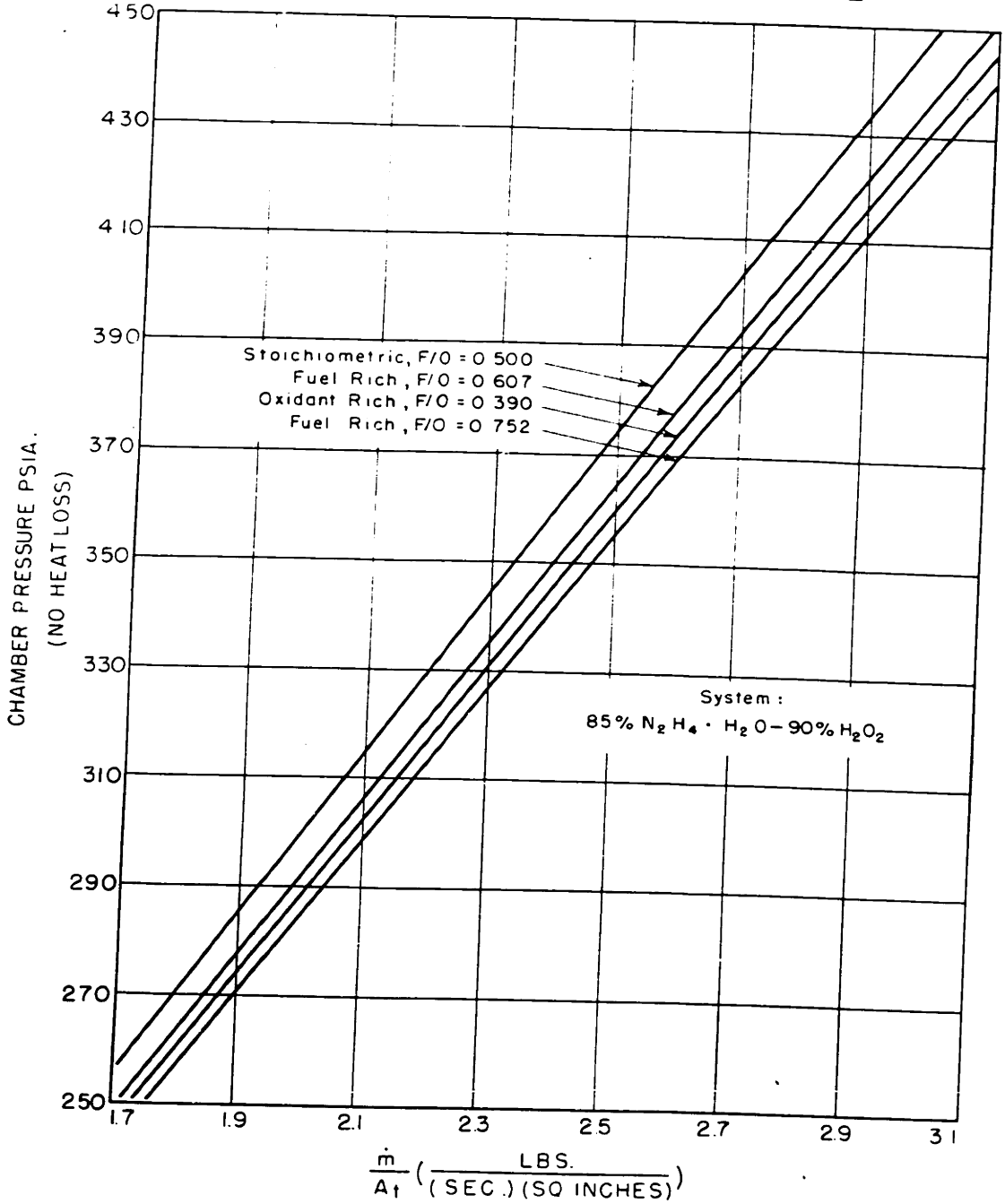

FIG.6 EFFECT OF HEAT LOSS ON CHAMBER PRESSURE FOR A GIVEN MASS FLOW RATE

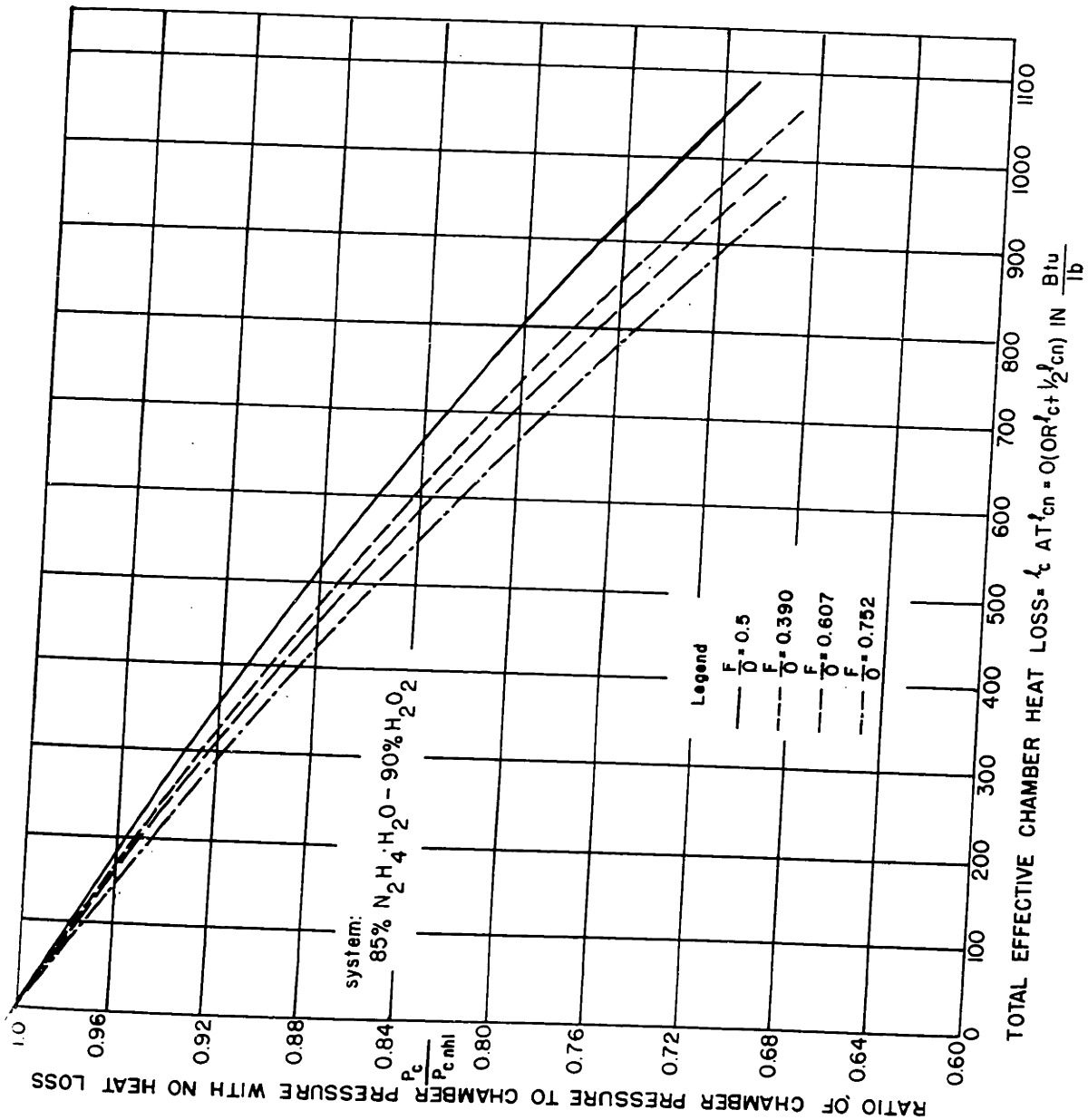

FIG. 7 · THEORETICAL SPECIFIC IMPULSE FOR ADIABATIC NOZZLE EXPANSION AS A FUNCTION OF $\frac{\dot{m}}{A_t}$ AND $\frac{P_c}{P_{c\,nhl}}$

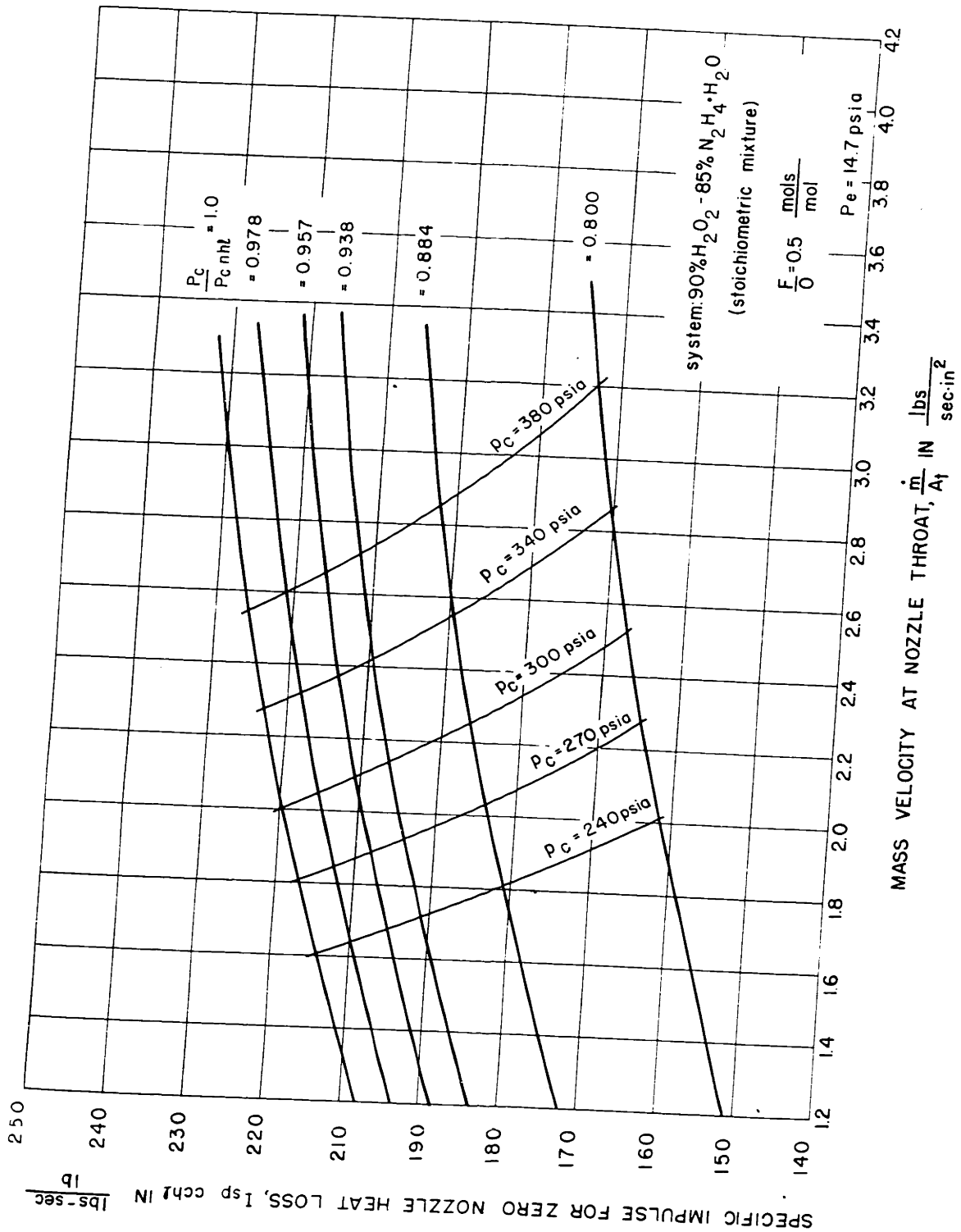

FIG. 8 EFFECT OF DIVERGING NOZZLE HEAT LOSS IN SPECIFIC IMPULSE (THEORETICAL CALCULATIONS)

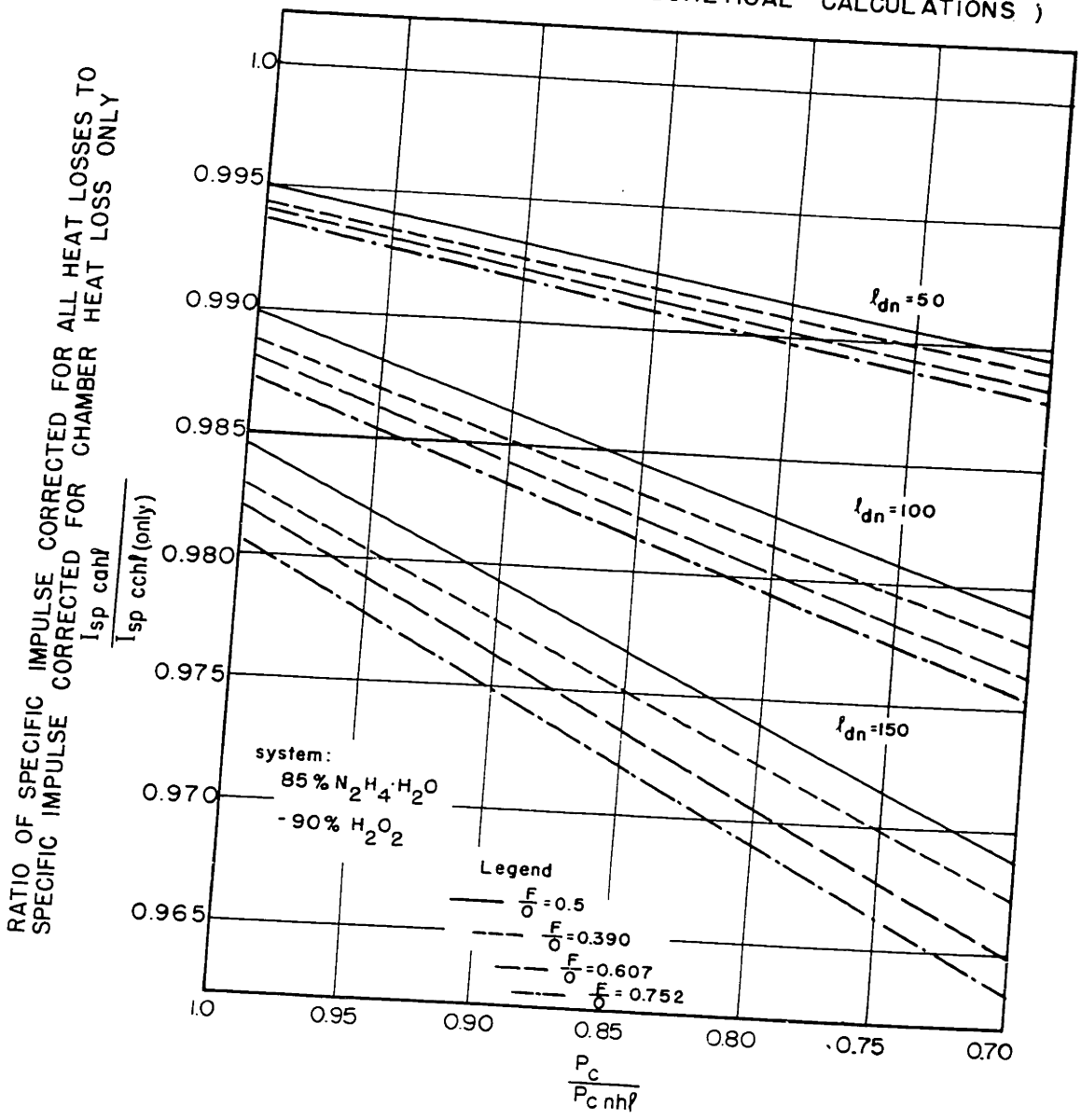

specific impulse as a function of the important variables. (See Figures 5, 6, 7, and 8). This made it possible for theoretical values corresponding to any combination of variables occurring in a given experimental run to be read immediately from these plots. This was done for each individual run and the theoretical values thus obtained were compared with the corresponding experimental values.

Figure 5 is a sample of the working plot which shows the theoretical chamber pressure which should be obtained under conditions of no heat loss at a given mass flow rate per unit of nozzle throat area. Figure 6 is a sample of the working plot which takes account of the effect of heat loss on chamber pressure. Figure 7 is a typical working plot used to take account of the effect on specific impulse of the heat loss in the chamber and converging nozzle. Figure 8 shows the corresponding plot which enables the additional correction for diverging nozzle heat loss to be made.

The detailed procedure for using these plots to obtain the theoretical performance for a given run under various conditions of heat loss and combustion chamber inefficiencies and to correct experimental performance for measured heat losses is best understood by reference to the sample calculations of Appendix K.

The corresponding working plots for the other propellant systems tested in this thesis as well as tables of all the calculated points from which all of these plots were constructed are presented in Appendix R.

APPARATUS AND PROCEDURE

The experimental program carried out in support of this thesis consisted of the reaction of concentrated peroxide with various fuels in a flow system with the hot gases thus produced being continuously exhausted from the reaction chamber to the atmosphere through a converging-diverging nozzle in a manner equivalent to a small rocket motor. A flow system was felt to be the most practical method of studying the reaction of various fuels with peroxide. Yet, it was imperative to keep the scale of operation as small as possible in order to minimize the danger in handling the potentially hazardous chemicals and to reduce the total propellant requirements of the system.

Requirements to be Met by Apparatus

In designing the apparatus for this study, several rather special but important requirements for obtaining the desired data were considered. One of the chief objectives of the work at the start was to study the nature of the combustion reactions between peroxide and various fuels and to investigate the reasons for smooth or rough burning. In most reaction motors, irregular combustion and fluctuating feed rates are inseparably interrelated due to the dependence of flow rates upon the back pressure and the dependence of combustion chamber pressure upon the flow rate. One of the chief problems in designing

the present apparatus was to achieve a really constant flow rate on such a small scale using a feed system of small capacity but which was essentially free from response to the pressure fluctuations in the reaction chamber. Only in this way could the combustion irregularities be freed from the tendency for self-magnification through resultant irregularities in flow rates. Thus, in order to determine the true causes of irregular combustion with assurance, a positive displacement feed system appeared necessary.

Due to the tendency for peroxide to decompose in the presence of most ordinary metal surfaces or especially in the presence of dirt, scale, rust, many metal oxides and other impurities, it is necessary to use special care in its handling. Therefore, all parts of the feed system in which the peroxide was to be handled would apparently necessitate construction from specially cleaned and polished stainless steel, or pure aluminum or tin. Ordinary pumps, pump lubricants, valves and valve packings would probably not suffice.

It was also desirable in designing the feed system to make provision for easily and quickly changing the flow rates of either or both propellants in order to make possible control of both the total flow rate and the mixture ratio during a run or variations in these conditions in different runs.

In addition, in the interest of safety it seemed necessary to provide a sheltered and baricaded space inside of which the apparatus could be operated by remote control from the outside. It appeared desirable to confine all the feed tanks and feed lines, in short all the propellant supply inside the test room also, if at all possible.

In designing the reaction motors themselves it also seemed logical to pattern them after larger scale rocket motors of conventional design insofar as possible, in order to make the results of the present study as nearly suitable as possible for application to the design and study of larger reaction motors.

Description of Actual Apparatus

The investigation of the liquid propellant systems employing high strength peroxide was carried out in a series of small reaction chambers. Each was equipped with a method of injection for the liquid reactants and an exhaust nozzle for the gaseous reaction products and operated as a small jet motor or so-called micro rocket motor. The auxiliary equipment consisted of a stationary-mount test stand and a suspension-mount thrust stand for testing the micro-rocket motors, a positive displacement feed system for supplying propellants to either stand, and the necessary instrumentation for measuring and recording data and controlling the operation - all built

FIGURE 9

FLOW SHEET OF MICRO-ROCKET FEED SYSTEM

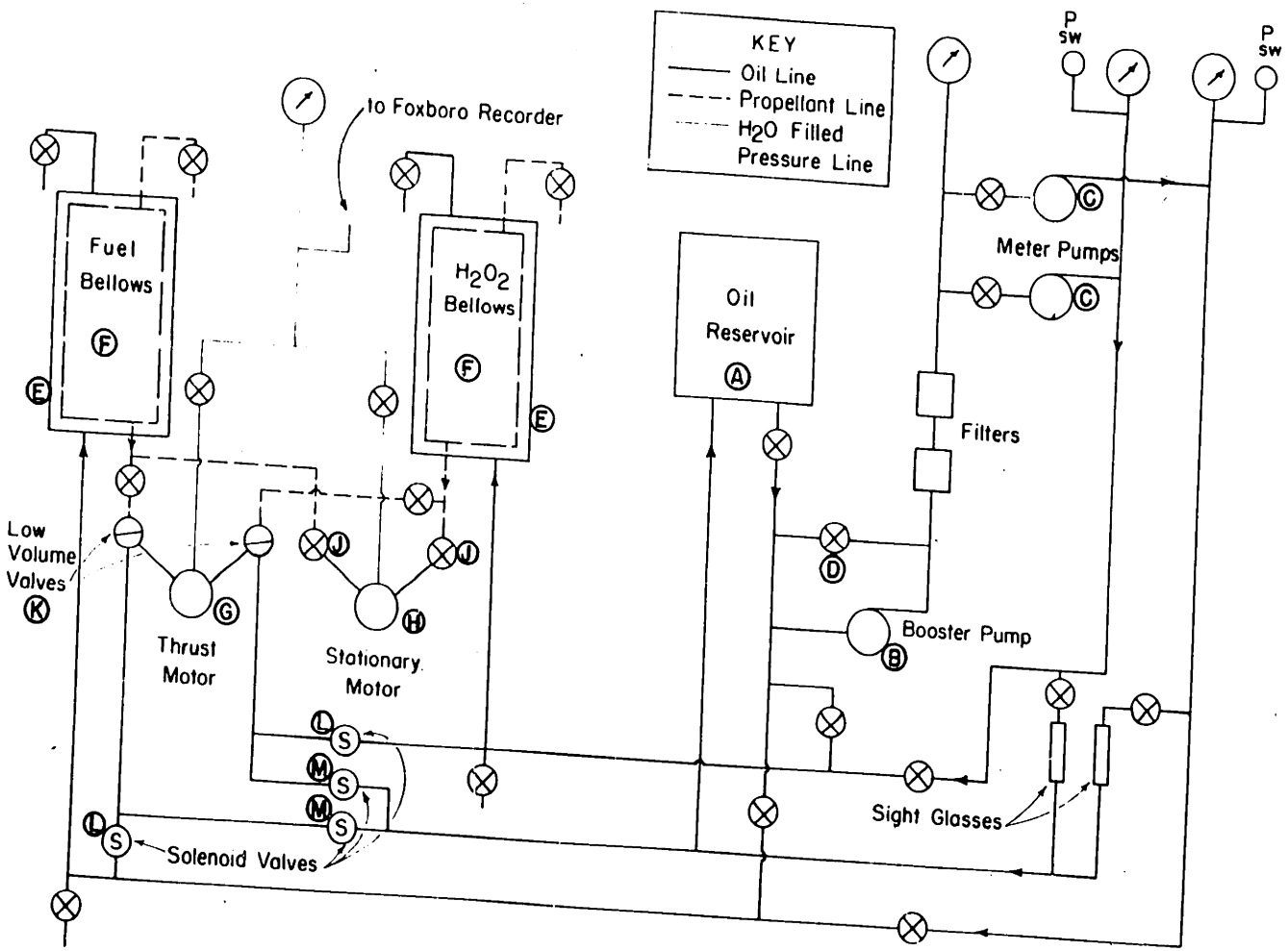

in and around a completely enclosed test cell constructed of one inch armor plate. In addition to the general brief description of apparatus which follows, other details are presented in Appendix A.

Feed System

Figure 9 is a flow sheet of the hydraulic circuit used in feeding the propellants to the reaction motors under test conditions. The unique feature of this system is the provision for positive displacement feeding of the liquid propellants. This is accomplished by the use of Zenith metering gear pumps operated from a synchronous motor drive. If the feed lines from the pumps to the rocket motor injector are free of gas, the positive displacement of these gear pumps is transmitted to the propellant flowing into the combustion chamber and the resultant flow rates are substantially constant regardless of combustion chamber pressure.

As seen in Figure 9 , the propellants are not actually handled by the pumps but are displaced by the hydraulic medium (SAE 50 lubricating oil), from bellows type containers located inside the test cell. It is thus possible to keep the propellant supply tanks and all propellant lines inside the test cell.

During a run, oil feeds by gravity from the storage reservoir (A) into the booster pump (B). This booster pump, a small Viking gear pump, furnishes filtered oil to the inlet of the two Zenith metering pumps (C), at a pressure

of 40 - 75 psia, the exact valve being determined by the setting of the by-pass valve (D). The two independent oil streams then flow through bulkhead fittings in the cell wall to the oil pots (E) which house the propellant bellows (F). The propellants are displaced from inside the bellows containers (F) to the reaction motors on either the thrust stand (G) or the stationary stand (H).

Manual valves (J) with extension handles through the cell wall are used to start and stop runs on the stationary stand. Balanced diaphragm valves (K) controlled by oil pressure are used for this purpose on the thrust stand. The oil pressure on the back side of these diaphragm valves is controlled by solenoid valves (L) and (M) in the pumping circuit. The solenoid valves (L) is normally open while (M) valves are normally closed thus placing oil pressure equal to the pumping pressure behind the diaphragm valves (K). To initiate propellant flow, solenoids (M) and (L) reverse positions simultaneously reducing the back pressure to atmospheric and allowing the propellant to lift the diaphragm, open the valve port and enter the combustion chamber of the thrust motor.

The bellows containers were constructed of stainless steel and carefully cleaned and polished inside. All propellant lines were made of 1/4" stainless steel tubing and Parker three piece stainless steel flare fittings. All valves in these lines were stainless steel with teflon or koroseal being used as gaskets or packings. The oil

FIGURE 1.0
BELLOWS POT ASSEMBLY

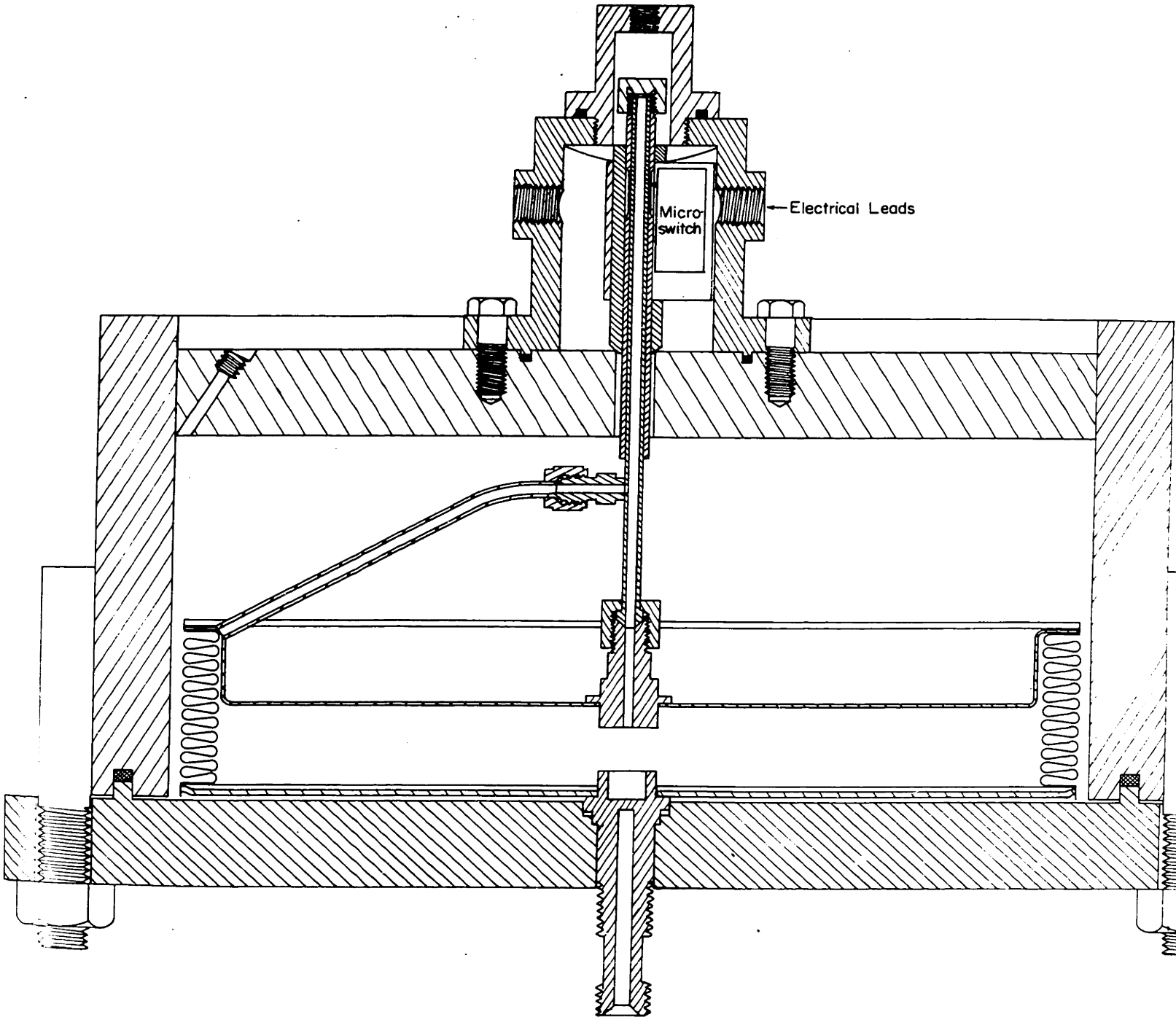

Figure 11

Bellows Tank and Oil Pot Assembly

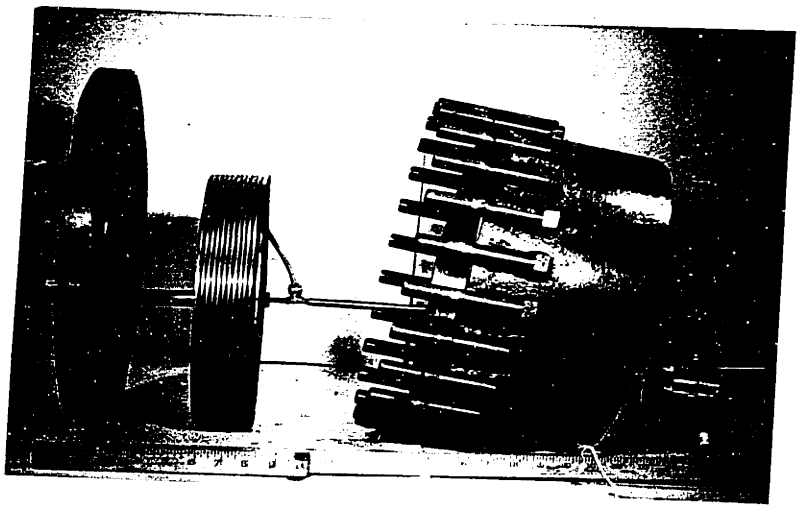

Disassembled

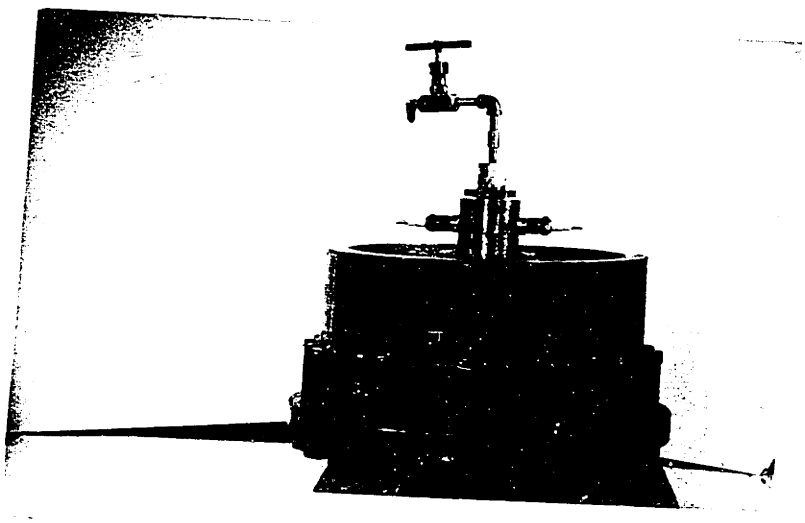

Assembled

Figure 12

Pumping Stand

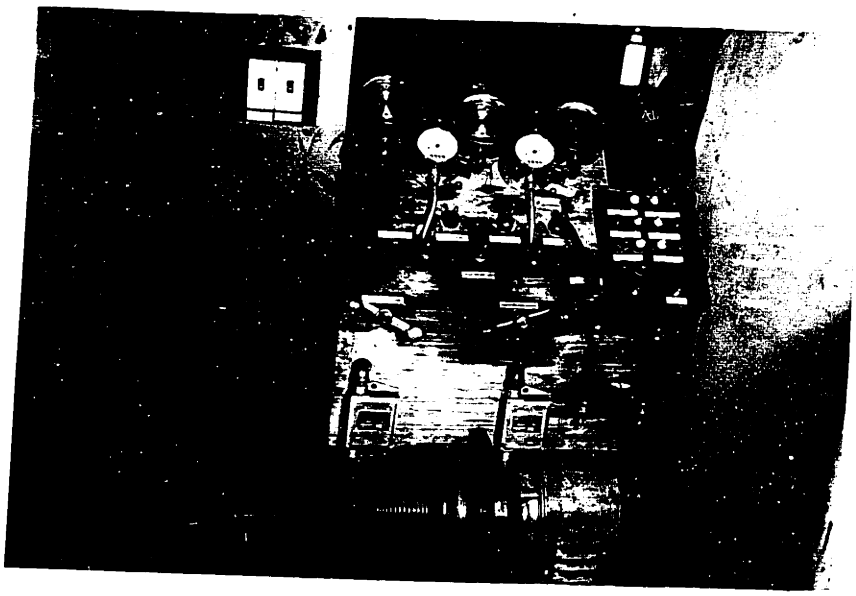

FIG.13 PUMPING STAND EQUIPMENT SHOWING VARI-SPEED DRIVES (SIDE VIEW)

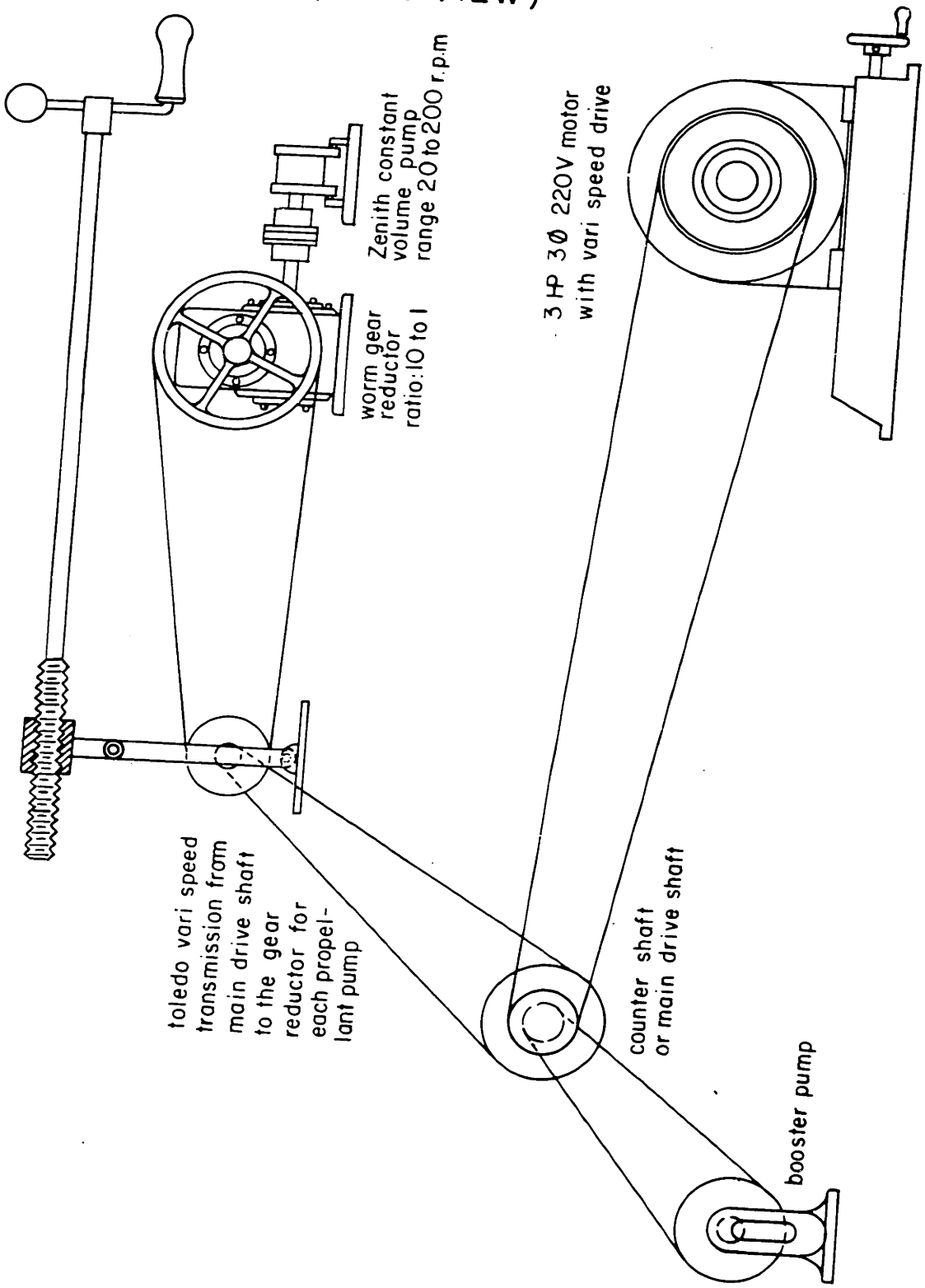

circuit of Figure 9 consisted of brass flare fittings and 3/8" copper tubing with ordinary brass, bronze or mild steel valves.

The section view diagram of Figure 10 illustrates the arrangement of one of the propellant bellows and oil tank assemblies in operating position. Pictures of this same equipment are shown in Figure 11. These bellows containers are about twelve inches in diameter with a capacity of nearly 3500 cc., but they were deflected sufficiently to deliver only about one liter of propellant in any given run. A maximum stroke of 3/4 of an inch was allowed, this motion being restricted by micro limit switches located in the housing on top of the oil pot and actuated by grooves cut in the bellows bleed tubes. (See Figure 10).

Pumping Stand

The metering pumps and the electric motor used to drive them were incorporated with the necessary auxiliary equipment on a portable pumping stand. A photograph of the control panel and front end of this stand is shown in Figure 12. The schematic drawing of Figure 13 shows the arrangement of the main drive motor, the pumps, the Toledo Timer variable speed transmissions and the gear reductors. Most of this equipment is located under the front panel on platforms at two levels as shown. The main drive motor (A) is a 220V-3 phase -60 cycle, 1800 rpm., synchronous three horse-power motor "with vari-speed drive". The booster pump (B)

FIGURE 14
TEST CELL

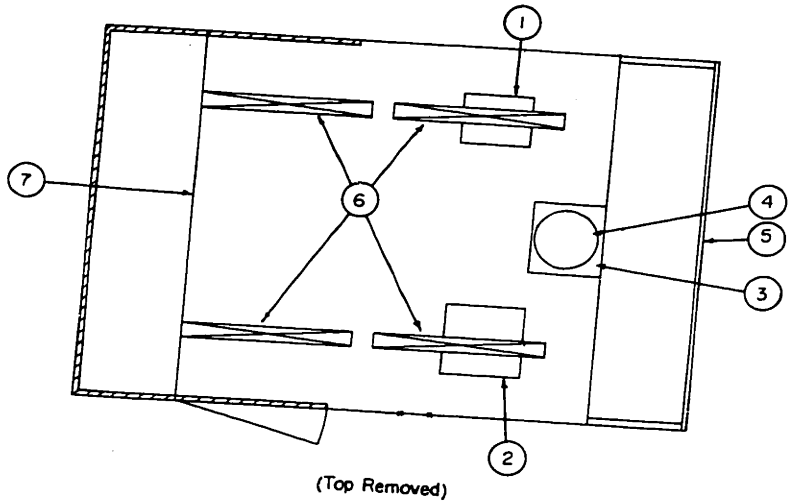

(Top Removed)

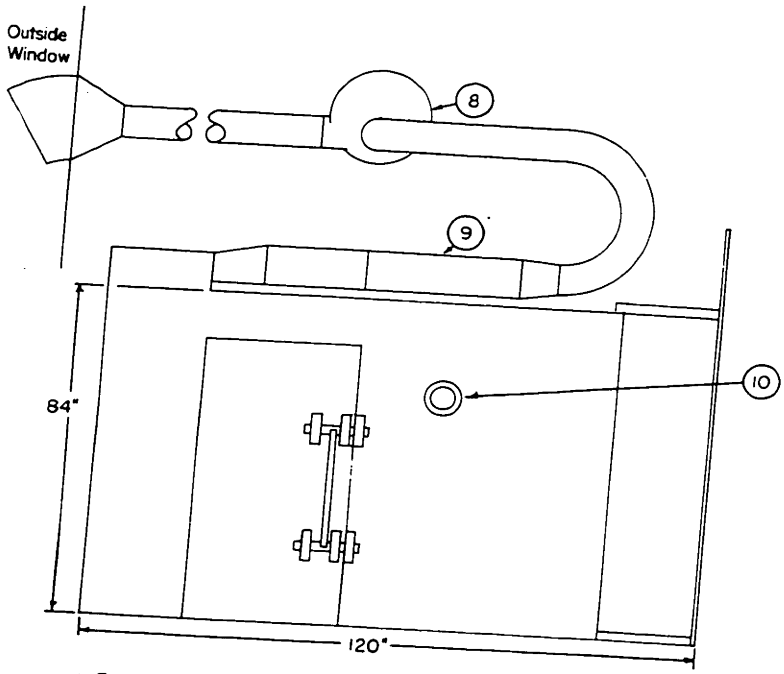

1. Thrust Stand
2. Stationary Stand
3. Fuel Pot Mounts
4. Fuel Pot
5. Panel Board
6. Fluorescent Lights
7. Work Bench
8. Ventilation Fan
9. Baffled Sound Trap
10. Observation Window

zzzzzz Designates Sound Insulation

is driven off of the main drive shaft (C). However, the metering pumps, only one of which is shown (D), were each driven off of a gear reductor (E) through a separate Toledo Timer variable speed transmission (F) from the main drive shaft. Variations in total flow could be made by adjusting the vari-speed drive on the electric motor, while changes in the fuel-oxidant ratio were accomplished by adjusting one or the other of the Toledo variable speed transmissions for the individual metering pumps.

The speed of each pump could be adjusted from 20 to 240 rpm. The rated delivery of these No. 5 Zenith pumps is 2.92 cc., per revolution and the measured delivery in calibration tests was always 2.94 $\pm$ 0.03 cc., per revolution. Thus, the flow rate of each propellant could be varied from about 60 to 720 cc. per minute. These flow rates were measured by the readings of the tachometers attached to the high speed of the gear reductors. These Boston Gear reductors have a ten to one speed reduction and therefore the tachometer readings were ten times the actual speed of the pumps.

Test Cell Arrangement

Figure 14 is a layout of the test cell showing the arrangement of such fixtures as the door, window and the ventilation system as well as that of the test equipment within the cell.

Control Equipment and Instrumentation

The heart of the control equipment used in operating

FIGURE 15

WIRING DIAGRAM FOR MICRO-ROCKET TEST CELL

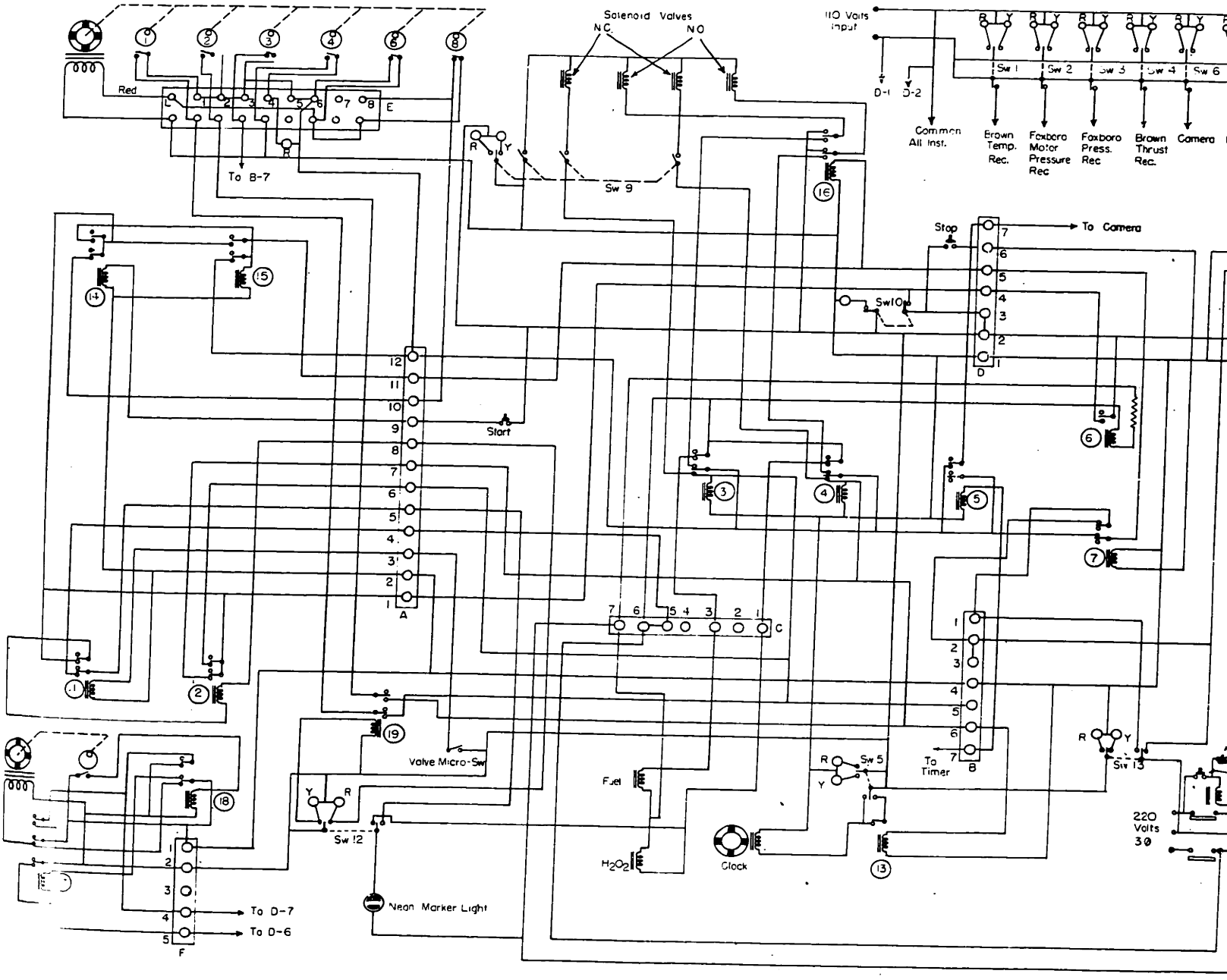

Figure 16

Panel Board

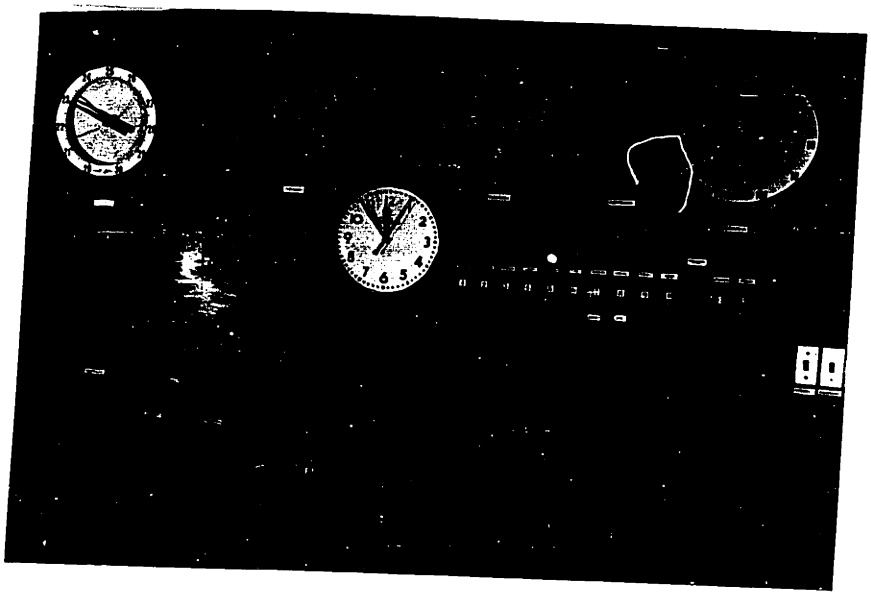

the micro-rocket test stand was the sequence timer. This was an automatic regular device manufactured by the Automatic Temperature Control Co. of Philadelphia under the name "Series 2400 Cam Timer". It consists of a synchronous motor geared to a cam shaft with each of the six individually adjustable cams available to operate a switch at any desired and predetermined time of the timer cycle. By adjusting and setting the cams at their proper positions, the entire sequence of events and operations necessary to initiate a run can be made to take place on a predetermined timing schedule.

This careful control of the injection process was necessary to prevent premature injection and subsequent accumulation of one propellant before the other arrived in the motor to initiate the "self-igniting" combustion reaction. If not prevented, this occurrence could have lead to "hard starts" or possibly damaging explosions.

The use of the sequence timer was not necessary for operation of the stationary stand when manual valves were used to start a run as was generally the case.

The wiring diagram of the entire control circuit and power circuit for the test cell is shown in Fig. 15.

Figure 16 is a photograph of the main instrument panel board of the micro-rocket test cell. In addition to the various instrument switches and pilot lights and the two manual valve handles, the five main instruments pictured here are a Brown Electronik Potentiometer for recording temperatures as measured by a Platinum-Platinum +13% Rhodium thermocouple,

FIGURE 17 COMBUSTION CHAMBERS

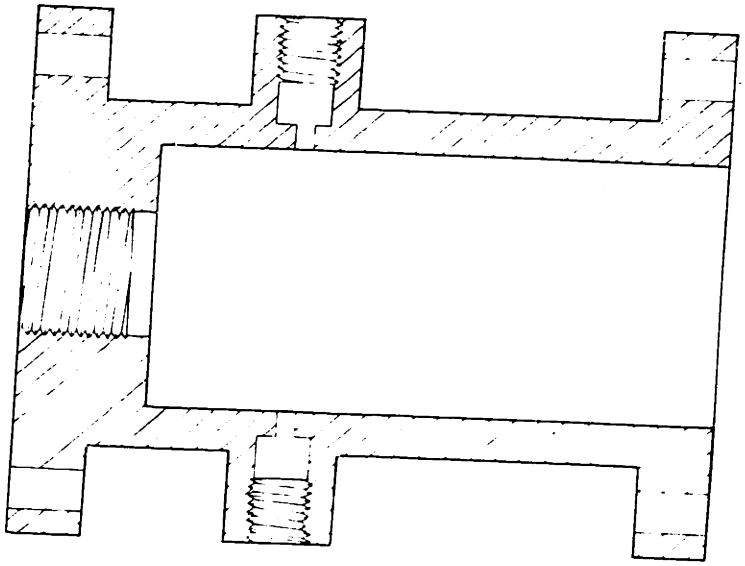

Diagram a, Stationary Stand Motor A

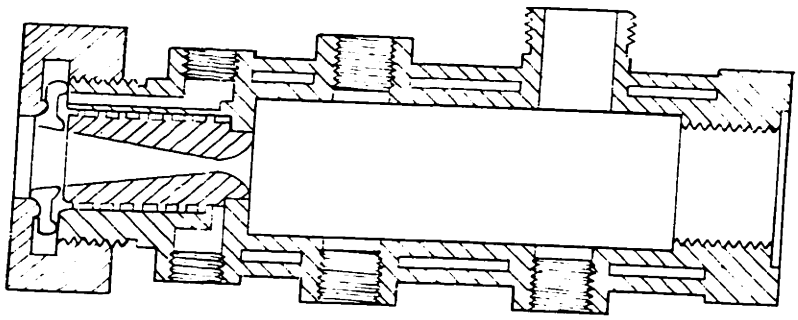

Diagram b, W Motor

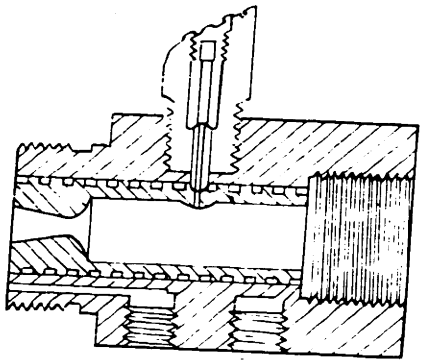

Diagram c, X Motor

Figure 19

Micro-Rocket Motor A

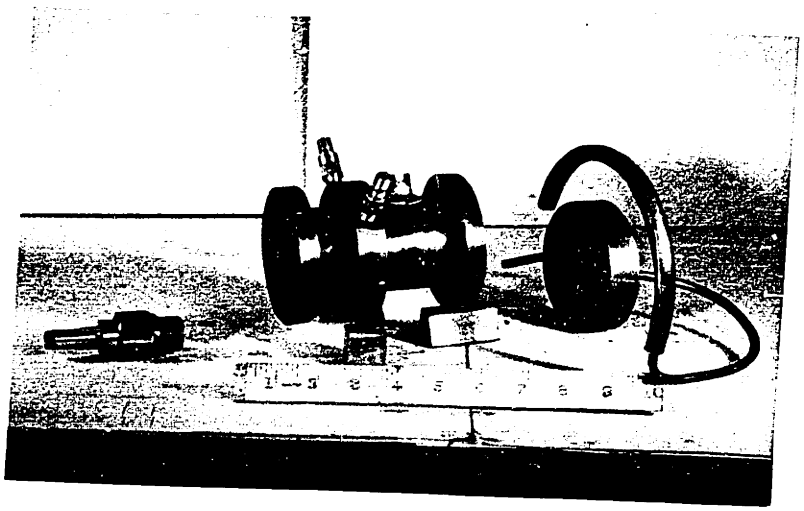

Disassembled - Showing G. M. gage, Motor and Nozzle

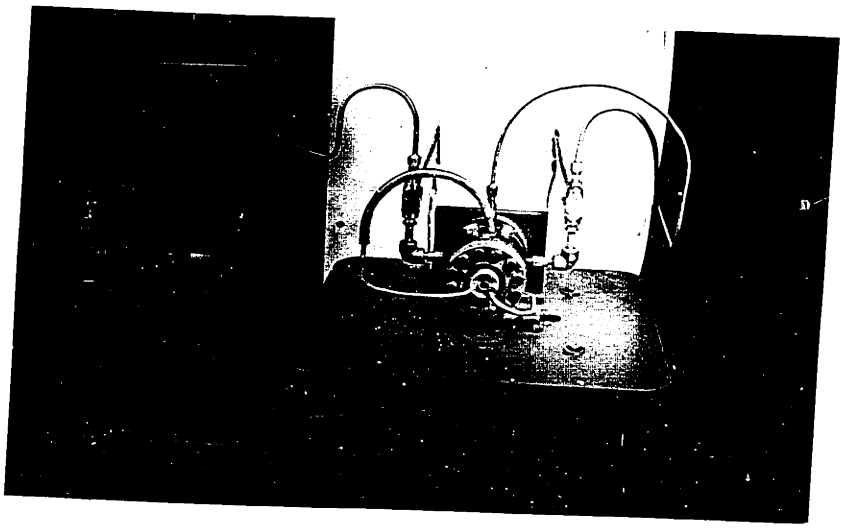

Assembled and in Position for Operation
on Stationary Stand

Figure 20

Micro-Rocket Motor W

two Foxboro recorders for measuring chamber pressure and fuel feed pressure, another Brown Electronik Potentiometer for recording millivolt output from a strain gauge bridge used to measure thrust, and the Telechron Electric Clock with sweep second-hand used for measuring time.

The other measuring instruments were the recording tachometers and pressure gauges shown previously on the pumping stand panel, a Leeds and Northrup portable potentiometer used in measuring cooling water temperatures and motor wall temperatures in determining heat transfer rates, and the electronic equipment and recording camera used in connection with the General Motors capacitance type pressure indicator for measuring fluctuations in combustion chamber pressure. This General Motors pressure gauge and associated equipment are described further in Appendix A and are described completely in a paper by Grinstead, Frawley, Chapman and Schultz (16).

The design of the thrust stand and the strain gauge circuit for measuring thrust is discussed in A ppendix B.

Combustion Chambers and Injectors

The four different designs of combustion chamber used in the micro-rocket studies are sketched in Figures 17 and 18. Photographs are shown in Figures 19 and 20. Two of these, motors A and B were used on the stationary stand while the other two, motors X and W were used on the thrust stand. The volume of these combustion chambers varied from about 0.5 to 12.5 cubic inches. The exact sizes are given in

FIGURE 21 STATIONARY MOTOR WATER-COOLED EXHAUST NOZZLE

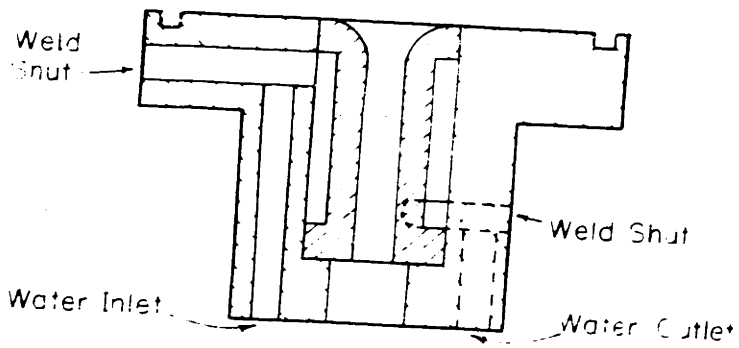

Dotted Lines Indicate Drill Holes In Another Plane

FIGURE 22 INJECTORS

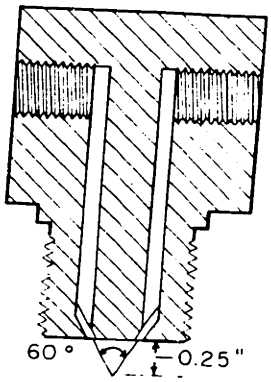

Diagram - A
60° Open Injector

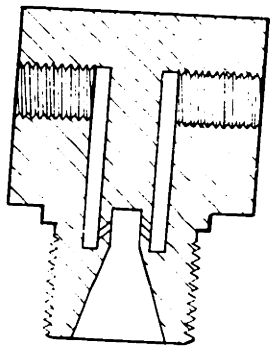

Diagram - B
90° Reverse Injector

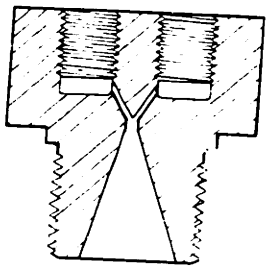

Diagram - C
60° Confined Mixer Injector

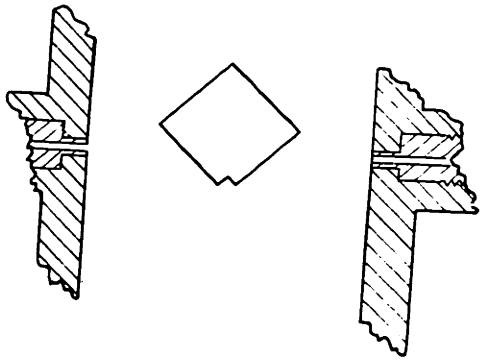

Diagram - D
180° Open Injection With Target
(Top View)

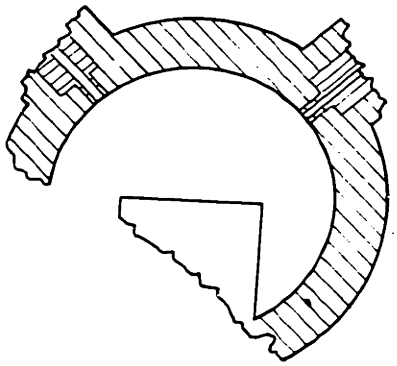

Diagram - E
90° Open Injection With Target
(End View)

Appendix A. Each motor was used with several different sizes of exhaust nozzle except motor X where the nozzle is an integral part of the combustion chamber. A typical nozzle for use with motor A is shown in Figure 21. The design of the passages of all of these supersonic converging-diverging exhaust nozzles is quite similar. The theory for this design is presented in Appendix D.

The five chief types of injection tested in the micro-rocket studies are depicted in Figure 22. One condition was common to all of these methods of injection, namely each produced but a single stream of each propellant which issued in almost every case from a simple drilled orifice 0.04" in diameter (No. 60 drill size). All of these injectors as well as those of lesser importance are discussed in Appendix A.

Making A Run

Briefly, the experimental procedure ordinarily involved in making a run consisted of the following steps:

1.) The motor to be used was installed on the test stand with its injector and exhaust nozzle properly assembled. Connections were made between the propellant valves and the injector, between the combustion chamber pressure tap and the line to the pressure gages, and between the cooling jackets and the water lines, all by means of Parker three-piece stainless steel flare fittings with 1/4" stainless tubing.

2.) If the General Motor capacitance-type pressure indicator was being used, it was connected to the amplifier and oscilloscope equipment, which was then turned on to warm up. The equipment was set for the proper gain and intensity of the cathode ray and the recording camera was focused and loaded.

3.) If thermocouples were being used, they were connected to the measuring potentiometer through a selector switch, the cold junction thermos was filled with ice water, and the potentiometer standardized.

4.) The fuel bellows was filled by gravity from a stainless steel funnel allowing liquid to run out the top of the bellows "bleed" tube before capping it. Then the top opening through the bellows pot was closed and oil pumped in until it displaced all the air from the space surrounding the bellows and finally flowed from the bleed valve atop the plug which closed the bleed tube opening in the pot.

5.) Charts were installed in the recording instruments and the pens checked to be sure they were inking properly.

6.) The sequence timer was checked to insure that it started from the zero position of its cycle and that the timing cams were set properly. The electric clock was set at 12 o'clock to prevent errors in recording the time of the run and the initial readings on each of the tachometers which count the

revolutions of the "fuel" and "peroxide" oil metering pumps was recorded.

7.) The cooling water was allowed to flow until its temperature levelled off and then the flow rates were set at the proper values by means of the appropriate needle valves.

8.) The peroxide bellows was filled by the same procedure as used with the fuel bellows and the bellows pot likewise pumped full of oil. This operation was purposely delayed until the other preparations were substantially complete so that the peroxide would be closed up in the bellows as short a time as possible before the start of a run. This reduced the gas formation from the decomposition of the peroxide to a minimum.

9.) A final check was made of the panel board switches to be sure all the equipment to be used was energized with power while unused equipment was shut off.

10.) The thrust stand cradle was freed (if a thrust stand run) and the electronic thrust recorder standardized.

11.) The metering oil pumps were set at the correct speeds by adjustment of the main variable V-belt drive from the synchronous motor and the Toledo timer drives on the individual pumps. When the manual oil by-pass valves were closed, the entire

system would then be pressurized to some value as determined by adjustable relief valves in each line, usually about 300 psia. or the expected operating pressure for the run.

12.) If heat loss data were being taken (i.e., thrust stand operation), containers were placed under the water outlets of the various cooling jackets and the resulting flow was later measured after a timed interval of three to four minutes which included the duration of the run.

13.) Then the test cell door was closed and the sequence timer energized to start the run. This started the camera first, and then after allowing a few seconds for the camera motor to reach synchronous speed, actuated the propellant valves initiating the flow of first the fuel and, a fraction of a second later, the peroxide to the injector and motor. The recording tachometers on the oil metering pumps were engaged by solenoids simultaneously with the opening of the respective propellant valves. Also, as the second or peroxide valve was opened, the electric clock was started and the neon flash bulb by means of which timing lines were placed on the film was lighted.

14.) Most of the pertinent data were recorded continuously throughout the run by the electrical instruments with timing by means of calibrated synchronous motor drives.

The peroxide feel pressure was measured by visual readings only and the same is true of the inlet and outlet temperatures of the cooling water thermocouples.

15.) The apparatus was designed on the basis of using approximately 1 liter of 90% H_2O_2 per run. At the flow rates generally employed, the duration of the run was limited to a maximum of from 90 to 150 seconds. Most of the runs actually lasted for from 60 to 150 seconds. Often the oscilloscope camera, which recorded the instantaneous time-pressure record, was only used for the first 30-60 seconds of a run, with the camera motor being shuft off manually in the middle of the run.

16.) After sufficient data had been obtained under equilibrium conditions, the run was stopped by de-energizing the sequence timer. This simultaneously stopped the flow of reactants, the clock and the recording tachometers. However, the system remained pressurized as in the pre-starting stage until the manual by-pass valves were opened.

17.) Shortly after the completion of the run, the cooling water flow was stopped and the time of flow from the start of collection recorded. Later the amount of water collected from each cooling jacket was measured and the average flow rates thus obtained.

FIGURE 23

THRUST STAND AND SUSPENSION ASSEMBLY

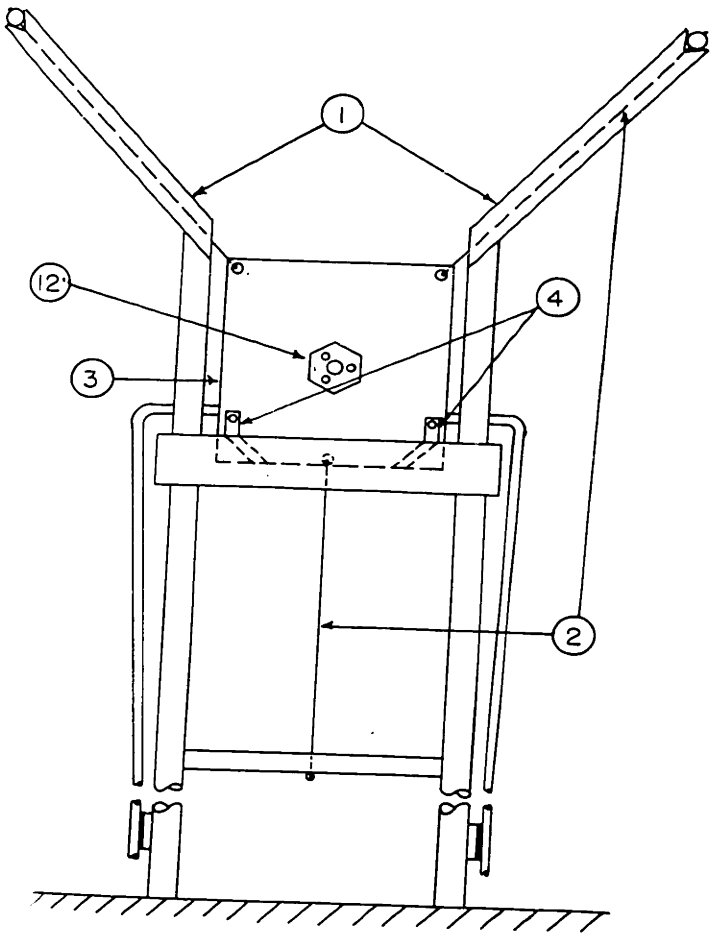

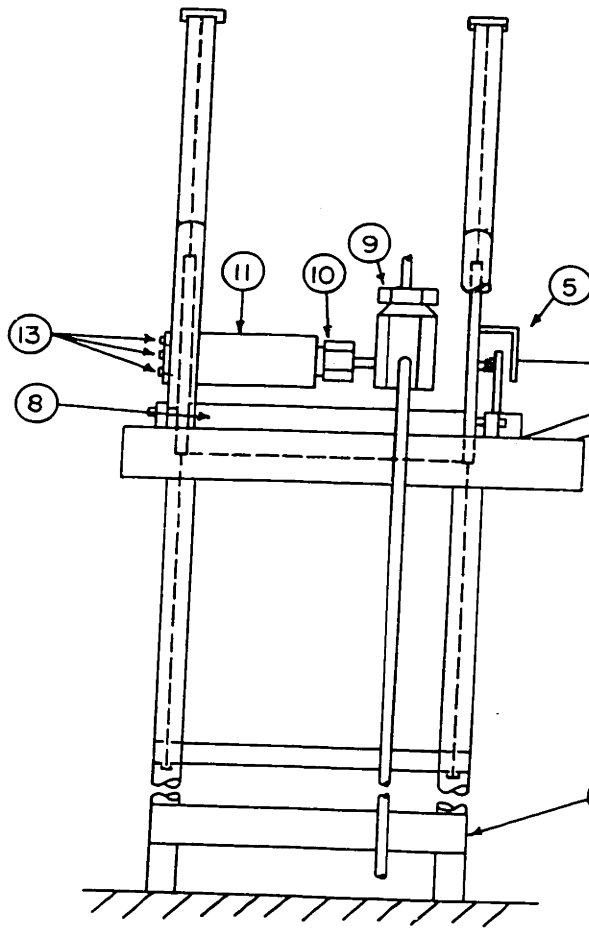

1. Suspension Arms
2. " Cables
3. Cradle
4. " Lock Down
5. Thrust Jack Assembly
6. Weight Pan
7. Lower Fitting Strap
8. Upper " "
9. Propellant
10. Fuel Injector
11. Motor
12. Nozzle Retainer
13. Motor Mounts

18.) As soon as possible after the run, the thrust stand was calibrated by means of static weights placed on a scale pan connected via a ball bearing pulley to the thrust cradle. The cable connector from the pulley to the cradle was aligned with the axis of the reaction motor exhaust nozzle as shown in Fig. 23. This assured the equivalence of a pound weight to a pound of reaction force exerted by the ejection of gases from the nozzle without applying directional correction factors. An effort was made to keep the tension in the suspension cables of the thrust cradle constant and to keep the connecting lines unchanged in all respects, so that the resistance to movement of the cradle in operation would remain a constant percentage of the total thrust. Appendix B contains a discussion of the design of the thrust stand and its measuring system.

Check calibrations of the thrust system on the same day usually matched within at least 1%. Since calibrations were made immediately after each run, the only source of greater error in thrust measurements was an occasional uncertainty as to the exact reference or zero reading which should be used for a given run. This uncertainty was caused by a gradual change in reference zero after the rapid drop to an apparent zero at the end of a run. This discrepancy seldom amounted to more than 3% of the total thrust, however.

FIG. 24 RECORDER CHARTS

RUN W - 3

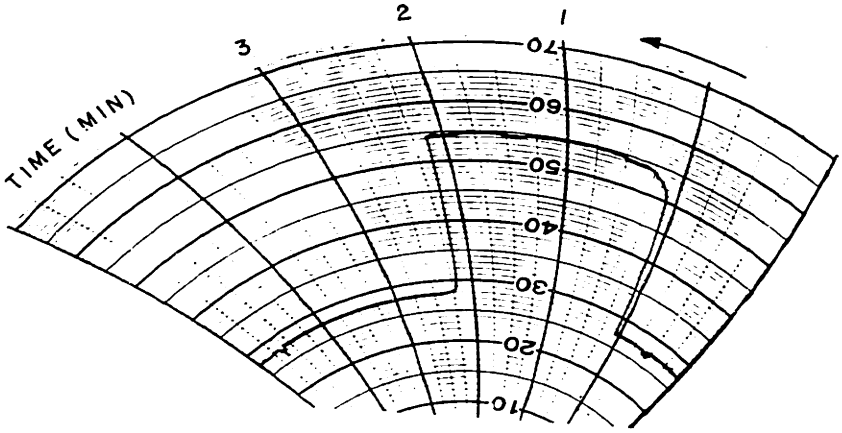

THRUST RECORDER CHART

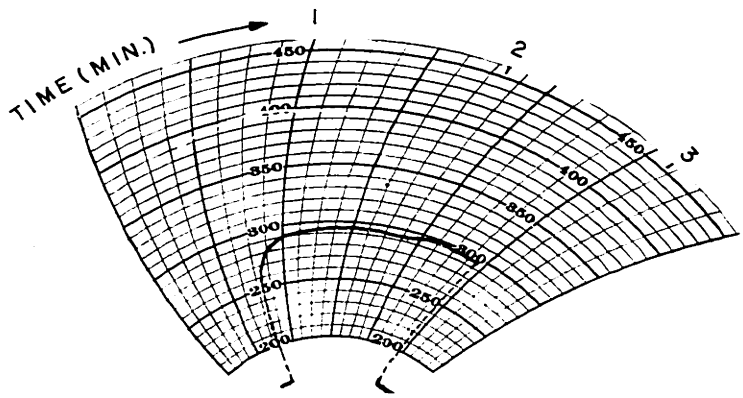

CHAMBER PRESSURE RECORDER CHART

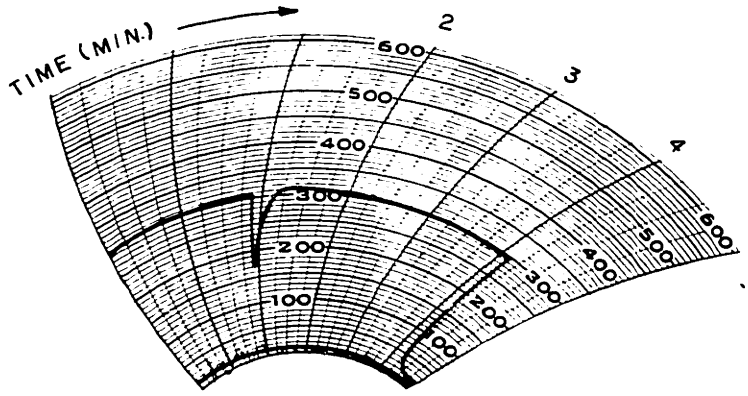

FUEL FEED PRESSURE RECORDER CHART

19.) After calibrating the thrust stand, the cradle was again locked in place. Then the bellows pots were opened and oil pumped back from the pots to the oil reservoir, equivalent to the amounts pumped in during the run. Finally, the bellows containers themselves were opened, leaving the apparatus in the original position ready to refill for another run.

20.) Finally, the throat diameter of the exhaust nozzle which had been used was measured with a Starrett hole gauge, to complete the data record for the run.

A set of charts from the various recording instruments for a typical run is shown in Fig. 24. These indicate how the operation builds up slowly to equilibrium conditions during a transient period of approximately 30 seconds and then levels off for the remainder of a run. This time lag in reaching equilibrium is primarily due to the small scale of operation and the appreciable amount of energy required to bring the apparatus up to the temperature of steady-state operation.

Techniques in the Preparation and Handling of Chemicals

1.) Hydrogen Peroxide:

The hydrogen peroxide used in these tests was supplied by the Buffalo Electro-Chemicals Co. of Buffalo, N. Y., as a 90 weight percent aqueous solution known as "C.P. Becco Hydrogen Peroxide 90%". It is said to be a very pure product with no known stabilizers or impurities added. It has been shown that if dust, dirt, and other catalytic impurities can be excluded, concentrated peroxide is most stable when really pure.

The so-called stabilizers for peroxide are actually, for the most part, anti-catalysts which should be added to slow down catalytic action in case of later contamination. In any case, this Becco 90% Peroxide as received has a very good stability with a measured decomposition rate in a 250 ml. pyrex volumetric flask of only 0.0027 per cent per hour at 50°C. Its conductivity measures 9.3×10^{-6} ohm^{-1} cm^{-1} and its ph (diluted 10 fold) is about 5.0. It was stored at room temperature in the same special vented shipping drums (constructed of 99.6% pure aluminum) in which it was received. These drums are shipped with 250# net weight of peroxide which is approximately 75% of full capacity. When stored in these drums at room temperature the peroxide concentration dropped by less than 1/2% per month.

This Becco hydrogen peroxide was used substantially as received except in the early runs when it was diluted with distilled water to a concentration of 80% by weight before use. The only addition which was usually made was that of 20 to 40 parts per million of phosphoric acid (H_3PO_4) just before use. This very small amount of acid appeared to give the solution increased stability to decomposition especially in the stainless steel bellows container from which the propellants were fed to the reaction motor.

The chief source of danger with concentrated peroxide is that of possible contamination. Because of the highly exothermic heat of reaction of the decomposition reaction, a small amount of impurity may cause sufficient decomposition and heat evolution to exceed the rate of heat loss for the system. In

FIGURE 25

THE DENSITY OF AQUEOUS HYDROGEN PEROXIDE SOLUTIONS AS A FUNCTION OF CONCENTRATION AT VARIOUS TEMPERATURES

(Data Of Huckaba & Keyes)

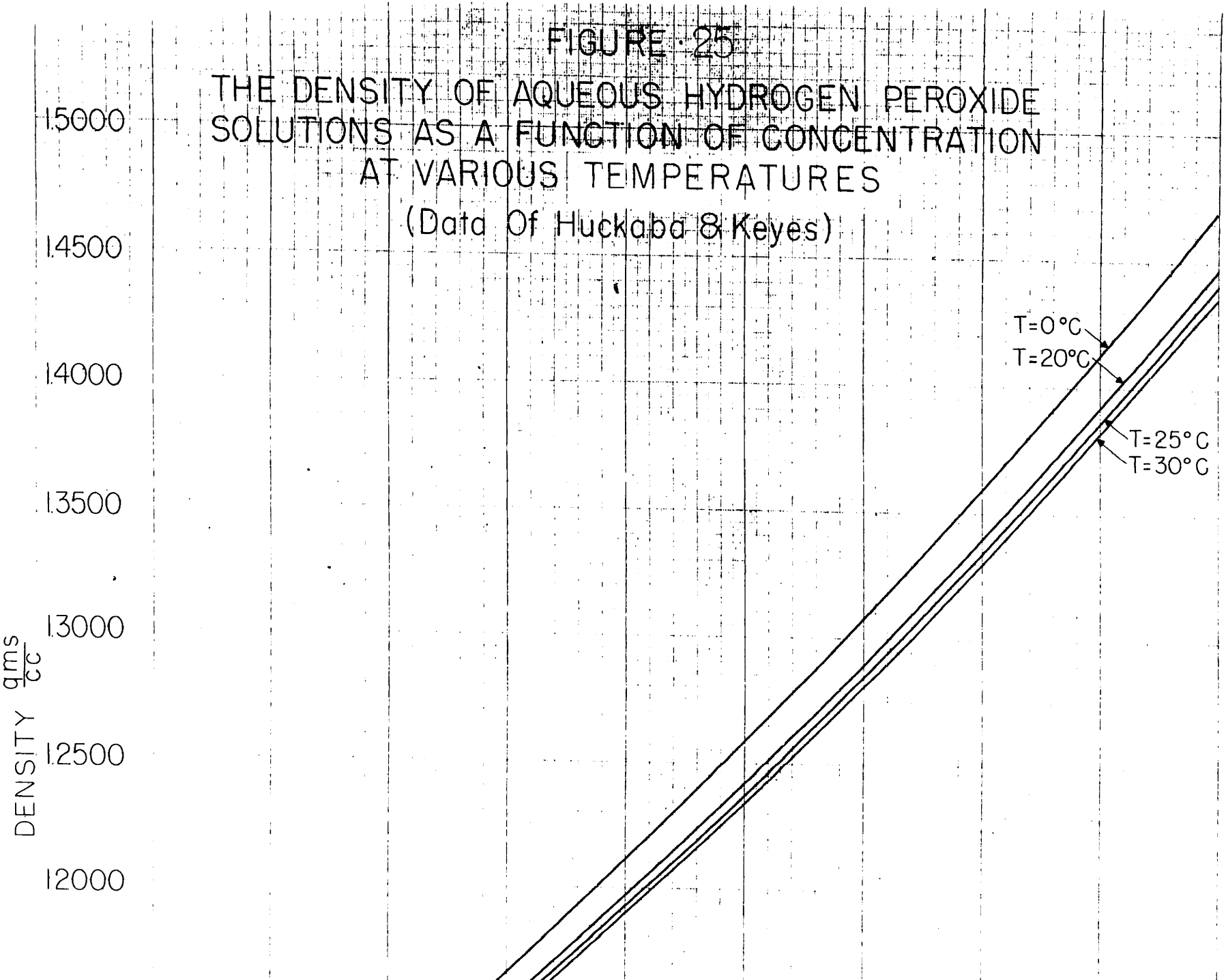

this case the temperature will gradually rise and the reaction speed will grow at a continuously increasing rate until it finally reaches explosive violence. It appears to be practically impossible to detonate pure peroxide although when strong peroxide is mixed with small percentages of organic materials it can be easily detonated in many cases.

Strong peroxide is also a fire hazard. Spillage or leakage can easily cause exposed organic matter to inflame, particularly if there is any dirt or other catalytic material present. For this reason great care should be taken in its handling. Spilling it on the skin will cause severe burns unless it is quickly washed away with large quantitites of water. There is also danger of setting the clothing on fire resulting in additional burns. Most serious accidents with peroxide have been of this nature.

The concentration of the hydrogen peroxide which was used for reaction motor tests was checked at least once a week by making a careful determination of the density by means of an analytical balance. The densities thus determined corresponded to peroxide concentration between 89 and 91% in all cases when compared with the density data of Huckaba and Keyes (19), (Figure 25). Accordingly, the peroxide strength was considered as constant at 90% (or 80% in early runs) for purposes of comparing experimental and theoretical performance.

2.) Hydrazine Hydrate:

The hydrazine hydrate was obtained from the Fairmount Chemical Co., of Newark, N. J., as an 85 weight percent

aqueous solution for which the only specification is that of "pure". It was stored in the 40-lb. glass carboys in which it was received and showed no deterioration on storage provided it was kept tightly closed and not allowed to come in contact with air or oxygen. The standard "Helman" fuel which was used in the present test work consisted of this 85% hydrazine hydrate solution with the addition of the following salts as catalysts:-

1.07 g/liter of $Na_2Fe(CN)_5 NO.2H_2O$

0.47 g/liter of CuCN

0.39 g/liter of KCN

The amounts given above are those used as standard and referred to as the normal amounts of catalyst. Solutions were also tested containing 2 times and 5 times this normal amount of catalyst and are referred to as 2X Helman and 5X Helman. These final solutions were made up in only two-liter quantities and were never stored for a very long time before use. However, indications are that with the combined catalyst given above, the solution would remain quite stable in glass, stainless or mild steel vessels, over a considerable period, provided air were excluded. If only the copper cyanide complex is used as catalyst, copper tends to separate or be replaced in solution by iron when stored in steel containers.

In addition to precautions taken to prevent chance air oxidation of the "Helman" fuel, care in its handling was observed because of the small amount of cyanide it contained. Also, hydrazine has been found to produce a rash on certain "allergic"

persons if allowed to wet their skin. In addition, waste should be avoided because of its extremely high cost.

The concentration of the hydrazine hydrate solution as received was quite constant. This was checked occasionally by titrating a sample against a known standard solution of hydrochloric acid. All determinations made in this manner resulted in equivalent strengths for the hydrazine hydrate between 84.5 and 86.0 percent. Accordingly, the hydrazine hydrate concentration was assumed constant at 85% for purposes of making theoretical performance calculations.

3.) "Naphferrol"

The so-called "Naphferrol" fuel consisted of a solution of 200 grams of ferrous beta naphthalene sulfonate-tri hydrate per liter of anhydrous methyl alcohol. The ferrous salt of this sulfonic acid was prepared from the sodium salt which was obtained from the American Cyanamid Co. Analysis of the product for the elements indicated that it was at least 99% pure ferrous beta-naphthalene sulfonate-tri hydrate or its isomers. However, 3 to 5% of the material would not dissolve in the methanol and was believed to be the alpha isomer. Accordingly, 200 grams of soluble material was added with the accompanying insoluble material being filtered off. It is believed that the "Naphferrol" thus prepared was composed of materials of approximately 99% purity, (both the methanol and the ferrous salt of the sulfonic acid).

No storage or handling difficulties were experienced with "Naphferrol", provided it was kept in tightly stoppered

containers. When exposed to air, however, it appeared that the ferrous salt was slowly oxidized to the insoluble ferric state. Also, plugging difficulties sometimes resulted from the solid residue which remained if the methanol was allowed to evaporate from the solution in a small passage or pipe line. The plugs thus formed could usually be removed by solution with fresh methanol.

Precision of Measurements

1.) Flow Rates:

The delivery per revolution of the metering gear pumps is constant to within better than 1% under all conditions. This was checked in the frequent calibrations of the gear pumps used for the tests here reported. Since the same tachometers used in the motor operations were also used in these calibration tests, this consistency can also be applied to the operation of the tachometers. Hence, the only appreciable errors in flow rate measurement, under the present system would be caused by leaks or unnoticed changes in pump rates during a run. The total numbers of revolutions recorded on the individual tachometers together with the duration of the run served as a measure of the average pumping rates. Thus, by comparing these average pumping rates with the set rates, an additional check on any otherwise unnoticed variations was effected. However, these figures were never different by more than 1%. It is, therefore, believed that flow rates as measured were always accurate to within $\pm$ 1% except for a few runs in which slight leaks occurred. In any runs where appreciable leakage

was noticed the results were withheld from serious consideration.

2.) Pressure Measurements:

The calibrations of the Foxboro recorders used to measure the chamber pressure and fuel feel pressures were consistent to within at least 1% or about as close as they could be read. The 12-inch Heise bourdon pressure gage which was used in the calibrations had been previously calibrated with an Ashton deadweight tester. The proper mean pressure readings were sometimes in doubt on the chamber pressure recorder due to rapid fluctuations or to failure to reach a perfectly constant mean equilibrium pressure. However, in good runs, this chamber pressure measurement should be accurate to within ± 1%, while in a few cases it is possibly in error by as much as 2.0%.

3.) Thrust Measurement:

Calibrations of the thrust measuring system with loads applied in the form of dead weights were consistent to within at least 1%. In a good run, therefore, this quantity can be assumed accurate to ± 1%. However, in many cases, there was sufficient fluctuation in the record under the "equilibrium attained" part of the run or enough lag in assuming a final reference zero which was perfectly constant at the end of a run, to introduce a possible error of as much as 2.5% in reading the thrust from the chart.

4.) Nozzle Throat Diameter:

The nozzle throat diameters were measured to the

nearest 0.0005 inches. However, due to non-circularity caused by thermal deformation and slight solids accumulation or partial plugging, the diameter as measured might be incorrect by as much as 0.002 inches in some cases. This represents a maximum error in the quantity, nozzle throat area, of about

$$\frac{2 \times 0.002}{0.130} \times 100 = 3\%.$$

In most runs, however, no plugging occurred and this error would amount to less than 1.5%.

5.) Heat Losses and Average Heat Transfer Rates:

These derived quantities are based on two types of measurements, namely those of cooling water flow rates, and cooling water temperatures. The cooling water flow rates obtained were an average for a period of time approximately double the duration of the actual run. While this average rate was determined to an accuracy of at least 1%, the instantaneous rate at the equilibrium conditions of the run might have been in variance by up to a maximum of 3-5%. The temperature measurements were likewise precise to within at least 1% but due to fluctuation with time in some runs, (i.e., failure to attain a perfectly constant value at equilibrium), it appears that the mean value used might be in error by 3-5%. For most runs the heat loss measurement was, therefore, accurate to within 5%. In a few runs this error might approach 10%, however, if all errors were cumulative.

6.) Concentration of Reactants:

In all cases these concentrations were known within at least $\pm$ 1% and probably within $\pm$ 0.5%.

7.) Instantaneous Pressure Measurements and Magnitude and Frequency of Pressure Fluctuations:

Static calibrations of the General Motors' capacitance-type pressure indicator at room temperature were quite consistent. However, a relatively small increase in temperature caused considerable change in the capacity of the indicator condenser. Heating the condenser plate with hot water to a temperature of approximately 200°F. at atmospheric pressure caused a greater shift of the cathode ray on the oscilloscope screen than application of 500 psi pressure. While the gauges used were all water-cooled, they may easily have approached the temperature of boiling water (at least 212°F). In fact, in most runs there was definite evidence on the pressure time film record of a gradual shifting of the cathode ray in the direction of higher pressure throughout most of the run. For this reason the absolute magnitude of the pressures indicated by the General Motors' gauges cannot be reliable except for the first few seconds of each run. However, the relative magnitude of the pressure fluctuations obtained from the film record should still be significant. Since the mean pressure is known from the Foxboro bourdon tube pressure record, the actual magnitude of the fluctuations can be estimated by obtaining a new calibration factor by comparison of the total mean displacement of the cathode ray and this known mean pressure. When used in this manner, the General Motors' pressure indicator served as a reliable measure of the magnitude and frequency of the pressure fluctuations existing in the micro rocket motor combustion

chambers. These gauges are designed for sensitivity to impulses of up to 5000 cycles per second frequency. The principal fluctuations measured were never faster than 150 cycles per second although there were occasionally smaller secondary fluctuations superimposed on the larger ones.

The thermal effect mentioned above was substantially eliminated in a few runs by placing a short water-filled line between the combustion chamber and the gauge. The pressure was then transmitted to the pressure-sensitive diaphragm of the gauge by means of the column of water. This added inertia may have affected the speed of response but evidently the upper limit was still above the frequencies of the main fluctuations existing in the present case because no appreciable drop in the characteristic frequencies recorded was noted.

RESULTS AND DISCUSSION OF RESULTS

The reaction motor is an extremely simple engine as regards number of working parts and principles of operation. However, the physical and chemical processes which are consummated in the course of its operation are really quite complex, especially combined as they are in a short space of time with superimposed effects of one upon the other. By making certain simplifying assumptions it is possible to distribute the total inefficiencies of the experimental operation of the reaction motor between its two principal parts, the combustion chamber and the exhaust nozzle. The function of the combustion chamber is to provide the space for effecting the release of the potential or chemical energy bound up in the reactants while the exhaust nozzle is the means for converting this source of random energy into the useful, directed, translational energy of the exhaust jet. The mechanism by which the energy is released in the combustion chamber usually involves the performance of some sort of oxidation - reduction reaction. It is this reaction which is of most interest to the chemical engineer. It may involve very simple compounds such as hydrogen and oxygen or much more complex molecules such as nitric acid and aniline.

Most of the reactions which are usually carried out in rocket combustion chambers are so complex that very little is known of the mechanism or of the overall reaction rates or the rates for the controlling steps of the reaction. Most

oxidation reactions are assumed to involve chain reactions, and molecules or radicals which are known chain carriers are generally conceded to be helpful in promoting rapid or complete combustion. Even in the case of the reaction between hydrogen and oxygen for which the mechanism is fairly well understood, the time required to complete the reaction in a given motor cannot be predicted because of the importance of factors other than the chemical reaction rate. For example, since it is impossible or at least generally inadvisable to mix the fluid reactants prior to their entrance into the combustion chamber, the rate and efficiency of mixing and/or of vaporizing the reactants in the case of liquids is probably of equal importance to the chemical reaction rate in determining the efficiency of combustion which can be obtained in a given chamber. In the usual case, then, this entire process of injection, mixing and subsequent reaction in a rocket combustion chamber obviously will be influenced by the method of injection used, the chemical and physical properties of the reactants and their combustion products, the amounts of each or the mixture ratio, the size and shape of the combustion space, the amount of turbulence produced, the method of ignition and the chemical kinetics of the reactions involved. The analysis of the effect of each of these factors from measured overall performance of the motor would be an extremely difficult task because of the interdependence which exists amoung them. However changes in performance with changes of

various experimental conditions can often be explained at least qualitatively from theorectical considerations of some of these factors.

The above picture is further complicated in the case of self-igniting fuel systems or where combustion catalysts are employed. For example, in the self-igniting fuel system, liquid phase mixing of the reactants is probably of much greater importance than the atomization or vaporization process.

Considering the multiplicity of variables in the design and operation of the combustion chamber of a rocket, it is not surprising that it is so difficult to predict the effects of a single variable under conditions not experimentally studied, either from purely theoretical considerations or from other not directly related experimental results. Until more research has clarified the effects of the separate variables or more extensive development has covered a wider field of rocket motor experimentation, such will be the case, however.

The present thesis is directed towards a relatively unexplored phase of the field of rocket engineering with the hope of developing a general micro-rocket technique of practical utility. The critical appraisal which has been made of the possibilities of this technique should be generally applicable under any presently forseen conditions. However, some of the more specific results as to performance of the actual equipment used may be limited to the present scale of operation

or the special propellant systems studied because of the complex nature of the processes involved. For example the methods of injection used are so different from those commonly employed in conventional sized motors, that the present injection studies may be of no importance for predicting large scale injector performance. In fact some of the best methods of injection used here could not be used in a practical motor due to the necessity of a positive displacement feed system. The present indications concerning the specific methods, equipment and propellants will need to be tested on other systems on the same scale as well as with the same systems and equipment design on a larger scale. An adequate comparison with conventional size motor operations cannot be made at the present time since almost no larger scale test results are now available on the present propellant systems.

Qualitative Evaluation of Combustion Performance

The performance obtained in each run was evaluated qualitatively by visual and auditory observations during the run and by consideration of the average frequency and magnitude of the pressure fluctuations picked up by the G.M. capacitance type gauge. Visual observations usually made were as to the color and intensity of the exhaust jet, its steadiness and the sharpness of the shock wave pattern and flow pattern. A good indication of the smoothness of operation was obtained by listening to the sound of the operating motor. Very rough runs were characterized by intermittent

loud knocking and an unsteady exhaust jet could be heard as well as seen.

The magnitude of the pressure fluctuations on the records obtained from the G.M. gauge was evaluated percentage of the total mean pressure of the run by making two linear measurements on the film. The frequency of the fluctuations was obtained by counting the number of pressure waves and the number of neon flashes (1/60th of second intervals) over a given length of film.

TABLE 1

RELATIVE ROUGHNESS OF OPERATION WITH VARIOUS INJECTORS AND DIFFERENT PROPELLANTS

RUN NO.	PROPELLANT SYSTEM	MOTOR	INJECTOR	MAXIMUM FLUCTUATIONS $\pm \frac{\Delta p}{p_{av}}$	FREQUENCY OF FLUCTUATIONS $\frac{\text{cycles}}{\text{sec.}}$	REMARKS
B-1 thru B-10	80% H_2O_2- 85% $N_2H_4H_2O$	2"x4"	180° no target	$\frac{60}{350}$	40 (not always regular)	Clear shock waves in jet (about 10" long)
B-10 thru B-19	same	same	90° with target	$\frac{60}{400}$	42 (very regular)	Rougher sounding than above. Jet irregular and spitting.
B-20 and B-21	same	same	60° confined mixing	$\frac{15}{350}$	20 to 60 (not regular)	Very clear strong steady jet (12" long with 7 shock waves clearly visible)
C-1 thru C-7	same	same	90° with target	$\frac{100}{400}$	41-42 (very regular)	Very rough sounding. Jet varied rapidly from bad to good.
D-1 thru D-3	same	same	180° confined mixing	$\frac{100}{400}$	very irregular	No jet visible - just sparks
D-4 thru D-7	same	same	same injector (eroded)	$\frac{30}{400}$	irregular	Better than the average jet with open injectors but shock waves not too sharply defined.
D-8, D-9 and E-1	same	same	180° with target	$\frac{70}{400}$	42	Very good jet - clear shock waves most of time but some unsteady periods.
E-2	90% H_2O_2- 85% $N_2H_4H_2O$	same	same	$\frac{100}{400}$	41	
E-3 and	same					

1.) Effect of Methods of Injection

Table 1 summarizes the determinations of relative roughness of the micro motor operation for the various methods of injection as measured by the G.M. capacitance type pressure indicator and the visual and auditory observations made during the tests. The most consistently smooth pressure records as well as the strongest, sharpest and most symmetrical exhaust jets were obtained with the 60° confined mixing injector (diagram C Fig.22). With the hydrazine hydrate - hydrogen peroxide combination, many other types of injection were tested.

The original methods of injection in which the streams enter from the side walls of the motor and meet and mix in the center of the wide-open combustion space (See diagram a and b Fig.22) were characterized by an amazingly regular frequency of the fluctuating pressure wave. In all these runs whether the streams impinged at 180° or at 90° and whether with or without a target, the pressure fluctuated through practically the entire record of every run at a frequency of 40 - 42 cycles per second. Sample records of two of these methods of injection are shown in Fig. 26. The amplitude of these fluctuations varied somewhat from one run to another and within a given run but the frequency was always the same. This is in direct contrast with the other methods of injection in which the streams enter from the end of the motor and have from the start a directional momentum

Figure 26

Sample G. M. Capacitance Gage – Oscilloscope Film Records

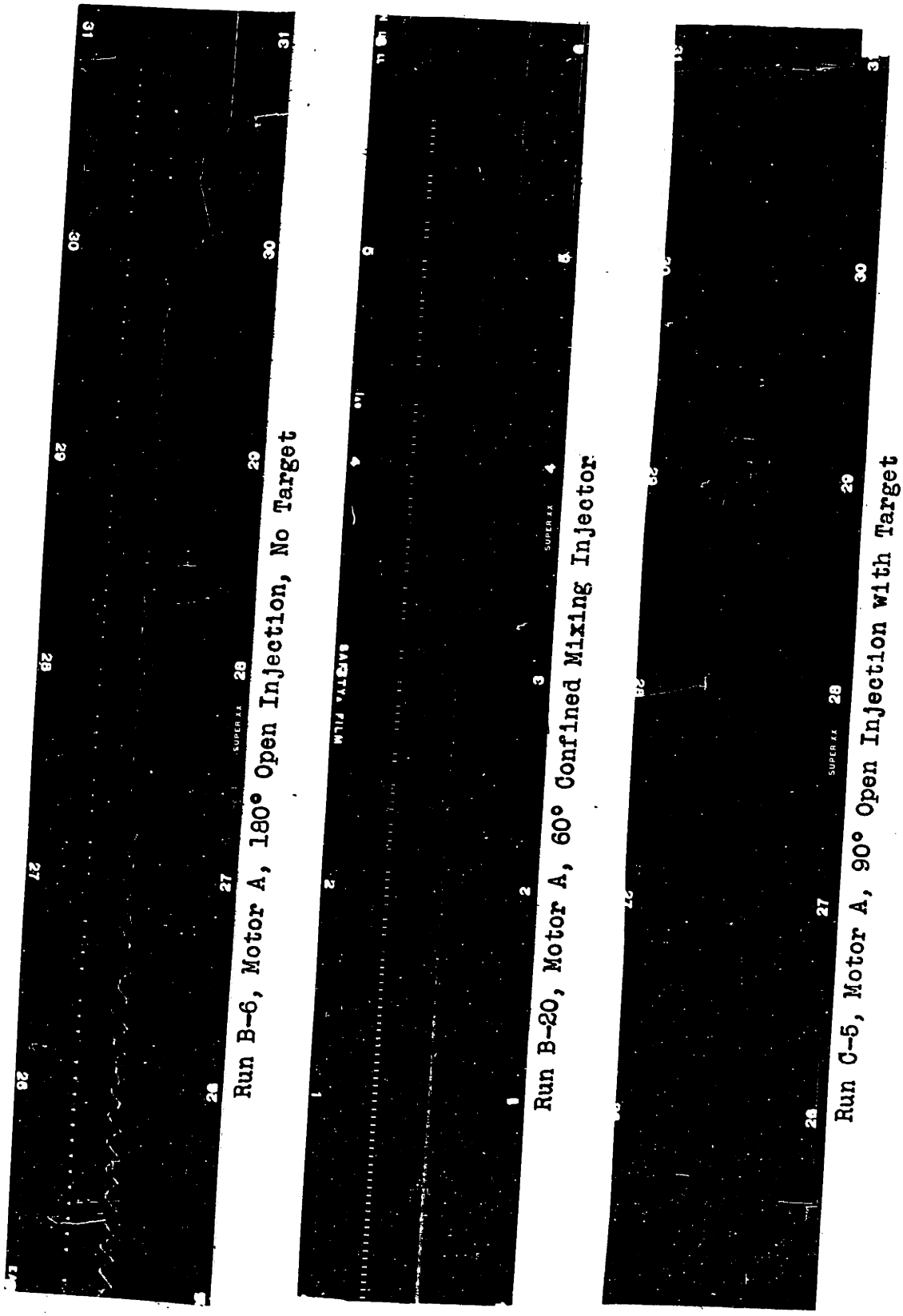

Run B-6, Motor A, 180° Open Injection, No Target

Run B-20, Motor A, 60° Confined Mixing Injector

Run C-5, Motor A, 90° Open Injection with Target

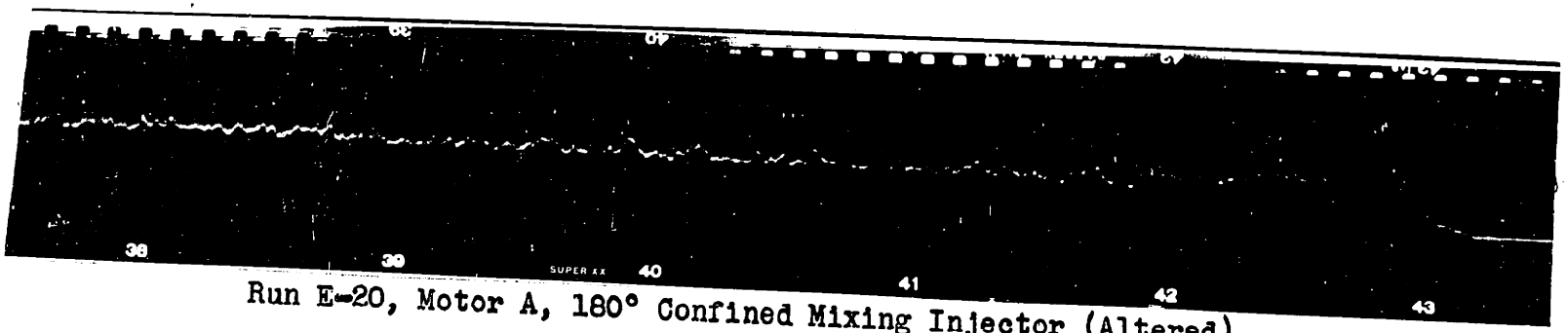

Run E-20, Motor A, 180° Confined Mixing Injector (Altered)

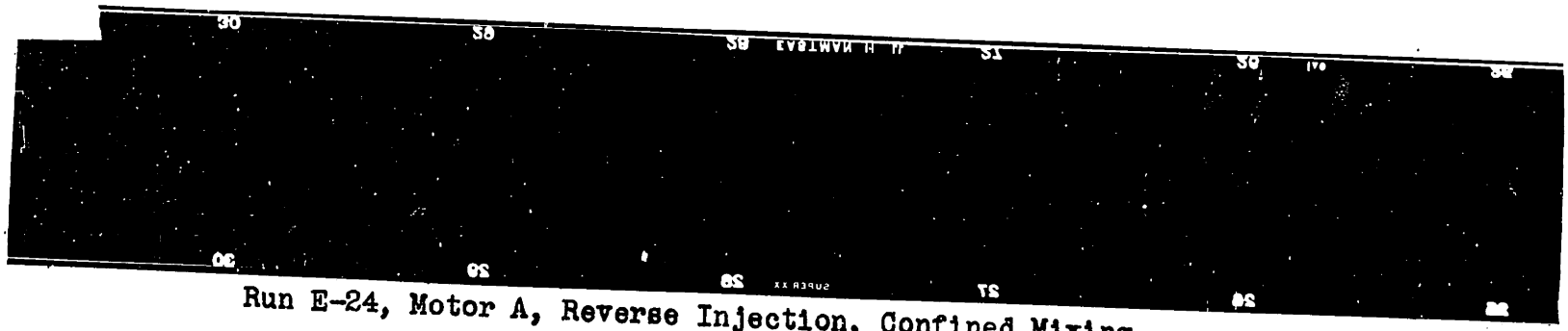

Run E-24, Motor A, Reverse Injection, Confined Mixing

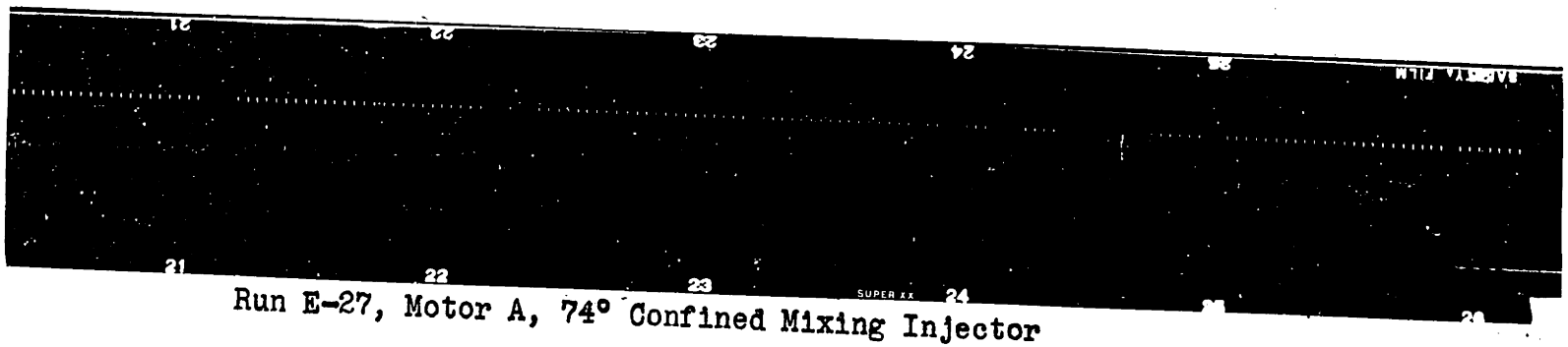

Run E-27, Motor A, 74° Confined Mixing Injector

Figure 26 (cont.)

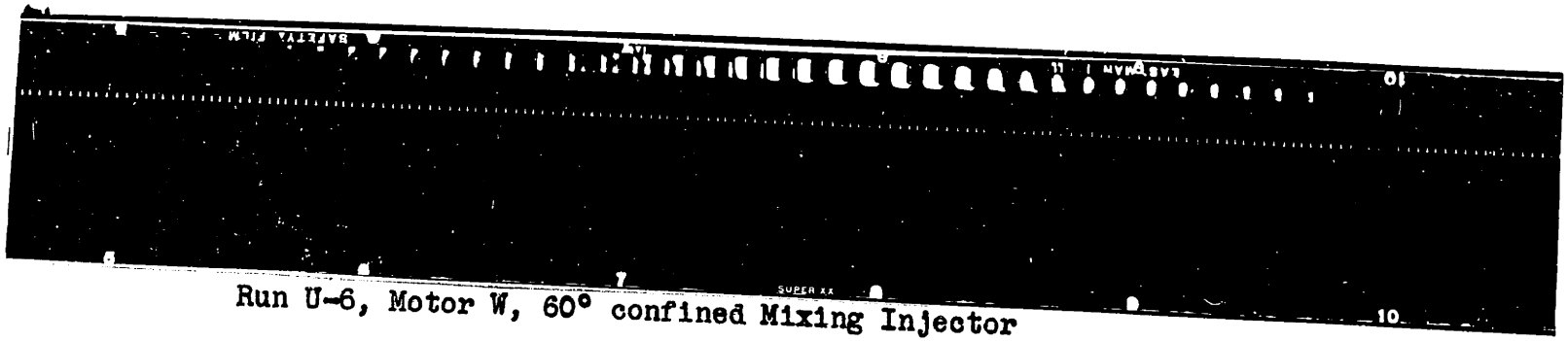

Run U-6, Motor W, 60° confined Mixing Injector

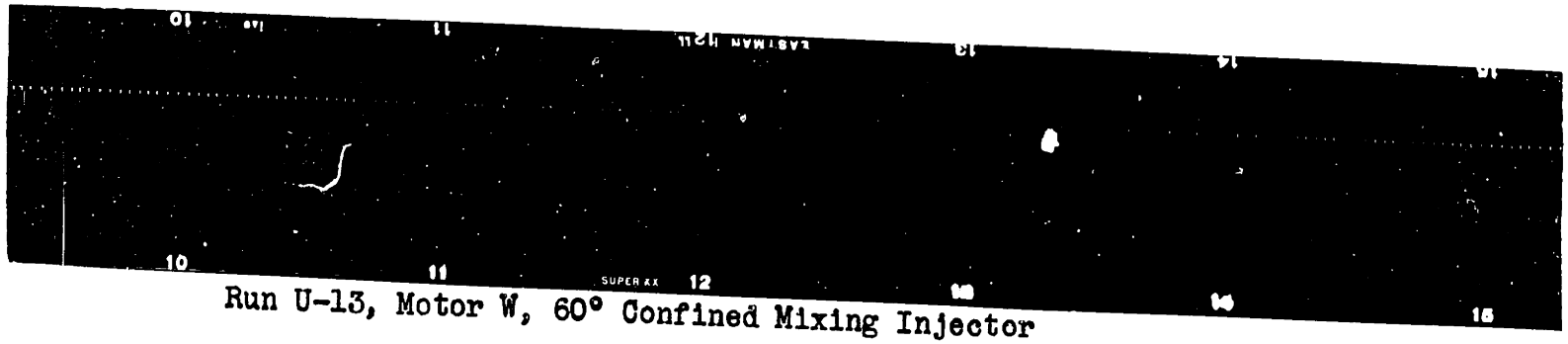

Run U-13, Motor W, 60° Confined Mixing Injector

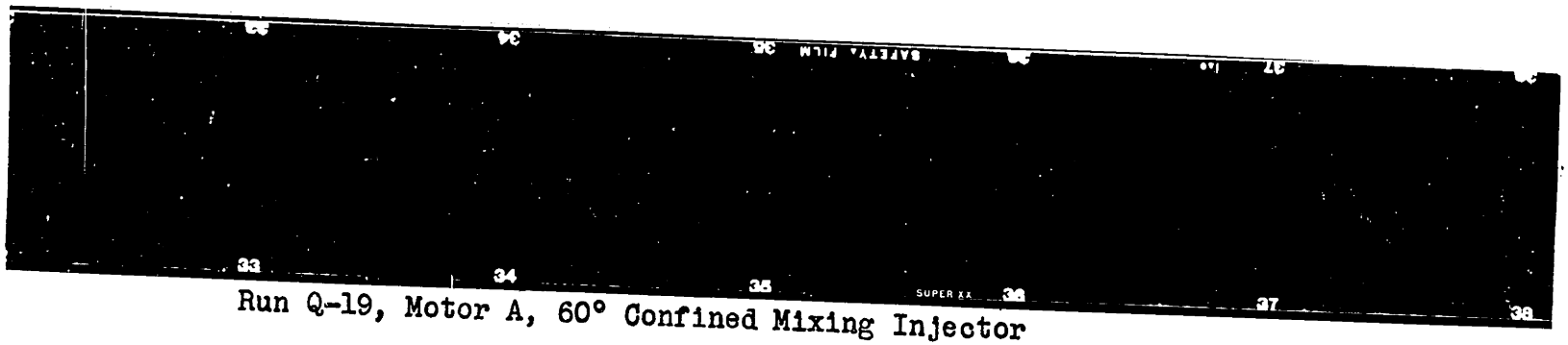

Run Q-19, Motor A, 60° Confined Mixing Injector

Figure 26 (cont.)

more or less in line with the axis of the cylindrical combustion chamber. In all these injection methods, any roughness which did appear in the pressure record showed no regular frequency for any appreciable length of time.

This roughness of combustion of the open injection methods is undoubtedly traceable to the unprotected location of the injection orifices. Since each stream of liquid propellant traveled an average distance of about one inch across the open combustion chamber before meeting the target or intersecting the other stream, there was ample opportunity for the gaseous combustion products and pressure waves resulting from the combustion reactions to interfere with the jets and cause misalignment or poor impingement. This misalignment of jets would naturally tend to repeat itself due to the pressure surge of the delayed reactions caused by poor mixing. However, it is surprising that this fluctuating pressure wave should occur so regularly from this source of variation. It is possible that this regular type of pressure fluctuation was due to changes in flow rates corresponding to the natural frequency of the propellant feed system and caused by the slight compressibility of the liquids which actually exists or the compressibility of the small amounts of gases formed in or trapped in the hydraulic system.

A series of confined mixing injectors similar to the 60° model discussed above were also tested. The chief variation in the various models of this type of injector was

in the angle of impingement. Angles of 74, 90, 135 and 180° were also tested. Initially runs with the 135° and 180° confined mixing injectors were extremely rough. The pressure fluctuations of the G.M. gauge were quite wild and quite irregular and the exhaust jet was scarcely visible except for incandescent solid particles contained in it. These runs were accompanied by loud knocks and jarring noises and vibration of the entire motor as well as by high pitched screaming noises in some cases. However, operation of one 180° injector was continued in this manner for two or three runs with gradual improvement as the confined mixing section was eroded away to a much larger diameter of approximately one quarter of an inch. As this erosion took place, the runs gradually became smoother in sound and in magnitude of the pressure record fluctuations while the appearance of the jet also improved. Fig. 26 shows a sample record of the 180° injector after considerable erosion had occured and the magnitude of the fluctuations had become fairly small. In the case of 90° and 74° confined mixing injectors, combustion was fairly smooth as measured by the magnitude of the pressure fluctuations. However, their operation was much less consistent than that of the 60° injector and the exhaust jet was not nearly as clear. Erosion also occurred in these injectors although more slowly and to a lesser extent than with the 180° and 135° models. Fig. 26 is a record of one run made with a 74° angle model.

The pressure fluctuations of these wider angle confined mixing injectors are believed to be caused by recycling of part of the reactants in the mixing chamber until the resident time of these fuel particles exceeded the ignition delay time. In this case the resulting explosion would undoubtedly clear the mixing chamber completely, after which normal flow would return and the same process repeat itself again and again. The irregularity of the fluctuations of the G.M. gauge pressure record in this case are more to be expected since very small changes in the dimensions of the injector orifices or mixing chamber could change the flow pattern and resultant mixing appreciably.

Other end-position, single-piece injectors which showed promise were the reverse injection model (diagram e, Figure 22), the 60° one-piece open-impingement type (diagram d, Figure 22) and the confined mixing spray injector of [redacted] page 193 of Appendix A. The one piece 60° open impingement injector gave smooth pressure records and fairly strong, clear exhaust jets in a very consistent manner. However, it was slightly inferior in all these respects to the 60° confined mixing injector. This was especially noticeable in the quality of the exhaust jet. The exhaust jet from the 60° confined mixing injector contained more clearly visible standing shock waves and all these shock diamonds as well as the jet itself seemed more symmetrical. The reverse impingement injector produced runs with pressure records equally as

smooth as the one-piece 60° open-impingement model. However, the nature of the exhaust jet which it produced varied considerably from run to run as well as slightly during a given run. In some cases the exhaust jet from runs using this injector was scarcely visible and seldom were as many as four shock wave diamonds clearly visible whereas six or more are usually seen with other good injectors.

The confined-mixing spray injector produced one exceptionally good run in which a silver-soldered joint in the injector was melted by the heat. However, in other runs with very minute changes in design, it produced fairly rough pressure records and only moderately sharp exhaust streams. This performance as well as that of some of the two-stream confined-mixing injectors indicate how sensitive this type of injection is to minor changes in physical dimensions.

Roughness of combustion as measured by the above standards, especially the instantaneous pressure fluctuations, did not always indicate poor quantitative performance as measured by the mean chamber pressure obtained for a given flow rate. This will be seen later when the quantitative performances of various injection methods are compared.

2.) Effect of Combustion Chamber Size

The 60° confined-mixing injector was the only type tested extensively in a smaller combustion chamber in which a G.M. gauge was being used to record the instantaneous pressures produced. However, with this injector being used on the thrust stand in a smaller motor with an L* of 150

inches instead of 500 inches or more, not only was the amplitude of the pressure fluctuations greater, but the frequency of these changes was also noticeably increased. This can be seen by comparison of the sample records for runs B-20 and U-6 and U-13 shown in Fig. 26.

3.) Chemical Nature of Reactants

The 60° confined-mixing injector and the 60° one-piece open-impingement injector were also tested extensively with the Naphferrol-Peroxide combination. The G.M. gauge pressure records obtained in runs with this propellant combustion were more inconsistent for both of these injectors than had been the case with the hydrazine hydrate-peroxide combination in the same motor. In a given run the pressure fluctuations would vary by ±30 psia to ±70 psia from the mean. At the same time the frequency of the fluctuations varied considerably during a run but, as had never happened with these injectors with the hydrazine hydrate system, for periods of a few seconds these fluctuations stayed fairly constant. The frequencies of the pressure fluctuations in these regular periods varied from 17 to 120 cycles/sec. In the smoothest portions of a run, however, the pressure record with the Naphferrol system was quite similar to that obtained with hydrazine-hydrate and peroxide. Fig. 26 shows a sample record of this type taken while using the 60° confined mixing injector. While the fluctuations are larger and more rapid than with the same motor and injector while operating on

hydrazine hydrate, the fluctuations here still appear to be quite random in frequency.

Practical Operating Characteristics of the Propellant Systems Studied

One of the results of the micro rocket motor operation was an evaluation of the suitability of the various propellant systems for application to actual power cylces. In this regard the hydrazine based fuel proved to be definitely superior.

Two practical difficulties were experienced with operations using the Naphferrol fuel. The first of these was the difficulty in obtaining smooth starts in runs in which the propellant storage bellows were prepressurized. This difficulty was partially due to the small amount of gas which was trapped in the bellows and bellows pots and which tended to expand from the pressurized volume as the run started, thus flooding the motor with an excess of reactants. However the fact remains that with the same conditions exactly, no troubles whatsoever were experienced with "hard starts" in any runs with the hydrazine hydrate fuel combination. On the other hand "hard starts" or explosive starts were the rule with the Naphferrol - peroxide combination with a prepressurized system.

The second disadvantage of the Naphferrol fuel compared to the Helman fuel was its greater solid content (approximately 200 g of ferrous B Napthalene Sulfonate per liter). The combustion products contained considerable solid material due primarily to the iron content which

amounted to about two per cent by weight of the Naphferrol. As a result, plugging and solids accumulation were sometimes troublesome in parts of the system such as the exhaust nozzles and the injectors. Some injectors became plugged completely both during combustion and even when the equipment was idle. In the latter case, the plugging was due merely to the evaporation of the methanol from the Naphferrol solution leaving the ferrous β napthalene sulfonate in the orifices or manifolds. These plugs could be dissolved out with more methyl alcohol, but those formed during combustion were as solid as a welded joint. In only one rund did an exhaust nozzle become badly blocked in operating with Naphferrol, However, the nozzle throat areas were so small that a very small amount of solid accumulation effected a considerable change in the mass flow rate per unit area and therefore in the chamber pressure. A small amount of this partial plugging of the exhaust nozzle occurred even with the Helman fuel in which there was never more than 10 or 12 grams of metallic salts per liter. However, this occurred much more often with the Naphferrol combination. It seems probable that this difficulty would be considerably lessened in operation of an actual power plant or of a much larger scale motor. The chief difficulty caused by this occurrence in the present work was not in operation but in calculations of theretical performance due to the uncertainty in correcting the exhaust nozzle throat area for this effect.

FIGURE 27 PERCENTAGE OF THEORETICAL PRESSURE OBTAINED WITH VARIOUS INJECTORS FOR THE SYSTEM 80% H_2O_2 – 85% $N_2H_4 \cdot H_2O$

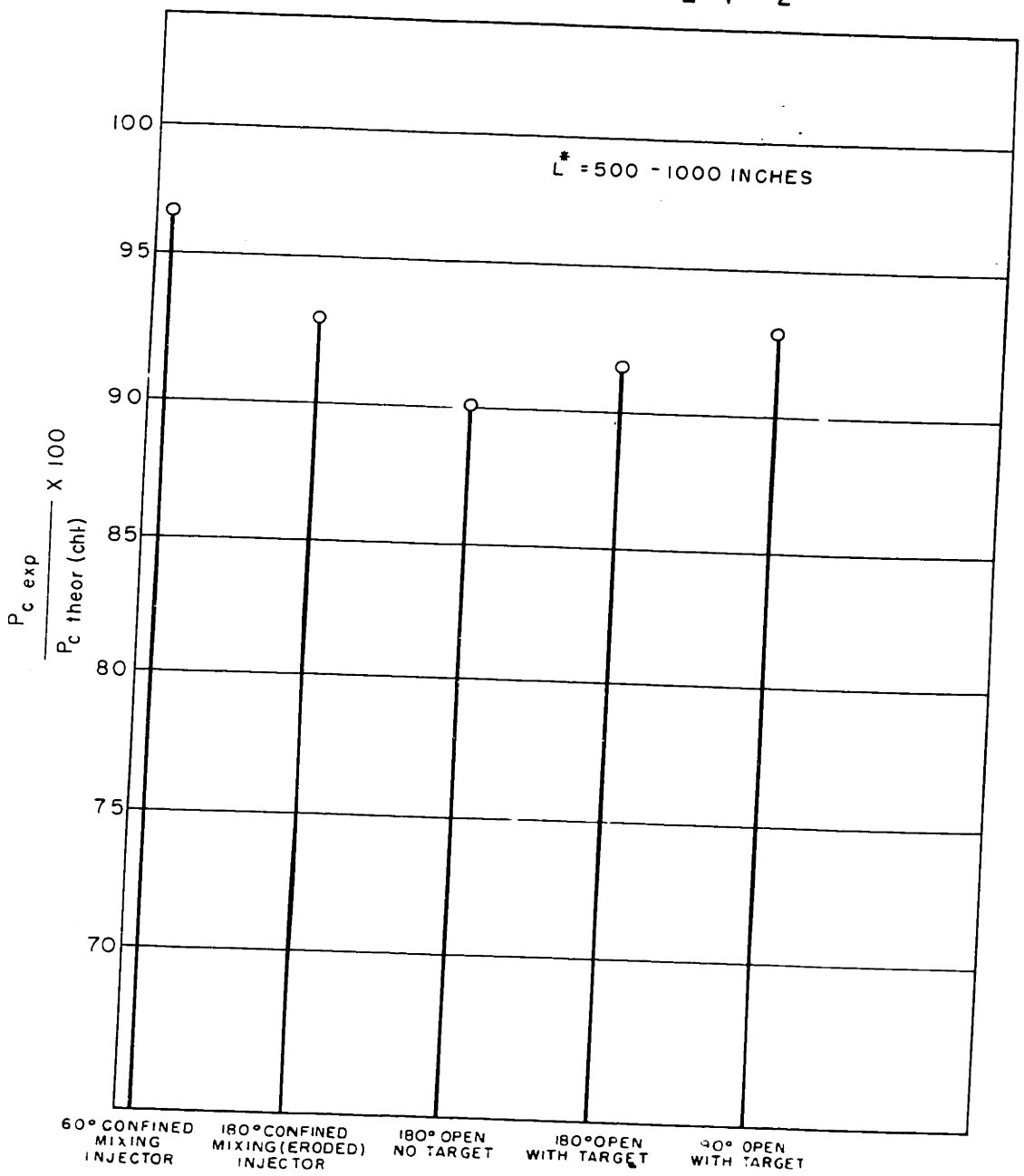

FIGURE 28 PERFORMANCE OF VARIOUS INJECTORS USED WITH THE SYSTEM 90% H_2O_2 - 85% $N_2H_4 \cdot H_2O$ IN DIFFERENT COMBUSTION CHAMBERS

FIGURE 29 PERFORMANCE OF VARIOUS INJECTORS USED WITH THE SYSTEM [NAPHFERROL - H_2O_2 (90%)]

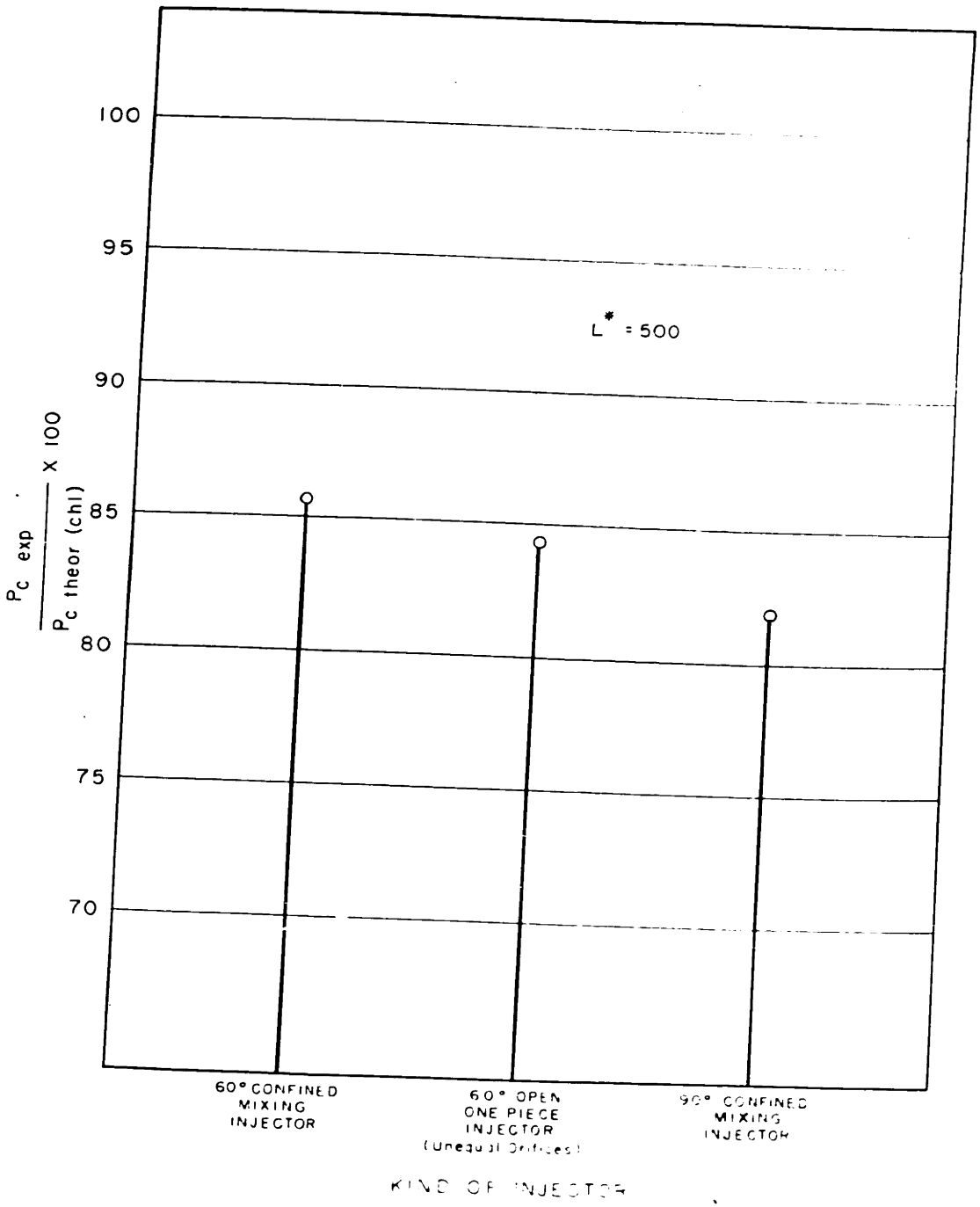

Quantitative Evaluation of Combustion Performance

The combustion chamber performance or efficiency of combustion as defined here is the percentage of the theoretical chamber pressure which is actually obtained experimentally. The usual definition of rocket combustion chamber efficiency is the percentage of the theoretical C* actually obtained experimentally. However since C* is equal to $P_c A_t g_o/\dot{m}$, it is directly proportional to the chamber pressure for a given mass flow rate per unit area and these two definitions are therefore indentical. As pointed out before this pressure ratio is not exactly the same as the usual definition of efficiency of combustion but is a good measure of it and quite sufficient for practical purposes.

1.) Effect of Methods of Injection

The results of the principal injector studies are shown for the various propellant systems in Figures 27, 28, and 29. It can be seen from these graphs that the 60° confined mixing injector gave the best performance of all injectors tested with each system, followed closely by the 60° open impingement one piece injector and the 90° reverse impingement injector. In the large combustion chamber with L* of 500 inches or greater, the average level of performance was 90 to 100% of theoretical with the hydrazine fuel for all methods of injection. For the Naphferrol fuel, this range was between 80 and 90% of theoretical for the three injectors tested which were the more promising of the types tested with

the hydrazine combination. The theoretical pressures with which the experimental pressure is compared in these plots has been corrected for the experimental heat loss. In the stationary stand runs the heat loss was estimated from theoretical calculations and a comparison of the theoretically calculated and experimentally obtained heat loss on the thrust stand motors. (See Appendix F).

With ordinary propellant systems the injectors are usually designed to accomplish two main jobs, mix the reactants and atomize them to present the maximum surface area for reaction and vaporization. In the use of self-igniting fuel systems, it has been assumed that the primary function which should be served by the injector was that of producing good mixing. Providing for vaporization and atomization seems unnecessary with these systems because the intense reaction which occurs in the liquid phase with such substances can almost instantly produce these changes. Conceivably, the entire combustion process might be essentially completed at the same time if really thorough mixing could be accomplished before this intense reaction had been iniated or at least before it had been proceeded far enough to break up and vaporize the reactants. The ultimate goal in mixing self-igniting reactants would therefore seem to be a method of producing complete and perfect mixing down to molecular dimensions almost instantly, or at least within the "ignition delay time" which is probably no more than a few milliseconds

in most cases especially in the case of "perfect" mixing. (Ordinary measurements of ignition delay time have been shown to vary with the method of mixing for a given fuel system. See Appendix G. If this "perfect" liquid phase mixing and resultant almost complete and instantaneous reaction were obtainable, space and provision for the more voluminous vapor phase mixing would not be necessary. While this ultimate in the mixing process obviously cannot be achieved in practice, special attempts at obtaining the best possible liquid-phase mixing appear to have made possible more economical use of the combustion spaces in the present studies. This conclusion is based on the results shown in Figure 28 which compares the performances of several methods of injection. In the top curve representing performance of the large stationary motor, there is little to choose between the performances of the three best injectors. However, in the bottom curve representing the smallest combustion chamber, the superiority of the confined mixing injector becomes more pronounced. This indicates that the improved liquid-phase mixing produced in the confined space of this injector results in more complete combustion when the available combustion space is critically small. Such a result is to be expected since a much larger volume is required for a given amount of mixing in the vapor state than for the same mixing in the liquid phase. Good liquid mixing is undoubtedly an asset in any kind of propellant system. However in a non-self-igniting

TABLE 2

EFFECT OF MICRO ROCKET HEAT LOSSES ON INITIAL ENTHALPY AND ON THEORETICALLY CALCULATED CHAMBER PRESSURE AND SPECIFIC IMPULSE

PROPELLANT SYSTEM	MIXTURE RATIO $F/F \approx o$	MOTOR	AV. COMB. CHAMB. HEAT LOSS Btu/lb.	AV. CHANGE IN INITIAL ENTHALPY (above products of combustion at 0°K)	AV. EFFECT ON CALC. CHAMBER PRESSURE	EXHAUST NOZZLE THROAT DIAM. inches	DIVERG. ANGLE °	AV. DIVERG. NOZZLE HEAT LOSS (Total) Btu/lb.	AV. TOTAL CHANGE IN INIT. ENTHALPY (using ½ nozzle/chamber)	AV. EFFECT ON CALCULATED SPECIFIC IMPULSE
$90\%H_2O_2$-$85\%N_2H_4$·H_2O	0.5	1"x3"	114	6.0%	3.0%	0.176	8°	75	8.0%	4.0%
" "	0.5	1"x3"	155	8.0%	4.0%	0.144	8°	113	11.5%	5.7%
" "	0.5	½"x1½"	55	2.8%	1.4%	0.147	20°	37	3.8%	1.9%
" "	0.55	1"x3"	158	9.0%	4.5%	0.144	8°	114	12.2%	6.0%
" "	0.55	½"x1½"	53	3.0%	1.5%	0.147	20°	36	4.0%	2.0%
" "	0.601	1"x3"	144	8.7%	4.3%	0.144	8°	100	11.7%	5.8%
" "	0.601	½"x1½"	43	2.6%	1.3%	0.147	20°	29	3.5%	1.7%
" "	0.438	1"x3"	153	8.5%	4.2%	0.144	8°	101	11.4%	5.7%
" "	0.438	½"x1½"	50	2.8%	1.4%	0.147	20°	34	3.7%	1.8%
$80\%H_2O_2$-$85\%N_2H_4O$	0.525	1"x3"	99	5.7%	2.8%	0.176	8°	57	7.3%	3.6%
$90\%H_2O_2$-Naphferrol	0.50	1"x3"	78	3.2%	1.6%	0.144	8°	98	5.3%	2.6%
" "	0.622	1"x3"	74	3.8%	1.9%	0.144	8°	97	6.4%	3.2%
" "	0.399	1"x3"	86	4.5%	2.2%	0.144	8°	99	7.1%	3.5%

system, it may be that no net gain would result if such improved liquid phase mixing were carried out at the expense of the degree of atomization and vaporization produced.

Even in self-igniting systems some gas-phase reaction and mixing is undoubtedly necessary to complete the combustion process in an actual motor. The extensive experimentation which would be necessary in order to determine the magnitude of the effect on combustion of such factors as turbulence and gas flow patterns has not been carried out. It has not even been possible to make an empirical study of the overall effect of varying the shape of the combustion since all motors used have employed cylindrical chambers with length to diameter ratios of about 2 to 1 or 3 to 1.

The shape of the combustion chamber is important since use of a design which is unsuitable for the injection system employed can result in complete loss of utility of part of the combustion space. However, the principle of using the smallest possible cross sectional area of the combustion chamber as the means of making most effective use of the combustion space, has recently received considerable acclaim in this country. This shape of combustion chamber gives a high concentration of flowing reactants, either liquid or gaseous, in terms of the mass flow per unit cross sectional area. This apparently makes possible active use of the entire combustion space and also insures the presence of high turbulence in all parts of the chamber merely due to the

violence of reaction and the changes in point conditions of pressure and temperature which are effected in the gas mass as combustion proceeds. Turbulence alone is ordinarily considered as being capable of effectively distributing or mixing very small masses or slugs of material but not individual molecules. Hence the final stage in the gaseous mixing process is probably accomplished by molecular diffusion of the various chemical species. This molecular diffusion occurs as a result of the thermal motion of the individual molecules. Theoretically then, completely intimate mixing should be the easier to attain, the higher the temperatures and the lower the molecular weight of the gases in the system. The role of turbulence in combustion is still very important, however because increased turbulence produces, increased surface for diffusion, and it is easier to increase the turbulence than to speed up molecular diffusion rates as much.

The inferiority in the quantitative performance of the original injection methods or so called "open" injection, in which the streams intersect directly in the center of the combustion space, is probably traceable primarily to their unprotected location. As stated previously, this open position made possible gaseous interference with the liquid jets and resulting misalignment and poor impingement. Because of the small diameter of the streams very small deflections would cause almost complete loss of liquid-liquid mixing especially in the cases where no targets were used. This

loss of liquid mixing could adversely affect performance and combustion efficiency. The actual loss in combustion efficiency of these systems is not as great as would be expected from the roughness of the G.M. gauge pressure records however. One reason for this may be the extremely large combustion chamber with which these open injection systems were always used. Obtaining good liquid-liquid mixing would probably be of less importance in such a large combustion space.

The use of single streams of each propellant as the fuel supply of the micro rocket motor constitutes of course a special case in the field of rocket injectors. While these streams are of approximately the size used in motors of conventional size which employ "jet" injectors, the distinction is that in the larger motor there are several hundred of these stream pairs. Therefore in a given run or at a given time in a run, the performance of a large motor is dependent upon the average performance of a large number of impinging stream pairs, whereas in the micro motor the performance of the entire motor is at all times dependent upon the operation of the single injector with its lone pair of liquid jets. This makes more probable the chance for erratic performance of an injector or method of injection from run to run and especially from time to time during a run. However, based on the experimental results of the present study, it can be said that at least with the present pumping and feed system, quite steady, reliable performance can be

Figure 30

Exhaust Jet from Micro-Rocket Motor

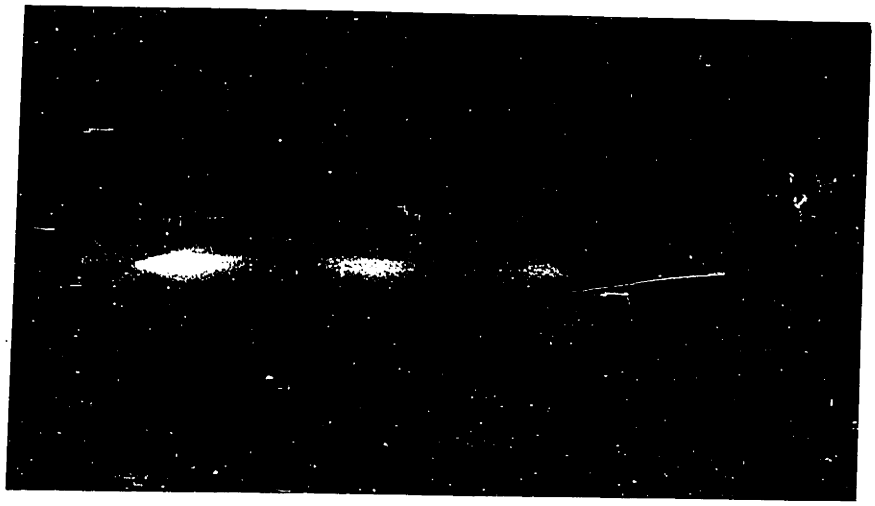

obtained with a single pair of injection streams.

The data curves of the recording instruments for a typical run are shown in Figure 24 ~~of Appendix E~~. These indicate that uniform operation was obtained, with a constant final equilibrium reading being reached in most cases. Also the spread of data points on the various performance curves is never more than ±10% and is less than ±5% except for a few scattered cases. Smooth pressure-time records on the G.M. gauge equipment and a steady uniform exhaust jet with from 3 to 8 clearly visible and fairly sharp shock-wave diamonds were usually obtained for most "in-line" methods of injection. Figure 30 is a single frame from a 16mm. motion picture of the exhaust jet from one of the runs with an open method of injection. In the case of the 60° confined-mixing injector, even clear shock diamonds could usually be seen.

2.) Chemical Nature of the Reactants

While only two completely different self-igniting systems have been studied, the two self-igniting fuels which were employed with the concentrated hydrogen peroxide in these two cases were quite different in chemical structure and properties. For example the ignition delay of the two fuels when mixed with 90% H_2O_2 in the standard delay tester were widely different. Compare 70 to 100 milliseconds for the Naphferrol combination and 12 milliseconds for the standard Helman. Appendix G gives a description of this reactor which was used on the Peroxide Project at M.I.T. in research

investigations of promising self-igniting fuels for use with peroxide. This appendix also gives the ignition-delay times of the various fuel combinations studied in this theses as measured in the standard delay tester, as well as those of some other fuel systems for comparison.

In the standard delay testing apparatus, the ignition delay time is defined as the time which elapses between the first contact of the two reactant streams and the first appearance of flame. The entire process is recorded on a motion picture film in a Fastax 8mm. camera driven at about 4000 frames per second and the results later evaluated from this film record. In a rocket motor the ignition delay time would more practically be defined as the time elapsed between the first mixing of the two propellants and the first appreciable rise in chamber pressure. This quantity was measured in the present study with the open methods of injection from the instantaneous time-pressure record obtained from the G.M. capacitance type gauge, with a correction for the average time required for the propellant streams to flow from the balanced diaphragm valves to the center of the motor. This average injection time was obtained by studying the injection process of a single propellant into an open combustion chamber by means of the Fastax high speed movie camera. Rocket motor ignition delay times defined in this way and measured by this technique proved to be somewhat longer than the standard "flame ignition delay" as would be

FIGURE 31 PERCENTAGE OF THEORETICAL COMBUSTION CHAMBER PRESSURE OBTAINED AS A FUCTION OF IGNITION DELAY TIME OF REACTIONS USED

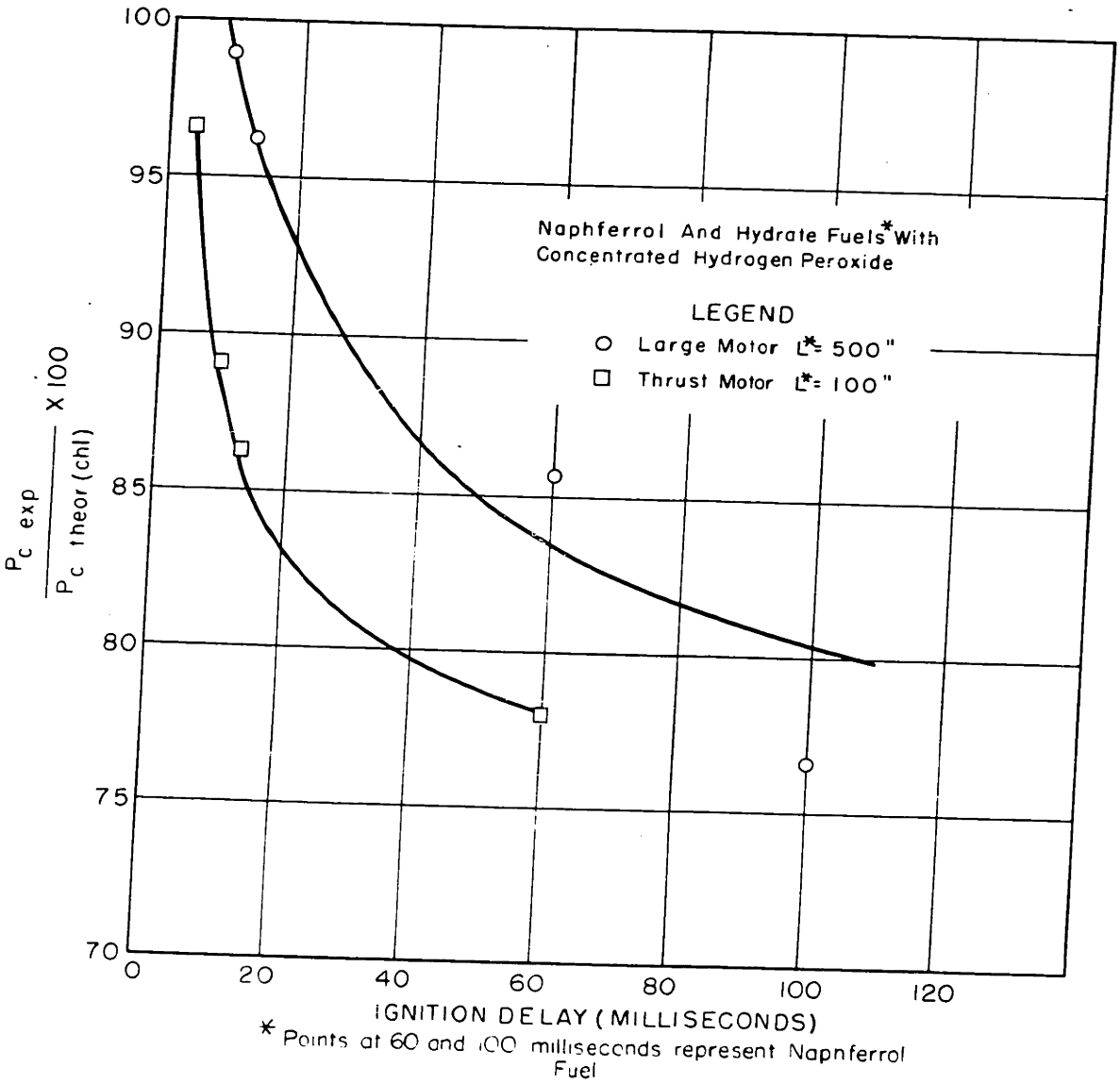

* Points at 60 and 100 milliseconds represent Napnferrol Fuel

expected. With same 90° open impingement on a flat target injection that was used in the standard delay tester, the average "rocket motor ignition delay" for the standard Helman-Peroxide fuel combination was 150 milliseconds compared with a delay of about 12 milliseconds in the standard delay tester before the appearance of flame. It seemed probable that approximately the same relative magnitudes would exist for the two types of delay with any self-igniting fuel-oxidant combination. Thus it seemed worthwhile to obtain a measure of this difference.

The ignition-delay time of the 85% hydrazine hydrate - 90% hydrogen peroxide combination in the standard delay tester was found to be a function of the amount of catalyst in the hydrazine fuel or Helman and also of the concentration of the reactants themselves. (A more complete list of factors affecting ignition delay is given in Appendix G). Since both the concentration of the catalyst in the Helman fuel and the concentration of the peroxide solution was changed somewhat in the micro-rocket motor studies, a chance to study the effect of these changes on combustion efficiency was afforded. As seen in Fig. 31 the combustion efficiency was found to be a smooth function of ignition delay. In fact for a given combustion chamber and method of injection, this dependence of percent of theoretical pressure obtained on the ignition delay time of the reactants could even be extended fairly well to include the Naphferrol-

peroxide combination.

General Comparison of the Propellant Systems
(hydrazine, hydrate / hydrogen peroxide and
Naphferrol / hydrogen peroxide)

As pointed out earlier in this section the hydrazine hydrate system proved to be generally cleaner, ignited more consistently, and burned more smoothly than the Naphferrol system under similar conditions. This was evident even from casual observation as well as from the roughness of the combustion as measured by the instantaneous pressure-time record from the G.M. capacitance-type gauge.

Most of the operational difficulties of Naphferrol are traceable to the large amount of solid material which it contains. Solid particles, probably iron oxides, were present at all times in the exhaust jet from the Naphferrol system. Accumulation of these solids in parts of the injector were a probable cause of some of the erratic pressure fluctuations obtained on the G.M. gauge equipment since these fluctuations were not consistently obtained and varied widely in magnitude and occured at several frequencies, which were constant for a short while.

The longer ignition-delay time for the Naphferrol-peroxide combination is obviously responsible for the hard starts and explosive starts which sometimes occurred for this system but which were never experienced with the hydrazine-based fuel. This longer ignition delay may also be at least

partially responsible for the pressure fluctuations obtained on the G.M. gauge. A long ignition delay could easily lead to breaks in the regular combustion process and a type of chuffing or "stop and start" reaction with its accompanying rise and fall in pressure. This is consistent with the quantitative results on the two systems indicating that the ignition dealy is a significant factor in determining the ease of combustion. The confined-mixing type of injector places more responsibility upon the "self-igniting" quality of the reactants to keep the entire combustion process going. In the open types of injection the reactants are more completely atomized and penetrate further into the combustion zone or that part of the combustion chamber where the high temperature gas reaction or flame propagation is already proceeding. Of course with the conventional methods of injection which are more similar to the present one-piece open-impingement injector, non-self-igniting fuels are employed successfully. [redacted]

The chief importance of the smoothness of combustion, in terms of those fluctuations which occur as rapidly as 60 cycles per second or more, may lie largely in the aid this knowledge would afford in analyzing the nature of the combustion. However, slower fluctuations, at least such as can be detected audibly as "knocking" combustion, have frequently been reported to affect rocket motor performance adversely not only due to accompanying poor combustion

efficiency but also by causing internal shocks and irreversible flow in nozzle performance with resulting nozzle losses of 5 to 10%.

Not only did the Helman type fuel perform more smoothly and consistently than the Naphferrol when used with concentrated peroxide in the micro motor studies, but the level of combustion efficiency as measured by the percent of theoretical chamber pressure obtained was also much higher regardless of the mixture ratio employed. With a given motor and method of injection, the dirrerence in these combustion efficiencies for the two systems was quite striking. This was found to be true for all the combustion chambers and methods of injection which were tested on both systems. The difference in the standard ignition delays for the two propellant systems is also quite appreciable. This correspondence between combustion efficiency and ignition delay would not logically be expected to prove very far-reaching, especially since completely non-self-igniting systems have given fairly good combustion, with efficiencies of 90 to 95% commonly reported in the literature. However, for the limited range of systems thus far studied on the micro-rocket stands, this dependence on ignition delay proved to be a very smooth relation as shown by the curves of Fig. 31. Other points on these curves resulted from using peroxide of varying concentration and from varying the amounts of catalyst in the Helman type fuels. Both of these changes

affected ignition delay as well as combustion efficiency of the motors to a small extent. This relation between combustion efficiency and ignition delay time is not completely unexpected however, especially with fuel systems in which one or both substances require a catalyst in order to be"self-igniting" or at least contain a catalytic material which affects ignition delay time. For, in this case, it seems only logical that a substance which catalyzes the oxidation-reduction reaction in the liquid phase of the mixed reactants would or at least might also catalyze the combustion reaction in the gaseous phase. Since both of the present fuels contain materials which can be classed as catalytic, this interpretation seems acceptable in the present case. This leads us to believe that catalysts which affect reactivity of the liquid reactants as measured by ignition delay, will in general prove useful in promoting the whole combustion process if it involves the same or similar reactants. This latter restriction may be necessary since the mechanism by which combustion is promoted by such catalysts may be their initiation of chain forming substances or chain carriers as a result of the type of reaction which they cause and accelerate either in the liquid phase or later on in the combustion process. At any rate, this relation between these catalysts which increases the ignitability of liquid-liquid reactants and combustion accelerators needs to be further investigated in order to determine their range of applicability or their

degree of selectivity relative to the fuels with which they will prove effective.

There can be little doubt of the beneficial effect on the combustion of the catalytic materials in the Helman (or hydrazine hydrate) fuel, at least on runs using combustion chambers with values of L* of 150 inches or lower. No appreciable effect of excess catalyst on combustion efficiency was noticed with runs in the large motor with an L* of 500 inches or over, which was used on the stationary stand. However, a careful study of this effect was not made on the large motor where excess catalyst was added in only a few runs merely to add color to the exhaust jet.

A report by the U.S. Naval Technical Mission (41) to Japan describes a study of the combustion of 80% H_2O_2 and the German C-stoff consisting of 30% $N_2H_4 \cdot H_2O$, 57% CH_3OH and 13% water with potassium cupro-cyanide added as a catalyst in the C-stoff. In this work, the Japanese experimenter employed a cylindrical combustion chamber with an L* of 195 inches, in connection with an intersecting conical sheet injector and a converging diverging exhaust nozzle. This motor produced a thrust of 175 lbs. at a chamber pressure of about 140 lbs./in^2. Upon varying the concentration of the $K_3Cu(CN)_4$ from 0 to 9 grams per liter of C-stoff in runs with this motor, no difference in performance was noted except for a peculiar sound in the combustion of the run with no $K_3Cu(CN)_4$ catalyst.

While this evidence conflicts with the observations

made in the present work, there are several possible explanations. One of the most obvious is that the precision of the Japanese work may not have been sufficient to detect the difference. Another is that with the relatively large combustion space and the particular method of injection used, there may not have been an appreciable difference produced in the combustion efficiency. Also the fuel used in the Japanese work was considerably different containing 57% of methyl alcohol and the catalyst was somewhat different since it contained no iron.

The combustion efficiency of the hydrazine-hydrate-peroxide propellant system has been found to be definitely superior to that of the Naphferrol-peroxide in all motors and with all injectors tested. The exact reason for this superiority is not apparent. The hydrazine-hydrate molecule is inherently less stable and more susceptible to oxidation under mild conditions than either methanol or ferrous naphthalene sulforate which are the two components of the Naphferrol fuel. However, it seems improbable that reaction rates would prove to be the factor controlling combustion efficiency under the conditions that exist in a rocket motor combustion chamber. Possibly the difficulty in vaporizing the solid component of the Naphferrol or any solid residue left from this component after the initial "self-igniting" reaction is a partial explanation of the lower combustion efficiency in the reaction of Naphferrol and hydrogen

peroxide.

3.) Combustion Chamber Volume or L*

All combustion chambers used in the present studies were cylindrical in shape with length to diameter ratios of about 2 to 1 or 3 to 1. Figures 17 and 18 of Page 84 are drawings of the various combustion chambers. No tests were made of the effect of changing the shape of the combustion chamber without a change in L* or relative combustion chamber volume.

The parameter L* is defined as the ratio of combustion chamber volume to nozzle throat area or V_c/A_t. Since for a given operating pressure A_t is approximately proportional to the mass flow rate of propellant for most propellant systems, L* is then an approximate measure of the volume available for reaction per unit mass of propellant.

Since all runs of the present study were carried out at a combustion chamber pressure near 300 psia, for a given propellant system L* is directly proportional to the average resident time of the reactants in the combustion chamber and is probably a good measure of the opportunity which is afforded for the combustion reactions to occur. However, it should be realized that the shape factor is important and the optimum L* for one length to diameter ratio may be different from that for another. The complete design of the best possible chamber requires the determination of the optimum L/D ratio or shape factor to insure arrival at

FIGURE 32 EFFECT OF L^* OR COMBUSTION CHAMBER VOLUME ON PERCENTAGE OF THEORETICAL PRESSURE OBTAINED

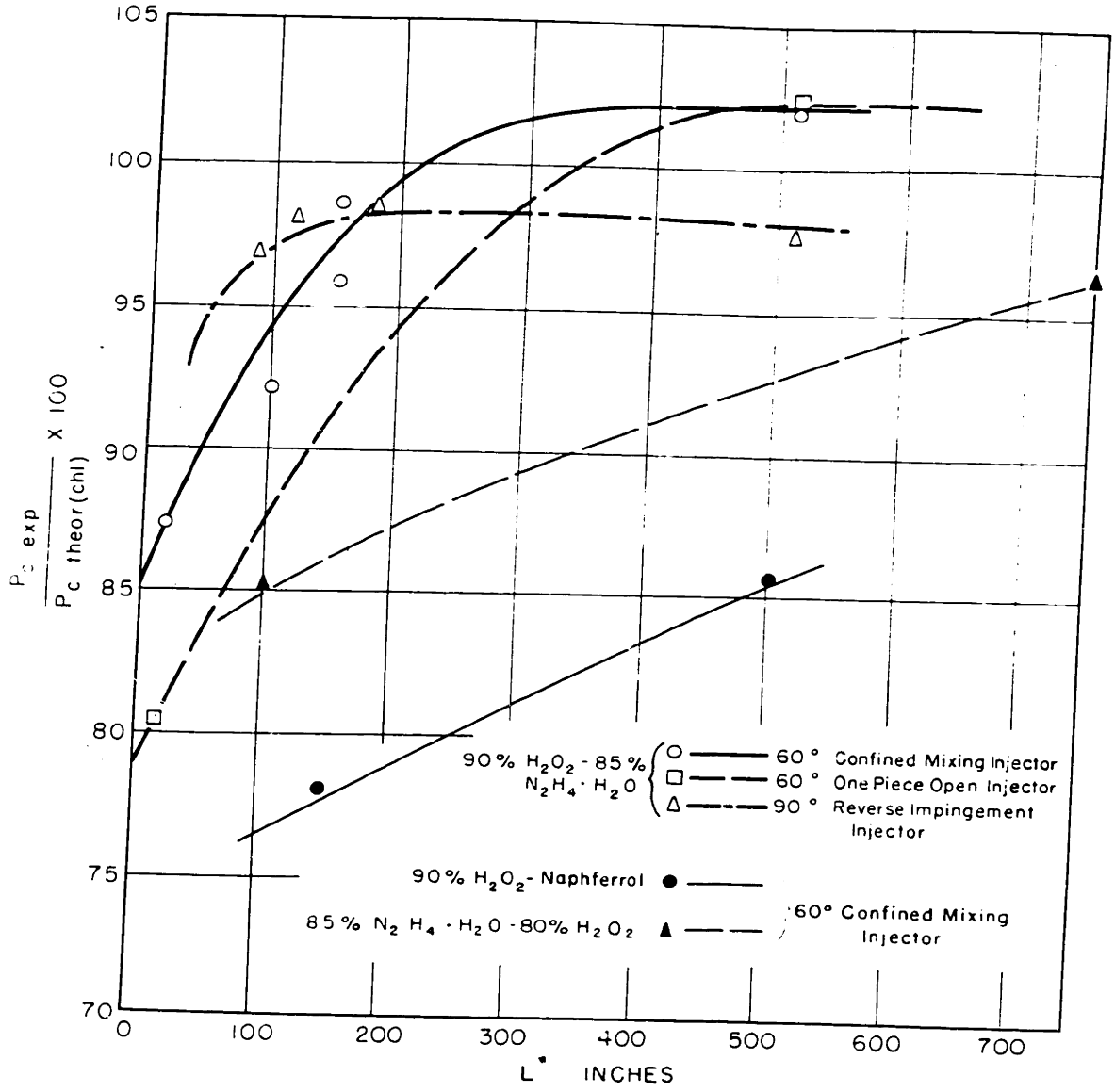

FIG. 33 EFFECT OF MIXTURE RATIO ON THE PERCENTAGE OF THE THEORETICAL CHAMBER PRESSURE EXPERIMENTALLY OBTAINED FOR THE SYSTEM 90 % H_2O_2 - 85 % $N_2H_4H_2O$

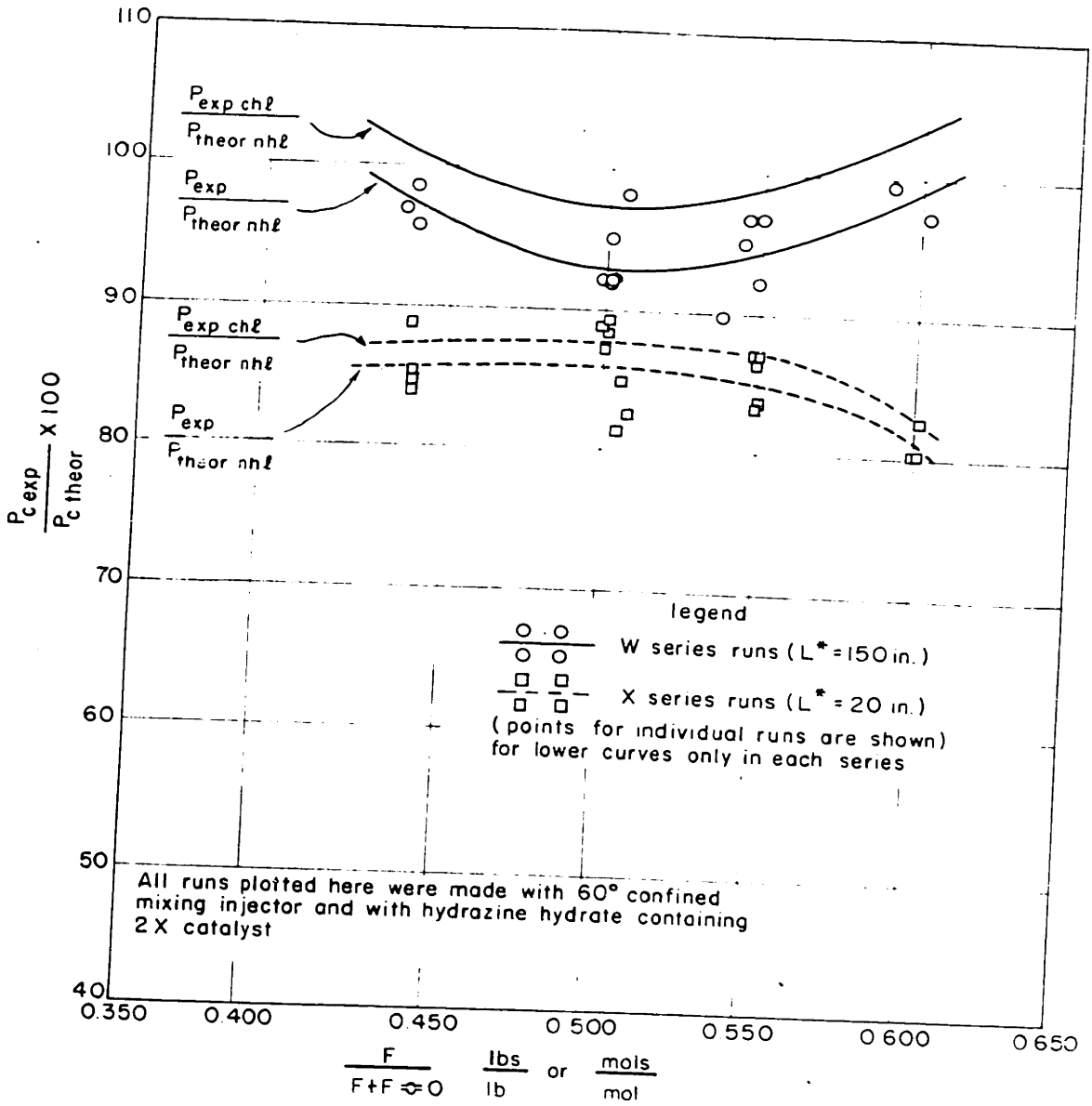

FIG. 34 EFFECT OF MIXTURE RATIO ON THE PERCENTAGE OF THE THEORETICAL CHAMBER PRESSURE EXPERIMENTALLY OBTAINED FOR THE SYSTEM 90% H_2O_2 - NAPHFERROL

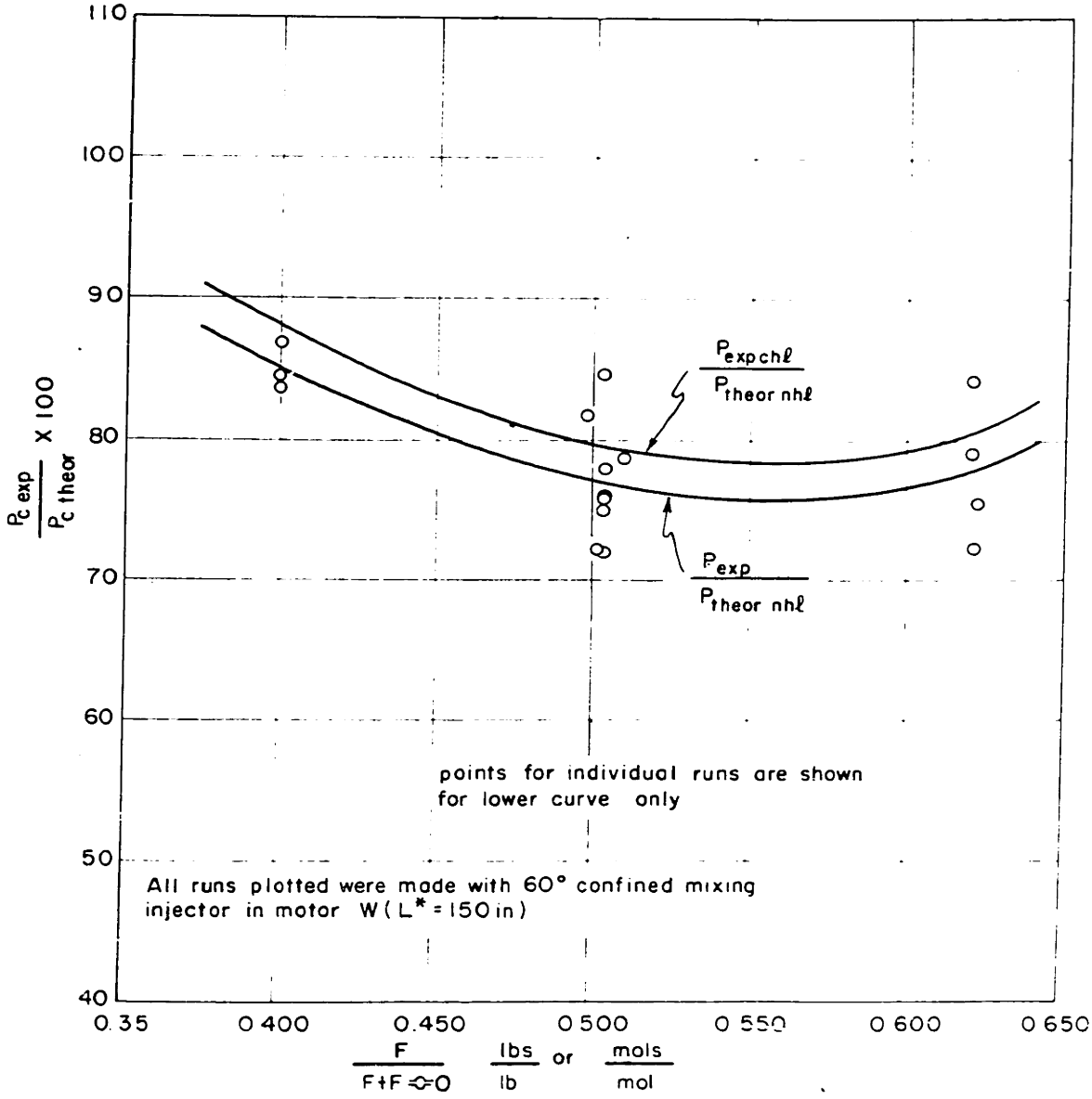

the design which represents the smallest possible L* that will produce a desired combustion efficiency. Some experimenters prefer to regard the major problem as the determination of the optimum diameter or cross sectional area and then to arrive at the optimum length of chamber for this diameter.

In the present study with a given propellant system, method of injection and motor design, combustion efficiency usually increases with increasing combustion space, up to a certain point at least. Under the conditions of the present study, as seen in Figure 32, the performance improved for the 90% H_2O_2 - 85% $N_2H_4 \cdot H_2O$ system up to L* values of about 200 inches, while there was at least still room for improvement with the Naphferrol system at L* values as high as 700 inches. For the three best methods of injection with the 90% H_2O_2 - 85% $N_2H_4 \cdot H_2O$ system, the combustion efficiency appeared to level off at a very high value of about 100% at L*'s of around 200 inches. While the other two systems studied had not reached 98% efficiency, at an L* value of 500 to 700 inches or more, this efficiency was nevertheless higher than was obtained in the smaller combustion chamber.

4.) Fuel to Oxidant Mixture Ratio

The effect of changing the mixture ratio on the combustion chamber efficiency for the two systems studied is shown in Figures 33 and 34. These runs were all made on the thrust stand where heat loss measurements were carefully

taken. Three average curves are shown for each set of runs. The lower curve in each case is the ratio of experimental chamber pressure to the theoretical chamber pressure calculated assuming no heat loss. The upper curves are for the ratio of experimental pressure to the theoretical chamber pressure corrected for heat loss and for the ratio of the experimental pressure corrected upwards for heat loss to the theoretical chamber pressure calculated assuming no heat loss. This last ratio is the one which should most nearly represent the performance that would be obtained in a conventional size motor (where heat loss is negligible) assuming attainment of the same combustion efficiency in both cases.

The mixture ratio function used in Figures 33 and 34 is called the generalized fractional fuel in the system and defined as the ratio of mols of fuel used to the sum of the mols of fuel plus the mols of fuel which are stoichiometrically equivalent to amount of fuel is the amount theretically required to react completely with the given amount of oxidant so as to produce only H_2O, CO_2 and N_2 in the reaction products. The advantage of this particular mixture ratio function used is that the stoichiometric mixture for all systems occurs at 0.5 and the entire range of mixtures from pure oxidant to pure fuel covers the range from 0 to 1.

The combustion efficiency curves of Figures 33 and 34 show no common shape for all cases nor even for the same system in the two different combustion chambers used. From

Figure 33, performance in the larger motor is seen to be definitely superior. However, due to the greatly expanded scale of these plots and to the spread of points at a given mixture ration, the exact shape of the three curves in the two plots cannot be considered as definitely fixed.

If the effect of the mixture ratio on combustion efficiency is accepted to be as shown in the curves Figures 33 and 34, one possible explanation which can be applied fairly consistently to all three curves is the following: In general it can be said that in a rocket motor combustion chamber, the overall reaction rate may be controlled either by the velocity of the chemical reaction or by the efficiency of the physical mixing processes, more probably by the latter. In either case, an excess of one reactant aids in the rapid completion of the combustion process. In the most usual fuel-oxidant propellant system composed of all of the elements C, H, O and N, the oxidant consists of only O, H and N while the fuel consists of C plus some or all of the other three elements. Under this condition, an excess of oxident is more likely to minimize the mixing problem than an excess of fuel. This is true because the excess fuel must be mixed with the products of reaction in order for the carbon to reach chemical equilibrium and release all of the available energy whereas the excess oxidant need only be decomposed to yield O_2 and H_2 and N_2 if H and N are present since these compounds are substantially the equilibrium state for these

elements in most combustion gas mixtures. Although H_2 does enter into the water gas equilibrium, this is a relatively unimportant reaction as it involves both heat release and molecular weight. Accordingly the most probable effect of mixture ration upon combustion efficiency would be expected to find performance at oxidant rich mixtures superior to that at stoichiometric as well as that at fuel rich mixtures. Combustion efficiency at fuel rich mixtures might be expected to be about the same as that at stoichiometric in general but perhaps slightly higher or lower for certain systems depending upon individual fuel and oxidant compositions. The curves of Figures 33 and 34 are seen to be in fair accord with this picture. The most striking inconsistency is in the fuel rich mixtures of the two curves of Figure 33. In the larger motor (W) the combustion efficiency for the peroxide-hydrazine hydrate system at fuel rich mixtures is higher stoichiometric, whereas in the smaller motor (X), the reverse is true. No reason for this is evident from the above analysis. In fact since the fuel is composed only of H, N and O, the problem of mixing excess fuel with products of combustion is not present and therefore the superior performance obtained in Motor W would be expected. The cause of the reverse behavior in the case of Motor X may be due to the increased importance of liquid-liquid mixing in this very small volume motor. ($L^* = 20$ inches). In this hypothesis, the possibility of effecting nearly complete liquid-liquid mixing

down to molecular dimensions within the ignition delay time is assumed. With an almost homogeneous liquid mixture the "self-igniting" reaction can almost immediately produce a combustion mixture which is almost completely reacted to chemical equilibrium, thus effecting a tremendous saving in space which would otherwise be required for vapor-vapor mixing and reaction. Since the stoichiometric mixture of the hydrogen peroxide - hydrazine hydrate system is much more nearly in equal volumes than the very fuel rich mixture of Figure 33, the nearly homogeneous liquid mixture required for the instantaneous ignition combustion reaction postulated above would be more closely achieved in the case of the stoichiometric mixture.

Overall Motor Performance

The overall efficiency of a rocket motor is ordinarily considered to depend upon the efficiency of its two main parts, the combustion chamber and the exhaust nozzle. The chief reason for making the measurements of thrust and overall motor performance is to obtain data which will serve as a check on the combustion efficiency as well as a measure of nozzle efficiency.

All of the factors which have been discussed thus far have been connected with the performance of the rocket motor combustion chamber which is generally taken to include the converging section of the exhaust nozzle. Any additional inefficiency in the overall rocket motor performance, therefore, must be introduced in the diverging section of the exhaust nozzle.

The efficiency of a well designed converging-diverging, de Laval type nozzle, can be predicted fairly well in most cases. (Some of the theoretical considerations of nozzle design are presented in Appendix D). Those exhaust nozzles which are commonly used on rocket motors for actual propulsion employ rather wide divergence angles but generally maintain between 96 and 98% efficiency in most cases when operated at a single design condition. Consequently the determination of the inefficiency of the exhaust nozzle is not ordinarily a major problem in the experimental study of a rocket engine. However, an attempt has been made to

FIG. 35 VARIATION OF SATTERFIELD ENTHALPY FUNCTION AND THEORETICAL AND EXPERIMENTAL SPECIFIC IMPULSE WITH MIXTURE RATIO FOR THE SYSTEM 90% H_2O_2 - 85% - $N_2H_4 \cdot H_2O$ (W SERIES RUNS)

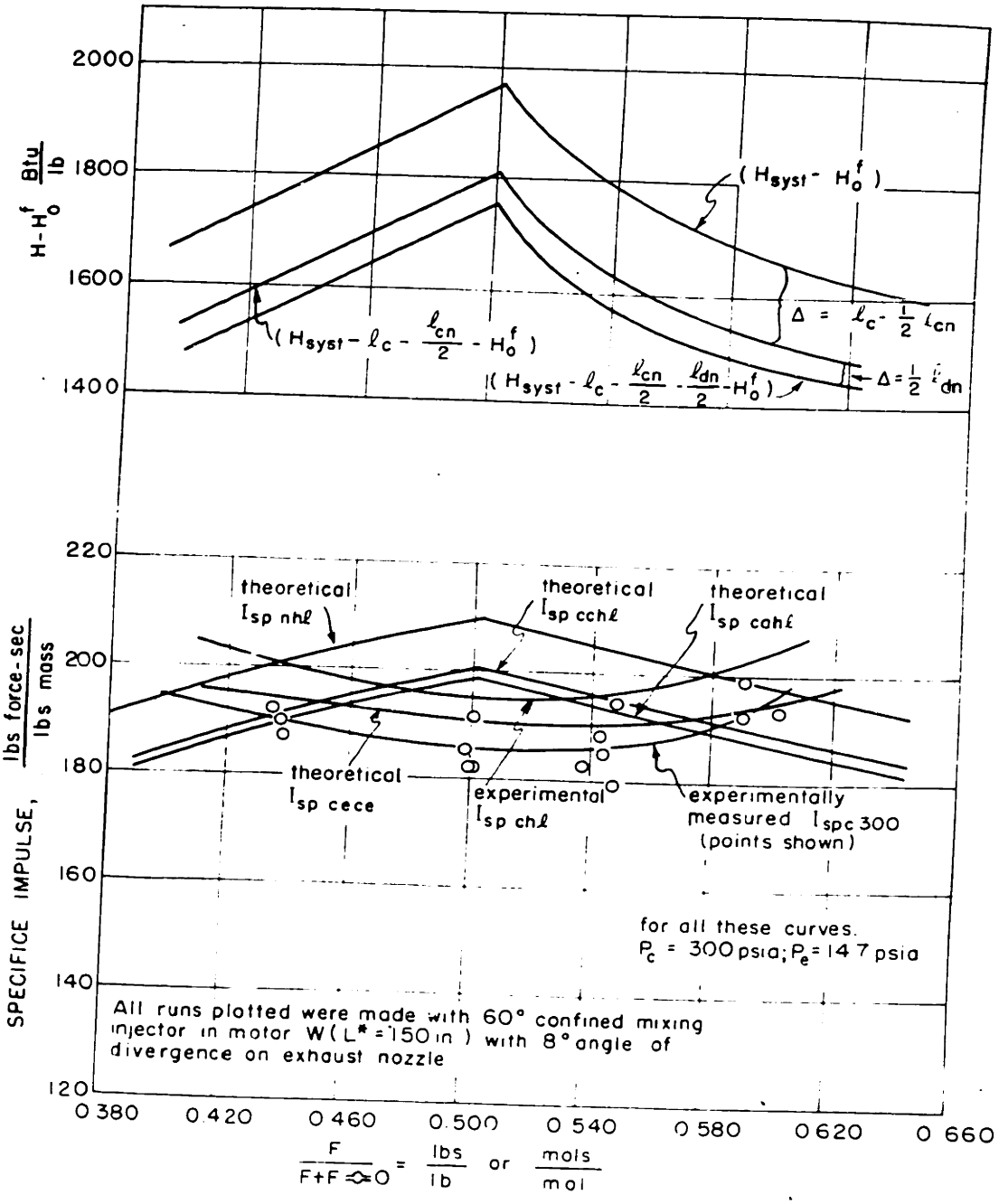

FIG. 36 VARIATION OF SATTERFIELD ENTHALPY FUNCTION AND THEORETICAL AND EXPERIMENTAL SPECIFIC IMPULSE WITH MIXTURE RATIO FOR THE SYSTEM 90% H_2O_2 - 85% $N_2H_4H_2O$ (X SERIES RUNS)

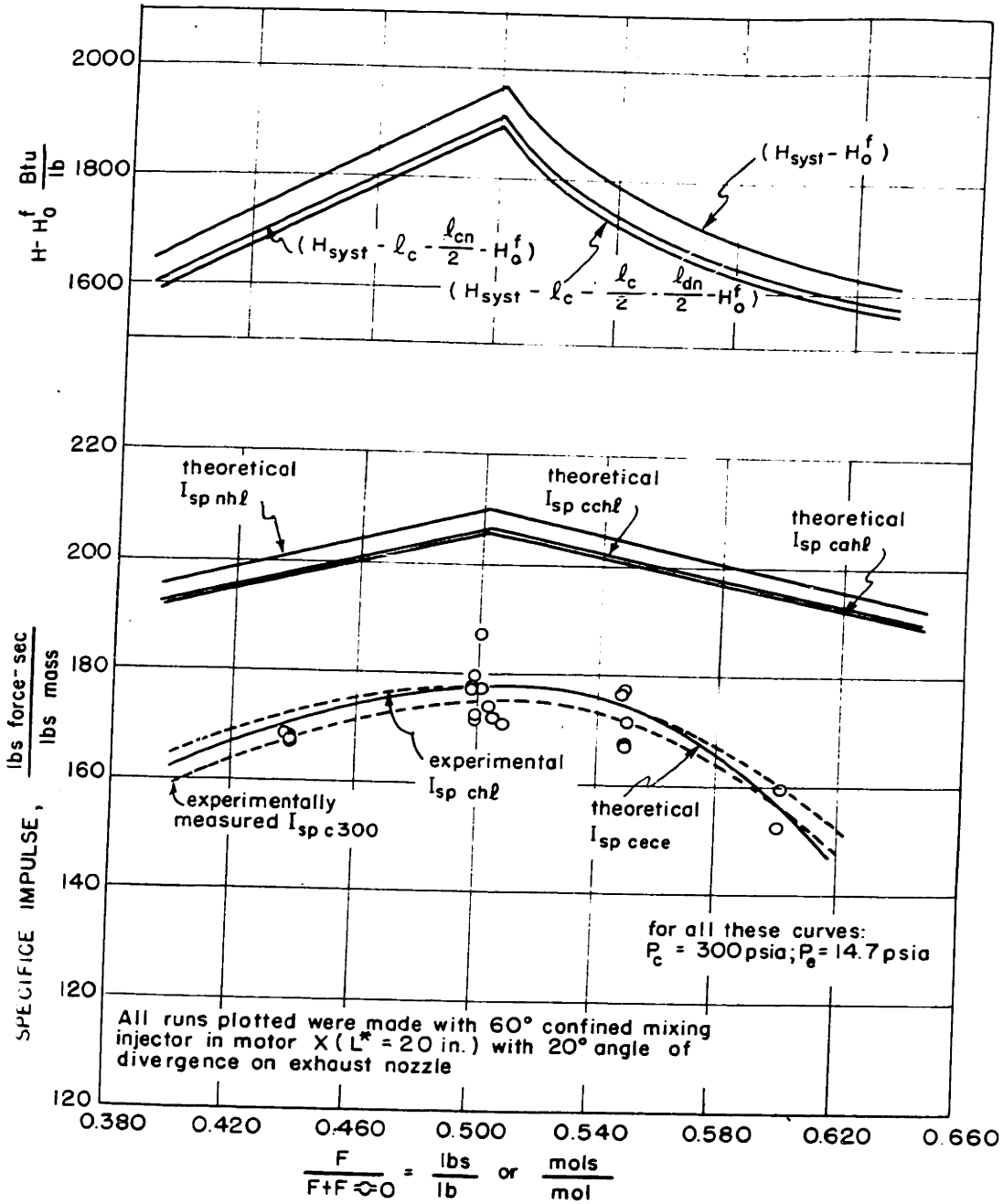

FIG. 37 VARIATION OF SATTERFIELD ENTHALPY FUNCTION AND THEORETICAL AND EXPERIMENTAL SPECIFIC IMPULSE WITH MIXTURE RATIO FOR THE SYSTEM 90% H_2O_2 NAPHFERROL (Y SERIES RUNS)

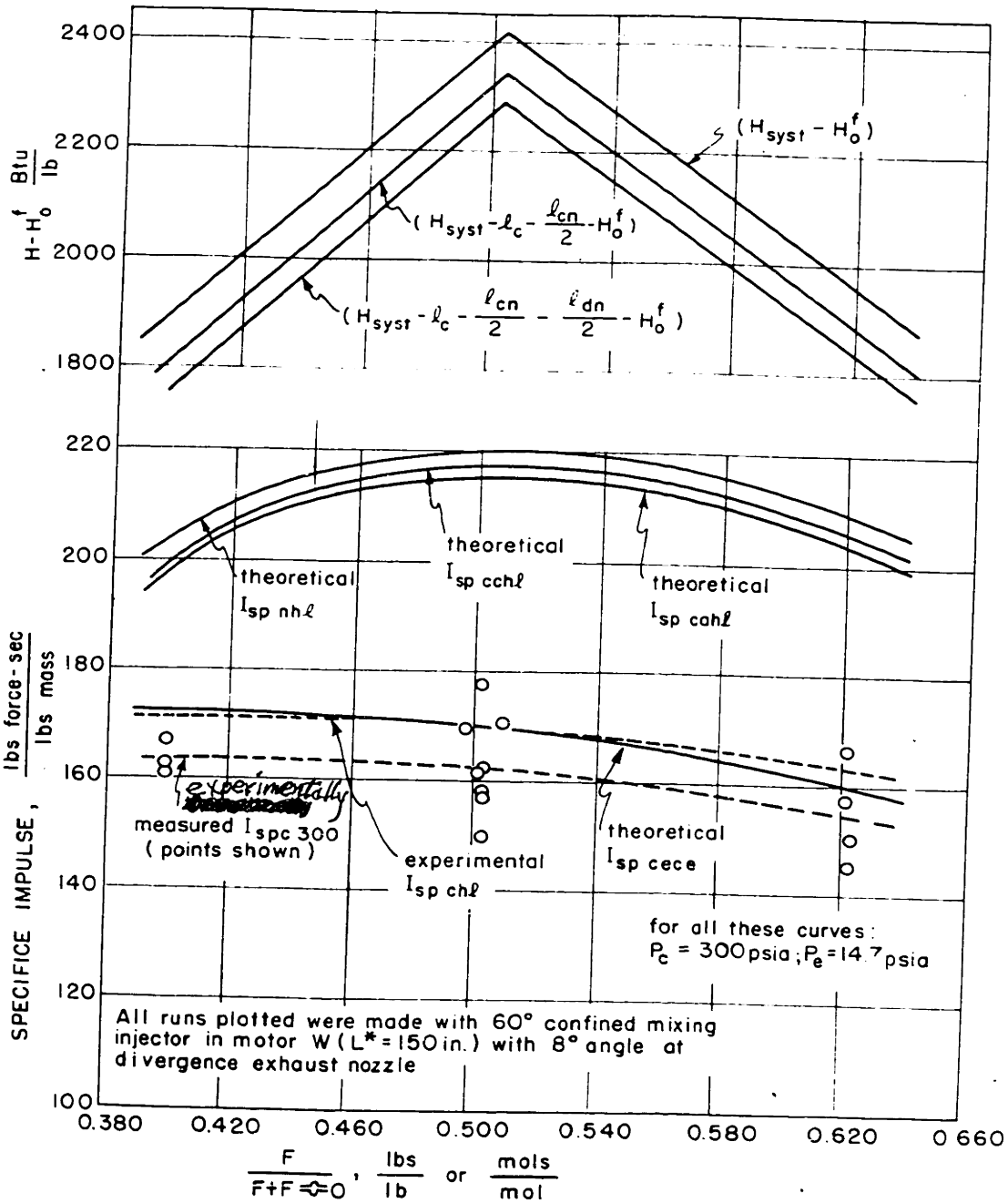

evaluate the efficiency of the exhaust nozzles used in the present study in order to complete the evaluation of the micro-reaction motor technique and thus determine if there are any appreciably larger losses due to the small scale of operation.

These overall performance figures for the two propellant studies are presented as curves of specific impulse against the same parameter, generalized fuel fraction, previously used in the lower part of Figures 35, 36 and 37. It should be recalled that the specific impulse is calculated from the ratio of thrust force and mass flow rate being defined as the total impulse produced per pound of propellant used. Comparison of these experimental curves with those for theoretical specific impulse which are also presented (both corrected to a chamber pressure of 300 psia) show a deviation in each case which parallels that of the corresponding curve of combustion chamber efficiency versus the generalized fracional fuel function presented previously in Figures 33 and 34.

As with combustion chamber efficiency, the overall performance of the one-inch diameter motor (Motor W) with an L* of 150 inches was much higher for the hydrazine-based system than for the Naphferrol system even in spite of the fact that theoretically the specific impulse of the latter system sould be the higher. This emphasizes the importance of good combustion chamber efficiency as was obtained in the

case of the 85% hydrazine hydrate - 90% hydrogen peroxide system. Even when used in a smaller combustion chamber (Motor X) of 1/2 inch diameter and L* of only 20 inches, this system gives comparable overall performance to that of the Naphferrol system in the larger motor as seen by comparison of the experimental curves of Figures 36 and 37.

As with the values of combustion efficiency, these overall performance figures are subject to slight corrections due to the unusually high amount of heat loss which is special to "micro" rocket operation. Again the theoretical performance can be corrected downwards for the effects of an equivalent amound of heat loss to that actually experimentally measured or the experimental performance figures can be corrected upwards for the additional energy which would have been available had the heat loss not taken place. These corrected curves based on an arm expansion process from 300 to 14.7 psia ps.2 are also presented in Figures 35, 36 and 37. However, the individual points are shown only for the uncorrected experimental curve to avoid confusion. These corrected curves obtained using working plots similar to those presented in the section of Thermodynamics. Three heat loss correction curves are shown for each set of data. The first is a correction of the theoretical specific impulse for the average amount of heat lost in the combustion chamber and in the converging nozzle. The second is an additional correction to this theoretical figure for the average

amount of heat lost in the diverging nozzle. The third correction curve represents a correction of the experimental specific impulse upwards for the effect of the combined heat losses of both chamber and exhaust nozzle. This curve represents most nearly the overall performance that should be obtained on a conventional size reaction motor provided the same efficiencies of the combustion process and of the expansion process through the exhaust nozzle were obtained.

Nozzle Efficiency

Nozzle efficiency is usually judged by a comparison of the experimentally measured nozzle coefficient, C_F, with the theoretical value of this parameter. The experimental value of C_F is easily obtained from the measured quantities in the following defining equation

$$C_F = \frac{F}{P_c A_t}$$

The theoretical value of C_F is a function of the isentropic exponent γ or C_p and MW and the pressure ratio P chamber/P exhaust as seen from Equation 46 (a or b) of the Thermo. Section. Since the experimental chamber pressure is known, this theoretical value of C_F can be calculated if γ can be estimated. This maximum value of C_F at the optimum nozzle design increases with increasing pressure ratio for a given γ as well as with decreasing values of γ for a given pressure ratio. Since γ tends to increase for the gaseous reaction products of a given propellant system as combustion is less and less complete, the theoretical value of C_F assuming complete combustion will not be the same but will be higher than the theoretical value of C_F for some actual measured combustion efficiency. Therefore, it would appear that for those cases in which combustion efficiency is appreciably lower than 100%, that the theoretical value of C_F should be calculated using the properties of the real gas mixture rather than those of the gas mixture theoretically resulting from complete combustion.

The experimental and theoretical values of C_F were calculated for each thrust stand run and are included for comparison in the tables of calculated values in Appendix P. For the reason given above, the theoretical value of C_F was calculated using the estimated properties of the actual combustion gas mixture. In most runs the experimental value of C_F is between 95 and 100% of the theoretical value. However, in a few runs these figures reach the extremes of 94 and 102%. Values in excess of 100% must obviously be due to either experimental errors or incorrect theoretical assumptions or both. In any case the variation in these figures for check runs is rather large and only an average value of nozzle inefficiency for all check runs has much significance.

This comparison of the average nozzle efficiency of several runs under fixed conditions can be made more easily from the specific impulse curves however. A sample calculation is made in Appendix K showing how the theoretical specific impulse which would be reached by the system in question with the experimentally obtained combustion efficiency can be approximated fairly closely. This is done by correcting the energy available (or the combustion temperature in other words) sufficiently to produce the experimental pressure without correcting the gas composition at all from that corresponding to complete combustion to equilibrium conditions and then calculating the specific impulse for a gas mixture of this initial temperature and gas composition expanding from 300 to 14.7 psia. This was done for each run

and the average curves are shown (without data points) on Figures 35, 36 and 37. Comparison of these curves with the curves through the measured experimental data points is a good indication of the average nozzle efficiency for each nozzle.

This comparison indicates that in the case of the nozzle with an 8° angle of divergence, which was used in runs with Motor W, the nozzle efficiency was about 98% (97 to 99%) for various mixture ratios for the Hydrazine Fuel System and about 96% (95 to 97%) for the Naphferrol combination. In runs on the X motor (1/2" diameter) with an L* of only 20 inches, an exhaust nozzle with a 20° angle of divergence was used. In these runs which were all made with the Hydrazine fuel, the nozzle efficiency averages about 98% at all mixture ratios.

Thus it appears that the average nozzle inefficiency lies between 5 and 1% at all of the mixture ratios studied in both systems. The overall average nozzle efficiency for both nozzles used and for both systems studied appears to be about 97% which is very little if any lower than that obtained with conventional size motors. However, a greater part of the performance loss with the nozzles of conventional size motors is due to the larger angles of divergence which are used. The theoretical effect of divergence angle on thrust or specific impulse is discussed in Appendix D on Nozzle Design. The friction losses in the micro size exhaust

nozzles are therefore probably somewhat higher than in larger scale nozzles which might be expected because of the larger ratio of surface area to mass flow rate.

The experimental results on the hydrazine hydrate fuel system indicate about the same inefficiency for the 8° divergence angle nozzle as for the 20° divergence angle design. Since the theoretical thrust correction factor for the 20° angle of divergence amounts to nearly 1%, the friction losses on the two nozzles would appear to be 2% and 1% respectively. However, this difference is small and can be regarded only as an indication of the trend because of the possible experimental error and because of approximations in the theoretical calculations. Since the surface area is larger for the small angle of divergence, this apparent difference in friction losses is in the right direction at least.

Accuracy and Precision of Results

The probable and maximum errors in the individual experimental measurements of this thesis have already been discussed in the section dealing with Apparatus and Procedure. These figures were estimates based on the apparent precision of the individual measurements plus recognition of the frequent careful calibrations which were made on all instruments and an estimate of the accidental error in making the various readings required. On this basis, these maximum and probable errors in individual measurements can be summarized as follows:

Quantities Used in Calculating Theoretical Chamber Pressure

Quantity	Estimated Max. Error	Estimated Probable Error
mass flow rate, $\dot{m}$	1%	0.5%
nozzle throat area	3%	1.5%
heat losses	10%	5.0%

Quantities Used in Experimentally Determining Chamber Pressure

pressure, P_c	1%	0.5%

Quantities Used in Calculating Theoretical Specific Impulse

pressure, P_c	1%	0.5%
pressure, P_e	1%	0.5%
Heat losses	10%	5.0%

Quantities Used in Calculating Experimental Specific Impulse

Quantity	Estimated Max. Error	Estimated Probable Error
Thrust Force, F	3%	1.5%
Mass flow rate, $\dot{m}$	1%	0.5%

In addition to the errors in experimental measurements, in calculating theoretical performance figures there are additional sources of error due to theoretical approximations and assumptions. The correlations of the generalized Satterfield chart represent a maximum deviation of 1% from the calculation of the same quantities rigorously. The quantities of molecular weight and temperature are usually obtained from this source and are therefore subject to maximum errors of 1% and probable errors of about 1/2%. There are also small errors in the evaluation of the isentropic exponent γ due both to use of the generalized Satterfield data in calculating this quantity in some cases and to approximations concerning the proper mean value to be used. However, due to the low temperature and relative lack of dissociation in the systems of this thesis this latter error is extremely small. Moreover, an error of one percent or less in γ will cause no appreciable error in either P_c or I_{sp} as pointed out previously in the section on Thermodynamics by use of figures 2 and 3. Consequently the effect of errors in γ will be neglected in the present analysis of probable

FIG.38 THRUST FORCE VERSUS PRODUCT OF CHAMBER PRESSURE AND NOZZLE THROAT AREA FOR RUNS WITH STOICHIOMETRIC MIXTURE OF 90% H_2O_2 AND 85% $N_2H_4H_2O$

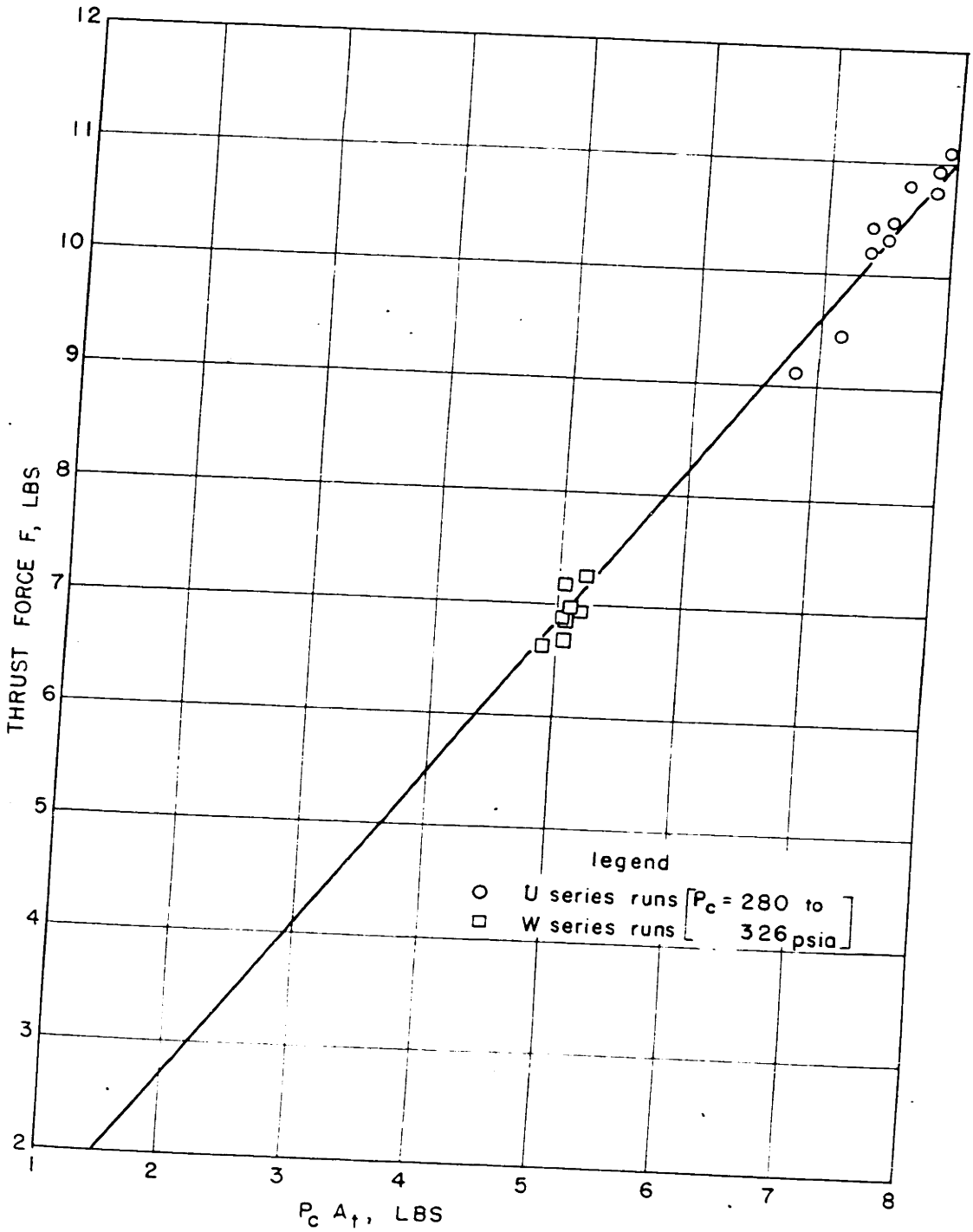

error in results.

It should also be noted that errors in measured heat loss are diminished by at least one tenth in their effect on calculated chamber pressure or specific impulse since the corrections of these quantities due to heat loss never amount to more than 10%.

Using these figures tabulated above for experimental errors and the above estimates of errors due to methods of making theoretical calculations, the maximum probable and most probable errors in the calculated results of comparisons between experimental and theoretical chamber pressures or between experimental and theoretical specific impulse values can be calculated to be as follows:

Result	Maximum Probable Error	Most Probable Error
Comparison of Theor. & Exp. P_c	3.54	1.75
Comparison of Theor. & Exp. I_{sp}	3.46	1.73

To give an idea of the precision of the measurements of Thrust, (F), chamber pressure, (P_c) and nozzle throat area, (A_t), which are required to measure nozzle thrust coefficient, (C_F), Figure 38 contains a plot of F against the product $P_c A_t$ for W and U Series runs on the stoichiometric mixture of 85% $N_2H_4 \cdot H_2O$ and 90% H_2O_2. High combustion efficiency was obtained in all these runs and the chamber pressure in all lies between 280 and 320 psia. Hence

a straight line through the origin should pass through or near most of the points, or in other words C_F should be constand within about 1% for all these runs. It can be seen from Figure 38 that such a line does fit the experimental points within ±3%. Therefore a precision of within 2% on these three combined experimental measurements is indicated.

Importance of Heat Loss in Micro Rocket Studies

The heat loss in the combustion chamber and the exhaust nozzle of the micro rocket motors was measured on the thrust-stand runs. From this data the actual experimental performance figures were corrected according to theory to values they would have in an adiabatic system, such as is approached in a 1000 lb. thrust motor. (See Appendix F).

The effects of these heat loss corrections can be seen in the curves of combustion chamber performance and overall performance previously given in Figures 33, 34, 35, 36 and 37, for the two systems studies extensively. The actual average amount of heat lost per pound at each mixture ratio of the two systems studied is shown on the enthalpy curves above the overall specific impulse performance curves of Figures 35, 36 and 37. There are three enthalpy curves shown on each of these plots. The top curve represents the initial enthalpy (above the products of reaction at 0°K) of the unburned mixture assuming the reactants enter the system in each case at 300°K. The second curve is derived from the first by subtracting the average heat loss in the combustion chamber plus one half the average heat loss in the converging nozzle in Btu's per pound of reactants at each mixture studies. The third curve is derived from the second by subtracting at each mixture ratio studied one half of the average heat lost in the diverging nozzle in Btu's per pound of reactants. From these curves on the three plots it can be seen

that the maximum total change in initial enthalpy thus affected occurs at an $F/F + F_{H_2O}$ ratio of 0.607 in the system 85% Hydrazine Hydrate / 90% Hydrogen peroxide operating in the combustion chamber with L* of 150 inches and with an exhaust nozzle with an 8° angle of divergence. The change in initial enthalpy due to the loss of heat in the chamber and converging nozzle amounts to 8.99% while the total change in initial enthalpy for motor and entire nozzle heat loss is 12.22%. In the smaller combustion chamber with a 20° angle of expansion in the exhaust nozzle all the heat loss quantities are much lower. This is due to the much smaller surface for heat transfer per pound of reactants. In the larger motor with an 8° angle of expansion exhaust nozzle but operating with the Naphferrol system the heat loss quantities are somewhat lower. In this case the decrease is largely in the combustion chamber and is probably due to the lower temperatures existing in most of the chamber due to slow and/or poor combustion.

The effect of these heat losses on the performance parameters of the micro motor operation is much less however than on the initial enthalpy of the system. Table 2 shows the maximum percentage change in enthalpy for each system studied in each motor and with each exhaust nozzle and the corresponding maximum percentage change in the combustion efficiency and the specific impulse which resulted from these heat losses.

The net corrections which these heat losses effect in the final performance figures can be seen to be quite small. This means that the chance of errors being introduced in making these corrections is correspondingly small. Therefore, the reliability of these corrected results can be considered to be essentially the same as that of the original experimental results. This in effect eliminates most of the disadvantage of the micro motor technique of obtaining qualitative performance compared to the operation of a large scale reaction motor where such corrections can be eliminated completely. This is true because the time and trouble of making the corrections is small compared to the extra effort and expense involved in operating a larger reaction stand. The important thing is that the corrections can be made without introducing appreciable error. While the percentage of the initial enthalpy lost as heat to the surroundings might be somewhat larger for a really "hot" propellant system, the correction calculations should still be applicable with less than one percent error with heat losses up to double the amounts measured in the maximum case of the present work.

The results reported here offer a good indication that the heat loss on a 10 lb. thrust motor is not sufficient to affect the reaction rate appreciably. The chief evidence of this is the extremely high combustion efficiency which was reported on motor W runs, where the highest heat loss of all was measured. Since most reaction rates increase with

temperature, some slight impairment of combustion efficiency might theoretically be expected with heat losses of 10% or more, but the present indications are that is not at all serious.

FIGURE 39
THERMOCOUPLE WELL POSITIONS IN MOTOR B

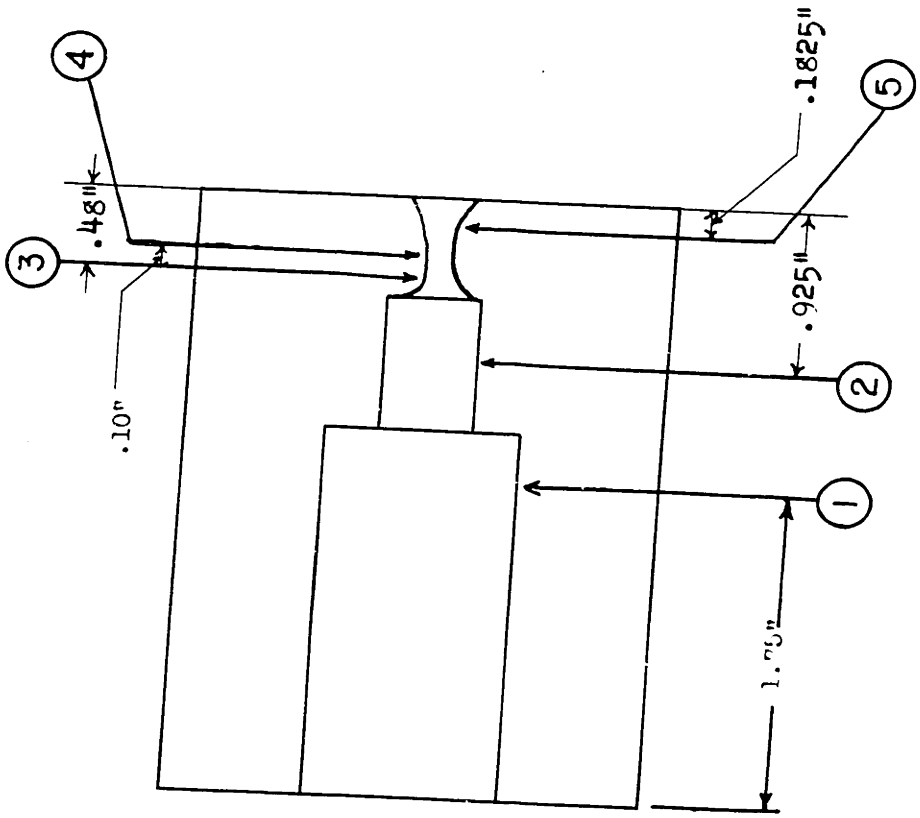

Average Heat Transfer Rates in Combustion Chamber and Exhaust Nozzle

In the course of measuring heat losses on the thrust-stand runs, average heat transfer rates were obtained for the combustion chambers and exhaust nozzles of Motors W and X. The average values of these average rates for all check runs are given in Table 3 for comparison of the effects on these rates of such factors as chamber diameter, propellant system and exhaust nozzle design.

Attempts were made to obtain point values of the heat transfer in Motor B on the stationary stand by obtaining temperature gradients through the thick copper wall using four radially placed thermocouples at each of several stations along the length of the motor. This work was done by Borden (9). While the probable accuracy of his measurements is not high, the results are interesting for comparison with the average heat transfer rates given above. This motor was operated with the 90° reverse impingement injector on a stoichiometric mixture of 85% $N_2H_4 \cdot H_2O$ and 90% H_2O_2 in all cases. At a flow rate of about 0.0365 lbs. per second the following point heat transfer rates (averaged for three or more runs) were obtained at the positions stated and shown in Figure 39.

TABLE 3

AVERAGE HEAT TRANSFER RATES IN MICRO ROCKET MOTORS

(60° confined mixing injector)

A. COMBUSTION CHAMBERS

PROPELLANT SYSTEM	$\frac{F}{F/F=0}$ in $\frac{lbs.}{sec.}$	$Q^{Av.}_{chamb.}$ $\frac{Btu}{sq.in..sec.}$ for 1" diam. chamb.	$Q^{Av.}_{chamb.}$ $\frac{Btu}{sq.in..sec.}$ for 1" diam chamber
80%H_2O_2-85%$N_2H_4 \cdot H_2O$	0.526 0.0558	0.496	-----
90%H_2O_2-85%$N_2H_4 \cdot H_2O$	0.500 0.0557	0.581	-----
" "	0.500 0.0365	0.568	0.946
" "	0.549 0.0350	0.601	0.873
" "	0.600 0.0370	0.567	0.776
" "	0.438 0.0363	0.590	0.929
" "	0.500 0.0365	0.601	2.470*
90%H_2O_2-Naphferrol	0.500 0.0367	0.345	-----
" "	0.622 0.0401	0.312	-----
" "	0.399 0.0399	0.361	-----

* For a short ½" diam. section added to chamber W when operated with a 20° angle nozzle.

B. EXHAUST NOZZLES

PROPELLANT SYSTEM	$\frac{F}{F/F=0}$ in $\frac{lbs.}{sec.}$	$Q^{Av.}_{nozzle}$ $\frac{Btu}{sq.in..sec.}$ for 8° Angle nozzle	$Q^{Av.}_{nozzle}$ $\frac{Btu}{sq.in..sec.}$ for 20° Ang. nozzle
80%H_2O_2-85%$N_2H_4 \cdot H_2O$	0.526 0.0558	0.496	-----
90%H_2O_2-85%$N_2H_4 \cdot H_2O$	0.500 0.0557	0.581	-----
" "	0.500 0.0365	0.568	0.946
" "	0.549 0.0350	0.601	0.873
" "	0.600 0.0370	0.567	0.776
" "	0.438 0.0363	0.590	0.929
" "	0.500 0.0365	0.601	2.470*
90%H_2O_2-Naphferrol	0.500 0.0367	0.345	-----
" "	0.622 0.0401	0.312	-----
" "	0.399 0.0399	0.361	-----

Position (See Figure 39)	q_{Pos} in $\frac{Btu}{sq.in. \cdot sec.}$
(1) Near End of 1" diameter section	1.33
(2) Near End of ½" diameter section	1.58
(3) In converging nozzle section	3.90
(4) At nozzle throat	7.80
(5) In diverging nozzle section	2.80

These mean values usually checked within ±12% for the most widely differing runs. However, values between the individual thermocouples at a given station were sometimes in disparity by 25% from the average value for that run.

Scale of Operation

Having obtained complete operational data on two liquid propellant systems on a micro scale reaction motor, it should be possible to make a fairly accurate appraisal of the manner in which small scale operation affects general rocket motor performance. Based only on the results which have been pointed out and discussed already, it appears that the following remarks are now justified.

1.) The heat loss per pound is higher than in conventional size motors. However, at a 10 lb. thrust size the net effect of the maximum heat loss on performance figures appears to be reasonably small (5 to 10%) and fairly accurate corrections for this loss in energy can easily be made.

2.) Fairly simple methods of injection produce combustion efficiencies comparable to those measured in large scale rocket chambers. Micro motor injectors have the disadvantage of comprising a small number of units (a single one in the present study) but this difficulty has not proved serious since performance has not been very erratic. To be sure, injection methods specific to the micro-rocket could not be expected to prove of great utility in large-scale motors; on the other hand, the injection device is commonly a development problem on each new motor design.

3.) The combustion efficiencies and nozzle efficiencies are both high--of the same order as usually obtained in conventional rocket studies.

Scale of Operation

Having obtained complete operational data on two liquid propellant systems on a micro scale reaction motor, it should be possible to make a fairly accurate appraisal of the manner in which small scale operation affects general rocket motor performance. Based only on the results which have been pointed out and discussed already, it appears that the following remarks are now justified.

1.) The heat loss per pound is higher than in conventional size motors. However, at a 10 lb. thrust size the net effect of the maximum heat loss on performance figures appears to be reasonably small (5 to 10%) and fairly accurate corrections for this loss in energy can easily be made.

2.) Fairly simple methods of injection produce combustion efficiencies comparable to those measured in large scale rocket chambers. Micro motor injectors have the disadvantage of comprising a small number of units (a single one in the present study) but this difficulty has not proved serious since performance has not been very erratic. To be sure, injection methods specific to the micro-rocket could not be expected to prove of great utility in large-scale motors; on the other hand, the injection device is commonly a development problem on each new motor design.

3.) The combustion efficiencies and nozzle efficiencies are both high--of the same order as usually obtained in conventional rocket studies.

RESULTS OF TESTING THE VARIOUS METHODS OF CALCULATING THEORETICAL PERFORMANCE BY COMPARISON WITH THE RESULTS OF A THEORETICAL ANALYSIS USING A MOLLIER TYPE DIAGRAM

The various methods actually used in calculating theoretical performance in this thesis as well as those additional methods which were tried out for purposes of comparison have already been discussed in the section on Thermodynamics.

Of all of these methods, those carried out graphically with the aid of a Mollier diagram of the equilibrium combustion gases were on the soundest basis and could be carried out with most assurance. A Mollier diagram was constructed for the system 90% Hydrogen Peroxide and 85% Hydrazine Hydrate in stoichiometric proportions (as described in Appendix M). A similar diagram constructed by R. H. Boll ([C-1]) was available for the system red fuming Nitric Acid (6.5% NO_2) and Aniline in a mixture ratio of 3 lbs. acid to 1 lb. aniline. However, for general use the considerable labor involved in constructing such diagrams for the many different systems and mixture ratios which might be of interest almost precludes the use of this method. Accordingly the simpler analytical procedures previously presented were developed in the interest of obtaining methods of general utility. Due to some questionable assumptions or uncertain approximations in all of these

simpler calculating methods, it was desirable to test the accuracy of each. This was done for the two systems given above by comparing calculations for representative cases by each of these methods with similar calculations by the graphical technique on the Mollier diagram.

Sample calculations by all these various methods are performed in Appendix L. The accuracy of the manipulations involved in the graphical Mollier diagram procedure is estimated at well within 1%. Therefore use of this method as a standard seems justified.

1. System: 85% $N_2H_4 \cdot H_2O$ - 90% H_2O_2 (Stoichiometric mixture)

The results of the trial calculations for this system are presented in Tables 4 and 5.

TABLE 4

COMPARISON OF METHODS OF

CALCULATING THEORETICAL CHAMBER PRESSURE FOR THE

SYSTEM 85% $N_2H_4 \cdot H_2O$ - 90% H_2O_2 (Stoichiometric Mixture)

MASS.FLOW RATE PER UNIT AREA OF NOZZLE THROAT $\dot{m}/A_t$	TOTAL EFFECTIVE HEAT LOSS in Btu/lb. $l_c + \frac{1}{2} l_{cn}$	P_c (THEORETICAL) psia EQUATION METHOD 1A	EQUATION METHOD 1B	MOLLIER DIAGRAM METHOD 2
320 lbs/sec.·sq.ft.	0	333	335	335
320	100	326	328	324
320	200	318	320	318
320	280	312	314	309
340	0	354	356	360
340	100	346	348	350
340	200	338	340	341
340	280	331	333	330
300	0	312	314	314
300	100	305	307	306
300	200	298	300	298
300	280	292	294	290

TABLE 5

COMPARISON OF METODS OF

CALCULATING THEORETICAL SPECIFIC IMPULSE FOR

THE SYSTEM 85% $N_2H_4 \cdot H_2O$ - 90% H_2O_2 (Stoich. Mixture)

CHAMBER PRESSURE psia	TOTAL EFFECTIVE HEAT LOSS in $\frac{Btu}{lb.}$ $l_c \neq l_{noz.}$	I_{sp} (Theoretical) EQUATION METHOD 1A	EQUATION METHOD 1B	~~(THEORETICAL)~~ SATTERFIELD CHARTS METHOD 3	$\frac{lbs\text{-}sec.}{lb.}$ MOLLIER DIAGRAM METHOD 4
350	0	213.8	215.9	216.3	214.3
300	0	210.2	212.2	213.1	210.5
350	100	209.1	211.2	212.0	209.5
300	100	205.4	207.4	208.3	205.7
350	200	204.3	205.4	207.5	204.5
300	200	200.6	202.6	203.3	200.7
350	500	190.3	192.3	-----	190.2
300	500	186.4	188.3	-----	186.3

As discussed in the section on Thermodynamics, Method 1A for calculating chamber pressure refers to the use of equation 22c assuming the gas composition to be the same as the Satterfield fictitious gas composition with its specific heat being assigned a constant value obtained only from the contribution according to their molfractions of the pure gaseous components at the arithmetic mean temperature. Method 1B involves use of equation 22c also but the true average molecular weight is approximated closely using Satterfields reduced molecular weight charts and the specific heat is again evaluated at the arithmetic mean temperature in determining all γ's in equation (22c) but the effect of the reassociation reaction is considered by taking Cp equal to the slope of the actual enthalpy - temperature curve $\left(\frac{\partial H}{\partial T}\right)_p$. The average of the two values of this slope at the initial and final pressures is taken but this variation with pressure is small. Method 2 refers to the Mollier type diagram calculation which is almost completely rigorous in principle.

In calculating specific impulse, methods 1A and 1B correspond to methods 1A and 1B for calculating pressure in so far as methods of evaluating the terms for the equation are concerned. In this case equation (14c) is used. Method 3 refers to the use of the regular Satterfield reduced enthalpy and entropy charts at 300 psia and 14.7 psia to carry out the necessary enthalpy and entropy balances. Corrections in enthalpy and entropy with pressures differing from 300 or

14.7 psia are made according to the perfect gas laws. Method 4 refers to the use of the Mollier type diagram.

Examination of these figures in tables 4 and 5 reveals a maximum difference between the results obtained using the Mollier diagram and those from the other methods of analysis of less than 2% in all cases (usually about 1%). Since method 1A for calculating chamber pressures and specific impulse neglects the effects of dissociation and of reassociation during the expansion process, this indicates that these effects are negligible in most calculations for systems similar to this one (i.e. with combustion temperatures of 2200°K or less). The adiabatic combustion temperatures of the system 85% $N_2H_4 \cdot H_2O$ and 90% H_2O_2 is about 2135° K. Since method 1A is satisfactory for these systems, the other more general but more complicated methods are unnecessary.

2. System: Red fuming Nitric Acid - Aniline
(3 to 1 weight ratio)

The results of the trial calculations on this system are presented in Tables 6 and 7.

Methods 1A, 1B and 2 for calculating chamber pressure are the same as described above in connection with the Hydrazine system results.

Methods 1A and 4 for calculating specific impulse are the same as described above in connection with the hydrazine system results also. Method 2A and 2B both involve trial and error solution of the equation (8a)

$$\frac{Te}{Tc} = \left(\frac{Pe}{Pc}\right)^{\frac{\gamma''_{c-e}-1}{\gamma''_{c-e}}}$$

where $\gamma''_{c-e} = \dfrac{Mcp''_{c-e}}{Mcp''_{c-e}-R}$

with Mcp_{c-e} being evaluated from the slope of the enthalpy-entropy curve $\left(\frac{\partial H}{\partial T}\right)_p$. In method 2B this value Mcp''_{c-e} is evaluated at the logarithmic mean temperature while in method 2A, it is evaluated at the arithmetic mean temperature in order to determine the effect this substitution of for γ in Equation8a. In both cases an average value of slopes at the initial and final pressure is taken.

TABLE 6

COMPARISON OF METHODS OF

CALCULATING THEORETICAL CHAMBER PRESSURE

FOR THE SYSTEM RED FUMING HNO_3 - ANILINE (0.75 to 0.25 lbs./lb. mixture ratio)

MASS FLOW RATE PER UNIT AREA OF NOZZLE THROAT $\dot{w}/A_t$	TOTAL EFFECTIVE HEAT LOSS in Btu/lb. l_c / $\frac{1}{2}$ $l_{c.n.}$	P_c (THEORETICAL) psia EQUATION METHOD 1A	EQUATION METHOD 1B	MOLLIER DIAGRAM METHOD 2
260 lbs./sec.·ft.	0	272	280	283
260	328	260	268	271
320	0	335	345	348
320	328	324	330	331

TABLE 7

COMPARISON OF METHODS OF

CALCULATING THEORETICAL SPECIFIC IMPULSE

FOR THE SYSTEM RED FUMING HNO_3 - ANILINE (0.75-0.25 mixture)

CHAMBER PRESSURE atm	Isp (THEORETICAL) $\frac{\text{lbs.}\cdot\text{sec.}}{\text{lb.}}$			
	EQUATION METHOD 1A	EQUATION METHOD 2A	EQUATION METHOD 2B	MOLLIER DIAGRAM METHOD 4
20	214.2	222.0	218.1	220
40	231.7	237.8	235.2	237

Examination of these figures in Tables 6 and 7 reveals a maximum difference between the results using the Mollier diagram and those from any other methods of analysis of slightly over 4%. However, excluding method 1A the results check within about 1%. Since method 1A for calculating chamber pressure and specific impulse neglects the effects of dissociation and of reassociation during the expansion process, this indicates that these effects are no longer negligible in calculations for systems similar to this one (i.e. with combustion temperatures much above 2200°K). The adiabatic combustion temperature of this system is about 2940°K. While this is a fairly high combustion temperature, the interpolation number of this system is only 0.3 or 0.4 in the Satterfield system indicating much less dissociation than other systems of higher interpolation numbers (especially 0.8 to 1.0) would have at such high temperature. However, methods 1B and 2 check so closely with the Mollier diagram results that is seems probable that these techniques would be accurate within 2% at most even in the worst case of an interpolation number of 1.0 provided and were both evaluated and used in equation (14c). Therefore, the calculation methods 1B, 2 and 3 appear to be satisfactory for any system comprised of C, H, O and N.

In the present case, with the system red fuming nitric acid and aniline, there is very little difference in the results of methods 2A and 2B. However 2A is closer to

the Mollier diagram results and therefore evaluation of the molal heat capacity at the arithmetic mean temperature appears to be the more accurate type of average value for use in evaluating γ'' of equation (8a). According to the derivations of equation (8a) and (14c) which were made assuming the heat capacity to be linear with temperature, γ'' should be evaluated at the log mean temperature. However, as pointed out at that time in cases of appreciable dissociation the curve of c_p or M_{c_p} against temperature has considerable curvature (convex upward) over the range from T_c to T_e. Therefore, the use of the assumption of a linear relation between heat capacity and temperature would lead to an average value of C_p or M_{c_p} which is somewhat lower than the correct average. For this reason, use of the arithmetic mean temperature for evaluating γ'' is recommended in equation (8a) since the arithmetic mean is always somewhat higher than the logarithmic mean.

CONCLUSIONS

The performance of a micro-scale thrust motor has been found to be comparable to that commonly obtained by other investigators in much larger scale reaction motors provided that a suitable means of injecting and mixing the reactants is used (see conclusion 1 below) and provided that a feed system especially designed to produce steady flow is used (see conclusion 2 below), and provided that suitable corrections are made to the actual performance figures to allow for the effect ~~on performance~~ of heat losses [which are relatively high in a micro-scale motor] (see conclusion 3 below).

Micro-rocket motor testing appears to be a suitable means of making at least preliminary comparisons of the relative suitability of various propellant systems under given conditions. It appears that a propellant system which performs well under advantageous conditions in a small motor will also perform well under satisfactory conditions in a large scale operation. In fact, for a given propellant system, the performance obtained in a small motor with a good injector (corrected for heat loss) should approximate that which would be obtained in a large motor with a good injector. The micro-rocket technique is of course especially applicable to the study of propellant systems which involve

unusual compounds which are expensive or in short supply.

The amount of information which can be obtained on the performance of such equipment as injectors and combustion chambers by micro-rocket motor operation is open to question. The scale effects seem much too large and too poorly understood at present to make possible the design of a successful rocket motor of conventional size from a micro-scale design study alone. This is particularly true of the injector design. The shape and size of the combustion space required to achieve a given performance can be determined on the micro-reaction motor. However, owing to the importance of the injector configuration on this performance, the utility of this information is doubtful. In the present study using cylindrical combustion chambers with length to diameter ratios of 2 or 3, very little gain in performance was obtained by increasing the size of these chambers above an L* value of 200 inches.

Other specific conclusions are listed below:

(1) Injection methods - Several different types of injection have been tested and in the most promising type, studies have been made to determine the optimum design. The combustion reaction was much smoother and somewhat more complete when the point of injecting and mixing of the reactants was placed in the end or face

of the combustion chamber at the opposite end from the exhaust nozzle. Among these "in line" methods of injection from the combustion chamber face, a slight superiority in the performance of the confined mixing injector was noted. With this type of injector the maximum length of mixing section which could be used was about 1/8" and with this design large angles of inpingement led to very rough combustion and poor performance. However, with angles of inpingement of about 60°, performance was very good in both respects.

(2) One of the chief reasons for the smoothness and consistency of the operation of the micro-rocket motors is undoubtedly the constancy of the flow rates which was obtainable with the positive displacement feed system employed. Normally, operation with a single pair of injection orifices would be expected to vary tremendously due to changes in flow rates and/or mixing pattern of the jets. These fluctuations of individual orifices in a large motor tend to average out due to the large number of pairs of orifices which serve as the supply line for the motor. The achievement of an exhaust jet of uniform cross-section which was steady with time and accompanied by fairly consistent quantitative performance of the motor in check runs as well as during a given run is a long step in simulating large scale motor operation.

(3) The total heat losses of reaction motors of approximately 10 pounds thrust size have been found to be small enough to make the problem of correcting for them relatively simple. Amounting to only about 10 per cent of the total energy available, these losses would not be expected to quench the reaction rate sufficiently to affect the combustion efficiency very adversely. Over half of this total heat loss usually occurs in the combustion chamber proper. The net effect of the remaining heat loss which occurs in the nozzle is not significant, producing only about two or three per cent decrease in net performance figures. Accordingly, even an approximate method of correcting for this heat loss is sufficient. The exact distribution of this heat loss along the nozzle would be necessary to allow rigorously for its effect. However, assuming a uniform distribution along the length of the nozzle leads to the approximation that nozzle heat losses are one half as effective as combustion chamber heat losses. This makes possible a very simple but adequate method of handling the performance corrections which are due to nozzle heat losses. Thus another requirement for making micro rocket performance figures conform to the same basis as those obtained on larger motors can be met satisfactorily and with little additional effort.

(4) The experimental specific impulse obtained with the system, 85% hydrazine hydrate-90% hydrogen peroxide is consistently higher than that obtained with the system naphferrol-90% hydrogen peroxide, in spite of the fact that the theoretical values are higher for the latter system. The hydrazine hydrate fuel is also superior in ease and reliability of ignition as well as in smoothness of operation and suitability for use under service conditions.

(5) With self-igniting systems, a short ignition delay appears to be favorable not only in producing easy starting and consistent operation but also in aiding smoothness and completeness of combustion.

(6) Use of an exhaust nozzle divergence angle of less than 20 or 30° appears to be ineffectual since the increase in frictional losses tends to be greater than the saving in directional thrust.

(7) Suitable calculation methods have been devised for analyzing the performance of the combustion chamber and exhaust nozzle separately and for handling the heat loss corrections to each of these figures, making use of the generalized thermodynamic charts of Satterfield to minimize the labor involved. These methods have been applied in the simplest possible form consistent with the desired accuracy (of 1% or better) to the test results

of this thesis, and, in addition, have been tested with various modifications under conditions sufficiently representative to establish the range of applicability of each. In this connection a preliminary study has been made to determine the proper kind of average values of molal specific heat and/or isentropic exponent which should be used in the thermodynamic equations for fluid flow through the exhaust nozzle of a rocket motor. An indication has been given of the maximum error (less than 3%) caused by general use for all systems of the best kinds of simple averages for these quantities in calculating performance from these equations.

RECOMMENDATIONS

The micro-thrust motor appears to be a tool of sufficient utility that it should be considered for testing and comparing the experimental performance of various propellant systems as well as in development programs of actual reaction engines. Its position might be considered as comparable to that of bench scale operations in chemical process development work. Admittedly, the micro rocket is under a disadvantage as a test vehicle at the present time due to the dearth of experience in applying results on such a small scale to motors of practical sizes. However, wide use of this technique would soon provide much of the additional experience needed to establish a fair knowledge of scale effects in this field and there are many cases even now where it might prove to be a desirable starting point in research studies on jet engines.

It is felt particularly that the micro rocket technique should be extended to cover a greater range of fuels and oxidants especially to encompass several systems in the class of non-self-igniting propellants, and also to cover a wider range of types of injection systems, especially methods of injection which are more similar in type to those conventionally used in larger scale motors. In connection with the need for more experience in directly

comparing large scale and small scale results, larger scale testing of the concentrated hydrogen peroxide systems studied in this thesis would be helpful.

Whether in large scale or small scale tests, additional investigations should be carried out to determine the extent of applicability of ignition catalysts as combustion catalysts and the degree of selectivity of this catalytic effect for the fuel-oxidant system with which it must be used.

The operation of the micro-rocket equipment was generally quite satisfactory. However, one very desirable improvement would be the substitution of a more streamlined propellant storage tank and displacement device for the bellows container and oil pot which were used in the present study. This would simplify the displacement of all air and gases from the system on filling and would insure the achievement of a truly positive displacement feed system. This type of feed system is ideally suited to the determination of the smoothness of combustion which is inherent in a given fuel system, injection method, or motor design.

APPENDIX

APPENDIX A

DETAILED DESCRIPTION OF APPARATUS

The investigation of the liquid propellant systems employing high strength peroxide was carried out in a series of small, so-called "micro," rocket motors. The volume of the motor combustion chambers varied from about 0.5 to 12.5 cubic inches but the actual scale of operation was more constant, with the thrust force generated being between 5 and 12 lbs. in most cases.

Several practical reasons dictated the adoption of the smallest feasible scale of operation for these tests. The most important of these reasons were the high cost and scarcity of the propellants to be used--particularly hydrazine, the inadequate facilities or provision for safely handling large amounts of hazardous materials, the desire to investigate more fundamentally the nature of the chemical propellants and the character of operation of the reaction motor than would be possible on a large scale development project, and the greater economy in all phases of the program which small scale operation would effect. Consideration of these factors led to the decision to design the micro-rocket test stand equipment on the basis of consuming approximately one liter of 90% hydrogen peroxide per run. This is equivalent to a maximum theoretical thrust of 10 to 20 lbs. for most peroxide-fuel systems based on a minimum run duration

of 60 seconds. For the systems actually studied in this thesis the maximum thrust on this basis would be about 15 lbs. For operating conditions from 300 psia chamber pressure to 14.7 psia exhaust pressure, 15 lbs. thrust from these systems requires a nozzle throat diameter of about 0.21 inches. The nozzle throat diameters range from 0.125 inches to 0.20 inches in most runs here reported.

Test Cell Arrangement

In order to provide a suitable test cell of sufficient strength for even these limited quantities of propellants to be handled safely, a steel cubicle was assembled from one inch armour plate in one of the basement rooms in building 2. Figure 14 is a layout of this test cell showing the arrangement of fixtures such as the ventilation system and also of the test equipment which is within the cell. The sound absorbing panels which were used to insulate the inner walls of the cell and the baffles of the exhaust duct of the ventilation system, completely eliminated any noise disturbance in the outer control room or any of the neighboring class rooms. All the control instruments were located outside of the cell, mostly on the front panel board, with the connecting lines and wiring passing into the cell through bulkhead fittings in the wall. The pumping stand and auxiliary instruments were also located outside the cell for convenience in control and observation. However, none of the propellant lines passed outside the cell. Instead the oil was pumped by means of two

special positive displacement gear pumps from an external resevoir through the cell wall and into the large pots which housed the bellows-type propellant storage containers, displacing equal amounts of the liquid propellants into the reaction motors.

Hydraulic System

Figure 9 is a flow sheet of the complete hydraulic system employed in feeding the propellants to the reaction motors under test conditions. The distinguishing feature of this system is the ability to achieve substantially constant rates of flow of propellants into the combustion chambers, irrespective of fluctuations in the pressure existing in this combustion chamber. This is accomplished by use of Zenith metering gear pumps operated from a synchronous motor drive with a completely gas free system throughout. As actually used the system did not quite achieve true positive displacement. Due to the complicated shape of the bellows container and oil tank and the large cross sectional area of both, between 25 and 50 cc. of gas remained trapped in each bellows and oil tank assembly after filling. A small additional amount of gas accumulated after the peroxide bellows was finally capped from the slow decomposition of the peroxide. A gas pocket of 40 cc. at atmospheric pressure would be reduced to about 2 cc. at 300 psia, the usual operating pressure. An effective pressure fluctuation of 15 psi from this mean of 300 psia would change this gas volume

by 0.105 cc. This is equivalent to from 3 to 1% of the usual total flow for 1 second of each propellant of sufficient to stop flow completely for from 1/20th to 1/60th of a second. However, it is believed that with reasonably smooth combustion, very little if any of the pressure fluctuations were effectively transmitted to the storage containers and the enclosed air pockets. Consequently, it can be said that for the better (i.e., smoother) injection systems at least, there was probably no superimposed effect of combustion chamber pressure fluctuations upon the smoothness of the combustion even with this small amount of gas trapped in the system.

As shown in the flow diagram of Fig. 9, each oil pump circuit contained a pressure operated switch which was set at approximately 1000 psi. These were Meletron Model 310 pressure switches adjustable for actuating pressures from 200 to 1200 psi. If the pressure in either pump circuit reached 1000 psi these switches would automatically shut off the power to the main motor drive. Each oil pump circuit was also arranged with the necessary manual valves (as shown) to either pump oil into bellows pots (as would be the case during the run) or to return the oil from the pots to the reservoir at the end of the run.

The main propellant valves usually used on the thrust stand were of the balanced diaphragm type in which the

pressure exerted by the propellant on the valve port side of the diaphragm was opposed on the opposite side by the oil pressure from the same oil pump circuit used to displace the propellants from the bellows pots plus a small spring load to insure positive sealing. The opposing oil pressure behind the diaphragms is controlled by two high pressure solenoid valves in each circuit. These valves were type K-10-12 Solenoids made by the General Controls Company for use on 115 volt-60 cycle current. As used here, the first valve in the oil circuit from pump to valve was normally open while the second valve in the line from valve to oil reservoir was normally closed. In this way oil pressure was maintained on the back side of the valve diaphragm equal to the opposed propellant pressure until at the start of the run when both valves reversed positions. This action reduced the pressure on the oil side to atmospheric and allowed the pressurized propellant to lift the valve diaphragm and enter the motor. To stop the run the solenoid valves were reversed to their original position thus applying oil pressure to return the diaphragm to the closed position. The balanced diaphragm valve bodies were constructed of stainless steel except for parts not exposed to propellants where mild steel was used. The diaphragms were made from 0.015" thick sheet Monel which was tin plated and the seats were made from Teflon. Ordinary stainless steel globe valves with

extension handles through the test cell wall were usually used on the stationary stand.

Pumping Stand

A photograph of the pumping stand is shown in Fig. 12. However, the drawing of Fig. 13 shows more clearly the arrangement of the main drive motor, the pumps, Toledo variable speed transmissions gear train, and gear reductors. Only one set of these items is shown in the sketch. The motor was a 220V-3 phase - 60 cycle, 1800 rpm, synchronous, 3 horsepower model "with vari-speed drive" made by the U. S. Electrical Company. The booster pump was an ordinary Viking gear pump which was driven off the main drive shaft to furnish a feed pressure of about 40 - 75 psia to the inlet of the two metering pumps. The Toledo Timers were of the manufacturer's type-designation "1 A." The gear reductors were Type U.D.-10 with a 10 to 1 speed reduction made by Boston Gear Works. The main feed pumps were No. 5 Zenith metering pumps of the largest size available in these special gear pumps designed for metering viscose rayon spinning solutions. The vital dimensions of these pumps is held to a tolerance of $\pm$ 0.000025" with complete interchangeability of parts. The No. 5 Zenith has a rated delivery of 2.92 cc. per revolution. The measured delivery in our calibration tests was always 2.94 $\pm$ 0.02 cc. per revolution at a speed

of 160 rpm and with discharge pressures from 200 to 700 psia. At a speed of 80 rpm the delivery was 2.94 ± 0.03 cc. per revolution over the same range of discharge pressures. The measuring tachometers were attached to the high speed side of the gear reductors and consequently ran at ten times the actual speed of the feed pumps. They were panel mount instruments with built in counters made by the Reliance Tachometer Company and with an operating range from 200 to 2400 rpm (corresponding to pump speeds of 20 to 240 rpm). The solenoids used to engage and release the tachometer counter buttons were Trombetti F-324 models with a 5-lb. pull and a 1-1/4" stroke for use with 220 volt-60 cycle current. Variations in total flow rate and in fuel oxidant ratios were accomplished by adjusting the main vari-speed motor drive and the Toledo variable speed transmissions to the individual metering pumps. Thus the total flow rate could be changed without affecting fuel to oxidant ratio by adjusting only the main motoring drive while the fuel to oxidant ratio could be varied in such a way as to maintain constant total flow rates by making adjustments on both of the Toledo Timer transmissions to the separate feed pumps.

Bellows Assembly

The section view diagram in Fig. 10 illustrates the arrangement of one of the propellant bellows and oil tank assemblies with associated equipment. Pictures of this same

equipment are shown in Fig. 11. The bellows shown was constructed from a Fulton Sylphon corrugated expansion tube of 0.010" thick stainless steel by attaching the one flate head and one dished head (both of 16 gauge stainless) at the ends by means of a continuous spot weld around the edge of each. This produced a bellows container of about 3500 cc. capacity with welded connections in each end plate. There were ten corrugations in each bellows tube wall each about 5/8" deep, giving the container a major diameter of about 12 inches and a minor diameter of about 10-3/4" with a total length at the neutral position of about 2-5/8". The maximum total stroke of the bellows which was allowed was about 3/4 of an inch, which delivered approximately 1 liter of propellant. The limit switch which was a micro switch operated by grooves cut in the bleed tube was set to throw at 3/8 of an inch above the neutral position on filling or 3/8 of an inch below the neutral position when feeding propellants during a run. When thus actuated, this switch (on either bellows assembly) would shut off the power to the main motor drive, thus acting as a safety device to prevent stressing the bellows sufficiently in either direction to cause permanent damage or excessive wear in the corrugated joints which would shorten the life of the bellows. Since one end of the bellows was free to move, the pressure differential across the bellows

wall was very small (probably less than 2 psia over the stroke used). Under these conditions there was no necessity for great strength in the bellows container. From the bottom outlet of each bellows container, 1/4" stainless steel tubing was used to complete the piping circuit in a parallel arrangement to each of the test stands. Appropriate stainless steel manual valves were installed in each line to both stands to enable easy switchover to operation on either stand.

Electrical Control Equipment

The heart of the control equipment used in operating the micro-rocket test stand was the sequence timer. This was an automatic regulator device manufactured by the Automatic Temperature Control Company of Philadelphia under the name "Series 2400 Cam Timer." It consists of a synchronous motor geared to a cam shaft with each of the six individually adjustable cams available to operate a switch at any desired and predetermined time of the timer cycle. By adjusting and setting the cams at their proper positions, the entire sequence of events and operations necessary to initiate a run can be made to take place on a predetermined timing schedule. The timing program usually used for a run on the thrust stand was as follows:

1. Start the oscilloscope camera motor.
2. After 10 seconds to allow camera to reach synchonous speed and the cathode ray to return to its zero position on the scope, actuate solenoid valves

which control fuel propellant valve. (Also the solenoids which engage the fuel tachometer counter.)

3. From 0.1 to 0.2 second later, actuate solenoid valves which control peroxide propellant valves. This cam also actuated the peroxide tachometer counter solenoid and started the electric clock and the neon light which gave timed flashes on the film in the oscilloscope camera.

This careful control of the injection process was necessary to prevent premature injection and subsequent accumulation of one propellant before the other arrived in the motor to initiate the "self-igniting" combustion reaction. If not prevented, this occurence could have led to "hard starts" or possibly damaging explosions.

The use of the sequence timer was not necessary for operation of the stationary stand when manual valves were used to start a run as was generally the case. These valves were standard Lunkenheimer 1/4" or 1/8" standard pipe size stainless steel globe valves in which Koroseal rings were substituted for the string packing. The valve stems were also extended out through the cell walls by means of 5/16" diameter steel rods welded to the original handle stubs. A 6-sided cam on the peroxide valve stem acting on a microswitch was used in many runs to turn the neon timing light on and off six times per revolution as the valves were being

opened to start the run. In order to open the two valves quickly and simultaneously, the valve stems were geared together and a wheel type handle on the fuel valve used to open both valves at once for a time. In most cases, however, the runs on the stationary stand were started by one person opening both valves together--one with each hand--using the regular valve handles. While this required several motions to get the valves wide open, they were substantially open after the first motion. In this case the neon timing light was turned on by the first motion of the peroxide valve stem by means of a simple cam on the valve stem acting on the micro-switch.

A check list was employed in preparing for each run to assure the attention to all the necessary details and especially to insure making the changes required to shift operations from one stand to the other. A row of instruments switches was installed on the panel board with accompanying pilot lights to enable the various circuits to be changed and checked to conform to the different standard usages in effect in making runs on the two stands. Each safety shut-off switch also operated a pilot light in order to indicate immediately which one of the several possible switches had been actuated when a run was stopped in this manner. The wiring diagram of the entire control circuit and power circuit for the test cell is shown in Fig. 15.

FIGUREA-I CALIBRATION CURVE FOR FOXBORO PRESSURE RECORDER

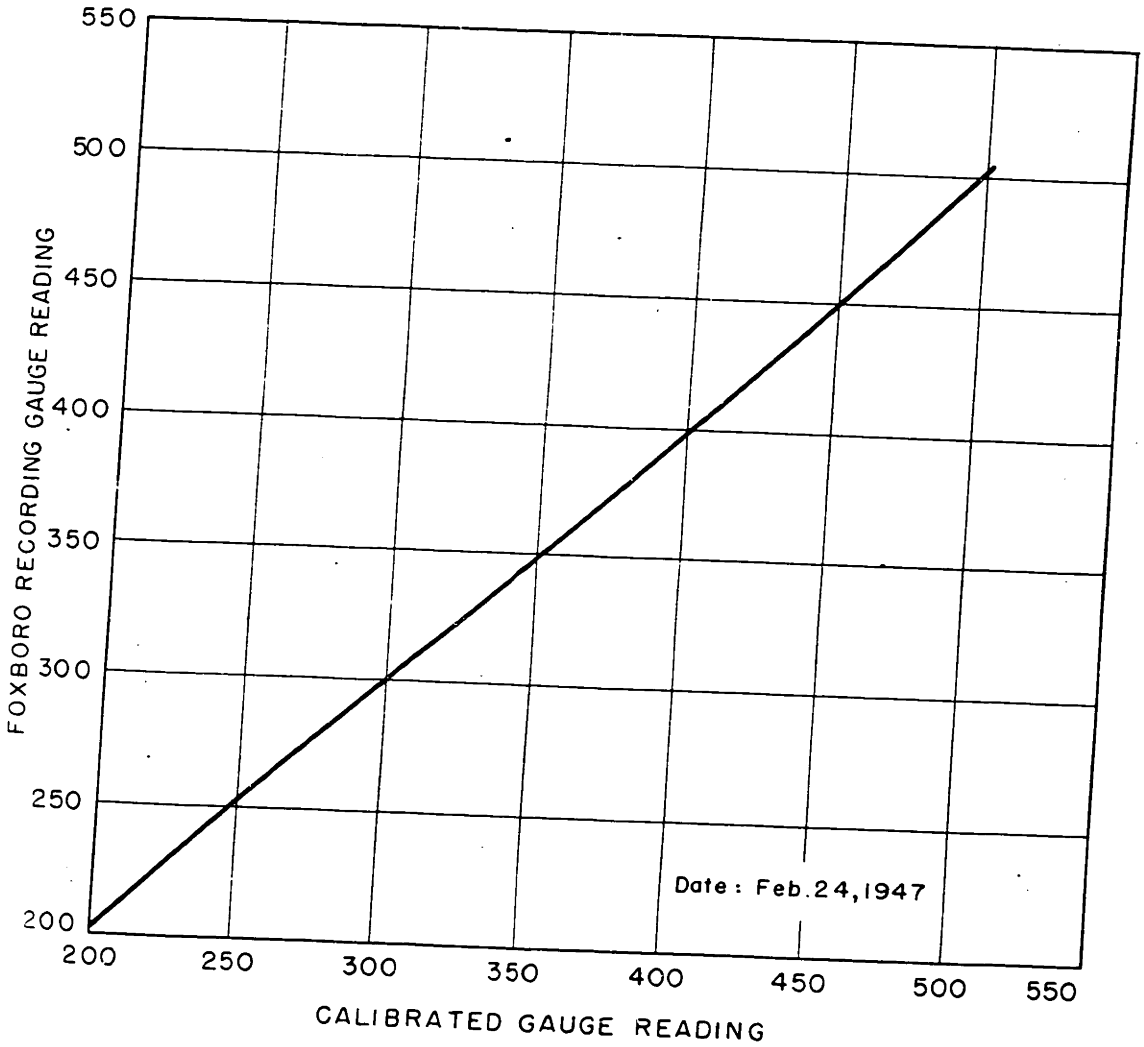

FIGURE A-2 CALIBRATION OF THRUST RECORDER

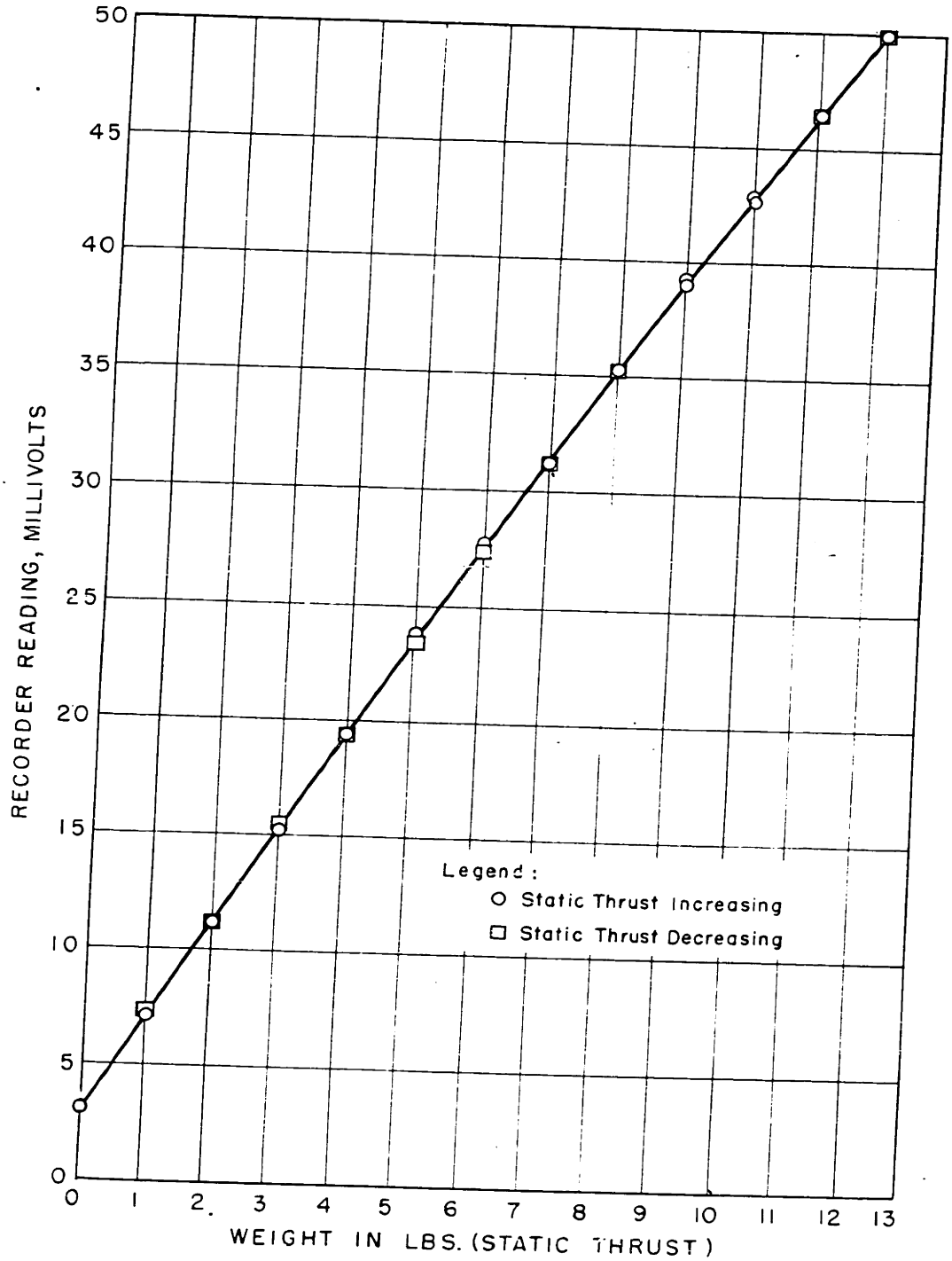

FIGURES A-2A & A-2B

FIGURE A2A CALIBRATION CURVE FOR GENERAL MOTORS CAPACITANCE PRESSURE INDICATOR

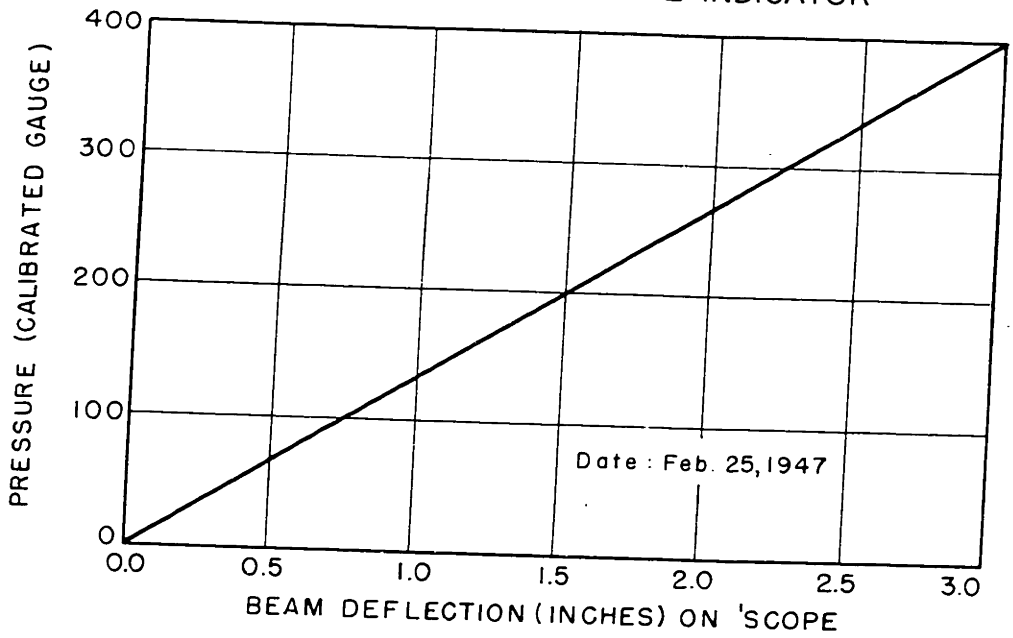

FIGURE A2B CALIBRATION CURVE FOR FEED PRESSURE RECORDING GAUGE

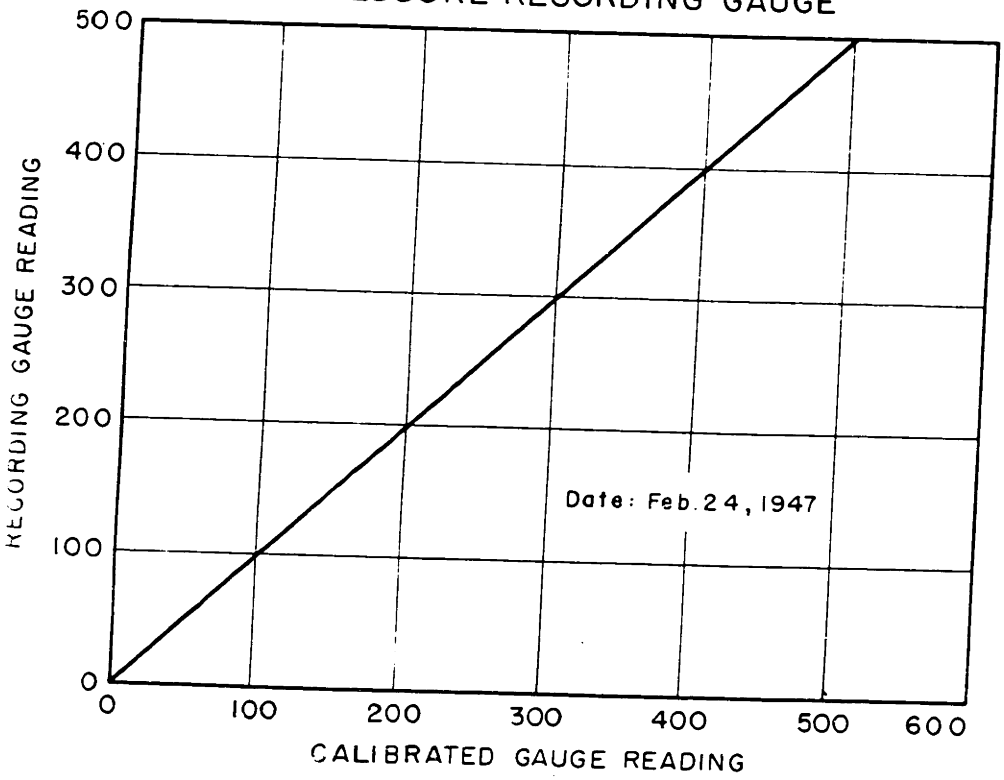

Instrumentation

Fig. 16 is a photograph of the main instrument panel board. In addition to the various instrument switches and pilot lights and the two manual valve handles, the five main instruments pictured here are a Brown Electronik Potentiometer for recording temperatures as measured by a Platinum-Platinum + 13% Rhodium thermocouple, two Foxboro recorders for measuring chamber pressure and fuel feed pressure, another Brown Electronik Potentiometer for recording millivolt output from a strain gauge bridge used to measure thrust, and the Telechron Electric Clock with sweep second hand used for measuring time.

The pressure recorders and thrust recorders were calibrated frequently and typical calibration curves are shown in Fig. A-1, A-2, and A-2A & A-2B. Calibration of the thrust measuring system was actually made after each run at least in the range of thrust measured, while calibrations of the pressure recorders was made every two or three months. The very frequent thrust calibrations were necessary mainly because of the gradual change in potential of the dry cell battery which was used to furnish current to the strain gauge bridge.

The only other measuring equipment used which has not yet been mentioned in this description of apparatus was the General Motors Capacitance type pressure indicator

FIGUREA-4COPPER-CONSTANTIN THERMOCOUPLE CALIBRATION

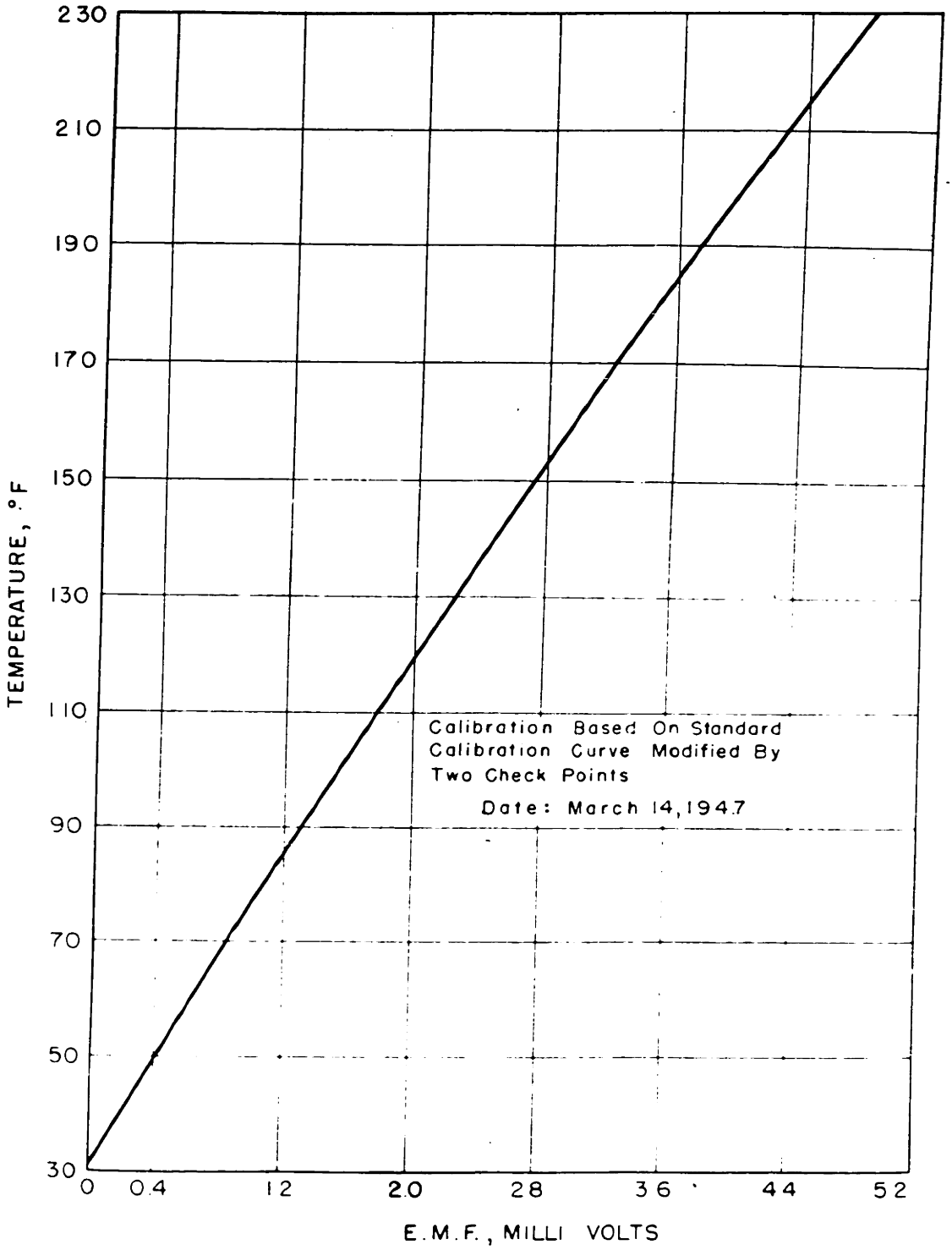

FIGURE A-5

THERMOCOUPLE CIRCUIT

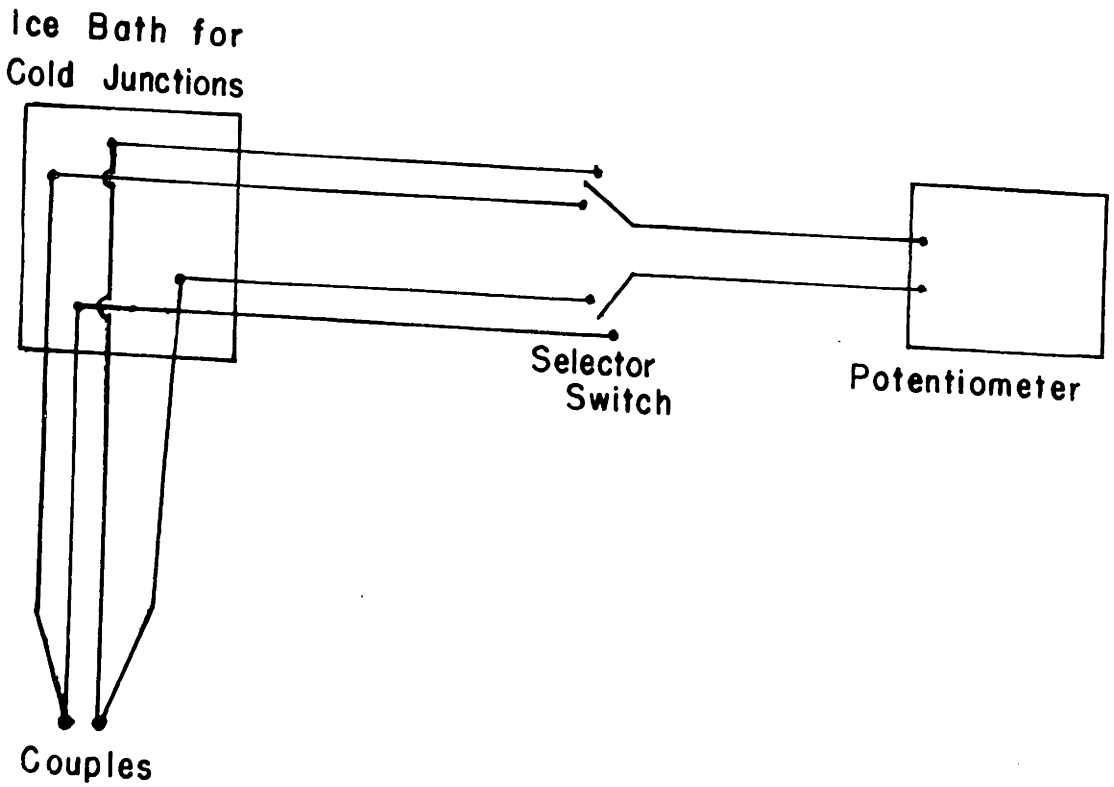

Figure A-8 6

Recording Camera and Oscilloscope
and Auxiliary Equipment Used
with G. M. Capacitance Gage

Oscillator - Detector Unit, Power Supply,
Oscilloscope, Gear Box, Camera and Motor

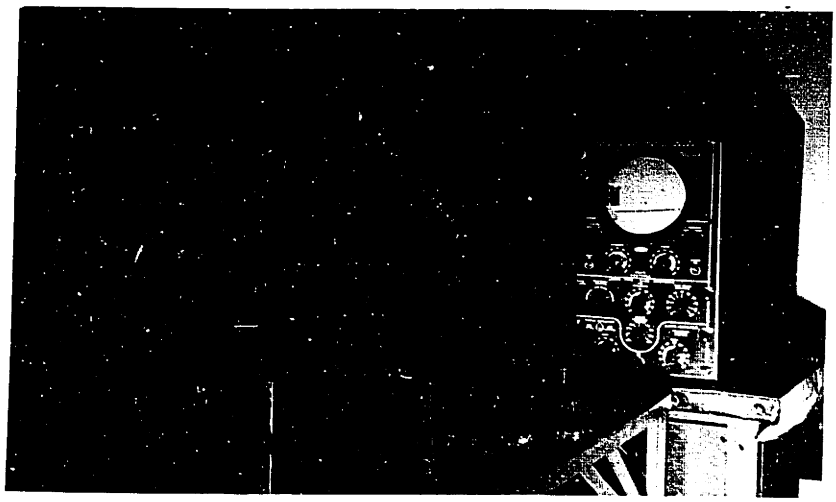

Motor, Camera, and Oscilloscope

FIGURE A-7 GENERAL MOTORS PRESSURE INDICATOR

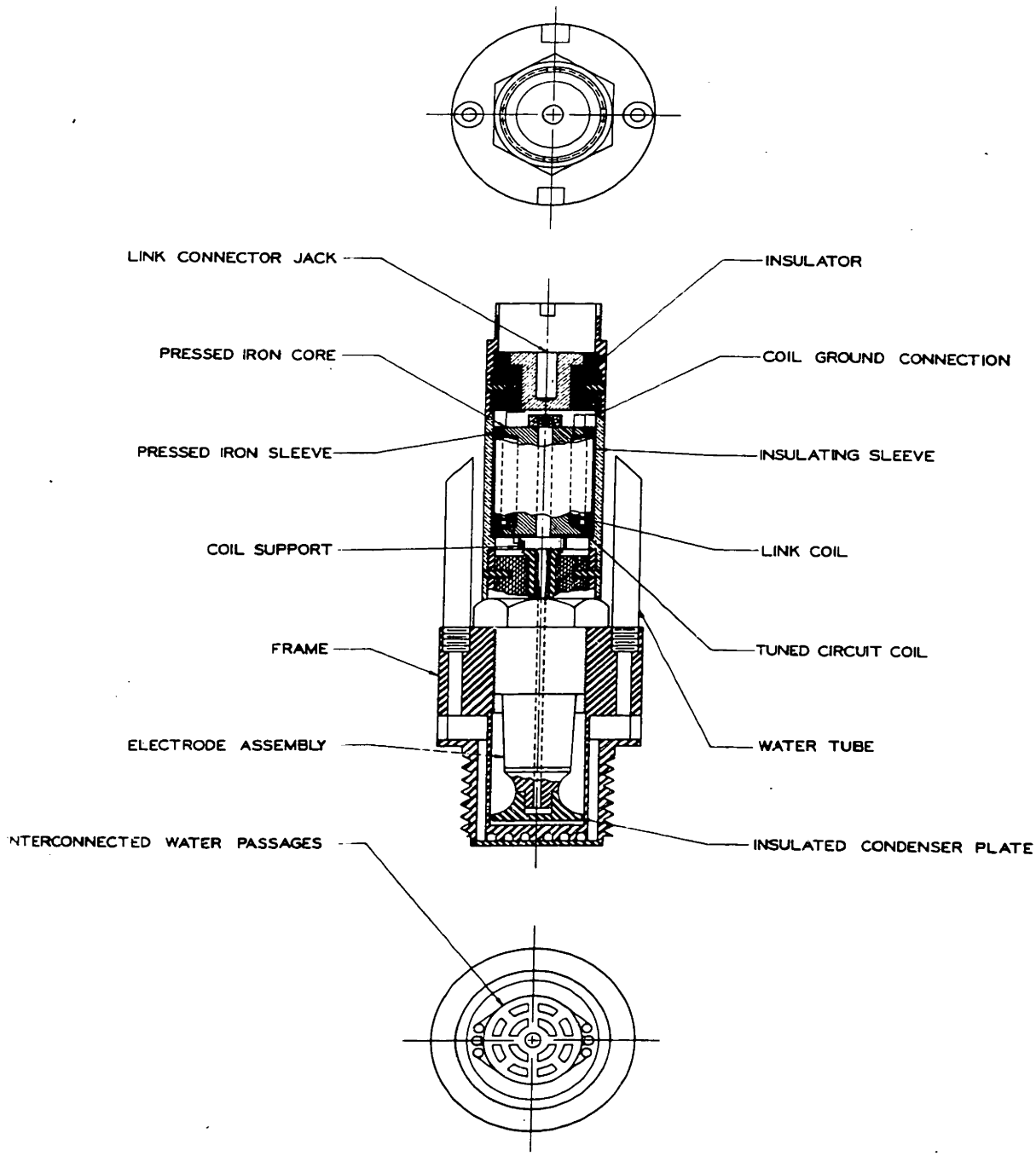

■ Fig. 6 – Cutaway view of water-cooled condenser-plate indicator – high-pressure type

and associated equipment including oscilloscope and recording camera and the Leeds and Northrup Portable Potentiometer which was used in measuring cooling water temperatures and motor wall temperatures in determining heat transfer rates, as well as in some early attempts to use a tungsten-molybdenum thermocouple for measuring temperatures inside the motor combustion chamber. Calibration curves for the Tungsten-Molybdenum couple are given in Appendix C. Calibration curves for the cooling water couples of copper-constantin are given in Fig. A-4. A typical thermocouple circuit is shown in Fig. A-5.

Fig. A-6 is a photograph of the electronic equipment used with the G. M. capacitance type pressure gauge including the oscilloscope and recording camera. Fig. A-7 is a cross section view of the water-cooled indicator itself, 18 mm. thread size, which is the type used in the present work. Grinstead et al have given a paper describing this gauge and the electronic circuit used with it. Briefly the principle of operation of the instrument is as follows: The pressure sensitive element or diaphragm forms one plate of an insulated condenser. In order to obtain a diaphragm of high natural frequency of response and good elasticity with a diameter of only 18 mm. or less, a total deflection of only 0.0003" was chosen for the maximum operating pressure. In order to make the change of capacity with pressure

nearly linear, the air gap between condenser plates was then made approximately 0.003". With the 18 mm. indicator which was used in the present work, a diaphragm thickness of 0.065" is employed in order to give a maximum deflection of 0.0003" at 800 psia. The natural frequency of responce of this diaphragm would then be at least 10,000 cycles per second.

The condenser thus formed in the indicator together with the coils in the top section forms a circuit which is loosely coupled to a high frequency oscillator and close coupled to a diode detector unit, power supply, and modified Du Mont type 208 cathode ray oscillograph. The power supply consists of a positive 350 volt side as well as a negative 350 volt side to furnish power for the balancing circuits necessary for direct coupled amplification in the oscilloscope. Static calibration and low frequency fluctuations can be measured by the direct coupled amplifier. In ordinary use the unbalance of the circuit due to the change in capacitance of the condenser indicator is measured by the output of the oscillator-detector unit. This output is amplified and appears on the oscilloscope screen as a deflection of the cathode ray beam along the horizontal axis, increasing pressure causing a shift to the left. An increase in the temperature of the indicator produces a change

FIG. A-8 OSCILLOSCOPE CAMERA AND CAMERA DRIVE
(top view)

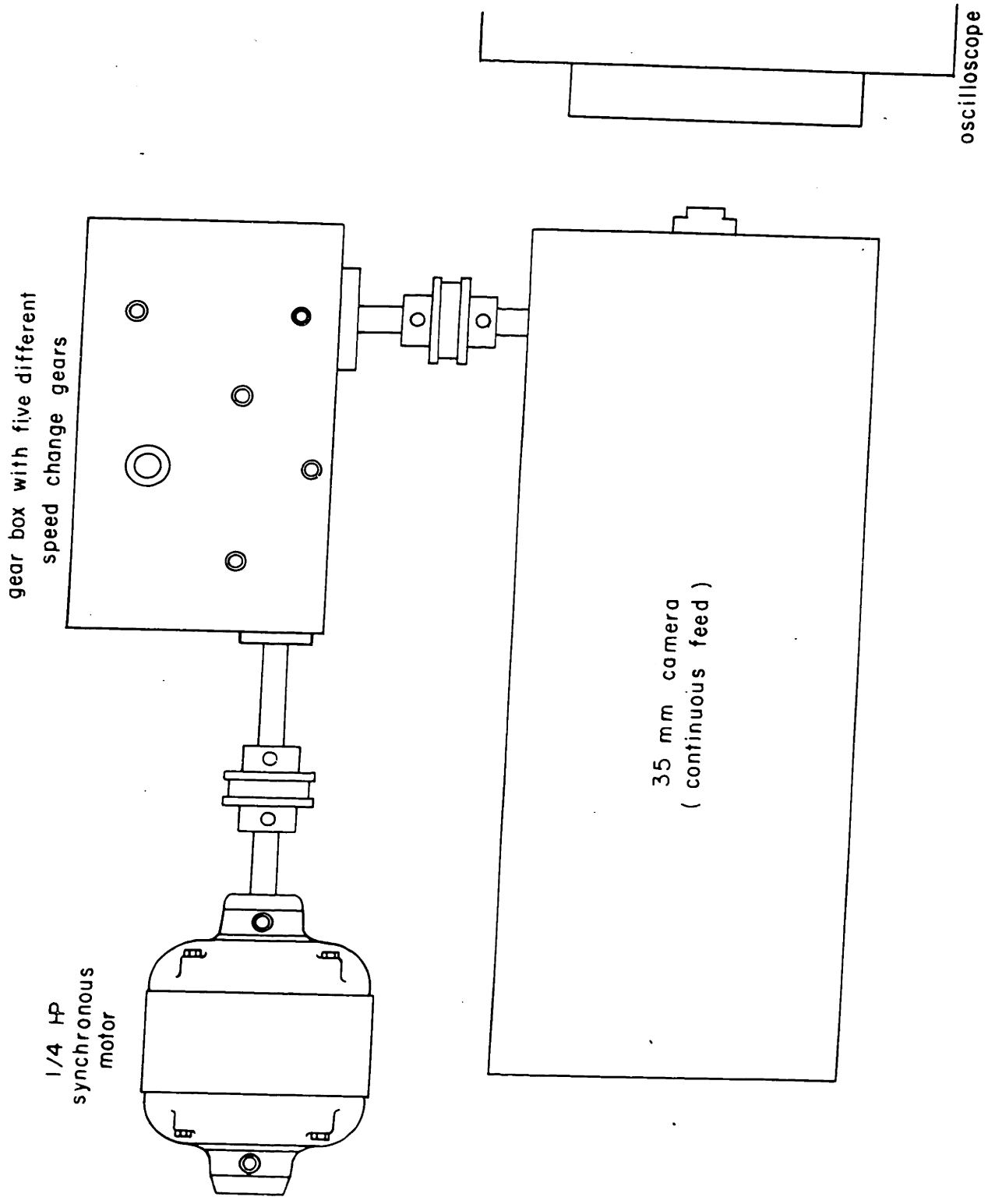

FIG.A-9 CHANGEABLE SPEED GEAR BOX DRIVE FOR RECORDING CAMERA FOR OSCILLOSCOPE
(SIDE VIEW)

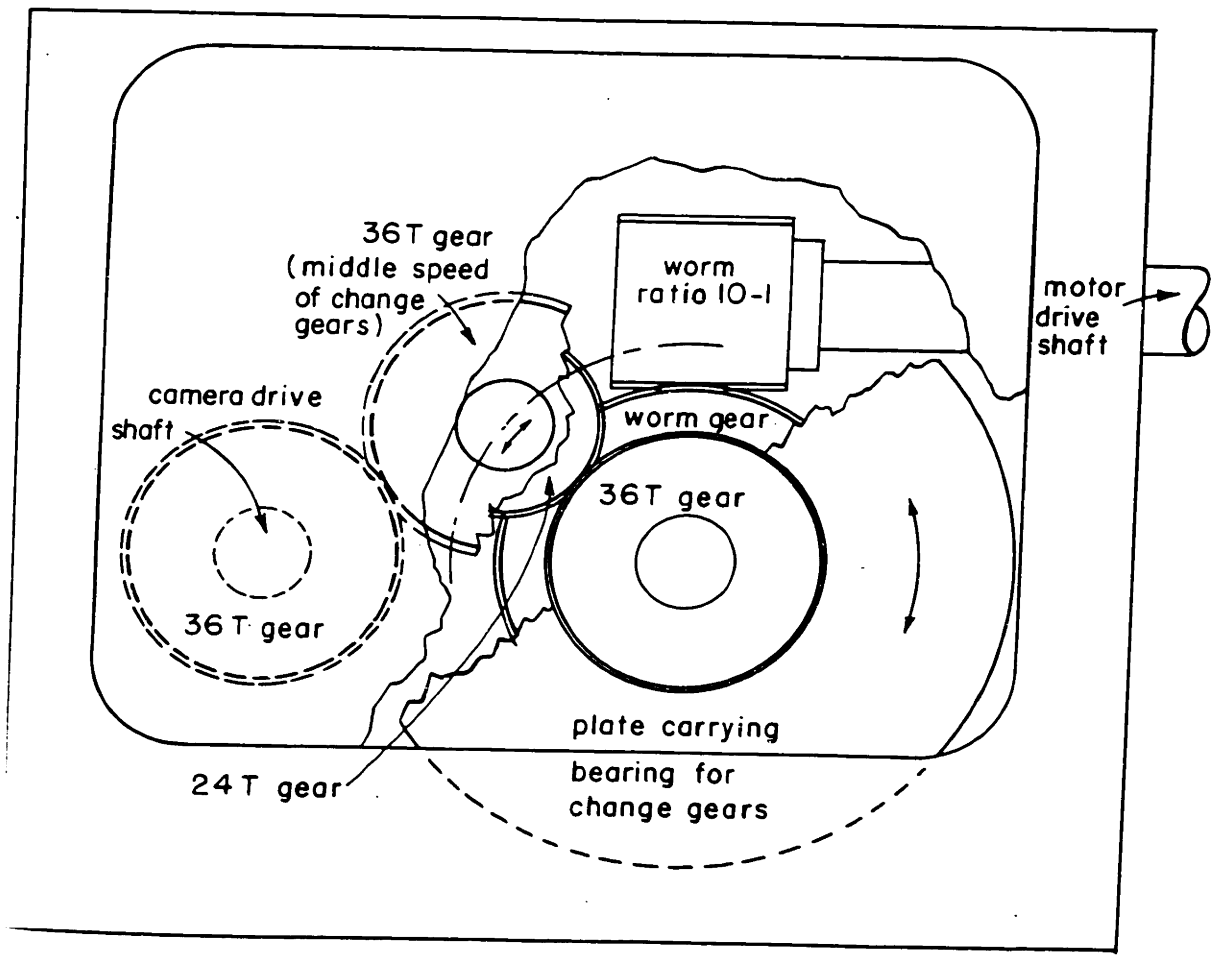

in the same direction.

The camera used to record this deflection of the cathode ray beam on the oscilloscope screen, was an old style 35 mm. movie camera which was modified to run continuously by removing the jerk feed and shutter mechanism. It was then operated through a gear box by a G. E. 1/4 horsepower-110 volt-60 cycle electric motor made to operate nearly synchronously at about 1800 rpm by milling flats on the rotor. See Fig A-8. The custom built gear box of Fig. A-9 was equipped with change gears so that the camera film speed could be varied in stages from 33 ft./min. to 16-1/2 ft./min. to 11 ft./min. to 8-1/4 ft./min. to 5-1/2 ft./min. With this synchronous camera drive, the movement of the 35 mm. film provided a time axis for the pressure record of the run. As a check, however, timing lines were placed on the border of the film by a neon light which when operated on 220 volt-60 cycle alternating current flashed off and on 60 times per second. With this system of timing, the oscillograph sweep circuit, which could have been employed to provide an electrical time axis, was not used. The lens used with this camera was a Summar with 5 cm. focal length and F:12.5 aperture. Super XX 35 mm. film was sufficiently sensitive to the cathode ray trace even at the fastest camera film speeds. The lens was used slightly folded to

give a complete view of the 5 inch diameter oscilloscope screen from a distance of 1 foot. External light was shielded from the light path between oscilloscope and camera by a loose cloth covering stretched over the top of the two instruments. This enabled an observer to watch the movement of the cathode ray beam on the scope screen while the run was in progress and at the same time that the film record was being made.

Combustion Chambers

The four different designs of combustion chamber which were used in the micro-rocket studies are sketched in Figures 17 and 18. Two of these, motors A and B, were used on the stationary stand while the other two, motors X and W, were used on the thrust stand. The exhaust nozzles shown are one of several which were used with a given motor in all cases except motor X where the nozzle is an integral part of the combustion chamber. The extra nozzles used were generally of a different size but of the same design as the one pictured in all details such as type of cooling passage, expansion ratio, shape of converging section and diverging cone angle. However, with motor W one of the extra nozzles for a few runs had a 20° included angle of divergence instead of 8° as is the case with the one shown. In this case the combustion chamber was extended by a 3/4" cylindrical length of 1/2" diameter. The theory of design of

Figure A-10

Micro-Rocket Motor B

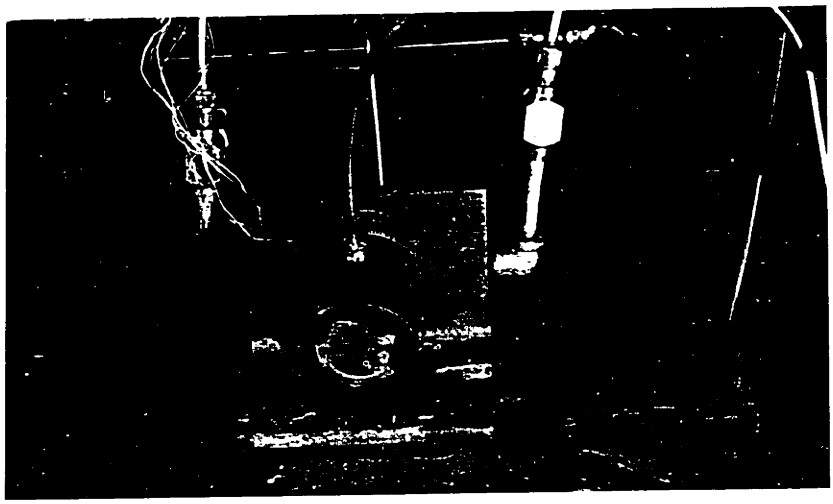

the converging-diverging supersonic nozzle is considered in Appendix D.

The two stationary motor combustion chambers, A and B, were thick walled cylinders with no enclosed coolant passage surrounding them. Chamber A was constructed of mild steel and Chamber B of copper and both were cooled by a stream or film of water flowing over the outside surface. The picture of Fig. A-10 shows motor B in position, ready for a run on the stationary stand. This motor was used primarily in a thesis study on heat transfer by Borden. Motor A is shown in the pictures of Fig. 19. It was the first combustion chamber constructed and was used for all preliminary test work such as trying out new propellant systems or new methods of injection. This was the only combustion chamber with which the G. M. capacitance type pressure indicator was used extensively. No heat transfer measurements were made with motor A, however.

The two thrust motors, W and X, were constructed of stainless steel including the nozzle part of motor X. All other exhaust nozzles were made of solid copper, chrome plated on the inside contour. Each of these combustion chambers was cooled by water flowing through the enclosed cooling passage, which was a 3/32" annular passage in the case of motor W and a rectangular spiral groove 1/16" side by 3/64" deep in the case of motor X. Cooling water flow

rates and inlet and outlet temperatures were measured in runs with these thrust motors to obtain the heat loss rates at equilibrium. The G. M. gauge was used in some runs with Motor W but the motor X combustion chamber was equipped with only one small side connector which was used as a pressure tap to the Foxboro recorder. Motor X was used only with the propellant system 85% Hydrazine Hydrate - 90% Hydrogen Peroxide but Motor W was used to study both this system and the Naphferrol - Peroxide combination.

Injectors

The five chief types of injection tested in the micro rocket studies are depicted in Fig. 22. One condition was common to all these methods of injection, namely, each employed a single stream of each propellant and except for some injectors used with the Naphferrol-peroxide combination, all these injection orifices were 0.04" in diameter (No. 60 drill size).

The first method of injection used was modeled after the standard mixing device picture in Fig. A-19 which was used by the Fuels Ingestigation Group of the Peroxide Project in measuring the ignition delay times for self-igniting fuel systems. In this device the two propellant streams impinge upon the center of a flat plate target placed just above the point of intersection of the two streams. In this way the streams strike the plate just

FIGURE A-11
STATIONARY STAND

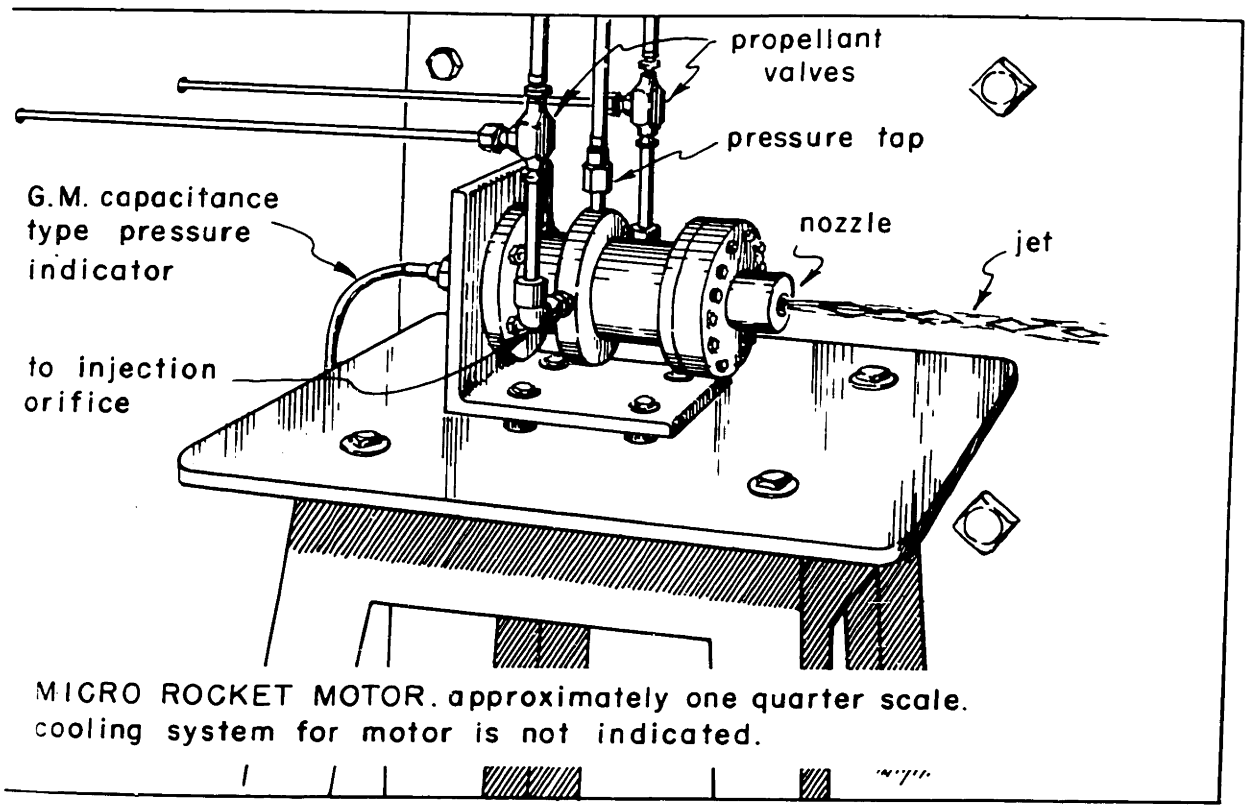

MICRO ROCKET MOTOR. approximately one quarter scale.
cooling system for motor is not indicated.

Figure A-12

Micro-Rocket Motor A Showing

90° Open Injection System With Target

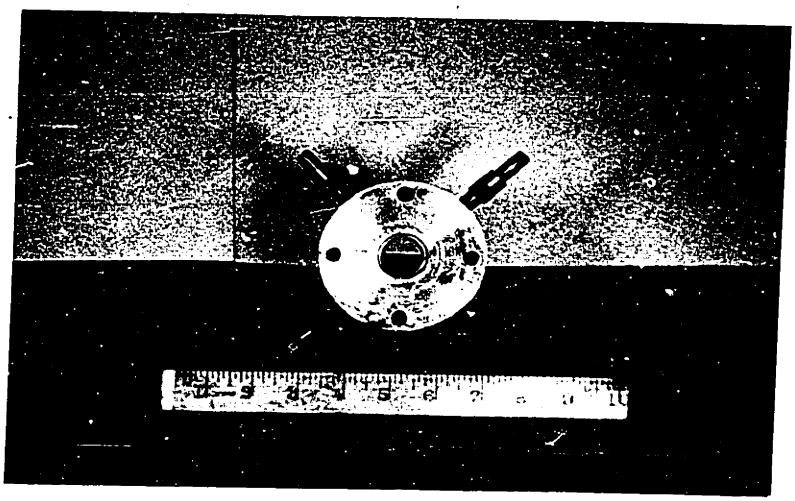

before they would intersect each other and then bounce into each other more in the form of films than unbroken rods. This follows the theory advanced by the German researchers that best mixing is obtained between two liquids in the form of films where the surfaces are somewhat spread out but before the streams have broken up into droplets. This type of injection was used only in the original motor combustion chamber A. Here the two injection nozzles were located on the circumference of the 2" diameter chamber at a point one inch down stream from the back end face of the motor where the injector is usually located. This type of injection is represented by diagram B of Fig. 22 and is also shwon with injection nozzles and target assembled in the picture of Fig. A-12. This type of injection where the streams meet out in the open in the central part of the combustion chamber has been designated "open injection" in the present work. One modification of this same system of open injection which was also tried in the original motor used the same 90° impingement but without the target. In this case the streams met in mid-air and while mixing scattered in all directions, although the direction of the net resultant momentum of the combined streams was downward toward the motor wall opposite the injection nozzles.

Figure A-13

Micro-Rocket Motor A Showing

180° Open Injection System with Target

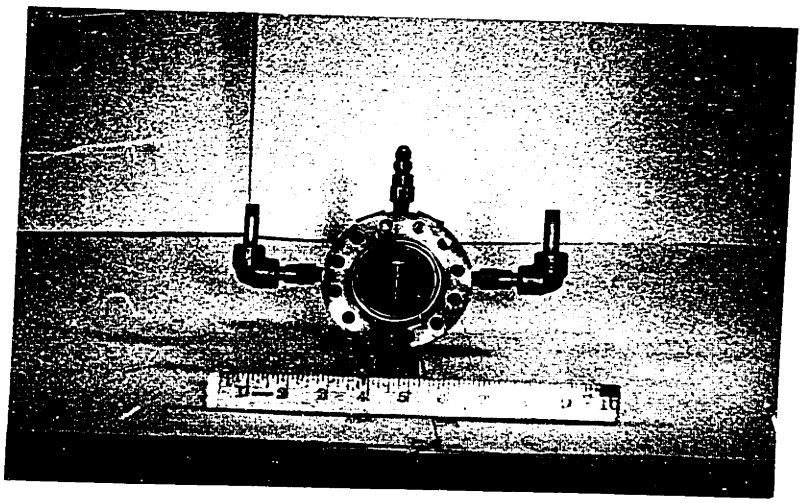

Another type of open injection employed directly opposed streams coming from the sides of the 2" diameter chamber at 180° to each other. In one case the streams impinged on opposite sides of 90° prism and met at the apex of this prism in the form of thin sheets of liquid. This arrangement is shown in diagram of Fig. 22 and in the picture of Fig. A-13. In a modification of this system the target was removed and the streams met head on in the center of the combustion chamber. In this case the resultant mixed liquid would spread out in all directions in a symmetrical mushroom pattern, the exact shape of which would depend upon the relative momentum of the original streams and the amount of interference created by the gas evolution resulting from the combustion of the reactants in the surrounding spaces.

Diagram D of Fig. 22 is a representation of the so-called "single piece" open injector. This injector was attached to the various combustion chambers through the back end plate where the injectors of a conventional rocket motor are usually located. In this case the pair of fuel streams met at a point 1/4 of an inch from the injector face at an angle of 60° to each other, each at 30° to the longitudinal axis of the motor. In this case the direction of injection of the liquid reactants was directly in line with the direction of flow of the combustion

Figure A-43

Micro-Rocket Motor Injectors

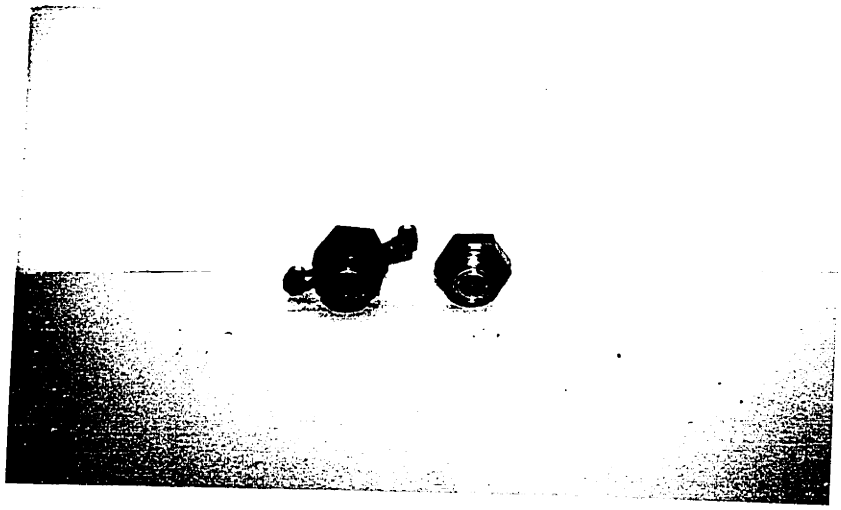

60° Open Impingement and

60° Confined Mixing Injectors

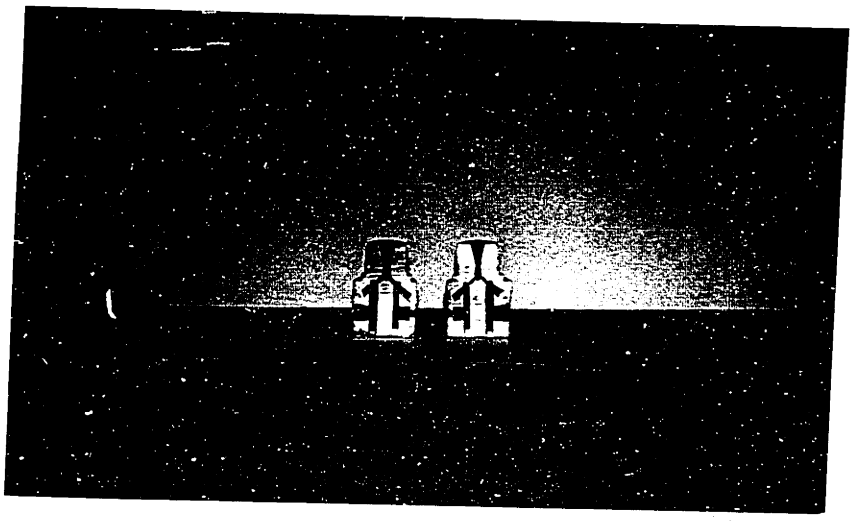

90° Confined Mixing

Injector, Cut In Half

gases through the combustion chamber and out the exhaust nozzle. With the Naphferrol-Peroxide system, the orifices of this injector were of unequal sizes, with the fuel hole held constant at No. 60 drill size (0.04" in diameter) while the peroxide hole was increased to a No. 54 drill size (0.055" in diameter).

Diagram C of Fig. 22 shows another in-line system of injection. This is the so-called pre-mix injector or "confined mixing" injector which was also attached through the back end plate of the motors. In this case the propellant streams meet and mix in a very small cylindrical passage (usually 0.08" in diameter) and then pass into the main combustion chamber through a short diverging conical passage (usually of 25-30°). In this way the reactants are held within a confined space for a time, which should produce more intimate mixing by prevent the complete separation of the liquids at the first reaction of the self-igniting propellants. Several different models of this injector were studied, with the main variables being the angle of impingement and the length of the cylindrical "confined-mixing" chamber. The angles of impingement studied were 60°, 74°, 90°, 135°, and 180° while the length of the mixing chamber was varied from 0.10" to 0.25". The diameter of the mixing chamber was also changed in a few cases.

Another model of this injector is shown cut in half in Figure A-43

Diagram E of Fig. 22 depicts a so-called reverse injection injector. This is again similar to the original mixing device used in measuring ignition delays, since the streams of liquid impinge at 90° on a flat surface. However, in this case the streams originate from orifices which are initially much closer together and the surrounding space is much more confined. Also this injector is located in the end plate of the motor instead of the sides of the combustion chamber wall as with diagram D. After bouncing off of the bottom of the impingement well, the reactants flow out into the main combustion chamber through another diverging conical passage. During this time they are flowing in the same direction in which the gaseous products eventually continue in passing right on out through the exhaust nozzle. In the open system of diagram B, on the contrary, the liquids enter in a direction which is perpendicular to or across the direction of gas flow and therefore is subject to more interference by these moving gas streams. The only other injector which was tried in the micro-rocket motors was a type of spray nozzle which was modified to give a short confined space just before the final spray orifice in which the two liquid reactants could be mixed together, before being ejected into the combustion chamber in the form of a conical spray. One of these nozzles which was made from a Monarch Stainless steel oil-burner

spray nozzle is shown in the sketch below.

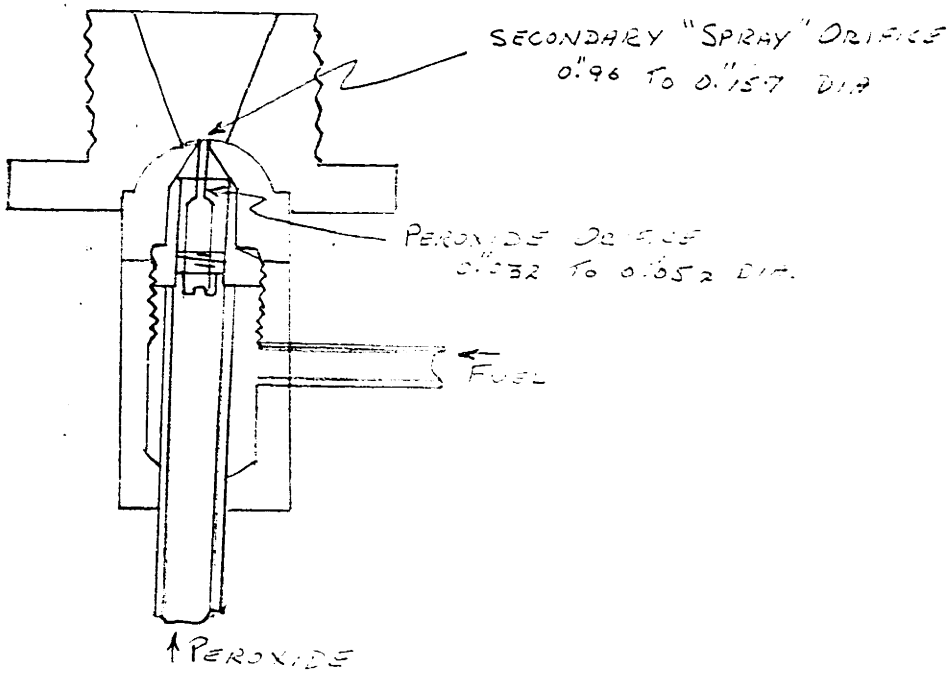

With this type of injector the inside, or primary orifice for the peroxide stream was varied from 0.032" diameter to 0.052" diameter while the outside or secondary orifice through which the mixed or combined streams enter the combustion chamber was varied from 0.096" diameter to 0.157" diameter. The fuel passage up to the mixing chamber consists of 3 or 4 spiral grooves (1/32" x 1/32") equally

spaced around the cone shaped nose of the inner tip. A whirl is imparted to the mixed streams by this directional flow of the fuel in these slots which results in the cone shaped spray which finally emerges from the outer orifice. Even this spray was further confined however by a diverging cone shaped passages leading out to the combustion chamber proper, similar to the cone passages in the confined mix, two-stream injectors.

FIGURE A-14

THRUST JACK ASSEMBLY

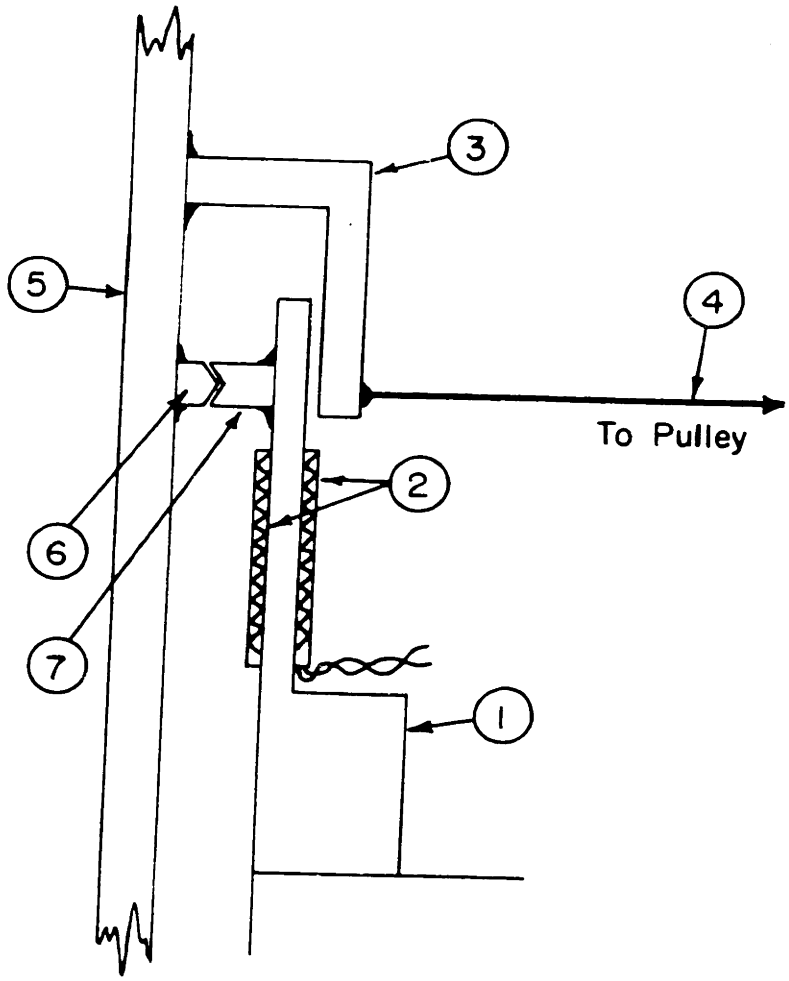

1. Dural Strain Gauge Beam
2. Stain Gauge
3. Calibration Jack
4. Calibration Wire
5. Cradle
6. Knife Edge
7. Thrust Jack (Agate Bearing)

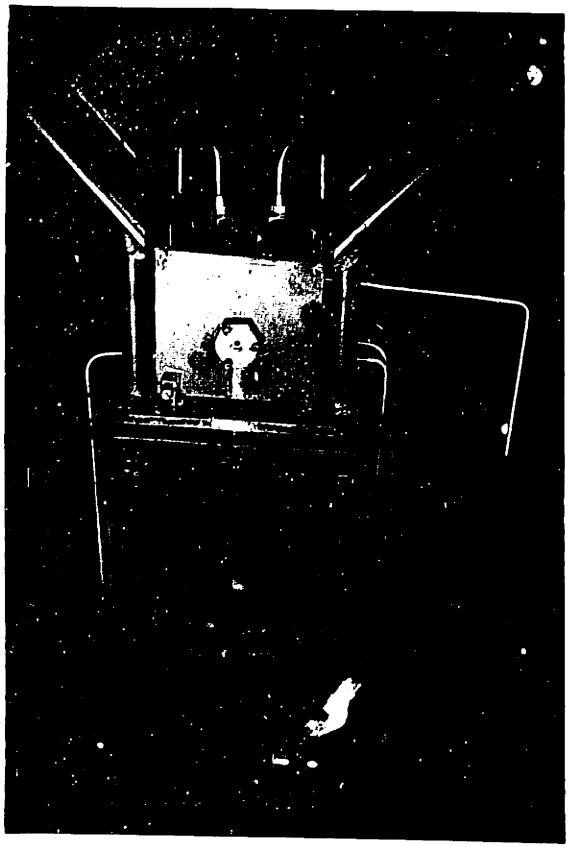

End View-Showing Exhaust Nozzle and Suspension System

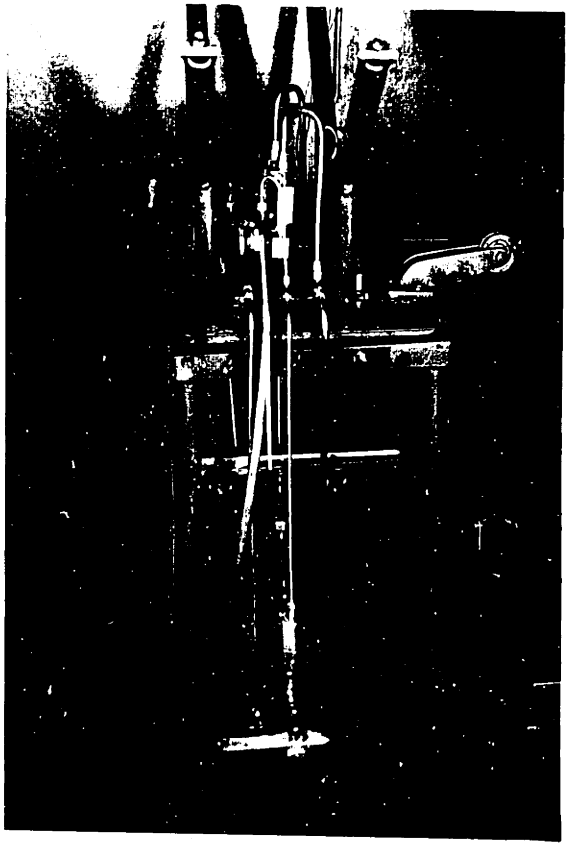

Side View-Showing Propellant Lines, Rocket Motor, Valves and Calibration System

Figure A-42
Thrust Stand

APPENDIX B

DESIGN OF REACTION STAND SUSPENSION AND THRUST MEASURING SYSTEM

Because of the small amount of thrust force obtained from the micro rocket motors, it was decided to employ for the thrust measuring system, that device which seemed to present the best possibilities for avoiding frictional effects. For this reason a strain gauge bridge cemented to a small cantilever beam which was deflected by the thrust force exerted by the motor was chosen as the instrument to be used. With this system the entire thrust force generated by the high velocity gas stream being discharged from the exhaust nozzle was transmitted directly against the cantilever beam via a knife edge contact against an agate bearing. The knife edge was actually mounted on one end of the thrust suspension cradle on the other end of which the nozzle of the motor itself was securely mounted. This arrangement is illustrated by the sketch of Fig. 23. The entire thrust stand assembly is shown in the pictures of Fig. A-42.

Thrust Bar

Dural was chosen for the cantilever beam because of its resistance to corrosion, its uniformity, and its

workability. When designed for a maximum stress of 10 to 13 thousand pounds per sq. in. (which is well within the elastic limit of the material) at the top thrust force of 20 lbs., the dimensions of the bar were as follows:

length	2"
width	3/4"
thickness	5/32"

These dimensions were determined from the flexure formula for beams [Given by Marks (26)]

$$S = \frac{Mc}{I} = \frac{Fxlxh/2}{bh^3/12} \qquad (1A)$$

where M = Force moment

S = Stress

c = Distance of outermost fiber from neutral axis

F = Force (Thrust)

l = Beam length

b = Beam width

h = Beam thickness

Solving for h from the above equation,

$$h = \sqrt{6Fl/bS} = \sqrt{\frac{6(20)(2)}{(3/4)(13,000)}} = \frac{5}{32}"$$

Under these conditions, the maximum deflection at the end of the beam on application of the 20 lbs. force will be given by the deflection formula for a concentrated load on a cantilever beam: [given by Marks (26)]

$$\delta = \frac{Fl^3}{3EI} = \frac{Fl^3}{3E(\frac{bh^3}{12})} = \frac{4Fl^3}{Ebh^3} \qquad (2A)$$

where δ = Deflection

I = Moment of Inertial

E = Young's Modulus of Elasticity

With the beam designed as above

$$\delta_{max.} = \frac{4(20)(2)^3}{(10)^7(\frac{3}{4})(\frac{5}{32})^3} = 0.0222"$$

This is an important quantity since it determines the amount of movement of the thrust cradle and consequently the amount of restraining force which will be exerted by the suspension wires and connected tubing lines due to this motion.

Strain Gauge Circuit

The strain gauge bridge was made up of four A-13 350 ohm gauges chosen because their width of about 3/8" made it possible to cement two gauges side by side on each side of the dural beam. A bridge of 4 gauges was used instead of a single gauge in order to eliminate temperature effects. As long as the temperature of both sides of the Dural bar was the same at all times, any temperature changes affected the resistance of the wire gauges on either side of the

bar equally. The electrical circuit used is shown in the diagram below.

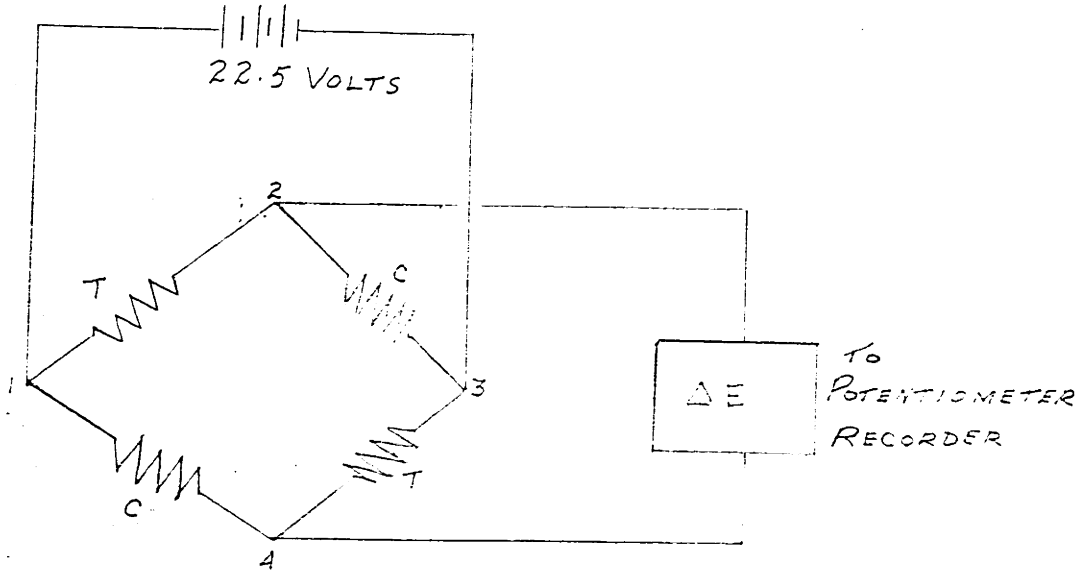

Gauges marked C are compressed by the deflection of the thrust bar, while those marked T are placed in tension.

The A-13 gauges are constructed of 0.001" diameter wire grids embedded in strips of paper and have a resistance of 350 ohms per gauge. Their change of resistance with

stress is given by

$$\frac{\Delta R}{R} = 2 \times \frac{S}{E} \qquad (3A)$$

which in this case would give

$$\left(\frac{\Delta R}{R}\right)_{max} = 2 \times \frac{13,000}{10 \times 10^6} = 0.0026$$

With the application of 22.5 volts to the terminals marked 1 and 3, the potential drop across terminals 2 and 4, from which the e.m.f. signal to the potentiometer is taken, would be given by

$$\frac{\Delta E}{E} = \frac{\Delta R}{R} \qquad (4A)$$

$$\Delta E_{max} = 0.0026 \ (22.5)$$

$$= 0.0585 \text{ volts or } 58.5 \text{ millivolts}$$

However, since the gauges are about 7/8" in length the effective length of the cantilever from the point of stress measurement is considerably less than the figure of 2 inches which was used in making the calculations above. This means that the stress at 20 lbs. thrust was actually nearer 10,000 psi. Accordingly at 20 lbs. thrust a maximum e.m.f. drop across terminals 2 and 4 of 45 m.v. was assumed and the Brown Electronik Potentiometer used to record the output signal from the bridge was built for an operating

range from 0 to 50 millivolts.

Thrust Cradle Suspension

The thrust cradle consisted of two 1/4" thick steel plates, 8 inches square joined near the lower edge by two 1/4" thick steel straps (3" x 8"). This formed a rigid frame work or cradle in which the test motors and auxiliary equipment could be mounted and through which the thrust force was transmitted to the cantilever strain gauge beam. This cradle was suspended by a total of 6 tension "wires," three on each end plate. These "wires" were actually 12 inch long galvanized wire cables of about 1/16" in diameter- each made up of several individual wire strands twisted together. They were stretched at each end to a tension of about 25 to 40 lbs. providing a torque resistance to prevent the movement of the cradle in any direction other than along the axis of the motor and exhaust nozzle. If this alignment had not been maintained, a component of the thrust force would have been measured instead of the total thrust.

Calibration System

The calibrating and pre-loading line was of the same 1/16" diameter cable as the suspension wires. It was attached to a steel arm extending from the rear face of the cradle over the top of the thrust bar. From this point of attachment to the top of the ball bearing pulley the cable was

perfectly aligned with the axis of the exhaust nozzle and cradle, using levels and a machinist's surface gauge. Passing over this pulley, the calibration cable then hung vertically due to the weight of the pan and preload weights which were used to bring the knife edge in firm contact with the thrust bar at the zero position. To calibrate the thrust system additional known weights were added to this dead weight load and the reading of the thrust (milli-volt) recorder noted. Since the calibrations were made immediately after each run with the same tension in the suspension wires and the same tubing connections made, the restraining force of these elements should have been the same in both cases and hence their effect eliminated. The tubing connecting to the cradle was all fastened rigidly to the stationary framework of the stand near the floor and then bent to form a right angle approach to the axis of the cradle just before being connected to it. These connections once made were then permanent and installing new equipment on the cradle involved only changes in the lines from the cradle framework to the equipment on the cradle.

Estimation of Magnitude of Restraining Forces on Cradle

1. Suspension Wires stretched to a tension of 40 lbs.

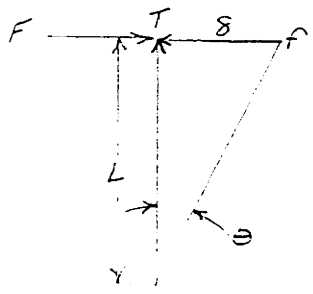

F = Thrust force

δ = Deflection

L = Length of suspension wires

T = Known tensile force in suspension wire

f = resisting force in direction of Thrust force = component of Tensile force in wire in that direction.

$$\tan \theta = \frac{\delta}{L} = \frac{f}{T} \qquad (5A)$$

$$\tan \theta_{max} = \frac{0.0222}{12} = 0.00185$$

$$\therefore \quad f = 0.00185(T)$$

$$= 0.74$$

With six cables the maximum restraining force due to all would be 6 x 0.074 or 0.444 lbs. out of a total thrust force of 20 lbs. In other words about 2% of the total thrust is taken up by the suspension wires.

2. Tubing connections to cradle

There were five pieces of 1/4" stainless steel tubing and two pieces of 3/8" copper tubing connected rigidly to the cradle from a point at the bottom of the stationary part of the thrust stand. The vertical distance between the two points of attachment was about 26.5 inches while the horizontal length of each piece of tubing was about 3

inches. This horizontal length of each section of tubing served as the lever arm through which the vertical length of tubing tended to be placed in torsional stress by the movement of the cradle. The entire length of tubing also tended to be deflected like a cantilever beam fixed at one end. Consideration of both of these mechanisms of producing a deflection in one of these tubing arm connections leads to the following equation:

$$\delta = F \left[\frac{b^3}{3EI} + \frac{a^3}{3EI} + \frac{ab^2}{E_s J} \right] \qquad (6A)$$

where δ = the total deflection of the cradle

F = the restraining force in the direction of movement of the cradle caused by all the stresses initiated in the tubing arm connection

b = the length of horizontal section of tubing

a = the length of the vertical section of tubing

E_s = modulus of rigidity or shear modulus

E = Young's modulus of elasticity

I = moment of inertia of the solid cross section of the tubing about a diameter or axis, as for a beam

$= \frac{\pi}{4}(r_o^4 - r_i^4)$

J = moment of inertia of the solid cross section of the tubing about the axis of the tubing

$= \frac{\pi}{2}(r_o^4 - r_i^4)$

a.) For one connection of copper tubing (3/8" O.D. by 3/10" I.D.)

Using Equation (6A):

$$0.0222 = F\left\{\frac{3^3 + (26.5)^3}{3(1.8 \times 10^7)(\frac{\pi}{4})(0.188^4 - 0.15^4)} + \frac{26.5(3)^2}{6.2\times10^6(\frac{\pi}{2})(0.188^4-0.15^4)}\right\}$$

$$0.0222 = F\left\{\frac{27 + 18{,}620}{(4.24 \times 10^7)(0.00123-0.00051)} + \frac{238.5}{(9.75\times10^6)(0.00123-0.00051)}\right\}$$

$$F = \frac{0.0222}{\frac{18{,}647}{30{,}200} + \frac{238.5}{7010}}$$

$$F = \frac{0.0222}{0.62 + 0.034} = 0.034 \text{ lbs.}$$

b.) For one connection of stainless steel tubing (1/4" O.D. by 0.035" wall)

$$0.0222 = F\left\{\frac{3^3 + (26.5)^3}{3(3.0\times10^7)\frac{\pi}{4}(0.125^4-0.09^4)} + \frac{26.5(3)^2}{12\times10^6(\frac{\pi}{2})(0.125^4-0.09^4)}\right\}$$

$$= F\left\{\frac{27 + 18{,}620}{(7.07\times10^7)(0.000244-0.000066)} + \frac{238.5}{(18.9\times10^6)(0.000244-0.000066}\right\}$$

$$\therefore F = \frac{0.0222}{\frac{18.647}{12,600} + \frac{238.5}{3360}}$$

$$= \frac{0.0222}{1.48 + 0.71} = 0.0143 \text{ lbs.}$$

Therefore the total restraining force due to all seven tubing connections is

$$F_{total} = 2(0.034) + 5(0.0143)$$
$$= 0.068 + 0.0715$$
$$= 0.14 \text{ lbs.}$$

out of a total thrust of 20 lbs. In other words about 0.7 of one per cent of the total thrust is taken up by the piping connections with the present thrust stand design. Of course, all of these restraining forces are accounted for in the calibration made after each run since conditions are presumably the same then as during a run.

APPENDIX C

CALIBRATION OF THE TUNGSTEN-MOLBDENUM THERMOCOUPLES

Although the tungsten-molybdenum thermocouple did not prove to be a successful means of measuring the temperature of the combustion gases in the micro-rocket motor, a typical calibration curve is presented here for future reference.

Originally, it had been expected that an unprotected thermocouple constructed of tungsten and molybdenum would be suitable for use in reducing gases up to a temperature of 2400°K at least. However, protection tubes were found to be necessary since the tungsten and molybdenum metals were both oxidized by even water vapor or carbon dioxide at temperatures as low as 2000°K. Satisfactory protection tubes constructed of Beryllia were obtained from the Norton Company of Worcester, Mass. However, the necessity of using the protection tubes so complicated the probe design and the correction calculations for radiation, that no reliable readings were ever obtained on an actual run.

Satisfactory calibration curves were obtained with an optical pyrometer using an electric carbon tube furnace to obtain the high temperatures. An atmosphere of nitrogen gas was maintained in the carbon tube in

FIG.A15 CALIBRATION CURVES FOR W-MO THERMOCOUPLE E.M.F VS TEMPERATURE

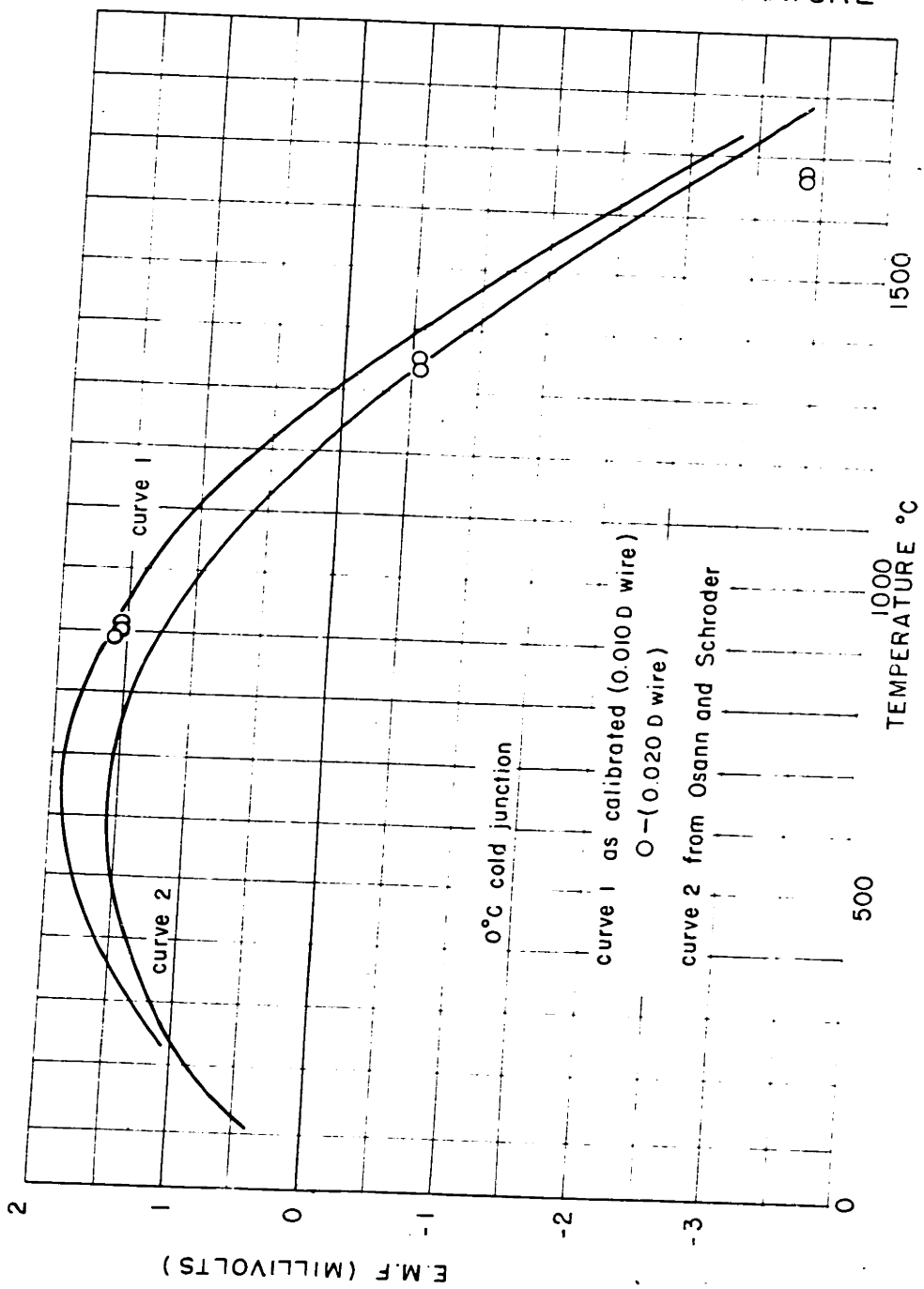

order to protect the thermocouple from oxidation. These calibration points for two different sizes of thermocouple wire are presented in Fig. A-15 together with an earlier curve of Osann and Schroder (31) for comparison.

Even with the nitrogen atmosphere, the tungsten and molybdenum wires became embrittled by heating to temperatures above 1500°C. This made it almost impossible to use a single couple for more than one run or calibration. However, the thermocouple wire which was used was tested for homogeneity and found to be very good with no stray effects of more than 2 or 3°C at temperatures of 600-800°C. The wire was obtained from Callite Tungsten Company of Union City, N. J.

APPENDIX D

NOZZLE DESIGN CONSIDERATIONS

Expansion Ratio

In the Thermodynamics section it was shown that

$$\dot{m} = p_c A_2 \sqrt{\frac{2g_o MW}{RT_c}} \sqrt{\frac{\gamma}{\gamma-1}} \sqrt{\left(\frac{T_2}{T_c}\right)^{\frac{2}{\gamma-1}} - \left(\frac{T_2}{T_c}\right)^{\frac{\gamma+1}{\gamma-1}}}$$

(See equation (20), page 31 of this thesis, which was derived assuming adiabatic reversible expansion of a perfect gas, with no reaction and constant C_p.)

In the case where point 2 is taken as the exit plane of the nozzle, this can be written:

$$\dot{m} = p_c A_e \sqrt{\frac{2g_o MW}{RT_c}} \sqrt{\frac{\gamma}{\gamma-1}} \sqrt{\left(\frac{T}{T_c}\right)^{\frac{2}{\gamma-1}} - \left(\frac{T}{T_c}\right)^{\frac{\gamma+1}{\gamma-1}}}$$

or

$$\dot{m} = p_c A_e \sqrt{\frac{2g_o MW}{RT_c}} \sqrt{\frac{\gamma}{\gamma-1}} \sqrt{\left(\frac{P_e}{P_c}\right)^{\frac{2}{\gamma}} - \left(\frac{P_e}{P_c}\right)^{\frac{\gamma+1}{\gamma}}} \qquad (7A)$$

Also in this section, it was shown that

$$\dot{m} = p_c A_t \sqrt{\frac{2g_o MW}{RT_c}} \sqrt{\frac{\gamma}{\gamma-1}} \sqrt{\left(\frac{2}{\gamma+1}\right)^{\frac{2}{\gamma-1}} - \left(\frac{2}{\gamma+1}\right)^{\frac{\gamma+1}{\gamma-1}}} \qquad (8A)$$

(See equation (22), page 32, which was derived on the same basis as (20) above.

From equations (7A) and(8A),

$$\frac{A_2}{A_t} = \frac{\sqrt{\left(\frac{2}{\gamma+1}\right)^{\frac{2}{\gamma-1}} - \left(\frac{2}{\gamma+1}\right)^{\frac{\gamma+1}{\gamma-1}}}}{\sqrt{\left(\frac{P_2}{P_c}\right)^{\frac{2}{\gamma}} - \left(\frac{P_2}{P_c}\right)^{\frac{\gamma+1}{\gamma}}}} \qquad (9A)$$

The quantity A_2/A_t is defined as the expansion ratio of the nozzle and equation (9A) is a theoretical expression for this quantity in terms of γ, P_2, and p_c (based on the several simplifying assumptions given before). In spite of these assumptions, equation (9A) is accurate enough to be used for designing actual nozzles using an average value of γ and the known or desired values of p_2 and p_c. In fact use of more refined equations is seldom justified because of the empirical allowance for friction which must be made in an actual nozzle and because of the relative insensitivity of motor performance to the value of p_2, which is actually reached in the experiments, (provided it is greater than $p_{atm.}$).

Design of Nozzles for Micro Thrust Motors

All of the nozzles for the present study were designed to operate at approximately 300 psia chamber pressure. The throat area A_t would be determined from equation (8A) or one of this same form for the desired mass flow $\dot{m}$. These areas for the studies reported here were between 0.016 and 0.04 sq. in.

All of the exhaust nozzles were designed with a gently rounded approach or converging section. The shape of this section was approximately by a conical section of 60° to 40°. This is approximately the approach angle commonly used although very irregualr approach surfaces can be used with less than 2% inefficiency being introduced in any case.

The correct expansion ratio was estimated from equation (9A). For example, if p_c = 300 psia, and p = 15 psia and γ = 1.2, substitution in equation (9A) will yield a value of $(A_e/A_t)_{theor.}$ = 3.7.

The value usually used in designing the micro-rocket nozzles was 3.5. From this ratio and the nozzle throat area, the exit plane area of the nozzle could be specified. However, the divergence angle of the nozzle was still undetermined. Kisenko (44) reports optimum performance for a de Laval type nozzle when the total divergence angle is between 20-25°. However, Keenan (45) recommends divergence angles of less than 12°. Accordingly some of the micro rocket exhaust nozzles were designed with divergence angles of 8° while others have included angles of 20°.

Performance Correction for Pressure

In order to correct experimental thrust or specific impulse to a chamber pressure slightly different than

the experimental chamber pressure, equation (14) of page 30 of the section on Thermodynamics can be used. This states that

$$I_{sp} = \sqrt{\frac{2RT_c}{g_o MW}} \sqrt{\frac{\gamma}{\gamma-1}} \sqrt{1-\left(\frac{P_e}{P_c}\right)^{\frac{\gamma-1}{\gamma}}}$$

If the two pressure $p_{c_{exp.}}$ and $p_{c_{standard}}$ are at all close together, T_c, MW, and γ will be substantially the same at both pressures for the same efficiency of combustion. In this case

$$\frac{I_{sp(exp.\ corrected)}}{I_{sp\ (exp.)}} = \frac{\sqrt{1 - \left(\frac{P_e}{P_{c\ standard}}\right)^{\frac{\gamma-1}{\gamma}}}}{\sqrt{1 - \left(\frac{P_e}{P_{c\ exp.}}\right)^{\frac{\gamma-1}{\gamma}}}} \qquad (10A)$$

If combustion efficiency is fairly high (80% or more) it will make little difference in this correction term (right side of equation (10A) whether the γ corresponds to theoretical combustion gas (produced by 100% combustion)) or to actual experimental conditions. This is especially true if the system is fairly cool and there is little dissociation. Accordingly, this substitution of theoretical working fluid properties in making this correction was employed in the present work, whether the correction was actually made by means of equation (10A) or from the comparison of calculated performance at

several pressures by means of Satterfield's charts and the pressure interpolation chart. Whichever method was used for calculating this theoretical performance, this comparison for two different pressures could be made directly from the working graphs on which theoretical performance was plotted over a whole range of conditions.

APPENDIX E

MATERIALS AND TECHNIQUES USED IN HANDLING PEROXIDE

Precautions in Handling Peroxide

Concentrated hydrogen peroxide solutions can be handled easily and safely if a certain amount of care is exercised. Hydrogen peroxide is not an exceptionally corrosive liquid and is almost completely free from corrosive and irritating fumes at room temperature. The chief danger is of its becoming contaminated with dirt or other catalytic material or mixed with organic liquids or other organic matter.

When pure, concentrated hydrogen peroxide is quite stable and has been found to be insensitive to shock. However, mixtures of peroxide and alcohol and other organic fuels have been detonated by means of blasting caps. Also owing to the exothermic nature of the decomposition reaction, a relatively small amount of contamination can start a vigorous reaction in a large container of peroxide which will reach explosive violence especially if there are insufficient escape vents.

Another danger with concentrated peroxide is that of fire. As a concentrated source of oxygen, it makes ignition and combustion of any combustible material easier and quicker to achieve. Spillage should be avoided if possible and quickly

washed away with large quantities of water when it does occur. Because of this danger glass containers without a surrounding metal container should not be used for storing or transporting peroxide. The strong peroxide solutions are, themselves, irritating to the skin and will attack the tissues producing soreness or near burns. Contact with the skin should be avoided if possible and even small amounts quickly washed away with water if such contact does occur.

Peroxide should never be stored for long periods of time in unvented containers or trapped in closed spaces. However, any vents should be carefully protected to prevent foreign material from gaining entrance in this way.

Materials for Use with Hydrogen Peroxide

A. Metals

The best metals for long time storage of concentrated peroxide are aluminum and tin. When very pure, these are ideal. Pyrex glass is also completely satisfactory for storage in that it furnishes a very inactive surface, however, it is inferior as regards structural strength and possible damage and breakage with resultant spillage. Stainless steel is also quite safe for moderately long time storage. However, loss of peroxide due to slow decomposition will take place at a somewhat higher rate in most cases in stainless than in tin, glass or aluminum. Stainless steel has the property of

becoming passivated upon use with peroxide so that the decomposition rate on such surfaces usually drops with continued use and will finally become very good in this respect. Types 316, 347 and 304 have been found to be among the best varieties of stainless steel for use with peroxide.

All these metals, especially stainless steel, require pretreatment in order to obtain the most inactive surface which they can possibly present to peroxide decomposition. The smoother the surface which is obtained, the less the chance for any peroxide decomposition -- other things being equal. A truly smooth and polished surface can usually be obtained by electropolishing but even mechanical polishing and buffing is helpful. After the best possible smoothness and polish is obtained for the surface, a chemical treatment is necessary. First, an alkali treatment to remove grease and dirt is carried out. This is followed by an acid pickle and a water rinse. Then the container surface should be passivated by immersion in peroxide for as long a time as possible (at least 24 hours and preferably one week). Dilute peroxide should be used first, with more concentrated solutions being applied later.

Stainless steel has the big advantage of good weldability. Much care is required, however, to produce a weld which is inactive to strong peroxide. If possible, an inert atmosphere

should be provided during the welding operation to
the formation of oxides and scale. In any case the
should be ground and cleaned of flux and scale if p
then pickled and treated chemically as for the othe
surfaces described above. Chromic Acid cleaning so
should never be used for glass or any other surface
used with peroxide, since chromic oxide is a strong
for peroxide.

Other metals can be used for pipe lines or othe
faces which contact peroxide only for the duration o
of an experimental test. However, stainless steel i
mended even here especially if there is a chance of
temperatures. Copper, mild steel, and Monel in very
amounts have been used in this work for such applica

B. Plastics, Gasket Materials, and Lubricants

Of the plastic materials which have been exp
to peroxide during this work, the following have prov
be most inert toward and least affected by concentrat
hydrogen peroxide (given in order of rating):

1. Teflon
2. Polyethylene
3. Koroseal
4. Saran
5. Vinylite
6. Neoprene

Inspite of its complete chemical inertness toward peroxide, Teflon is not an ideal gasket material because it is subject to "cold flow." The same is true of Polyethylene to a lesser extent. Koroseal is more rubber-like and ideal for gaskets but is somewhat affected by the peroxide, gradually hardening, apparently because of deplasticization. Of course, pure tin can be used for hard gaskets but for elastic-type gaskets either Koroseal or Teflon must be used. With Koroseal, this will necessitate occasional substitution of a new gasket when the old one becomes too hard. On the other hand with Teflon, a counteracting mechanism for continually squeezing the gasket back into shape or a complete confinement will be necessary in order to avoid its "cold flowing" out of shape.

Silicone grease and silicone oils appear to be satisfactory lubricants for contact with strong hydrogen peroxide. The arochlors which are partially chlorinated diphenyl compounds can also be obtained in a range of chlorination which produces oily liquids which are suitable lubricants. These compounds also appear unaffected by peroxide. Ordinary lubricating oils are initially completely immiscible with peroxide and produce no visible decomposition. However, if mixed with peroxide continuously for several days, a partial emulsion can be formed between the two liquids. While this mixture could not be detonated by use of a number eight blasting cap submerged in the

liquid at 300 psia pressure, the indication of possible emulsification is at least a potential source of danger, since the oil is a rather combustible material.

Ordinary talcum powder appears to be inactive towards strong peroxide solutions and furnishes a small amount of lubrication for a time.

FIGURE A-16 SURFACE TO VOLUME RATIO AS A FUNCTION OF THRUST FORCE

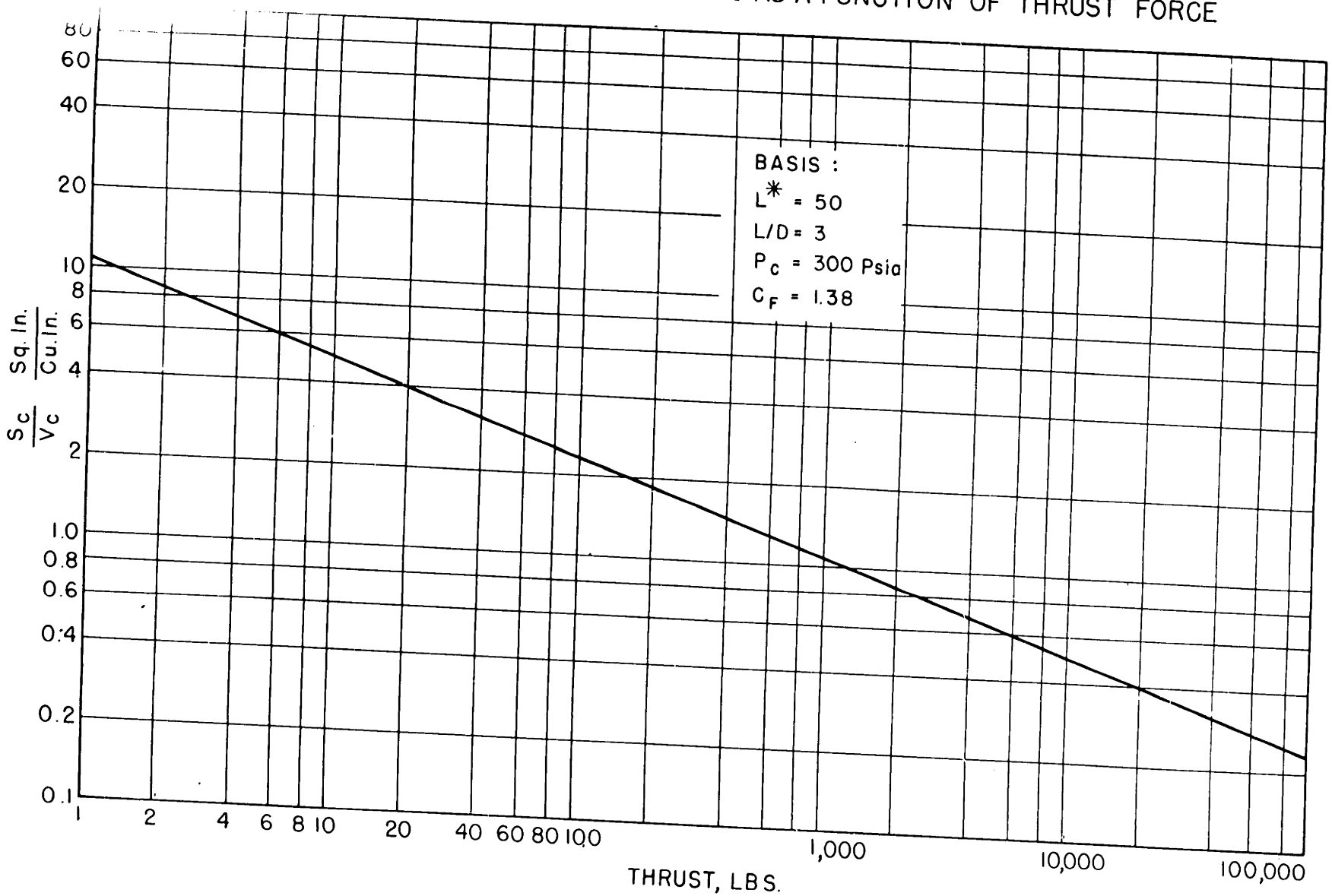

APPENDIX F

THEORETICAL AND PRACTICAL CONSIDERATIONS OF THE EFFECTS OF HEAT LOSS ON REACTION MOTOR PERFORMANCE

Effect of Scale of Operation on Heat Loss

Figure A-16 shows the change in surface to volume ratio for combustion chambers of various size thrust motors. It was constructed assuming the following design conditions for cylindrical shape motors:

$L^* = 50$ inches
$L/D = 3$
$P_c = 300$ psia
$C_F = 1.38$

Assuming the use of the same propellant system and the attainment of the same efficiency of combustion in all motors, then the chamber volume, V_c, is directly proportional to the mass flow rate, $\dot{m}$. Hence, the relative values of the surface to volume ratio, S_c/V_c, in the graph of Fig. A-16 for any two thrust sizes are the same as the relative values of the ratio of surface to mass of propellants available, $S_c/\dot{m}$, for the same thrust sizes. Accordingly, it appears that the ratio of surface to mass flow rate for a 10 lb. thrust motor is 4.65 times that of a 1000 lb. thrust motor on the above basis.

The heat transfer rate due to convection is given by

q/S in Btu/sec. x sq. ft. $= h\Delta T$

where h is the corrective heat transfer coefficient and ΔT is the temperature difference or driving force. Or assuming the same ΔT in all combustion chambers regardless of size, $q/A \propto h$. According to McAdams[27], for heat transfer from a gas flowing in a horizontal tube:

$$h = \frac{0.027 C_p G^{0.8} \mu^{0.2}}{D^{0.2}} \qquad (11A)$$

where G is the mass flow velocity, μ is the viscosity and D is the diameter. On the above design basis all of these quantities should be the same for each motor except D.

Also $V_c = \frac{\pi}{4} D^2 L$

and since $L = 3D$

$$V_c = \frac{3\pi}{4} D^3$$

$$100 V_{c(10 \text{ lb. thrust})} = V_{c(1000 \text{ lb. thrust})}$$

$$\therefore \quad 100\, D_{(10 \text{ lb. thrust})} = D_{(1000 \text{ lb. thrust})}$$

$$\text{or} \quad D_{1000 \text{ lb. thrust}} = 4.65\, D_{(10 \text{ lb. thrust})}$$

and from equation (11A)

$$h_{1000 \text{ lb. thrust}} = \frac{h_{10 \text{ lb. thrust}}}{1.36}$$

The radiation heat transfer rates will also increase with

diameter somewhat although the exact function can not be given and depends considerably on the temperature of the system and the gas composition. However, approximately we can say that

$$\left(q/A\right)_{10\,\text{lb. Thrust}} = 1.36\left(q/A\right)_{1000\,\text{lb. thrust}}$$

Therefore the heat loss for the entire combustion chamber per lb. of propellant, $q/\dot{m}$ in Btu/[redacted] lb. should be related as follows:

$$\left(q/\dot{m}\right)_{10\,\text{lb thrust}} = 4.65 \times 1.36\left(q/\dot{m}\right)_{1000\,\text{lb Thrust}}$$

$$= 6.32\left(q/\dot{m}\right)_{1000\,\text{lb Thrust}}$$

It is probable that a similar relation would exist for the heat loss in the nozzle, although this cannot be said with as much certainty.

Since the experimental results of this thesis indicate a maximum effect of heat loss on performance of a 10 lb. thrust size combustion chamber with an L* of 50 inches of about 4%, this analysis would indicate that the effect in a similar motor of 1000 lb. thrust size would be only about 1/2%. Or, instead of an effective heat loss of about 120 Btu/lb. on the hydrazine hydrate-peroxide system, in a

FIGURE A-17 HEAT CAPACITY VS. TEMPERATURE OF PURE GASES

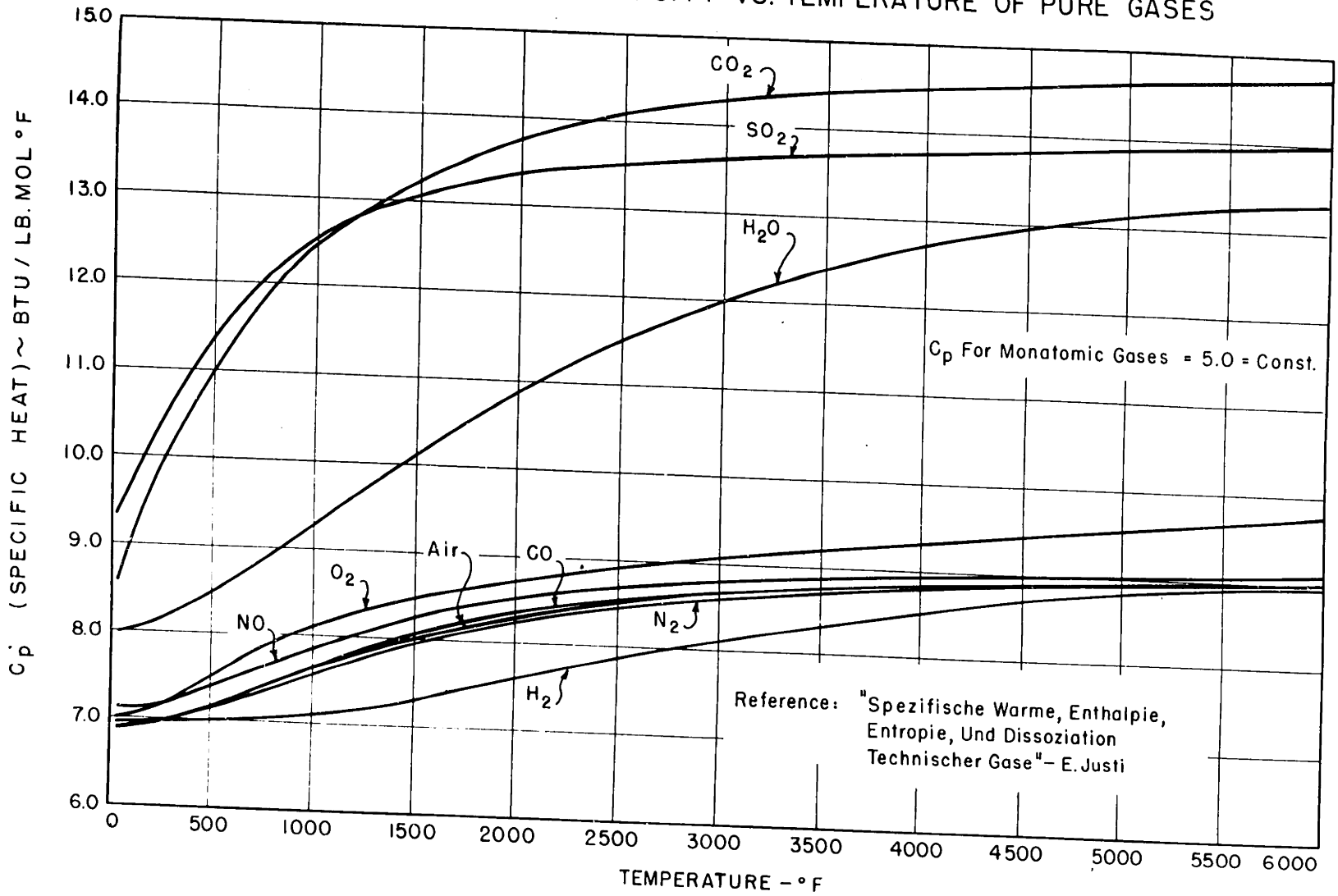

1000 lb. thrust motor this would only amount to 20 Btu/lb. of propellants. This analysis at least indicates the order of magnitude of the heat losses to be expected on various sizes of thrust motor.

Comparison of Experimental Combustion Chamber Heat Losses with Those Predicted from Equations

System: 85% $N_2H_4 \cdot H_2O$ - 90% H_2O_2 (Stoichiometric)

Case I: Motor W (1" I.D. x 3" long)(3/32" stainless steel wall thickness)

Given : $\dot{m}$ = 0.0366 lbs./sec. or 132 lbs./hr. (W Series Runs)

T_c for this system at 300 psia = 3860°R or 2145°K

C_p for combustion gases at 3860°R = 11.76 $\left\{\begin{matrix} 85.6\% \ H_2O \\ 14.4\% \ N_2 \end{matrix}\right\}$ approx.

MW = 19.44

$\mu = 0.000097\ T^{\wedge}$ approx [See McAdams (28)] where μ = lbs./hr. x ft. and T = °K

Using equation (11A) once more for gases flowing in a horizontal tube or pipe,

$$h = \frac{0.027\, c_p\, G^{0.8}\, \mu^{0.2}}{D^{0.2}}$$

$$= (0.027)\left(\frac{11.76}{19.44}\right)\left[\frac{132}{\frac{\pi}{4}\left(\frac{1}{12}\right)^2}\right]\frac{\left[(0.00097)(2145)\right]^{0.2}}{\left(\frac{1}{12}\right)^{0.2}}$$

$$= 63.2\ \frac{Btu}{ft^2 \cdot hr \cdot {}^\circ R}$$

$$\therefore q_{convection} = hA\Delta T = 63.2\left(\frac{\pi}{12} \cdot \frac{3}{12}\right)(3860 - T_{iw})$$

(using lateral surface area only)

$$= 4.14\,(3860 - T_{iw})$$

$$q_{radiation} = (A)(0.173)\left[\varepsilon_{H_2O}\left(\frac{T_c}{100}\right)^4 - \alpha_{H_2O}\left(\frac{T_{iw}}{100}\right)^4\right] \quad (12A)$$

where ε_{H_2O} is the emissivity and α_{H_2O} is the absorptivity of water vapor.

From the emmissivity charts of McAdams(29)

$\varepsilon_{H_2O} = 0.085$ at P_{H_2O} L = (0.865)(20.5)(0.6)(1/12) = 0.887

which is for $P_T = 1.0$ atm. and $P_w = 0$.

The effect of total pressure can be estimated by extrapolating the curves of Egbert(13).

ε_{H_2O} at 20.5 atm. = 1.8 ε_{H_2O} at P_T = 1.0 atm.

$\therefore \varepsilon_{H_2O} = 1.8(0.085) = 0.153$

It has been found that T_{iw} is so small that the second term on the right hand side of equation (12A) can be neglected. Therefore, the heat transferred by radiation is given by

$$q_{rad} = (\pi 1/12 \times 3/12)(0.173)(0.153)(38.60)^4$$

$$= 3810 \text{ Btu/hr.}$$

At steady state conditions, the total heat transferred to the inside wall of the combustion chamber by both convection and radiation must be transferred through the

wall by conduction. Therefore

$$q_{total} = q_{conv.} + q_{rad} = \frac{k}{x} S_{AV} (T_{iw} - T_{ow}) \qquad (13A)$$

Since the temperature of the cooling water was usually about 600 to 650°R in the experiments of this thesis, we shall assume $T_{ow} = 700°R$.

Then

$$4.14 (3860 - T_{iw}) + 3810 = \frac{25}{\left(\frac{0.0938}{12}\right)} \left(\pi \frac{1.094}{12} \times \frac{3}{32}\right) (T_{iw} - 700)$$

Solving this for T_{iw} gives:

$$T_{iw} = 771°R.$$

Therefore from equation (13A),

$$q_{total} = 4.14(3860 - 771) + 3810 = 12,790 + 3810$$
$$= 16,600 \text{ Btu/hr. or } 4.61 \text{ Btu/sec.}$$

$\therefore l_{total}$, the heat loss per lb. of propellant in this motor chamber $= \frac{4.61}{0.0366} = 126$ Btu/lb. Compare this with the average measured experimental value for this system with this motor of 155 Btu/lb. In other words the calculated value is 81% of the experimentally measured value in this case.

An analysis similar to that above carried out for the X motor (1/2" I.D. x 3" long) with the same propellant

system indicates that

q_{total} should be = 11,800 Btu/hr. or 3.28 Btu/sec.

and $l_{total} = \frac{3.28}{0.0365} = 89.9$ Btu/lb.

The average experimental value for this system in this motor was 55 Btu/lb. In this case the calculated value is 163% of the experimentally measured value.

The chief reason for the difference in the relative magnitudes of the measured and calculated heat loss on the two motors is probably the difference in the experimental performance on the two motors. Motor X was only one half as long as Motor W and complete combustion was never attained in Motor X whereas it was usually quite complete in Motor W. The gas temperatures were therefore lower in Motor X and probably much lower for a large fraction of its length.

Prediction of Combustion Chamber Heat Losses On Motors Used on Stationary Stand

The heat loss on the large stationary stand motor (2" I.D. x 4" long) can also be calculated by the above analysis. For the same system, but with a mass flow rate of 0.0553 lbs./sec., these figures are:

q_{total} = 30,040 Btu/hr. or 8.35 Btu/sec.

$l_{total} = \frac{8.35}{0.0553} = 151$ Btu/lb.

Since this chamber is even longer than that of Motor W and good combustion efficiencies were also obtained here, it is probable that the heat loss here was actually greater than this estimated value. However, it is almost certain that it was no lower than this estimated quantity. Therefore, as a conservative estimate, this calculated heat loss was used as a correction to the experimental performance of the runs with this motor. To be sure, this is an approximation but it should be better than no correction at all. The effect of this amount of heat loss upon the calculated chamber pressure for a given run was only about 4%.

Similarly on the solid copper motor used on the stationary stand in connection with heat transfer measurements by Borden, the heat loss can be estimated. This motor consisted of a 2-1/4" length of 1" diameter followed by 3/4" length or 1/2" diameter. Therefore, at a mass flow rate of 0.0365 lbs./sec., from the previous calculations on 1" and 1/2" diameter motors:

$$\ell_{total} = \frac{2\frac{1}{4}}{3}(126) + \frac{3/4}{1\frac{1}{2}}(90)$$

$$= 94.5 + 45$$

$$= 140 \text{ Btu/lb.}$$

This also is felt to be a conservative estimate because the total length of the motor was as long as

Motor W and good combustion efficiencies were obtained.

Comparison of Experimental Exhaust Nozzle Heat Losses With those Predicted by Conventional Heat Transfer Ecuations

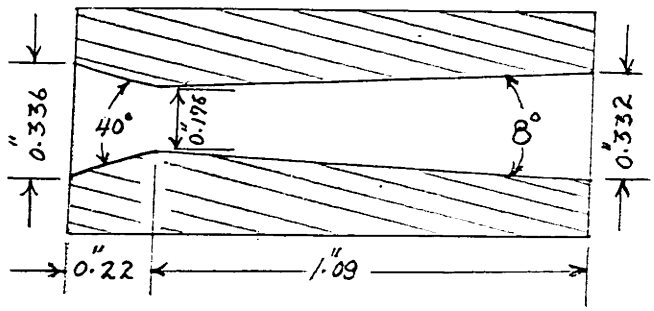

This nozzle sketched above was used in tests (U-Series) with the W-motor on the thrust stand, employing the system 90% H_2O_2 - 85% N_2H_4 H_2O as propellants. Experimental heat loss from the nozzle to cooling water in a spiral cooling jacket around the outside copper body was measured on these runs. In order to compare calculated heat losses with the experimental value for this nozzle, the following estimation of the expected heat loss was made using conventional heat transfer equations. Since the gas flow through the nozzle reaches sonic velocity in the throat and is supersonic throughout the diverging section, this method of handling the problem is not truly rigorous. An estimate of the maximum effect on this analysis of using a stagnation temperature instead of the true stream temperature is made

later using an assumed recovery factor of 1.0.

Calculation of Heat Transfer

The diverging section of the nozzle shown above is an 8° conical section and the surface area can be calculated from the dimensions of this frustrum of a cone. The converging section has a curved surface but it can also be closely approximated by a conical shape. This was done in order to simplify the equations for the surface area, S, of these sections.

x_n is defined as the distance along the axis of the converging section at any point from the entrance. It varies from 0 to 0.22".

x_d is defined as the distance along the axis of the diverging section at any point from the throat. It varies from 0 to 1.09".

y_n is defined as the radius of the converging (conical) passage at any point. It varies from $y_{n_o} = 0.168"$ to $y_{n_t} = 0.088"$.

y_d is defined as the radius of the diverging passage at any point. It varies from $y_{d_o} = 0.088"$ to $y_{d_e} = 0.161"$.

$$\therefore x_n = \frac{y_{n_o} - y_n}{\tan 20^\circ} = \frac{0.168 - y_n}{0.364} \qquad (14A)$$

and

$$x_d = \frac{y_d - y_{d_o}}{\tan 4^\circ} = \frac{y_d - 0.088}{0.0699} \qquad (15A)$$

The convectional heat transfer rate to the area of any infinitesimal segment of the nozzle length dx can be expressed by

$$dq_x = h_x \, dA_x \, \Delta T_x$$

Using equation (11A) this becomes

$$dq_x = \frac{0.027 \, c_{px} \, G_x^{0.8} / \mu_x^{0.2}}{D_x^{0.2}} \, dA_x \, (T_{gx} - T_{iwx})$$

or $$dq_x = \frac{0.027 \, c_{px} \, \dot{m}^{0.8} / \mu_x^{0.2}}{\left(\frac{\pi}{4}\right)^{0.8} D_x^{1.6}} \, dA_x \, (T_{gx} - T_{iwx}) \qquad (16A)$$

The following assumptions are made:

1) Assume that the inside wall temperature of the nozzle is constant at 1000°R (550°K). (Since the inside wall temperature of the chamber is estimated at about 800°R, this seems reasonable. Also Borden measured temperatures of about 400 to 500°F in this region of the thick walled copper motor.) While this temperature will vary slightly through the nozzle length, this variation will be very small especially in a copper nozzle.

2) Assume that the inlet gas temperature at the nozzle entrance is 2000°K. (Allowing for heat loss in chamber and incomplete combustion to reduce the adiabatic combustion temperature of 2145°K.)

3) Assume the inlet gas pressure to the nozzle is 300 psia and that the relationship between nozzle cross sectional area, pressure, and temperature as the gas flows through the nozzle is given by the expression for adiabatic, reversible expansion of a perfect gas.

$$\text{i.e. } \left(\frac{T_2}{T_1}\right) = \left(\frac{P_2}{P_1}\right)^{\frac{\gamma-1}{\gamma}}$$

and from equation (20) of the Thermodynamic section, p.31

$$\dot{m} = P_c A_2 \sqrt{\frac{2g_o MW}{RT_c}} \sqrt{\frac{\gamma}{\gamma-1}} \sqrt{\left(\frac{T_2}{T_c}\right)^{\frac{2}{\gamma-1}} - \left(\frac{T_2}{T_c}\right)^{\frac{\gamma+1}{\gamma-1}}}$$

since $\dot{m}$ is constant

$$P_c A_1 \sqrt{\frac{2g_o MW}{RT_c}} \sqrt{\frac{\gamma}{\gamma-1}} \sqrt{\left(\frac{T_1}{T_c}\right)^{\frac{2}{\gamma-1}} - \left(\frac{T_1}{T_c}\right)^{\frac{\gamma+1}{\gamma-1}}} =$$

$$P_c A_2 \sqrt{\frac{2g_o MW}{RT_c}} \sqrt{\frac{\gamma}{\gamma-1}} \sqrt{\left(\frac{T_2}{T_c}\right)^{\frac{2}{\gamma-1}} - \left(\frac{T_2}{T_c}\right)^{\frac{\gamma+1}{\gamma-1}}}$$

$$\therefore \frac{A_1}{A_2} = \left(\frac{T_2}{T_1}\right)^{\frac{1}{\gamma-1}} \sqrt{\frac{(T_c - T_2)}{(T_c - T_1)}} \qquad (17A)$$

This derivation assumes constant γ and MW and therefore constant c_p with no reaction in addition to those assumptions stated above. However, these approximations are more than justified for the present approximate

analysis or estimate of nozzle heat loss.

4) It is assume that the viscosity of the gas, μ in lbs/hr. x ft., is given by 0.000097T where T is in °K, in the range from 1000 to 2000°K. This approximation was found to fit the data presented on page 410-11 of McAdams quite closely.

5) It is also assumed that in the range of temperatures from 2000 to 1000°K, the molal heat capacity $M c_p$ of the gas mixture (85.6% H_2O and 14.4% N_2) is represented by $M c_p = 7.75 + 0.001955\ T$ where T is again in °K. This approximation was found to fit the data for this gas mixture within 1% over this range.

6) Assume that heat transferred by radiation in the nozzle is small enough to be neglected. Using these approximations equation (16A) becomes:

$$dq_{fx} = \frac{0.027(7.75 + 0.001955\,T)(\dot{m})(0.000097\,T)^{0.2}}{\pi y^2 (Re)^{0.2}} (2\pi y)\, dx\,(T - 550) \qquad (18A)$$

where R_e is the Reynolds number $\frac{DG}{\mu}$.

Here, $\dot{m}$ is constant and known and y is known in terms of x by equation (14A) and (15A); therefore, only T in terms of x is needed. This can be obtained by means of equation (17A) because $\frac{A_1}{A_2} = \frac{\pi y_1^2}{\pi y_2^2}$ and y is known in terms of x from either equation (14A) or (15A).

FIGURE A-18 TRUE TEMPERATURE OF GAS STREAM FLOWING THOUGH EXHAUST NOZZLE AS A FUNCTION OF CROSS SECTIONAL AREA OF NOZZLE PASSAGE

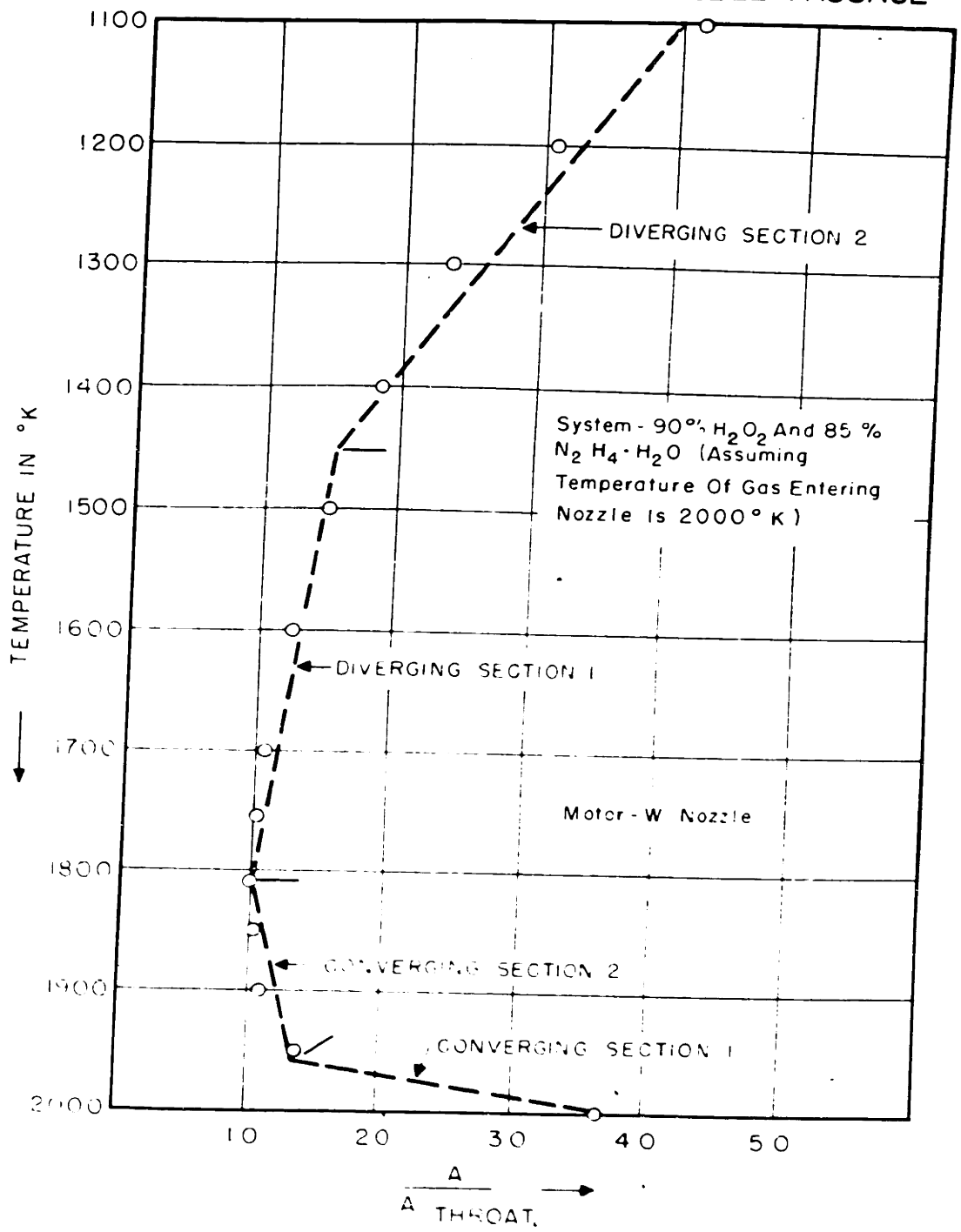

When A/A_{throat} was plotted against Temperature for the entire nozzle, it was found that the relationship between the two could be described quite accurately by linear equations provided the nozzle were divided into four sections. (See Fig. A-18) This was done and the heat transfer was integrated over the two converging sections and over the two diverging sections as follows:

Converging Section

No. 1. (From $x_n = 0$ to $x_n = 0.18$) T is essentially constant. Assume $T_{AV} = 1980$.

Then $M_{eff} = 7.75 + (0.001955)(1980) = 11.62$ Btu/lb.mol x °R.

and $\mu = 0.000097(1980) = 0.192$ lbs./hr. x ft.

$D = 2y = 2(0.168 - 0.364x)$

$$\text{and } Re = \frac{DG}{\mu} = \frac{4\dot{m}}{\pi D \mu} = \frac{4(0.0556 \times 3600)12}{\pi 2(0.168-0.364x)(0.192}$$

$$= \frac{7960}{(0.168-0.364x)}$$

$$\text{Then } dq_x \Big]_{x_n=0}^{x_n=0.18} = \int_0^{0.18} \frac{(0.027)(11.62)(0.168-0.364x)^{0.2}(0.0556\times3600)}{(19.44)(7960)^{0.2}\pi(0.168-0.364x)^2} \rightarrow$$

$$2\pi(0.168-0.364x)(1.8)(1480-550)\,dx$$

$$q_x(\text{converging section 1}) = -\frac{2758}{0.364}\int_0^{0.18}(0.168-0.364x)^{-0.8}(-0.364)\,dx$$

$$= -\frac{2758}{0.364}\left[\frac{(0.168-0.364x)^{0.2}}{0.2}\right]_0^{0.18}$$

$$= 2495 \text{ Btu/hr}$$

Converging Section No. 2 (From $x_n = 0.18$ to $x_n = 0.22$)

$$T = 1380 + 429\left(\frac{A}{A_t}\right) = 1380 + 429\,\frac{(2y)^2}{(0.176)^2}$$

$$= 1380 + 55{,}300(0.168 - 0.364x)^2$$

$$\mu = 0.000097\ T \quad (\text{assume } T_{AV} = 1890)$$

Then $\mu = 0.184$ lbs./hr. x ft.

$$c_p = 7.75 + 0.001955\left[1380 + 55{,}300(0.168 - 0.364x)^2\right]$$

$$= 10.45 + 108.1(168 - 0.364x)^2$$

$$Re = \frac{4(0.0556 \times 3600)12}{2\pi(0.168-0.364x)(0.184)} = \frac{8350}{(0.168 - 0.364x)}$$

Then $$dq_x\Big]_{0.18}^{0.22} = \int_{0.18}^{0.22} \frac{\left[10.45 + 108.1(0.168-0.364x)^2\right](0.027)(0.168-0.364x)}{19.44\,\pi\,(0.168-0.364x)^2\,(8300)^{0.2}}$$

$$\rightarrow 2\pi(0.168-0.364x)1.8\left[1380+55{,}300(0.168-0.364x)^2-550\right]dx$$

$$dq_x\Big]_{0.18}^{0.22} = \int_{0.18}^{0.22} \frac{1433\,dx}{(0.168-0.364x)^{0.8}} + 985{,}800(0.168-0.364x)^{3.2}\,dx$$

$$\rightarrow +110{,}500(0.168-0.364x)^{1.2}\,dx$$

$$\therefore q_x\,(\text{converg. sect. 2}) = \frac{1433}{0.364}\,\frac{(0.168-0.364x)^{0.2}}{0.2} - \frac{985{,}800}{0.364}$$

$$\rightarrow \frac{(0.168-0.364x)^{4.2}}{4.2} - \frac{110{,}500}{0.364}\,\frac{(0.168-0.364x)^{2.2}}{2.2}\Bigg]_{0.18}^{0.22}$$

$$= 658\ \text{Btu/hr}$$

$$\therefore q_{\text{total converging section}} = 2495 + 658 = 3153.\ \text{Btu/hr.}$$

Diverging Section

No. 1 (From $x_d = 0$ to $x_d = 0.286$)

From Chart $T = 2516 - 710\left(\frac{A}{A_t}\right) = 2516 - 710\left(\frac{2y}{0.176}\right)^2$

$= 2516 - 91800(0.088 + 0.0699x)^2$

$\mu = 0.000097T$ (assume $T_{av} = 1628°K$) See Chart (Fig. A-18)

then $\mu = 0.158$ lbs./hr. x ft.

$c_p = 7.75 + (0.001955)\left[2516 - 91800(0.088 + 0.0699x)^2\right]$

$= 12.66 - 179.3(0.088 + 0.0699x)^2$

$$Re = \frac{4(0.0556 \times 3600)12}{2\pi(0.088+0.0699x)(0.158} = \frac{9680}{(0.088+0.0699x}$$

Substituting all these quantities and equation (5) in equation (6A) and integrating between $x_d = 0$ and $x_d = 0.286$, we find

q(div. sect. No. 1) = 3564 Btu/hr.

Diverging Section No. 2 (From $x_d = 0.286$ to $x_d = 1.09$)

$T = 1664 - 143\frac{A}{A_t} = 1664 - 143\left(\frac{2y}{0.176}\right)^2$

$T = 1664 - 18500(0.088 + 0.0699x)^2$

$\mu = 0.000097T$ (Assume $T_{Av} = 1300$)

then $\mu = 0.126$ lbs./hr. x ft.

$c_p = 7.75 + 0.001955\left[1664 - 18500(0.088 + 0.0699x)^2\right]$

$= 11.01 - 36.18(0.088 + 0.0699x)^2$

$$Re = \frac{4(0.0556 \times 3600)12}{2\pi(0.088+0.0699x)(0.126)} = \frac{12,140}{(0.088+0.0699x)^2}$$

Substituting all these quantities and equation (5) in equation (6A) and integrating between γ_d = 0.286 and γ_d = 1.09, we find

q (div. sect. No. 2) = 4909 Btu/hr.

$\therefore$ q_{total} diverging section = 3564 + 4909 = 8473 Btu/hr. and q_{total} for entire nozzle = 8473 + 3153 = 11,626 Btu/hr. The average measured heat loss in the entire nozzle for the U-Series runs was 78 Btu/lb. This is equivalent to 78 x 0.0556 x 3600 = 15600 Btu/hr. In other words the calculated value is 75% of the experimentally measured value in this case, which is a fair check (as good as for the combustion chambers).

This theoretical analysis indicates that 72% of the total nozzle heat loss occurs in the diverging section of the nozzle. Accordingly, in the calculations of chamber pressure and other quantities which involve expansion only as far as the throat, 28% of the total nozzle heat loss was assumed to be transferred in the converging section. This figure is probably slightly higher than the correct percentage. However, it cannot be far in error, because even if the stagnation temperature had been used in calculating heat tranfer and the recovery factor for the entire surface assumed equal to <u>one</u> (i.e., constant heat transfer <u>rates</u> throughout nozzle), the converging section heat loss should still amount to 17% of the total heat loss since the

converging section surface area is 17% of the total. Also there would be a small amount of heat transferred by radiation in the converging section of the nozzle since this section can "see" the main gas mass in the combustion chamber. The difference in use of a 17% - 83% or a 28% - 72% split-up of nozzle heat loss would be negligible in the calculations of this thesis. In fact, all nozzle heat losses were neglected in the calculations of stationary stand runs, since only the converging section was needed here anyway and it was very small in all cases.

Estimate of the Effect of Nozzle Heat Losses Compared to Heat Lost Before the Nozzle

It has been assumed in correcting performance figures for nozzle heat loss that a given quantity of heat lost in the nozzle was equivalent to one half of that amount lost before the gas entered the nozzle, i.e., in the combustion chamber. The reasoning behind this is simple but appears safe enough considering the small effect of the nozzle heat loss on calculated quantities in this thesis.

The logic for the above assumption is as follows: If all of the nozzle heat loss were transferred within a differential length of surface just inside the entrance, it would be essentially the same as combustion chamber heat loss; however, if all of this nozzle heat loss were transferred within a differential length of surface just inside the nozzle exit, it would have no effect upon the performance of the motor. Therefore, provided this nozzle

heat loss is lost fairly uniformly over the entire expansion process (i.e., with respect to the pressure or temperature variable), the total sum of nozzle heat in question should be about one half as effective as combustion chamber heat loss. Therefore, one half of the appropriate nozzle heat loss (whether for the entire nozzle or just the converging section) is added to the combustion chamber heat loss and treated as such in all calculations of this thesis.

Some actual justification of the above procedure has been found in calculations on the Mollier type diagrams of the combustion products of the propellant systems Aniline - r.f. nitric acid and hydrogen hydrate-hydrazine peroxide. In calculating specific impulse from these diagrams for a given ratio P_c/P_e, it has been found that assuming all of the nozzle heat loss to be effected at the arithmetic average temperature between Tc and Te produces about one half of the effect of that caused when all of this heat is transferred ato nozzle entrance conditions (or chamber conditions). In calculations on the Mollier type diagrams, therefore, allowance is made for nozzle heat losses by assuming the entropy change for the gases flowing through the nozzle to be given by

$$\Delta S_{\text{nozzle}} = \frac{l_{\text{nozzle}}}{T_{c-2}}$$

FIGURE A-19

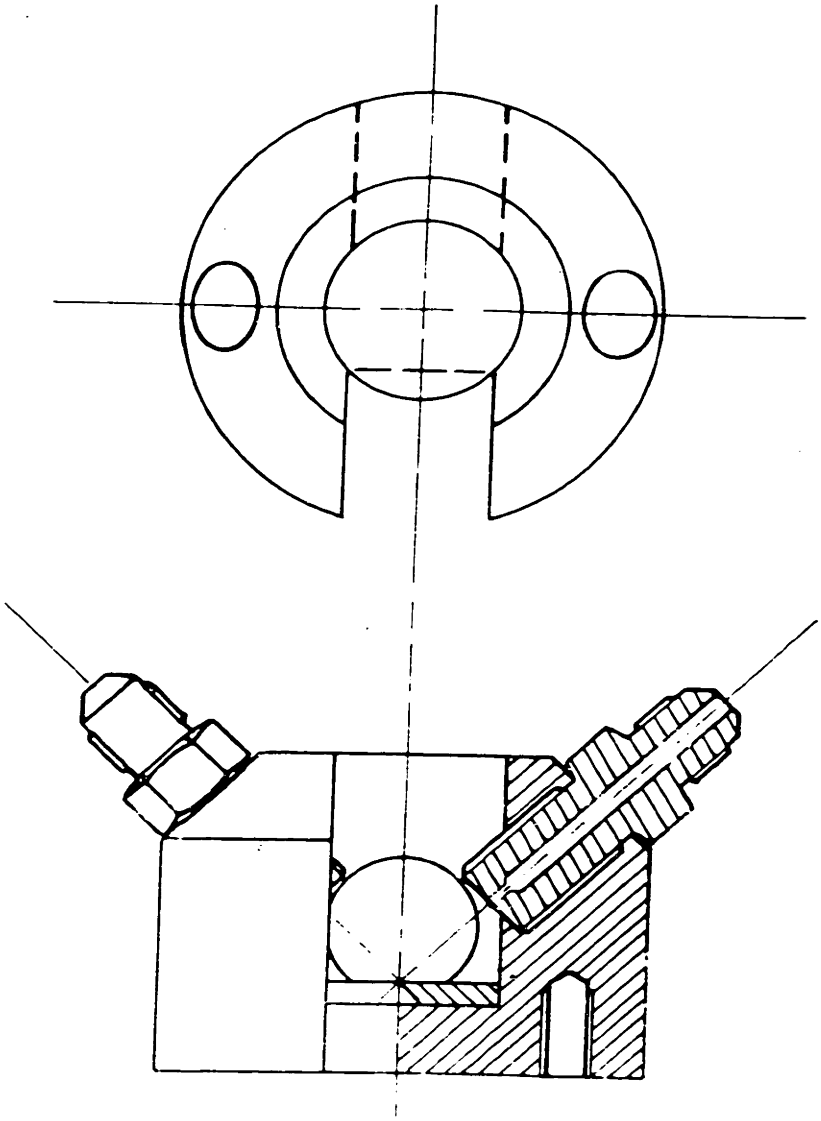

Reactor

For Ignition Delay Measurement

APPENDIX G

IGNITION DELAY MEASUREMENTS

The standard apparatus which was used by Kavanagh and coworkers (C-13) to measure ignition delays on the Peroxide Project at M.I.T. is shown in figure A-19. It consists of a semi-enclosed reactor into which the two reactants are injected simultaneously by means of nitrogen pressure (100 psia.) from the loops of $\frac{1}{4}$" diameter stainless steel tubing which are filled with about 2 ml. of each liquid before the test is made. The streams leave the 0.04" diameter orifices and travel less than an inch at a speed of about 100-150 ft./sec. before impinging at nearly the same point on the flat plate target at 90° to each other. The entire process is photographed by a Western Electric 8mm. Fastax camera operated at speeds of about 3000 frames/sec. and timed by a synchronous motor "clock" in the background of the photographic field.

This injection process is practically identical with one of the original open methods of injection which was used with the largest rocket motor (Motor A), which was operated on the stationary stand. In fact, this motor itself with wide open ends was substituted for the regular reactor in the standard ignition delay apparatus, and ignition delay measurements were made with the system 90% H_2O_2-85% $N_2H_4 \cdot H_2O$ (standard Helman catalyst) with all of the methods of open

TABLE A-7

SYSTEM OXIDANT-FUEL	APPARATUS OR METHOD OF INJECTION	AMOUNT AND NATURE OF CATALYST	TEMPERATURE °C	AVERAGE IGNITION DELAY TIME (sec.) (To appearance of flame)	REMARKS
90% H_2O_2- 85% $N_2H_4 \cdot H_2O$	STANDARD	"STANDARD HELMAN"IX	25°	0.009	
90% H_2O_2- 85% $N_2H_4 \cdot H_2O$	Rocket Motor (open ends) 90° with target injection	"STANDARD HELMAN"IX	25°	0.009	
90% H_2O_2- 85% $N_2H_4 \cdot H_2O$	Rocket Motor (open ends) 90° without target injection	"	25°	0.010	
90% H_2O_2- 85% $N_2H_4 \cdot H_2O$	Rocket Motor (open ends) 180° with prism target injection	"	25°	0.008	
90% H_2O_2- 85% $N_2H_4 \cdot H_2O$	Rocket Motor (open ends) 180° without target injection	"	25°	0.006	
80% H_2O_2- 85% $N_2H_4 \cdot H_2O$	STANDARD	"	25°	0.013	
90% H_2O_2- 85% $N_2H_4 \cdot H_2O$	STANDARD	"	0°	0.013	
90% H_2O_2- 85% $N_2H_4 \cdot H_2O$	STANDARD	"	100°	0.007	
90% H_2O_2-	STANDARD	" (60 days	25°	0.050	The increase in delay

injection using the regular photographic technique.

Other injection methods such as premix or confined mix types (similar to the confined mixing injectors used in the micro motor tests but usually constructed of glass) were also studied as to effect on ignition delay. The glass construction was necessary in order to measure the delay times photographically.

Table 1A-7 presents the best average measurements of the ignition delay time for all the propellant systems studied in this thesis as well as the values for other systems of interest. These results illustrate the effect of catalyst concentration, reactant concentrations, temperature and methods of injection (degree of mixing and confinement) on the ignition delay of a given propellant system, as well as the large differences in delays for different fuels and catalysts when used with the same oxidant. It should be pointed out that the effect of mixture ratios on the ignition delay of a given system is not studied on the standard delay time tester. In all cases the reactants are mixed in approximately equal volume amounts since the same amounts of each are used in each test and the streams are formed from equal size orifices under the same feed pressure.

In only one case was there any indication of the effect of mixture ratio of fuel and oxidant. In this experiment, a stream of peroxide from an 0.04" diameter orifice was injected at about the usual speed into a stagnant pool of 85%

injection using the regular photographic technique.

Other injection methods such as premix or confined mix types (similar to the confined mixing injectors used in the micro motor tests but usually constructed of glass) were also studied as to effect on ignition delay. The glass construction was necessary in order to measure the delay times photographically.

Table 1A-7 presents the best average measurements of the ignition delay time for all the propellant systems studied in this thesis as well as the values for other systems of interest. These results illustrate the effect of catalyst concentration, reactant concentrations, temperature and methods of injection (degree of mixing and confinement) on the ignition delay of a given propellant system, as well as the large differences in delays for different fuels and catalysts when used with the same oxidant. It should be pointed out that the effect of mixture ratios on the ignition delay of a given system is not studied on the standard delay time tester. In all cases the reactants are mixed in approximately equal volume amounts since the same amounts of each are used in each test and the streams are formed from equal size orifices under the same feed pressure.

In only one case was there any indication of the effect of mixture ratio of fuel and oxidant. In this experiment, a stream of peroxide from an 0.04" diameter orifice was injected at about the usual speed into a stagnant pool of 85%

hydrazine hydrate (with standard 1X Helman catalyst) which was contained in a 1 ml. beaker. In this case, a delay of 8 milliseconds was measured which is not significantly different from that (9 milliseconds) usually obtained with this fuel in the standard delay tester in which case the two reactants mix in approximately equal volume amounts.

One run on the standard delay tester was made with the system, red fuming nitric acid and aniline (no catalysts). The result of this measurement indicates a delay of around 150 milliseconds for this system.

FIGURE A-20 PRESSURE INTERPOLATION CHART FOR SATTERFIELD REDUCED ENTHALPY

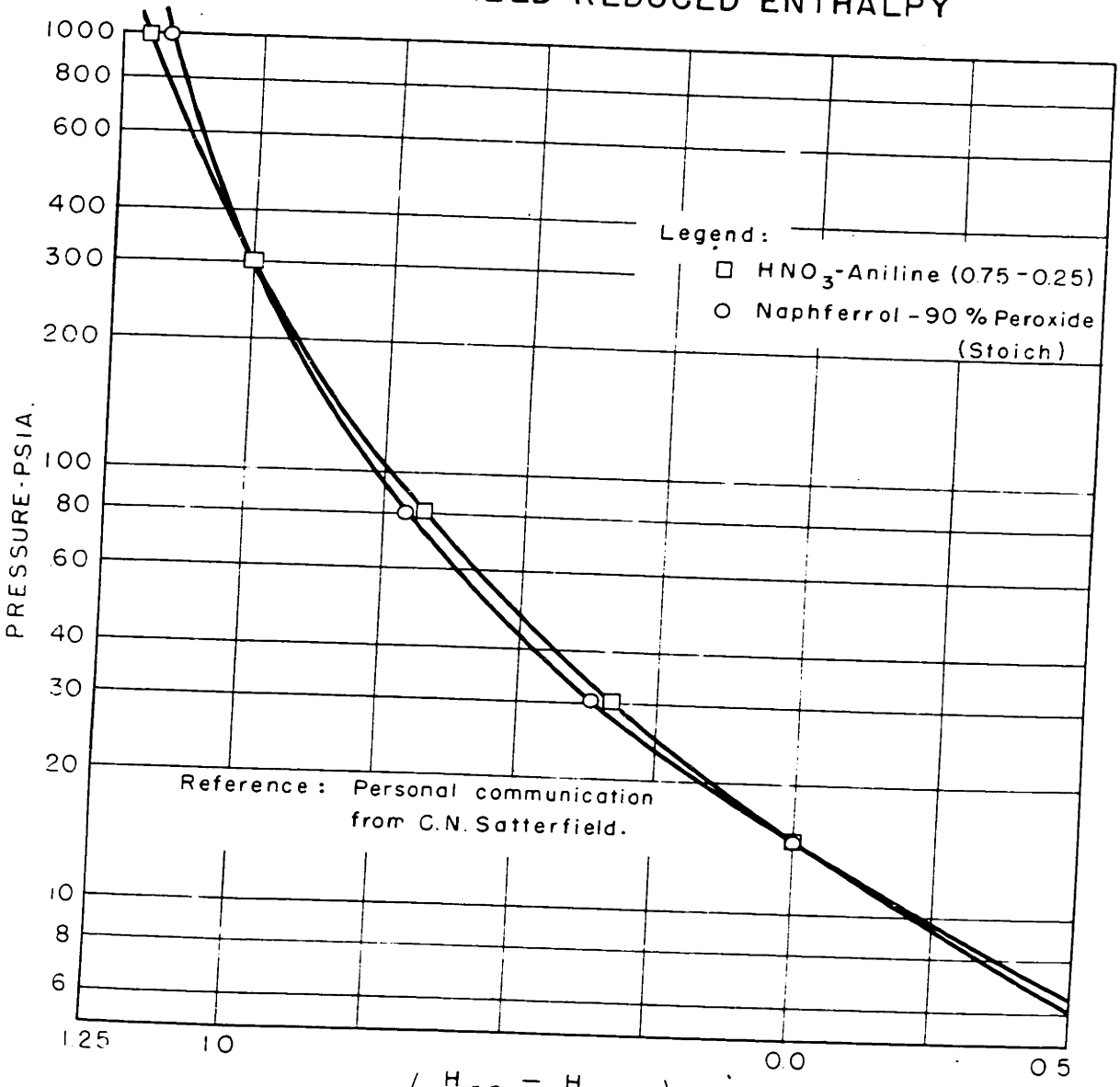

$$C = \left(\frac{H_{r\,p} - H_{r\,14.7}}{H_{r\,300} - H_{r\,14.7}} \right) T = 2800^\circ K$$

APPENDIX H

PRESSURE INTERPOLATION CHARTS FROM SATTERFIELD'S GENERALIZED THERMODYNAMIC CHARTS

Satterfield (30) has presented generalized thermodynamic charts of enthalpy and entropy at 300 psia and 14.7 psia pressures. These are applicable for almost any system composed only of C, H, O, and N, at temperatures up to 3200°K. A system has now been perfected by Satterfield for extending the pressure range for which these generalized data can be employed to that of 10-1000 psia. This is accomplished by use of one additional generalized extrapolation or interpolation plot such as that shown in Figure (A-29). By using the reduced enthalpy at 14.7 and 300 psia as tie points, the maximum deviation for all systems of points on this correction factor curve from the mean curve was held to about 10% within this pressure range. This correction quantity (C) is an addition or subtraction term to the reduced enthalpy at 14.7 psia compared with the difference between the reduced enthalpy at 300 and at 14.7 psia. The magnitude of this addition or subtraction term is never more than 15% of the base value of reduced enthalpy at 14.7 psia. Therefore, if this term is known within at least 10% the original accuracy of 1-2% which was obtained on the 14.7 psia and 300 psia charts will be retained in the values at any other desired pressure between 10 and 1000 psia.

FIGURE A 21 ENTHALPY (REDUCED) VS. TEMPERATURE AT VARIOUS PRESSURES FOR NAPHFERROL – PEROXIDE SYSTEM

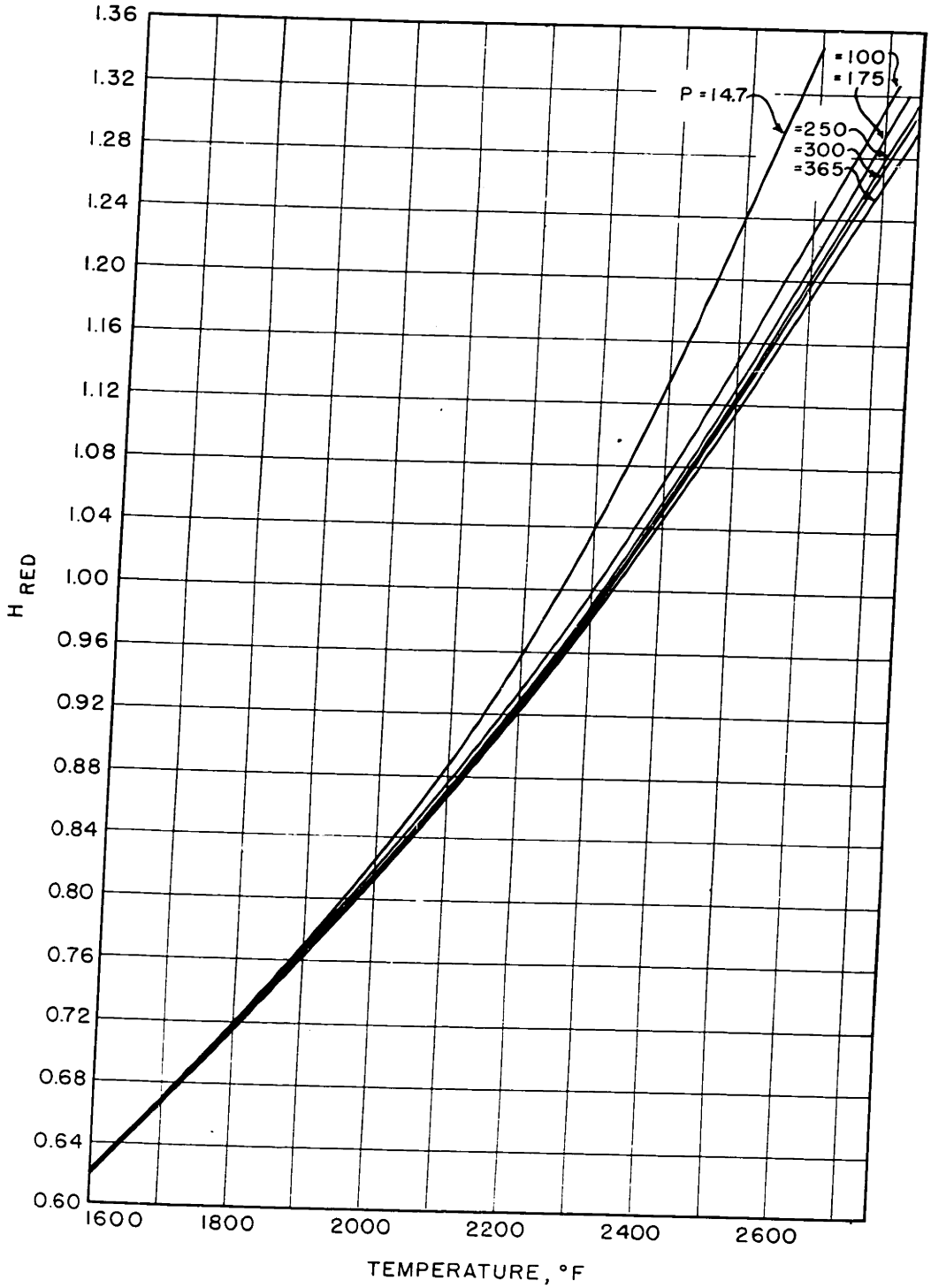

Construction of a Pressure Interpolation Chart for a Given System

In order to construct a chart of reduced enthalpy as a function of temperature for various pressures for a given system, it is necessary to use the curve of Figure A-20 together with the original 14.7 and 300 psia charts of Satterfield (3). The values of $H_{red_{14.7}}$ and $H_{red_{300}}$ are read from the original charts at several representative temperatures over the range of interest. Then values of C are read from Figure A-20 for several pressures over the range of interest. From the combination of these values H_{red_p} at the various temperatures for each of the desired pressures can be calculated and plotted as shown in Figure A-21 (for the system ~~red fuming nitric acid (6.5% NO_2) and aniline~~ 90% H_2O_2 - Naphtha (Catorich)). At a given temperature, the relative distances between the various lines of constant pressure are representative of the shift in the amounts of dissociation products which would be affected by an isothermal change in pressure at that temperature.

Use of the Pressure Interpolation Chart to Determine the Correct c_p or γ for an Expansion Process

In this thesis pressure interpolation charts for the various systems (such as Figure A-21) were used in two separate ways. In one case they were used to determine the difference in enthalpy at a given pressure, p, from that at 300 psia so that the corresponding entropy change could be calculated and thus the reduced entropy at pressure p could also be obtained

from the $S_{red_{300}}$ value of the original charts. The corresponding value of $S_{red_{14.7}}$ could then be found, from which the final temperature of the expansion process and hence $H_{red_{14.7}}$ could be evaluated. Thus ΔH for the process and, therefore, specific impulse could be obtained.

The second use of the pressure interpolation charts was in obtaining values of temperature and of γ for use in calculating performance from the various equations. Knowing $H_{1\ red}$ of the unburned system, T_c could be read directly from the chart at the known or guessed chamber pressure. The isentropic exponent, γ, was determined from M_{c_p} by the equation

$$\frac{M_{c_p}}{M_{c_p}-R} = \gamma$$

The heat capacity c_p in Btu/lb. is defined as

$$c_p = \left(\frac{\partial}{\partial T}\frac{H}{T}\right)_p$$

This slope in terms of reduced enthalpy, can be determined at any desired temperature and pressure simply by taking the tangent to the proper pressure line at the appropriate temperature. This value can be converted to be in terms of true enthalpy in the usual manner. While there is some question as to the proper average value of c_p which should be employed over a given expansion process, the c_p actually used in most cases was the arithmetic average of the two values of $\left(\frac{\partial}{\partial T}\frac{H}{T}\right)_p$ both read at the arithmetic mean temperature but on first the initial pressure line

and then on the final pressure line. The net effect of using other types of average c_p on the various calculated results is discussed in the main body of the thesis as well as in the sample calculations of Appendix L. The molecular weight value which is necessary to determine γ from this average value of c_p can be determined as outlined in Appendix I.

APPENDIX I

METHOD OF APPROXIMATING MOLECULAR WEIGHT FROM SATTERFIELD'S CHARTS

In order to calculate specific impulse I_{sp} by means of equations as by equation (14a), page 39 of this thesis, in addition to the value of the temperature T_c and the values of c_p which can be obtained from the pressure interpolation chart as indicated in Appendix H, the value of MW_{av} (over the process from p_c to p_e) and MW_c are also required, assuming T_e is not known (which is usually the case). Similarly, in order to determine the chamber pressure, p_c, by means of equations as by equation (22c), page 41 of this thesis, the values of MW_{av} (over the process from p_c to p_t) as well as MW_t are also required.

Satterfield(38) has presented generalized charts of reduced molecular weight for pressures of 300 psia and 14.7 psia. These reduced molecular weight values are based on use of a simplified gas composition which can be easily estimated for any system. These simplified gas compositions and molecular weight values calculated from them are accurate (within at least 1%) for all systems at temperatures below 2000°K. The true molecular weights can be obtained at any temperature up to 3200°K at either 14.7 or 300 psia from these two generalized charts.

In order to obtain true molecular weight values at other pressures from 10 to 1000 psia and at temperatures between 2000°K and 3200°K, it is necessary to use these two generalized molecular weight charts together with a pressure interpolation chart, such as Figure A-21 (discussed in Appendix H). This chart should contain both a 14.7 and 300 psia line and other lines of constant pressure in the range of interest. The molecular weight at the pressure, p, and temperature, T, in question can then be estimated as follows:

If p is greater than 14.7 psia,

$$MW_{p,T} = MW_{14.7,T} + \frac{H_{red\,14.7,T} - H_{red\,p,T}}{H_{red\,14.7,T} - H_{red\,300,T}} (MW_{300,T} - MW_{14.7,T})$$

If p is less than 14.7 psia,

$$MW_{p,T} = MW_{300,T} - \frac{H_{red\,p,T} - H_{red\,300,T}}{H_{red\,14.7,T} - H_{red\,300,T}} (MW_{300,T} - MW_{14.7T})$$

Point values of molecular weight, such as MW_c and MW_t can be obtained in this manner provided p_c, T_c and p_t and T_t are known or can be closely estimated.

Average Values of Molecular Weight

Some sort of average value of Molecular Weight is required in the general perfect gas relation between the pressures and temperatures of an adiabatic expansion, such as in equations (8a) and (8b) which were derived in the main body of this thesis. This same relation between temperatures and pressures is generally involved in equation-type calculations of either chamber pressure

or specific impulse, as shown by equation (22c) and equation (4c) previously presented.

The proper kind of average molecular weight for this case does not need to be determined separately, however, since it is always combined with the specific heat. As pointed out in the derivation of these equations in the thermodynamics section of this thesis, the average value of molal specific heat, M_{cp}, can be determined just as easily as the average value of c_p above and the appearance of Molecular weight in these equations, therefore, introduces no additional error.

APPENDIX J

ESTIMATION OF THE HEAT OF FORMATION OF FERROUS β NAPHTHALENE SULFONATE

Values of the heat of formation of ferrous β-napthalene sulfonate could not be located in the literature. Neither could this quantity be estimated from the rules for group contribution of Anderson, Beyer and Watson (4) nor by means of the method of Pauling (32) of summing up bond energies for an entire molecule because of the lack of values for the sulfonate group in both of these methods. However, M. Badoche (5) has studied the contribution of the sulfonate group to the heat of formation of similar compounds, and these figures were used in estimating the heat of formation of ferrous β-napthalene sulfenate.

Badoche(loc. cit.) measured the heats of combustion of 2-naphthol and 2-hydroxy-6 naphthalene sulfonic acid and those of 2-4 dinitro-1 naphthol and 2-4 dinitro-1 hydroxy-7 naphthalene sulfonic acid-dihydrate all at about 18-20°C. From these experimental figures, corresponding values of the heats of formation could be obtained as follows:

ΔH 2-naphthol	-32.6	kg.cal./g.mol
ΔH 2-hydroxy-6 naphthalene sulfonic acid	-190.0	"
ΔH 2-4 dinitro-1 naphthol	- 45.0	"
ΔH 2-4 dinitro-1 hydroxy-7 naphthalene sulfonic acid-dihydrate	-323.8	"

The 2-hydroxy-6-naphthalene sulfonic acidwas believed to contain 2 to 2.5% of water. The ΔH_f corrected for this was -173 kg.cal./g.mol instead of -190. Also the ΔH of 2-4 dinitro-1 hydroxy-7 naphthalene sulfonic acid-dihydrate was corrected for the water of hydration and the heat of hydration to give a value for ΔH_f of anhydrous 2-4 dinitro-1 hydroxy-7 napthalene sulfonic acid of -179.2 kg.cal./g.mol. Thus the contribution to the heat of formation due to the substitution of the ($-SO_3H$) group for th (-H) group amounts to (173-32.6)= -140.4 kg.cal./g.mol in the case of the 2-naphthol compound and to -(179.2-45)= -134.2 kg.cal./g.mol in the case of the 2-4 dinitro-1 naphthol.

Accordingly the contribution to the heat of formation of this sulfonate group substitution on a plain naphthalene ring was estimated to be 145 kg.cal./g.mol. Also the contribution to the heat of formation due to replacing the two hydrogen atoms of H_2SO_4 by an iron atom amounts to -24.14 kg.cal./g.mol. from heat of formation data given by Bichowsky and Rossini (6). Hence, the same contribution was assumed in forming ferrous β naphthalene sulfonate. The heat of hydration of Ferrous sulfate is given by Bichowsky and Rossini (6) as -3.3 kg.cal./ g.mol. H_2O in the tetrahydrate. Also M. Badoche (4) assigns a value of -3.9 kg.cal./g.mol.H_2O as the heat of hydration of the naphthalene based compounds (dihydrates) mentioned before. Accordingly a figure of -3.5 kg.cal./g.mol. H_2O was used for the heat of hydration of ferrous β naphthalene sulfonate-trihydrate. The heat of combustion of pure naphthalene (s)

is given in the International Critical Tables (20) as 1231.8 kg.cal./g.mol. from which the heat of formation can be calculated as 14.5 kg.cal./b.mol. Therefore, the heat of formation of the ferrous β naphthalene sulfonate was estimated as follows:

ΔH_f of 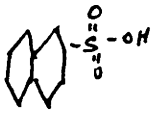 = 14.5 - 145 = -130.5 $\frac{\text{kg.cal}}{\text{g.mol}}$

ΔH_f of 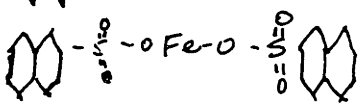 = 2(-130.5) - 24.14

= - 285.1 $\frac{\text{kg.cal}}{\text{g.mol}}$

ΔH_f of 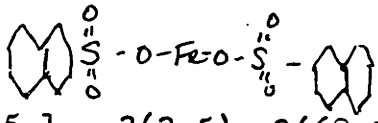 =

-285.1 - 3(3.5) -3(68.37) = 500.7 $\frac{\text{kg.cal}}{\text{g.mol}}$

Thus the heat of formation from the elements in their standard states of ferrous β naphthalene sulfonate-trihydrate is about 500 kg.cal./g.mol. at a temperature of approximately 293-300°K. If this value is accurate to within only 5%, the overall value for the Naphferrol fuel will still be almost 1% of the correct figure since ferrous β naphthalene sulfonate-trihydrate is only about 20% of the complete fuel.

Conversion to the Enthalpy Basis of this Thesis

The zero base state for enthalpy values in this thesis and in the Satterfield charts is not the usual one of the elements in their standard states at about 298°K but rather is assigned to the products of complete combustion (H_2O (g), CO_2, N_2, O_2 etc.) at 0°K and in the vapor state at a pressure of

one atmosphere. Accordingly the heat of formation value given above had to be converted to this basis before being used with the Satterfield charts in the calculations of this thesis. This conversion consists of adding the enthalpy of the elements in their standard states at 300°K above their products of complete combustion at 0°K to the enthalpy of formation calculated above.

This calculation is carried out as follows -- for one mol of ferrous ⊖ naphthalene sulfonate-trihydrate.

H_f (= -Q) or heat of formation from the elements	-500,000	cal./g.mol
Enthalpy of 7 H_2 at 300°K above H_2O(g) at 0°K	414,015	"
" of 4 1/2 O_2 at 300°K above O_2(g) at 0°K	9,342	"
" of 20 C at 300°K above CO_2(g) at 0°K	1,888,480	"
" of 2 S at 300°K above SO_2 (g) at 0°K	146,940	"
" of Fe at 300°K above Fe_2O_3(g) at 0°K	101,120	"
	+2,059,900	cal./g.mol

Therefore, the H_{system} for 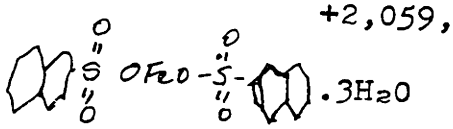 $.3H_2O$

$$= 2060 \text{ kg.cal./g.mol.}$$

$$\text{or } \frac{2060}{MW} = \frac{2{,}060{,}000}{524.3} = 3935 \text{ cal./gm.}$$

$$\fallingdotseq 3935 \times 1.8 = 7090 \text{ Btu/lb.}$$

The heat of formation of the products of combustion at 300°K which were used in this calculation were obtained from Bichowsky and Rossini (*loc. cit*) while the sensible enthalpies of these gaseous products above 0°K were obtained from the following sources:

H_2O	Wilson, E. B. Jr. (46)
O_2	Johnston, H. L. and Walker, M. K. (21)

CO_2 Kassel, L.S. (22)

SO_2 Bryant, W.M.D. (//)

Fe_2O_3 Kelley, K. K. (23)

Special Assumptions Involved with Naphferrol Fuel

The Satterfield charts are constructed for the four component systems C-H-O-N, and accordingly make no allowance for either sulfur or iron. However, in the Naphferrol fuel, both of these elements are present in such small amount that the generalized charts can still be applied with negligible error. The sulfur amounts to 12.2% by weight of the ferrous β naphthalene sulfonate-trihydrate but only about 2.4% by weight of the Naphferrol fuel. While the iron amounts to 10.6% of the ferrous β naphthalene sulfonate trihydrate but only about 2.1% by weight of the total Naphferrol fuel. When Naphferrol is used with stoichiometric proportions of hydrogen peroxide, it amounts to only about 20% by weight of the total propellant. Therefore, in this case, the sulfur would amount to only 0.5% by weight of the total propellant while the iron would amount to about 0.4% by weight of the total working fluid. In the most fuel-rich mixture studied neither of these components comprise as much as one per cent by weight of the working fluid.

Therefore, in performance calculations on the system Naphferrol - 90% H_2O_2, the folllwing special assumptions were made:

1.) All the sulfur was assumed burned to SO_2 (g) and all the Fe to Fe_2O_3(s) in all cases in the imaginary combustion process which is considered in determining the fictitious gas composition.

2.) The mass of the sulfur was added to that of the C in determining C/O, H/O, and N/O ratios which determine interpolation numbers for the various charts.

3.) The Fe_2O_3 was assumed to be ineffective in producing thrust or in other words the effective mass flow rate was assumed to be less than the actual mass flow by this amount. But, the average molecular weight was then calculated without considering the mols of Fe_2O_3. Actually the molecular weight of the Fe_2O_3 is so much higher than the average value of the other reaction products, that even if it is considered as effective in producing thrust as a gas of the same molecular weight, the net effect on the calculated specific impulse value is about the same. This is due to the rise in average molecular weight which even this relatively small amount of Fe_2O_3 produces.

It is believed that all of these assumptions are reasonable and represent a maximum possible error of 1% in the calculations of this thesis and a probable error of only about 0.1%.

APPENDIX K

Sample Calculations of Quantities Based on Experimental Data

Run W-3 which was made on the thrust stand using the W motor and the system 90% H_2O_2-85% $N_2H_4 \cdot H_2O$ has been chosen as a representative one. Figure 24 shows the chart records from the various recording instruments for this run. In addition to these measurements, the following data were taken:

Duration of Run: 2 min., 5 sec.

Pumping Rates set at 145 rpm Fuel; 136 rpm Peroxide

Tachometer Revolutions Counted during Run: = 303 rev. - Fuel

284 rev. - Peroxide

Thrust Calibration after Run: 7 lbs = 28.3 units on chart

6.5 lbs = 26.4 units on chart

Nozzle Throat Diameter: 0.144 inches.

Cooling Water Data:

A. Flow Rates:

(1) Combustion Chamber Jacket: 2.70 lbs/min.

(2) Nozzle Jacket: 2.54 lbs/min.

B. Temperatures

(1) Combustion Chamber: In 60.4°F; Out 178.4°F.

(2) Nozzle Jacket: In 62.8°F; Out 160.6°F.

From this data the following Calculations Were Made:

I. Directly Measured Performance

Total Fuel Consumed: $\frac{303 \times 2.93 \times 1.02}{454.5} = 2.00$ lbs

Total Peroxide Consumed: $\frac{284 \times 2.93 \times 1.40}{454.5} = 2.56$ lbs

Fuel/Oxidant Ratio in mols/mol $= \frac{2.00 \times 0.85 \times 1/50}{2.56 \times 0.90 \times 1/34} = 0.501$

$F/F + F\approx 0$ Ratio in mols/mol $= \frac{0.501}{0.501+0.5} = 0.5005$

Mass Flow Rate, $m = \frac{2.00 + 2.56}{125} = 0.0365$ lbs/sec

$\dot{m}/A_t$ or Mass Flow Rate per cent area of nozzle throat =

$$\frac{0.0365}{\pi/4(0.144)^2} = 2.245 \text{ lbs/sec}\cdot\text{in}^2$$

From chart and calibration points,

Thrust Force, F (Equilibrium) $= 6.5 + \left(\frac{27.1 - 26.4}{28.3 - 26.4}\right) 0.5$

$= 6.68$ lbs

Specific Impulse $= \frac{F}{m} = \frac{6.68}{0.0365} = 183.1 \ \frac{\text{lbs-sec}}{\text{lb}}$

From chart, P chamber (equilibrium) = 296 psia

by calibration curve, $P_c = 295 + 14.7$

$= 310$ psia

Characteristic Velocity $c^* = \frac{P_c A_{tgo}}{\dot{m}}$

$$= \frac{310(\ /4)(0.144)^2 32.17}{0.0365}$$

$$= 4450 \text{ ft/sec}$$

Nozzle Thrust Coefficient $C_F = F/P_c A_t$

$$= \frac{6.68}{310(\ /4)(0.144)^2} = 1.336$$

Total Chamber Heat Loss:

$$(1) q_c = 2.70\ (178.4-60.4)$$

$$= 318.5 \text{ Btu/min}$$

$$(2) q_{noz} = 2.54\ (160.6 - 62.8)$$

$$= 248.2 \text{ Btu/min}$$

Heat Loss Per Lb. of Propellant:

$$(1)\ l_{chamber} = \frac{318.5}{0.0365(60)} = 146 \text{ Btu/lb}$$

$$(2)\ l_{nozzle} \quad \frac{318.5}{60(0.0365)} = 113 \text{ Btu/lb}$$

Heat Transfer Rates:

$$(1) q_{chamber} = \frac{318.5}{60(\ )(1)(3)} = 0.567 \quad \frac{\text{Btu}}{\text{sec x in}^2}$$

$$(2) q_{nozzle} = \frac{248.2}{60(0.954)} = 4.31 \quad \frac{\text{Btu}}{\text{sec x in}^2}$$

These performance figures are presented for all runs in the tables of experimental and calculated data, see Appendix P.

II. Corrected Performance Figures

(Using Working plots - Figures 5, 6, 7 and 8)

A. Chamber Pressure

assume $l_{cn} = 0.28\ l_{nozzle}$

$= 0.28\ (113)$

$= 32$ Btu/lb

$l_{dn} = 113 - 32 = 81$ Btu/lb

$l_{eff} = l_c + 1/2\ l_{cn}$

$= 146 + 16 = 162$ Btu/lb

From Fig. 5, at $\dot{m}/A_t = 2.245$ lbs/sec x in^2 and for the stoichiometric mixture ratio.

Theoretical $P_{c\ nhl} = 336$ psia

From Fig. 6, at $l_{eff} = 162$ Btu/lb

for this same system $\left[\frac{P_{c\ chl}}{P_{c\ nhl}}\right]_{theor} = 0.9652$

Then $P_{c\ chl} = 0.9662\ (336) = 324.3$ psia

$$\frac{P_{c\ exp}}{P_{c\ th\ nhl}} \times 100 = \frac{310}{336} \times 100 = 92.3\%$$

$$\frac{P_{c\ exp}}{P_{c\ th\ chl}} \times 100 = \frac{310}{324.3} \times 100 = 95.5\%$$

To correct the experimental chamber pressure up for heat loss the following procedure was used:

on figure 6, at $\frac{P_{c\ exp}}{P_{c\ th\ nhl}} = 0.923$

$l_{equivalent}$ = 346 Btu/lb (This is the amount of heat which would have to be lost to produce the experimental pressure under the same experimental conditions except assuming that 100% efficiency of combustion were obtained in this case.

$(l_{equivalent} - l_{eff}) = 346 - 162 = 184$ Btu/lb

At this amount of heat loss, which is that equivalent in its effect to the combustion inefficiency of the actual run, $\frac{P_{c\ exp\ chl}}{P_{c\ th\ nhl}} = 0.9602$

$P_{c\ exp\ chl} = 0.9602\ (336) = 322.6$ psia.

This represents the approximate performance which should be obtained in a large motor with negligible heat loss if the experimentally measured combustion efficiency were constant.

B. Specific Impulse

From Fig. 7, at $\dot{m}/A_t = 2.245$ lbs/sec x in^2

and for the stoichiometric mixture ratio curves,

$I_{sp\ th\ nhl}$ (at $P_c/P_{c\ nhl} = 1.0$)

$= 212.7$ lbs-sec/lb

Assuming proportionality of $\dot{m}/A_t$ and P_c, the mass flow rate which would have produced an experimental pressure of 300 psia, with the same combustion efficiency, is

given by: $\left(\frac{m}{A_t}\right)_{P_{c\ exp} = 300\ psia} = \frac{300}{P_{c\ exp}} \left(\frac{m}{A_t}\right)_{exp}$

$$= \frac{300}{310}(2.245)$$

$$= 2.172 \text{ lbs/sec x in}^2$$

From Fig 7, at $m/A_t = 2.172$, for the same system,

$I_{sp\ th\ nhl}$ (at $P_c/P_{c\ nhl} = 1.0$)

$$= 211.9$$

$$I_{sp\ exp\ c300} = \frac{211.9}{212.7}(183.1)$$

$$= 182.4 \frac{\text{lbs-sec}}{\text{lb}}$$

From Figure 5, at $P_{c\ nhl} = 300$,

$$\left(\frac{\dot{m}}{A_t}\right)_{theor} = 2.003 \frac{\text{lbs}}{\text{sec x in}^2}$$

From Figure 7, at $\dot{m}/A_t = 2.003$ for the same stoichiometric system.

$I_{sp\ th\ nhl}$ (at $P_c/P_{c\ nhl} = 1.0$)

$$= 209.7 \text{ lbs-sec/lb}$$

Also from Fig. 7, at $\dot{m}/A_t = 2.003$ for the stoichiometric system, but at $\left[\frac{P_{c\ chl}}{P_{c\ nhl}}\right]_{theor} = 0.9652$

$$I_{sp\ chl} = 201.0 \text{ lbs-sec/lbs}$$

From Fig. 8 for the stoichiometric system at $l_{div.noz}$ = 81 Btu/lb, the ratio of specific impulse corrected for diverging nozzle heat loss to that not considering this heat loss or

$$\left[\frac{I_{sp\ cahl}}{I_{sp\ cchl}}\right]_{theor} = 0.991$$

$$\therefore I_{sp\ cahl} = 0.991(201) = 199.2 \text{ lbs-sec/lb}$$

From Fig. 7 for the stoichiometric system, at $\dot{m}/A_t$ = 2.172 and at $P_{c\ exp}/P_{c\ theor}$ n_{hl} = 0.923, the theoretical specific impulse corresponding to the experimental combustion efficiency and chamber heat loss but not corrected for diverging nozzle heat loss is given by $I^t_{spth\ cece}$ = 193.7, and correcting for diverging nozzle heat loss gives

$$I_{sp\ th\ cece} = 0.991\ (193.7)$$
$$= 192.0 \text{ lbs-sec/lb}$$

Comparison of this figure with the experimentally measured specific impulse gives an approximate value of the loss in performance due to nozzle inefficiency.

To correct the experimental specific impulse up for the measured heat loss, the following procedure is necessary:

assuming proportionality of $\dot{m}/A_t$ and P_c, the mass flow rate which would be necessary to produce an experimental pressure of 300 psia with no heat loss is given by

$$\left(\frac{\dot{m}}{A_t}\right)_{P_c \text{ exp chl} = 300 \text{ psia}} = \frac{300}{P_{c \text{ exp chl}}} \left(\frac{\dot{m}}{A_t}\right)_{exp}$$

$$= \frac{300}{322.6}(2.245)$$

$$\left(\frac{\dot{m}}{A_t}\right)_{P_c \text{ exp chl} = 300} = 2.088 \text{ lbs/sec x in}^2$$

From Fig. 7 at $\dot{m}/A_t = 2.088$ for the same system

$$I_{sp \text{ exp chl}} (\text{at } P_{c \text{ exp chl}}/P_{c \text{ th nhl}} = 0.9602)$$

$$= 192.0 \text{ lbs-sec/lb}$$

This represents the performance which should be obtained in a large motor with negligible heat loss but otherwise operating under the same conditions as in the actual experiment including the same combustion and nozzle efficiencies.

These values calculated above are also presented for all runs in Tables of experimental and calculated data in Appendix P.

APPENDIX L

Sample Calculations of Theoretical Performance

The general assumptions applicable to all the theoretical performance calculations have already been outlined in the section on Procedure. Also some additional assumptions applicable only to the Naphferrol system were stated in Appendix J. In addition to these rather general assumptions which amount merely to an idealization of the process, several additional approximations were employed in evaluating certain terms in the theoretical equations or in certain steps of the theoretical calculations when carried out by other methods. The reliability of these approximations was tested by trial calculations on the experimentally studied systems of this thesis as well as on the additional higher temperature system consisting of red fuming nitric acid and aniline. The results of these trial calculations are given and discussed in the main body of the thesis.

All of these approximations and assumptions and the differences between them and the various calculation methods will be made clearer by the examples of each which follow:

Chamber Pressure Calculations

Method 1A and 1B

Using Satterfield charts plus the equation

$$P_c = \frac{\dot{m}}{A_t}\sqrt{\frac{RT_c}{2g_o MW_t}}\sqrt{\frac{\gamma'_{c-t}-1}{\gamma'_{c-t}}}\sqrt{\frac{1}{\left(\frac{2}{\gamma_d+1}\right)^{\frac{2}{\gamma''_{c-t}-1}} - \left(\frac{2}{\gamma_d+1}\right)^{\frac{\gamma''_{c-t}+1}{\gamma''_{c-t}-1}}}} \qquad (22c)$$

In Method 1A all γ's are assumed the same and are evaluated from the average C_p of the gas mixture based on the C_p value of the pure gaseous components at the arithmetic mean temperature, thus neglecting the effect of reaction on C_p. In Method 1B it is assumed that all γ's can be evaluated from an average value of C_p obtained from the arithmetic avarage of $\left(\frac{\partial H}{\partial T}\right)_p$ at the arithmetic mean temperature and P_c and $\left(\frac{\partial H}{\partial T}\right)_p$ at the arithmetic mean temperature and P_t. This takes into account any heat of reaction effects on C_p.

Let us use the following example:

System: Red fuming nitric acid (6.5% NO_2) – Aniline

Mixture Ratio: 3 lbs acid – 1 lb aniline

Mass Flow Rate per unit area: 320 lbs/sec x ft^2 or

2.224 lbs/sec x in^2.

Total Chamber Heat Loss, l_c = 300 Btu/lb

Total Nozzle Heat Loss, l_n = 200 Btu/lb.

Take as Basis: 1 lb. of Propellant

or 0.75 lbs of r.f. HNO_3 (93.5% of 98% HNO_3)

plus 0.25 lbs of $C_6H_5NH_2$.

Then Mols of: $HNO_3 = \frac{0.98(0.935)(0.75)}{63} = 0.0109$

$NO_2 = \frac{6.5(0.75)}{100(46)} = 0.00106$

$H_2O = \frac{0.02(0.935)(0.75)}{18} = 0.00078$

$C_6H_5NH_2 = \frac{0.25}{93} = 0.00269$

Therefore, Atoms of H = 0.0109 + 0.00156 + 7(0.00269) = 0.03139

Atoms of N = 0.0109 + 0.00106 + 0.00269 = 0.01465

Atoms of C = 6(0.00269) = 0.01614

Atoms of O = 3(0.0109 + 2(0.00106) + 0.0078 = 0.0356

And the element ratios are: $\frac{C}{O} = \frac{0.01614}{0.0356} = 0.454$

$\frac{H}{O} = \frac{0.03139}{0.0356} = 0.882$

$\frac{N}{O} = \frac{0.01465}{0.0356} = 0.411$

The simplified gas composition can be estimated according to the method given with the Satterfield Thermodynamic charts. In this case, the result is (in mol fractions)

CO_2	0.1837
CO	0.2288
H_2O	0.3128
H_2	0.0881
N_2	0.1866
Total	1.0000

Then the average molecular weight of this simplified or fictitious gas mixture is given by

$$MW_f = 0.1837(44) + 0.2288(28) + 0.3128(18) + 0.0881(12) + 28(0.1866)$$

$$= 25.53$$

And on the Satterfield basis:

$$H_{f,o} = \frac{0.2288(120,184) + 0.0881(102,794)}{25.53}$$

$$= 1397 \text{ Btu/lb}$$

$$H_{f,2400} = (135,218)(0.0881) + (44,689)(0.3128) + 154,620(0.2288) + 0.1866(34,146) + 0.1837(54,031)$$

$$= 77,610 \text{ Btu/lb-mol or } \frac{77,610}{25.53} = 3040 \text{ Btu/lb.}$$

and $H_{system} = 0.25(16,130) + 0.065(0.75)(1.96) + 0.75(0.98)(0.935)(-226) + 0.75(0.02)(0.935)(-810)$

$$= 3617 \text{ Btu/lb.}$$

Considering the heat loss,

Assume $l_{cn} = 0.28 l_n = 0.28(200) = 56$ Btu/lb.

Then assume $l_{eff} = l_c + 1/2\, l_{cn}$

$$= 300 + 1/2(56) = 328$$

$$H_{system} = 3617 - 328 = 3289 \text{ Btu/lb}$$

Then

$$H_{red} = \frac{H_{syst'} - H_{f,o}}{H_{f,2400} - H_{f,o}} = \frac{3289 - 1397}{3040 - 1397} = 1.151$$

Assuming that we have no idea of the range of chamber pressure which should result in the present case, we must first make a preliminary estimate of this before proceeding.

First calculate the approximate value of $\dot{m}/A_t$ necessary to produce a chamber pressure of 300 psia. As outlined in the section on Procedure, arbitrary assumption of a value of 1.20 for γ will be accurate enough for this purpose. Therefore the only remaining quantities needed are T_c, and MW_c. T_c can be read from the pressure interpolation chart of Figure 4 . At $H_{red} = 1.151$, T_c (on the $P_c = 300$ psia line) is 2655°K. And from Satterfield's 300 psia reduced molecular weight chart, MW_{red} (at T_c = 2655°K) = 0.992. Then $MW_c = 0.992\ MW_f = 0.992(25.53) = 25.33$. So,

$$\frac{\dot{m}}{A_t} = P_c \sqrt{\frac{2g_o MW_c}{RT_c}} \sqrt{\frac{\gamma}{\gamma-1}} \sqrt{\left(\frac{2}{\gamma+1}\right)^{\frac{2}{\gamma-1}} - \left(\frac{2}{\gamma+1}\right)^{\frac{\gamma+1}{\gamma-1}}}$$

$$= 300\sqrt{\frac{64.4(25.33)}{1546(1.8)(2655)}}\sqrt{\frac{1.2}{0.2}}\sqrt{\left(\frac{2}{2.2}\right)^{\frac{2}{0.2}} - \left(\frac{2}{2.2}\right)^{\frac{2.2}{0.2}}}$$

$$= 300(0.01485)0.4590$$

$$= 2.045$$

$\dot{m}/A_t$ in the present case is 2.224.

Assuming proportionality of $\dot{m}/A_t$ and P_c, the approximate chamber pressure in the present case will be

$$P_c(\text{approx}) = \frac{2.224}{2.045}(300)$$

$$= 326 \text{ psia}$$

Now we are ready to carry out the exact calculation of the theoretical chamber pressure, P_c, for this case.

Method 1A

From the pressure interpolation chart (Fig. 4) the chamber temperature, T_c, is read at $H_{red} = 1.151$ and $P_c = 325$ psia: $T_c$here $= 2658^oK$ or 4790^oR

As shown in the Thermodynamics Section (see Equation 21)

$$\frac{T_t}{T_c} = \frac{2}{\gamma + 1}$$

This can be used to estimate the temperature at the throat of the nozzle. Assuming an arbitrary value of γ of 1.2,

$$T_t = \frac{2}{2.2} T_c = \frac{2658}{1.1} = 2416$$

$$\text{Then } T_{Av}\Big]_c^t = T_{\text{arith.mean}} = \frac{2416 + 2658}{2} = 2537^oK$$

or 4560^oR

From Figure A-10, the values of γ for the pure gaseous components can be ~~read~~ obtained at $T = 4560^oR$ as follows:

$$\gamma_{H_2O} = 1.1813$$
$$\gamma_{H_2} = 1.2961$$
$$\gamma_{CO} = 1.2885$$
$$\gamma_{CO_2} = 1.1558$$
$$\gamma_{N_2} = 1.2905$$

Therefore the approximate value of γ_{Av} (using the simplified gas composition) is given by:

$$\gamma_{Av} = 0.3128(1.1813) + 0.0881(1.2961) + (0.2288)(1.2885) + 0.1837(1.1558) + 0.1866(1.2905)$$

$$= 1.2319$$

MW_c is still $= 0.992 MW_f = 25.33$

So P_c can be calculated by

$$P_c = \frac{m}{A_t}\sqrt{\frac{RT_c}{2g_o MW_c}}\sqrt{\frac{\gamma-1}{\gamma}}\sqrt{\frac{1}{\left(\frac{2}{\gamma+1}\right)^{\frac{2}{\gamma-1}} - \left(\frac{2}{\gamma+1}\right)^{\frac{\gamma+1}{\gamma-1}}}}$$

$$P_c = 2.224\sqrt{\frac{1546(4790)}{64.4(25.33)}}\sqrt{\frac{1.232-1}{1.232}}\sqrt{\frac{1}{\left(\frac{2}{2.232}\right)^{\frac{2}{0.232}} - \left(\frac{2}{2.232}\right)^{\frac{2.232}{0.232}}}}$$

$$= 2.224\ (67.4)(2.161)$$

$$= 324 \text{ psia}$$

Which is very, very close to the assumed approximate value of 325 psia.

Method 1B

We can be sure that the chamber pressure calculated by Method 1A will not be in error by more than 25 psia and therefore the chamber Temperature (entering the nozzle will be very close to the value of T_c at 325 psia or 2658°K or 4790°R.

However, in order to fix the temperature at the throat very closely, it will be necessary to make a trial and error calculation between T_t and γ using equation (21) again.

$$\frac{T_t}{T_c} = \frac{2}{\gamma + 1}$$

1st Assume $T_t = 2416^\circ K$ (as calculated for $\gamma = 1.2$ in Method 1A),

Then $T_{Av}\Big]_c^t = 2537^\circ K$ (as before)

Also by equation (11) of this thesis

$$\frac{P_t}{P_c} = \left(\frac{T_t}{T_c}\right)^{\frac{\gamma}{\gamma-1}}$$

And an approximate value of P_t can be determined from this using the above figures and assuming $\gamma = 1.2$.

$$P_t = 325\left(\frac{2416}{2658}\right)^{\frac{1.2}{0.2}} = 183 \text{ psia}$$

From the pressure interpolation chart (Fig. 4), the slopes, $\left(\frac{\partial H}{\partial T}\right)_p$ or C_p can now be determined as follows:

$$\left(\frac{\partial H_{red}}{\partial T}\right)_P\Bigg]_{\substack{P = 325 \text{ psia} \\ T = 2537^\circ K}} = \frac{1.29 - 1.01}{(2914 - 2407)1.8} \qquad \frac{0.28}{507(1.8)}$$

so $$\left(\frac{\partial H}{\partial T}\right)_p\Bigg]_{\substack{P = 325 \text{ psia} \\ T = 2537^\circ K}} = (H_{f,2400} - H_{f,o})\left(\frac{\partial H_{red}}{\partial T}\right)_P\Bigg]_{\substack{P = 326 \text{ psia} \\ T = 2537^\circ K}}$$

$$= (3040 - 1397)\frac{0.28}{913}$$

$$= 0.505 \text{ Btu/lb R} = C_p$$

$$\text{and}\left(\frac{\partial H_{red}}{\partial T}\right)_P \Bigg]_{\substack{P=183\\T=2537}} = \frac{1.33 - 1.01}{(2928 - 2397)1.8} = \frac{0.32}{531(1.8)}$$

$$\text{so}\left(\frac{\partial H}{\partial T}\right)_P \Bigg]_{\substack{P=183\\T=2537}} = (3040 - 1397)\frac{0.32}{956}$$

$$= 0.550 \text{ Btu/lb°R} = C_p$$

$$\therefore C_{pav} = \frac{0.505 + 0.550}{2} = 0.528 \text{ Btu/lb°R.}$$

Since an average molecular weight is also required for use with the C_{pAv} in determining γ, the MW at the throat must also be estimated. This is done by the method outlined in Appendix I. From Satterfield's reduced molecular weight charts

MW_{red} (@ 300 psia and 2416°K = T_t) = 0.9963

MW_{red} (@14.7 psia and 2416°K = T_c) = 0.9958

From the relative spread of lines in pressure interpolation chart,

$\therefore MW_{red}$ (183 psia and 2416°K) = 0.9962

$\therefore MW_t = 0.9962\ (25.53) = 25.43$

$\therefore MW_{Av}\Big]_c^t = 25.38$

$$\therefore \gamma_{Av} = \frac{MW_{Av}C_{pAv}}{MW_{Av}C_{pAv} - R} = \frac{25.38(0.528)}{(25.38)(0.528) - 1.99} = \frac{13.39}{11.40}$$

$$= 1.173$$

Using this in equation (21) again

$$\frac{T_t}{T_c} = \frac{2}{2.173}$$

then $T_t = \frac{2}{2.173}(2658) = 2444^{\circ}K$

instead of $2416^{\circ}K$ as assumed.

Assuming now that $T_t = 2444^{\circ}K$, then

$$T_{Av}\Big]_c^t = \frac{2658 + 2444}{2} = 2551^{\circ}K$$

From equation (11),

$$P_t \text{ now} = 325\left(\frac{2444}{2658}\right)^{\frac{1.173}{0.173}} = 174 \text{ psia}$$

From the pressure interpolation chart (Fig. 4) the slope, $\left(\frac{\partial H}{\partial T}\right)_p$ or C_p, can now be determined more accurately as follows:

$$\left(\frac{\partial H_{red}}{\partial T}\right)_P\Bigg]_{\substack{P = 325 \text{ psia} \\ T = 2551^{\circ}K}} = \frac{1.29 - 1.01}{(2901 - 2407)1.8} = \frac{0.28}{498(1.8)}$$

$$\text{so } \left(\frac{\partial H}{\partial T}\right)_P\Bigg]_{\substack{P = 325 \text{ psia} \\ T = 2551^{\circ}K}} = (3040 - 1397)\frac{0.28}{896}$$

$$= 0.514 \text{ Btu/lb}^{\circ}R = C_p$$

$$\text{and } \left(\frac{\partial H_{red}}{\partial T}\right)_P \Bigg]_{\substack{P = 124 \text{ psia} \\ T = 2551^{\circ}K}} = \frac{1.33 - 1.01}{(2935 - 2397)(1.8)} = \frac{0.32}{538(1.8)}$$

$$\text{so } \left(\frac{\partial H}{\partial T}\right)_P \Bigg]_{\substack{P = 174 \text{ psia} \\ T = 2551^{\circ}K}} = (3040 - 1397)\frac{0.32}{969}$$

$$= 0.544 \text{ Btu/lb}^{\circ}\text{R} = C_p$$

$$\therefore C_{pAv} = \frac{0.514 + 0.544}{2} = 0.529 \text{ Btu/lb}^{\circ}\text{R}$$

The average molecular weight will not be changed by the slight change in $T_{Av}\Big]_c^t$ and P_t and can be taken still to be 25.38

$$\therefore \gamma_{Av} = \frac{25.38(0.529)}{25.38(0.529) - 1.99} = \frac{13.41}{11.42} = 1.173$$

which is the same as that calculated on the first attempt. Therefore this second trial was unnecessary except to prove this fact.

Now we are ready to calculate P_c from equation (22c).

$$P_c = \frac{\dot{m}}{A_t}\sqrt{\frac{RT_c}{2g_o MW_t}}\sqrt{\frac{\gamma'-1}{\gamma'}}\sqrt{\frac{1}{\left(\frac{2}{\gamma''+1}\right)^{\frac{2}{\gamma''-1}} - \left(\frac{2}{\gamma''+1}\right)^{\frac{\gamma''+1}{\gamma''-1}}}}$$

where $\gamma'' = \gamma_{Av}$(above) = 1.173

$$\gamma' = \frac{MW_t C_{pAv}}{MW_t C_{pAv} - R} = \frac{25.43(0.529)}{25.43(0.529) - 1.99} = \frac{13.40}{11.41}$$

so γ' also = 1.173 in this case

and $\gamma_d = 1 + \frac{\gamma'-1}{\gamma'}(\gamma_t)\left[1 - \frac{v_t}{MW_t}\left(\frac{\partial MW_t}{\partial v_t}\right)_s\right]$

where $\gamma_t = \frac{MW_t C_{pt}}{MW_t C_{pt} - R}$

From pressure interpolation chart,

$$C_{pt} = \left(\frac{\partial H}{\partial T}\right)_P \Bigg]_{\substack{P = 174 \text{ psia} \\ T = 2444^\circ K}} = \frac{1.29 - 1.01}{(2877 - 2388)1.8}(H_{f,2400} - H_{f,o})$$

$$= \frac{0.28}{489(1.8)}(1643) = 0.524 \text{ Btu/lb.}$$

so $\gamma_t = \frac{25.43(0.524)}{0.524(25.43) - 1.99} = \frac{13.33}{11.34} = 1.174$

From Satterfield's reduced Molecular Weight charts

$$\left.\frac{\Delta_{MW}}{MW}\right]_{2400}^{2500} = 0.0013 \doteq \left(\frac{\partial MW}{MW}\right)_t$$

$$\left.\frac{\Delta v}{v}\right]_{2400}^{2500} = \frac{1.8}{10.64} = 0.17$$

(obtained using the perfect gas law and the relation between T and P previously derived to calculate v_{2400}, v_{2500}, and v_t

$$\therefore \frac{MW_t}{v_t}\left(\frac{\partial MW}{\partial v}\right)_s = \frac{0.0013}{0.17} = 0.008$$

$$\therefore \gamma_d = 1 + \frac{1.173 - 1}{1.173}(1.174)(0.992)$$

$$\therefore \gamma_d = 1.173 \text{ also in this case.}$$

So

$$P_c = 2.224 \sqrt{\frac{1546(4790)}{64.4(25.33)}} \sqrt{\frac{1.173 - 1}{1.173}} \sqrt{\frac{1}{\left(\frac{2}{2.173}\right)^{\frac{2}{0.173}} - \left(\frac{2}{2.173}\right)^{\frac{2.173}{0.173}}}}$$

$$= 2.224\ (67.4)\ (2.199)$$

$$= 330 \text{ psia}$$

compared to 324 psia by method 1A.

Method 2

Graphical Procedure

Using the Mollier Type diagram constructed by R. H. Boll of the University of Michigan. To simplify the trial and error procedure which is necessary with this method, this Mollier Type chart for the system red fuming nitric acid and aniline was modified by the addition of lines of constant $(\partial p/\partial v)_s$ determined by the method outlined in Appendix M.

Basis of Method

It was shown in the Thermodynamic section (equation (27)) that the velocity of the gas in the nozzle throat could be expressed in the same form as the expression for the velocity of sound in a gas:

$$u_t = \sqrt{-g_o v_t^2 \left(\frac{\partial p}{\partial v}\right)_s}$$

from which we can write

$$-\left(\frac{\partial p}{\partial v}\right)_s = \frac{u_t^2}{g_o v_t^2}$$

Using the continuity equation $\dot{m} = \frac{u_t A_t}{v_t}$,

this becomes

$$-\left(\frac{\partial p}{\partial v}\right)_s = \left(\frac{\dot{m}}{A_t}\right)^2 \times \frac{1}{g_o} \qquad (19A)$$

Hence the point on the Mollier Type diagram which represents throat conditions can be limited to some point along one of the constant $\left(\frac{\partial p}{\partial v}\right)_s$ lines immediately, provided $\dot{m}/A_t$ is known.

One more relationship is needed to fix the exact point on this line however. This is obtained as follows starting with equation (1) of this thesis which states

$$dH + \frac{u\,du}{g_o} = dQ$$

Integrating this from chamber (nozzle entrance) to some point 2 along the length of the nozzle gives

$$H_2 - H_c + \frac{u_2^2}{2g_o} - \frac{u_c^2}{2g_o} = Q \qquad (20A)$$

If $\frac{u_1^2}{2g_o}$ can be neglected in comparison to the other terms

$$u_2 = \sqrt{2g_o(Q - \Delta H)} \qquad (21A)$$

Using the continuity equation $\dot{m} = \frac{A_2 u_2}{v_2}$

$$v_2 = \frac{A_2}{\dot{m}} \sqrt{2g_o(Q - \Delta H)} \qquad (22A)$$

or in terms of throat conditions

$$v_t = \frac{\sqrt{2g_o[Q - (H_t - H_c)]}}{\dot{m}/A_t} \qquad (23A)$$

Equation (23A) can be used in a trial and error calculation to determine the exact point along the line which represents throat conditions provided H_c and Q are known. In this case Q is the heat transferred Btu/lb ($= l_{cn}$) in the expansion process up to the throat. The procedure for using equation (23A) is as follows: A point on the known $\left(\frac{\partial P}{\partial v}\right)_s$ line is assumed to represent the throat condition, this fixes H_t & v_t. Since H_c, Q and $\dot{m}/A_t$ are known, v_t can also be calculated from equation (23A) and compared with v_t read from the chart at the assumed position. Guided by this deviation a new point on the

line is assumed and the process repeated until the two values of v_t check one another.

Sample Calculation (same case as calculated previously by Method 1A and 1B)

System: Red Fuming Nitric Acid (6.5%NO_2) - Aniline

Mixture Ratio: 3 lbs acid - 1 lb aniline

Mass Flow Rate: 0.0700 lbs/sec

Nozzle Throat Diameter: 0.200"

Chamber Heat Loss, l_c = 300 Btu/lb

Nozzle Heat Loss, l_n = 200 Btu/lb

The enthalpy basis for this Mollier Type diagram (Figure A-39) is different than that of the Satterfield charts which is used elsewhere in this thesis. In this case zero enthalpy is assigned to the elements in their standard states and on this basis the enthalpy of the unburnt system is as follows:

H_f for red fuming HNO_3 = -1237 Btu/lb

H_f for aniline = 150 Btu/lb

$$H_{system} = 0.75(-1237) + 0.25(150)$$
$$= -890 \text{ Btu/lb}$$

$$H_{system} = -890 - 300$$
$$= -1190 \text{ Btu/lb}$$

Assume as before that $l_{cn} = 0.28\ell_n = 0.28(200)$

$= 56$ Btu/lb

From equation (19A)

$$-\left(\frac{\partial p}{\partial v}\right)_s = \left(\frac{w}{A_t}\right)^2 \times \frac{1}{g_o}$$

$$-\left(\frac{\partial p}{\partial v}\right)_s = \frac{(320)^2}{32.17}$$

$= 3187$ lbs/ft^5

1st guess: Assume $H_t = -1450$ Btu/lb

Then from chart, $P_t = 12.8$ atm

$T_t = 4346^\circ R$

$S_t = 0.7410$

$$v_t = \frac{0.0286(4346)}{12.8} = 9.71 \text{ cu ft/lb}$$

From equation (23A)

$$v_t = \sqrt{\frac{2g_o\,[Q - (H_t - H_c)]}{w/A_t}}$$

$$= \sqrt{\frac{64.4\ \ -56 - (-1450 + 1190)\ \ 778}{320}}$$

$$= \sqrt{\frac{10,200,000}{320}}$$

$= 10.0$ cu ft/lb, which is too high.

2nd guess: Assume $H_t = -1435$ Btu/lb.

Then from chart,

$$P_t = 12.90$$

$$T_t = 4383^{\circ}R$$

$$S_t = 0.7440$$

$$v_t = \frac{0.0286(4383)}{12.9} = 9.73 \text{ cu ft/lb}$$

From equation (23A)

$$v_t = \sqrt{\frac{64.4[-56 - (-1435 - 1190)]778}{320}} = \sqrt{\frac{9460,000}{320}}$$

$= 9.62$ cu ft/lb which is too low

3rd guess: Assume $H_t = -1440$ Btu/lb

Then from chart $S_t = 0.7430$, $T_t = 4370^{\circ}R$

and from equation (23A)

$$v_t = \sqrt{\frac{64.4[-56 - (-1440-1190)\ 778}{320}} = \sqrt{\frac{9630000}{320}}$$

$= 9.72$ which checks.

Then assume $\Delta S\Big]_c^t = \frac{Q}{T_{Av}}\Big]_c^t = \frac{-56}{\frac{4990 + 4370}{2}} = -0.012$ Btu/lb x $^{\circ}R$

$$S_c = S_t + 0.012 = 0.7430 + 0.012$$

$= 0.7550$ Btu/lb x $^{\circ}R$

From the chart, at $H_c = -1190$ and $S_c = 0.7550$

$P_c = 22.5$ atm or 331 psia

Compared with 330 psia by Method 1B and 324 psia by Method 1A.

Specific Impulse Calculations

Method 1A and 1B

Using Satterfield charts plus the equation

$$I_{sp} = \sqrt{\frac{2RT_c}{g_o \frac{MC_{p'c-e}}{C_{p'c-e}}}} \sqrt{\frac{\gamma'_{c-e}}{\gamma'_{c-e}-1}} \sqrt{1-\left(\frac{P_e}{P_c}\right)^{\frac{\gamma''_{c-e}-1}{\gamma''_{c-e}}}}$$

Equation (14a) of Appendix C.

By defining $M_{cp'c-e}$ arbitrarily as $MW_c C_{p'c-e}$ this can be written

$$I_{sp} = \sqrt{\frac{2RT_c}{g_o MW_c}} \sqrt{\frac{\gamma'_{c-e}}{\gamma'_{c-e}-1}} \sqrt{1-\left(\frac{P_e}{P_c}\right)^{\frac{\gamma''_{c-e}-1}{\gamma''_{c-e}}}} \qquad (14c)$$

In method 1A all the γ's are assumed the same and are evaluated from the average C_p of the gas mixture based on the C_p values of the individual pure gaseous components at the arithmetic mean temperature, thus neglecting the effect of any reaction on C_p.

In method 1B it is assumed that all γ's can be evaluated from an average value of C_p obtained from the arithmetic average of $(\partial H/\partial T)_P$ at the arithmetic mean temperature and P_c and $(\partial H/\partial T)_P$ at the arithmetic mean temperature and P_e. This takes into account any heat of reaction effects on C_p.

System: 90% H_2O_2 - Naphferrol

Mixture Ratio: 3.5 lbs H_2O_2 - 1 lb Naphferrol

Stoichiometric = 0.269 mols Naphferrol (CH_3OH per mol H_2O_2

P_c = 240 psia

l_c = 75 Btu/lb

l_n = 70 Btu/lb

Take as Basis: 1 lb of Propellants

or 0.779 lbs of 90% H_2O_2

0.221 lbs of Naphferrol

Then Mols of: $H_2O_2 = \frac{0.90(0.779)}{34} = 0.02062$

$H_2O = \frac{0.10(0.779)}{18} = 0.00432$

$(C_{10}H_7)_2(SO_3)_2Fe \cdot 3H_2O = \frac{0.202(0.221)}{524.3} = 0.0000852$

$CH_3OH = \frac{0.798(0.221)}{32} = 0.00551$

Therefore, atoms of H = 2(0.02062) + 2(0.00432) + 20(0.0000852) + 4(0.00551) = 0.07362

atoms of C = 20(0.0000852) + 1(0.00551) = 0.00721

atoms of O = 2(0.02062) + 1(0.00432) + 9(0.0000852) + 1(0.00551) = 0.05184

atoms of S = 2(0.0000852) = 0.00017

atoms of N = 0.

And the element ratios are:

$$C/O = \frac{0.00721}{0.05184} = 0.1395$$

$$C + S/O = \frac{0.00738}{0.05184} = 0.1430$$

$$H/O = \frac{0.07362}{0.05184} = 1.420$$

$$N/O = 0$$

The simplified gas composition is then found to be(in mol fractions):

		Fe_2O_3 free basis
CO_2	0.1637	0.1639
SO_2	0.0040	0.0040
H_2O	0.8313	0.8321
Fe_2O_3	0.0010	0.0000

Then the average molecular weight of the gas (neglecting the Fe_2O_3) is given by:

$$MW_f = 0.8321(18) + 0.1639(44) + 0.004(64)$$

$$14.98 + 7.21 + 0.26$$

$$= 22.45$$

And on the Satterfield Basis:

$$H_{f,o} = 0$$

$$H_{f,2400} = 0.8313(44,689) + 0.1677(54,031) + 0.001(130,400)$$

$$= 46,490 \text{ Btu/lb or } \frac{46,490}{22.45} = 2066 \text{ Btu/lb}$$

and $H_{system} = 0.90(0.779)(848) + 0.10(0.779)(-810)$
$+ 0.202(0.221)(7090) + 0.798(0.221)(8784)$

$= 2408$ Btu/lb

Considering the heat loss,

assume,

$$l_{eff} = l_c + 1/2\ l_n = 75 + 1/2(70) = 110 \text{ Btu/lb.}$$

$$H_{system} = 2408 - 110 = 2298 \text{ Btu/lb.}$$

$$\text{then } H_{red} = \frac{H_{syst} - H_{f,o}}{H_{f,2400} - H_{f,o}} = \frac{2298}{2066} = 1.111$$

Method 1A

From the pressure interpolation chart (Fig. A-24), the chamber temperature, T_c, is read at $H_{red} = 1.111$ and $P_c = 240$ psia:

T_c here $= 2482^{\circ}K$

or $4470^{\circ}R$

By equation (11) of the Thermodynamics Section of this thesis,

$$\frac{T_e}{T_c} = \left(\frac{P_e}{P_c}\right)^{\frac{\gamma-1}{\gamma}}$$

A trial and error calculation between T_e and γ is necessary to fix γ precisely.

1st assume $\gamma = 1.2$

$$\text{then } T_e = 4470\left(\frac{14.7}{240}\right)^{\frac{1.2-1}{1.2}}$$

$= 2802^{\circ}R$

$$\text{therefore} \quad T_{Av}\Big]_c^e = \frac{2802 + 4470}{2} = 3636^\circ R$$

From Figure A-17, the values of γ for the pure gaseous components can be ~~read~~ obtained at $T = 3636^\circ R$ as follows:

$$\gamma_{H_2O} = 1.1898$$

$$\gamma_{CO_2} = 1.1567$$

then $\gamma_{Av} = 0.8321(1.1898) + 0.1679(1.1567)$

$= 1.1844$

Repeating the calculation of T_e using the value of gives:

$$T_e = 4470\left(\frac{14.7}{240}\right)^{\frac{1.1844 - 1}{1.1844}}$$

$$= 2898^\circ R$$

$$\text{therefore} \quad T_{Av}\Big]_c^e = \frac{2898 + 4470}{2}$$

$$= 3684^\circ R.$$

At this temperature,

$$\gamma_{H_2O} = 1.1893$$

$$\gamma_{CO_2} = 1.1566$$

and $\gamma_{Av} = 0.8321(1.1893) + 0.1679(1.1566)$

$= 1.1842$ which is practically identical with that obtained on the first trial.

Substituting these values in the expression for I_{sp} we get:

$$I_{sp} = \sqrt{\frac{2(1546)(4470)}{32.17(22.45)}} \sqrt{\frac{1.1842}{1.1842 - 1}} \sqrt{1 - \left(\frac{14.7}{240}\right)^{\frac{1.1842 - 1}{1.1842}}}$$

$$= \sqrt{19110}\ (2.5371) \sqrt{0.353}$$

$$= 208.4 \text{ lbs-sec/lb.}$$

Corrected for loss of Fe_2O_3,

$I_{sp} = 208.4(0.993) = 207.0$ lbs-sec/lb.

Method 1B

T_c still = 2482°K or 4470°R.

Again in order to fix γ precisely a trial and error calculation is necessary between T_e and γ in the expression:

$$\frac{T_e}{T_c} = \left(\frac{P_e}{P_c}\right)^{\frac{\gamma - 1}{\gamma}}$$

However, this time we will use the γ_{Av} of the method 1A as our first estimate,

Then T_{Av} = 3684°R or 2047°K

From the pressure interpolation chart (Fig. A-21) the slopes, $(\partial H/\partial T)_p$ or C_p, can now be determined as follows:

$$\left(\frac{\partial H_{red}}{\partial T}\right)_P \Bigg]_{\substack{P = 240 \text{ psia} \\ T = 2047^\circ K}} = \frac{1.04 - 0.70}{(2425 - 1767)1.8} = \frac{0.34}{658(1.8)}$$

$$\text{so } \left(\frac{\partial H}{\partial T}\right)_P \Bigg]_{\substack{P = 240 \text{ psia} \\ T = 2047^\circ K}} = (H_{f,2400} - H_{f,o})\left(\frac{\partial H_{red}}{\partial T}\right)_P \Bigg]_{\substack{P = 240 \text{ psia} \\ T = 2047^\circ K}}$$

$$= (2066)\frac{0.34}{1184}$$

$$= 0.593 \text{ Btu/lb} = C_p$$

$$\text{and } \left(\frac{\partial H_{red}}{\partial T}\right)_P \Bigg]_{\substack{P = 14.7 \text{ psia} \\ T = 2047^\circ K}} = \frac{1.04 - 0.70}{2348 - 1762} \qquad \frac{0.34}{586\ (1.8)}$$

$$\text{so } \left(\frac{\partial H}{\partial T}\right)_P \Bigg]_{\substack{P = 14.7 \\ T = 2047^\circ K}} = (2066)\frac{(0.34)}{(1054)}$$

$$= 0.666 \text{ Btu/lb} = C_p$$

$$C_{p_{Av}} = \frac{0.593 + 0.666}{2} = 0.629$$

Next to obtain an average value of the molecular weight. From Satterfield's reduced molecular weight charts

MW_{red}(at 300 psia and 2482°K = T_c) = 0.9858

MW_{red}(at 14.7 psia and 2482°K = T_c) = 0.9574

From the relative spread of the lines on the pressure interpolation chart,

$\therefore MW_{red}$ (at 240 psia and 2482°K = T_c)

$$= 0.9574 + (0.9858 - 0.9574)\frac{23}{24}$$

$$= 0.9846$$

$$\therefore MW_c = 0.9846 M_f = 0.9846(22.45)$$

$$= 22.15$$

From the reduced molecular weight charts again,

MW_{red} (at 14.7 psia and 1609°K = T_e) = 1.00

$\therefore MW_e = M_f = 22.45$

$$\therefore MW_{Av}\Big]_c^e = 22.30$$

$$\therefore \gamma_{Av} = \frac{MW_{Av} C_{pAv}}{MW_{Av} C_{pAv} - R} = \frac{22.30(0.629)}{22.30(0.629) - 1.99} = \frac{14.01}{12.02}$$

$$= 1.165$$

Using this to calculate T_e

$$T_e = 4470\left(\frac{14.7}{240}\right)^{\frac{1.165 - 1}{1.165}}$$

$$= 3007°R$$

$$T_{Av} = \frac{4470 + 3007}{2} = 3738°R$$

or 2077°K

This average temperature (2077°K) is only 30°K higher than that used before (2047). Therefore the first value of γ of 1.165 is close enough.

γ' however is based on MW_c not MW_{Av}

Therefore

$$\gamma' = \frac{22.15(0.629)}{22.15(0.629) - 1.99} = \frac{13.92}{11.93} = 1.167$$

Now we are ready to calculate I_{sp} from equation (14c), using these new values:

$$I_{sp} = \sqrt{\frac{2RT_c}{g_o MW_c}} \sqrt{\frac{\gamma'}{\gamma'-1}} \sqrt{1-\left(\frac{P_e}{P_c}\right)^{\frac{\gamma''-1}{\gamma''}}}$$

$$= \sqrt{\frac{2(1546)4470}{32.17(22.15)}} \sqrt{\frac{1.167}{1.167-1}} \sqrt{1-\left(\frac{14.7}{240}\right)^{\frac{1.165-1}{1\ 165}}}$$

$$= \sqrt{19390}\ (2.6464)\ \sqrt{0.317}$$

$$= 208.0 \text{ lbs-sec/lb.}$$

Corrected for loss of mass as Fe_2O_3

$$I_{sp} = 208.0(0.993) = 206.5 \text{ lbs-sec/lb}$$

Compared to 207.0 lbs-sec/lb by Method 1A.

Method 3

Using only Satterfield's charts.

Same case as calculated previously by Method 1A and 1B

Stoichiometric 90% H_2O_2 - Naphferrol

$P_c = 240$

$l_c = 75$ Btu/lb $\quad l_{noz} = 70$ Btu/lb

As before:

$MW_f = 22.45$, $MW_c = 22.15$

$H_{f,o} = 0$

$H_{f,2400} = 2066$

$l_{eff} = l_c + 1/2\, l_n = 110$ Btu/lb

$H_{syst} = 2298$ Btu/lb

$H_{red} = 1.111$

Gas Composition = 83.21% H_2O, 16.39% CO_2, 0.40% SO_2

$S_f = 0.8321(65.6) + 0.1679(76.63)$

$= 67.50$ Btu/lb-mol x ^oR or $\frac{67.50}{22.45} = 3.0$ Btu/lb x ^oR

From Satterfield's 300 psia reduced enthalpy chart

At $H_{red} = 1.111$ and at interpolation no. of 0.9,

$T_c = 2490^oK$.

From Pressure interpolation chart at $T_c = 2490$

$H_{red_{240\ psia}} = 1.116$

From Satterfield's 300 psia reduced entropy chart.

At $T_c = 2490$ and interpolation no. = 0.9,

$$S_{red\ 300} = 0.9645\ \text{Btu/lb} \times {}^{o}R$$

$$S_{red\ 240} = S_{red\ 300} + \frac{H_{red\ 240} - H_{red\ 300}}{T_c \times 1.8}\left(\frac{H_{f,2400} - H_{f,o}}{S_f}\right) + \frac{1.99}{MW_c}\cdot\frac{\ln\frac{300}{240}}{S_f}$$

$$= 0.9645 + \frac{1.116 - 1.111}{2490(1.8)}\ \frac{(2066)}{3.0}\ \frac{1.992.3 \log 1.25}{22.15(3.0)}$$

$$= 0.9645 + 0.0008 + 0.0067$$

$$= 0.9720$$

From the transformation figures to transfer to $S_{red\ 14.7}$

$$\Delta_{14.7} - \Delta_{300} = 0.014$$

$$S_{red\ 14.7} = 0.9720 + 0.014$$

$$= 0.9860$$

From Satterfield's 14.7 psia reduced entropy chart,

$S_{red} = 0.9860$ and interpolation no. = 0.9,

$$T_e = 1703^{o}K$$

From Satterfield's 14.7 psia reduced enthalpy chart,

at $T_e = 1703^{o}K$ and interpolation no. = 0.9,

$$H_{red\ 14.7} = 0.672$$

$$H_e = 0.672(H_{f,2400} - H_{f,o})$$

$$H_e = 0.672(2066)$$

$$= 1389 \text{ Btu/lb}$$

$$\Delta H = H_c - H_e = 2298 - 1389$$

$$= 909 \text{ Btu/lb}$$

$$I_{sp} = \sqrt{\frac{2\Delta H}{g_o}}$$

$$= \sqrt{\frac{2(909)(778)}{32.17}}$$

$$= 209.9 \text{ lbs-sec/lb}$$

or corrected for loss of the mass of Fe_2O_3

$$I_{sp} = 209.9(0.993)$$

$$= 208.4 \text{ lbs-sec/lb.}$$

Compared with answers of

207.0 and 206.5 by Methods 1A and 1B

Method 2

Using only the pressure interpolation chart which was derived from Satterfield's generalized correlations of thermodynamic properties as described in Appendix H.

System: Red fuming Nitric Acid - Aniline

Mixture Ratio: 3 lbs acid to 1 lb aniline

Chamber Pressure = 294 psia

Chamber and Nozzle Heat Loss - Both Negligible

As found with the same system in the first part of the appendix in the sample calculations of chamber pressure:

Simplified Gas Composition: 18.37% CO_2

22.88% CO

31.28% H_2O

8.81% H_2

18.66% N_2

$MW_f = 25.53$

$H_{f,o} = 1397$

$H_{f,2400} = 3040$

$H_{system} = 3617$

Therefore in this case,

$$H_{red} = \frac{3617 - 1397}{3040 - 1397} = 1.350$$

Method 2A

By equation (11) of this thesis,

$$\frac{T_e}{T_c} = \left(\frac{P_e}{P_c}\right)^{\frac{\gamma-1}{\gamma}}$$

T_c can be read from the pressure interpolation chart (Fig. 4), at $H_{red} = 1.35$ and $P_c = 294$ psia, as

$$T_c = 2942^\circ K$$

Since P_c and P_e are known (P_e is assumed = 14.7 for an ideal nozzle), the above relation can be used in a trial and error calculation to fix T_e and γ.

1st assume $\gamma = 1.2$

$$\text{Then } T_e = 2942\left(\frac{14.7}{294}\right)^{\frac{1.2-1}{1.2}}$$

$$= 1786^\circ K$$

$$\text{therefore } T_{\text{arith.mean}}\Big]_c^e = \frac{2942 + 1786}{2} = 2364^\circ K.$$

From the pressure interpolation chart (Fig. 4), the slopes, $(\partial H/\partial T)_P$ or C_p can now be determined as follows:

$$\left(\frac{\partial H_{red}}{\partial T}\right)_P \Big]_{\substack{P = 294 \text{ psia} \\ T = 2364^\circ K}} = \frac{1.29 - 1.01}{(2942 - 2395)(1.8)} \qquad \frac{0.28}{547(1.8)}$$

$$\text{so } \left(\frac{\partial H}{\partial T}\right)_P \Big]_{\substack{P = 294 \text{ psia} \\ T = 2364^\circ K}} = (3040 - 1397)\,\frac{0.28}{986}$$

$$= 0.466 \text{ Btu/lb} \times {}^\circ R$$

Similarly

$$\left(\frac{\partial H}{\partial T}\right)_P \Bigg]_{\substack{P = 14.7 \\ T = 2364^\circ K}} = (3040 - 1397)\,\frac{0.28}{920}$$

$$= 0.500 \text{ Btu/lb x } ^\circ R$$

$$\therefore C_{pAv} = \frac{0.500 + 0.466}{2} = 0.483 \text{ Btu/lb x } ^\circ R$$

The average molecular weight over the expansion process must also be determined to calculate γ. This is done as follows:

From Satterfield's Reduced Molecular Weight charts

MW_{red} at 300 psia and $2942^\circ K = 0.983$

MW_{red} at 14.7 psia and $1786^\circ K = 1.000$

$$MW_{red\ Av} = 0.9915$$

and $MW_{AV} = 0.9915(25.53) = 25.31$

$$\therefore MW_{Av} C_{pAv} = 25.31(0.483)$$

$$= 12.22$$

and $$\gamma_{Av} = \frac{12.22}{10.23} = 1.194$$

then

$$\frac{T_e}{T_c} = \left(\frac{P_e}{P_c}\right)^{\frac{1.194 - 1.00}{1.194}}$$

$$T_e = 2942\left(\frac{14.7}{294}\right)^{\frac{0.194}{1.194}}$$

$$= 1813^\circ K.$$

This value will not be changed appreciably by further repetitions of this process.

From the pressure interpolation chart, at $T = 1811^{o}K$ and at $P = 14.7$, H_{red} is seen to be 0.729.

$\therefore H_{red\ 14.7} = 0.730$

and

$$H_e = 0.730(H_{f,2400} - H_{f,o}) + H_{f,o}$$
$$= 0.730(3040 - 1397) + 1397$$
$$= 2597 \text{ Btu/lb}$$

so

$$H_c - H_e = 3617 - 2597$$
$$= 1020.$$

$$I_{sp} = \sqrt{\frac{2(1022)(778)}{32.2}}$$
$$= 222.0 \text{ lbs-sec/lb.}$$

Method 4

Using the Mollier Type Diagram constructed at Project Wizard of the University of Michigan (C-1) Fig A-30

On the enthalpy base of this chart as pointed out before in the chamber pressure calculation

$$H_{syst} = -890 \text{ Btu/lb}$$

From the chart, at $H_c = -890$ on the $P_c = 20$ atm. line, T_c is seen to be $5313^{\circ}R$

and $S_c = 0.8246$

Since there is no heat loss

$S_e = 0.8246$ and at the value of S on the $P_e = 1$ atm line,

$T_e = 3367^{\circ}R$

$H_e = -1890$

Therefore $H = 998$

and

$$I_{sp} = \sqrt{\frac{2(1000)(778)}{32.2}}$$

$$= 220 \text{ lbs-sec/lb.}$$

Compared with 222 lbs-sec/lb by Method 2A.

APPENDIX M

METHOD OF CONSTRUCTING THE MOLLIER TYPE DIAGRAM FOR THE SYSTEM 90% HYDROGEN PEROXIDE AND 85% HYDRAZINE HYDRATE (STOICHIOMETRIC)

The equilibrium gas composition, and the enthalpy, entropy and specific volume of this gas mixture were calculated for eight different temperatures at each of four different pressures for the system 90% H_2O_2 - 85% $N_2H_4 \cdot H_2O$ in stoichiometric proportions. This system is represented by the following element ratios: C/O = 0; H/O = 2.0; N/O = 0.337. The method used in calculating these equilibrium gas compositions was that previously used by Hottel and his co-workers (18) as well as others. It consists of a special procedure for carrying out the trial-and-error solution of the several (eight in this case) simultaneous equations which represent the material balances the equilibrium relationships for the system. The equilibrium constants for the various reactions were taken from Lewis and von Elbe (24). The entropy and enthalpy of the various components of the gas mixture were taken from Satterfield's (36) compilation of these data and were evaluated above the same base of zero value for both entropy and enthalpy at 0°K and one atmosphere of pressure.

FIGURE A-22

MOLLIER TYPE DIAGRAM
FOR SYSTEM 85% N_2H_4-H_2O
AND 90% H_2O_2
AT STOICHIOMETRIC MIXTURE
RATIO

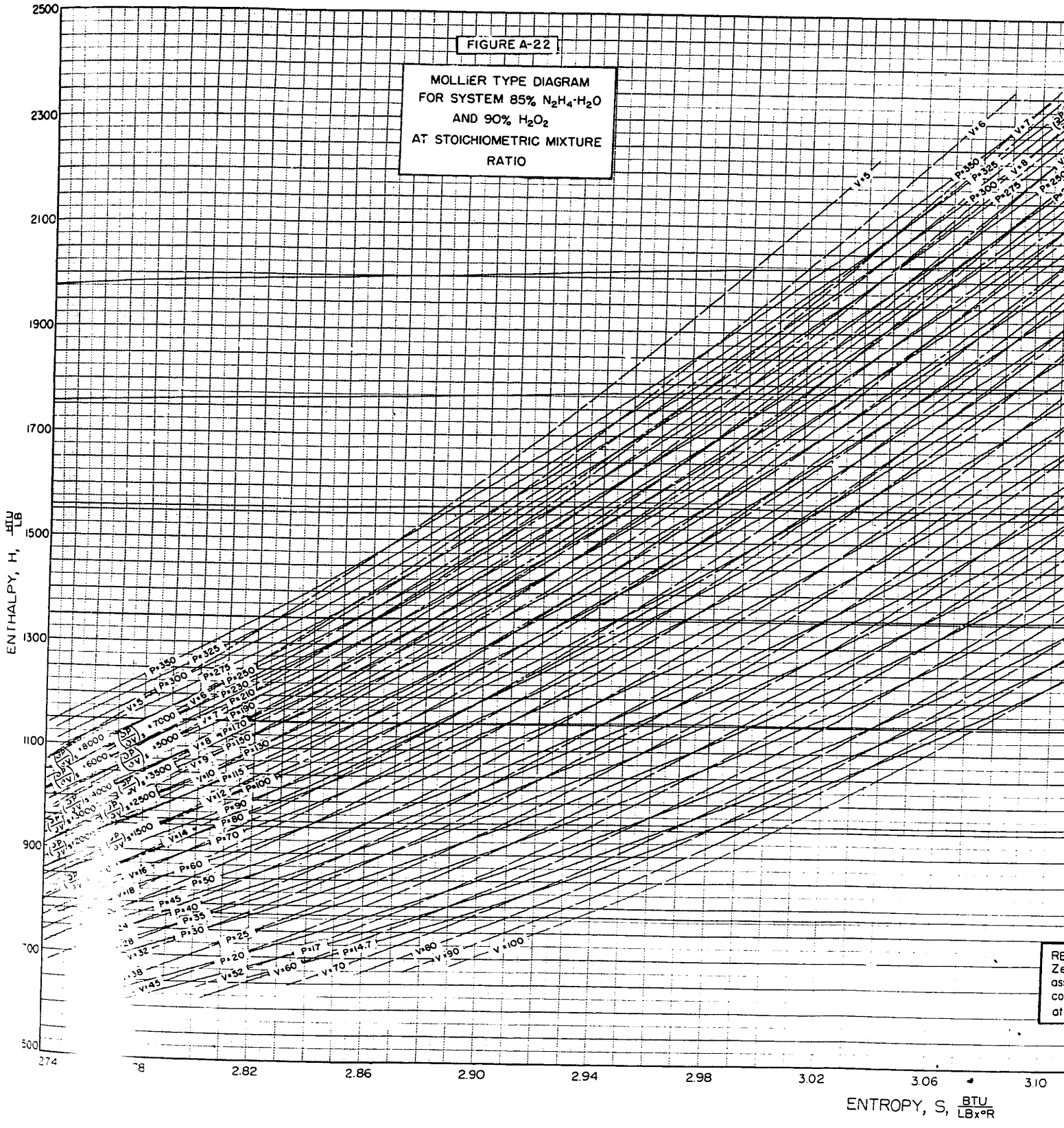

FIG A-23 PRESSURE - ENTROPY CHART FOR EQUILIBRIUM COMBUSTION PRODUCTS OF A STOICHIOMETRIC MIXTURE OF 90% H_2O_2 + 85% $N_2H_4 \cdot H_2O$ (REACTION ASSUMED FROZEN AT 1600°K)

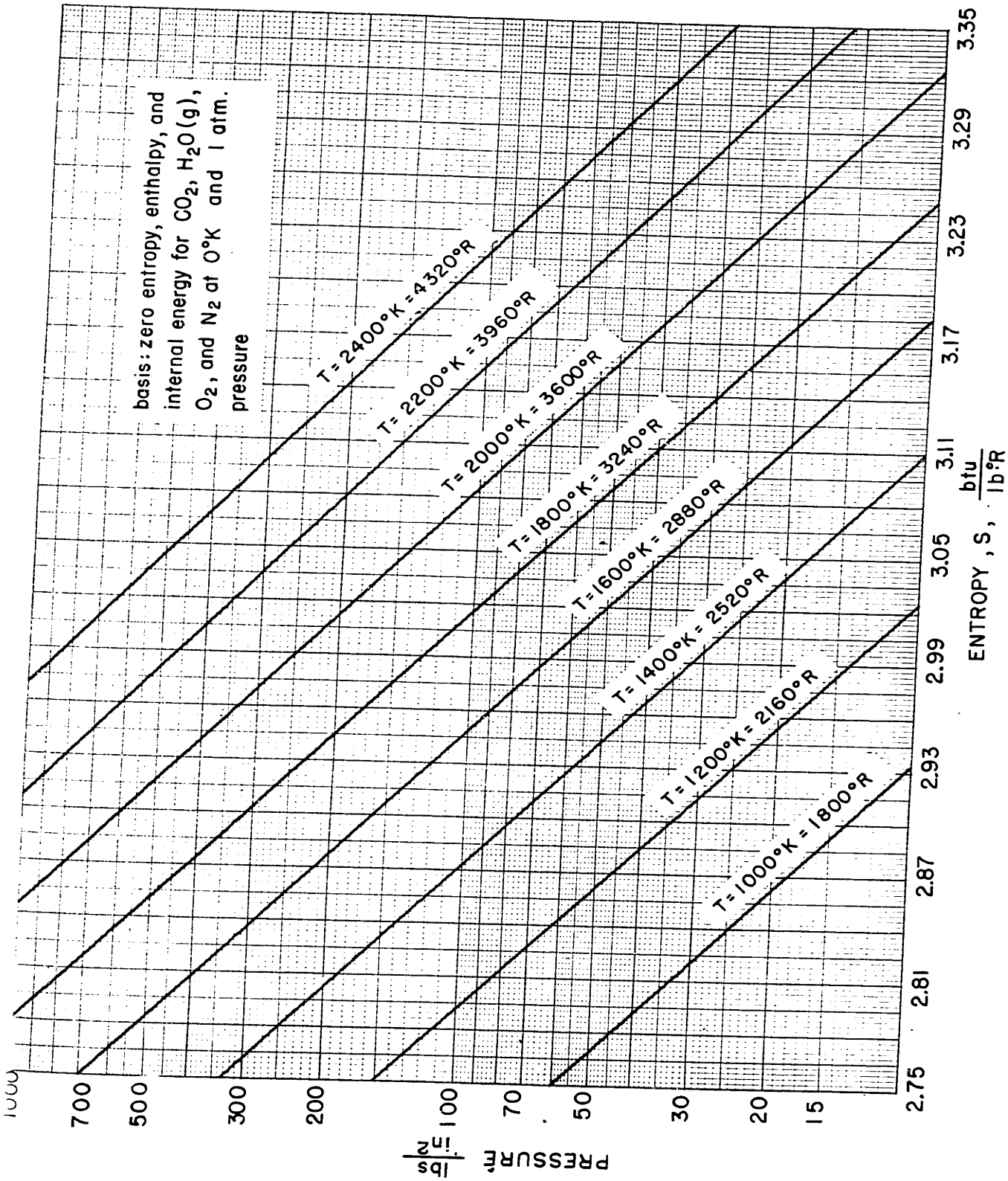

FIGURE A-24

VOLUME—ENTROPY CHART FOR EQUILIBRIUM COMBUSTION PRODUCTS OF A STOICHIOMETRIC MIXTURE OF 90% H_2O_2 + 85% $N_2H_4 \cdot H_2O$ (REACTION ASSUMED FROZEN AT 1600°K)

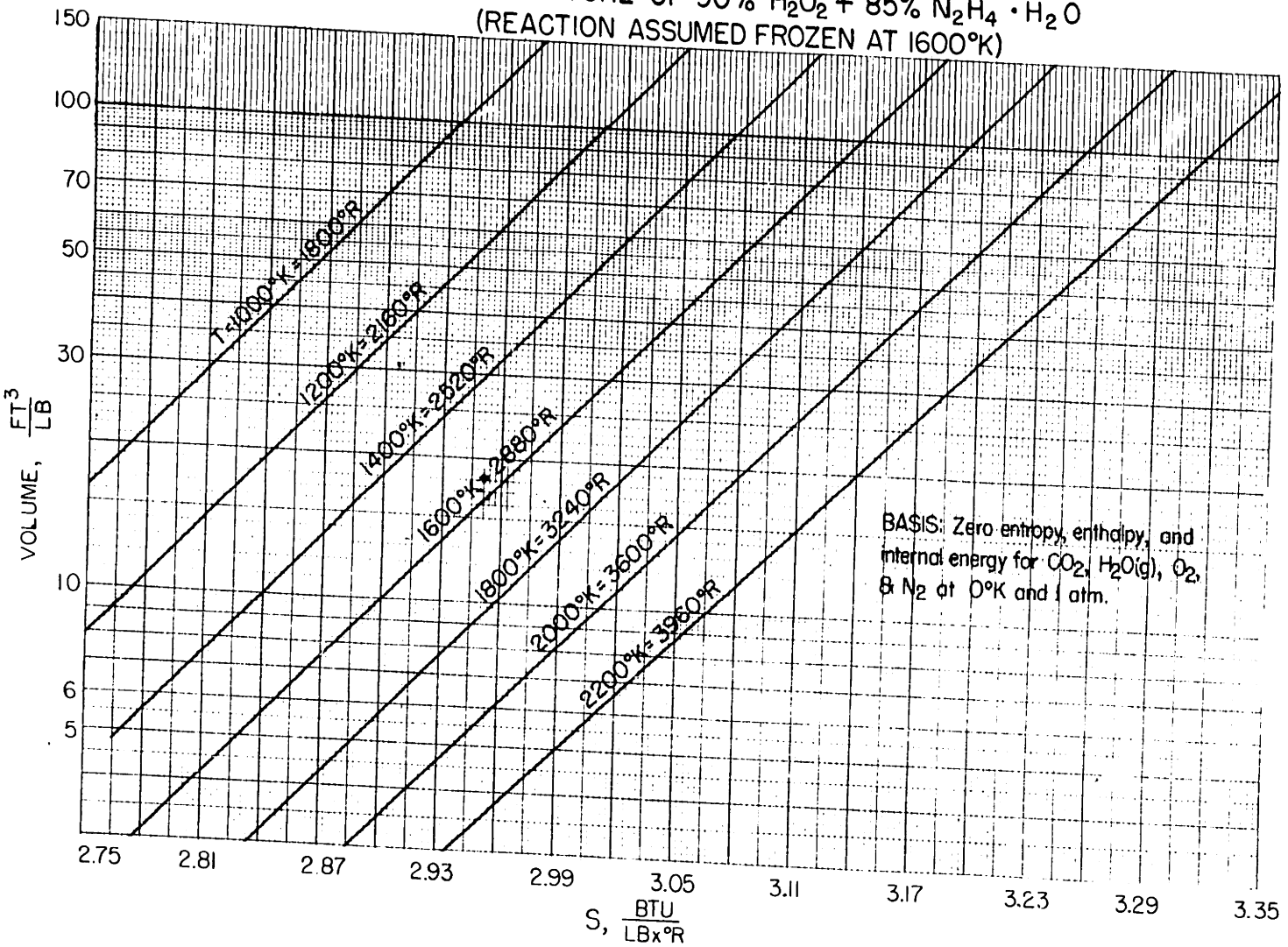

FIGURE A-25

VOLUME & PRESSURE vs ENTROPY CHART

CROSS PLOTTED FROM MOLLIER DIAGRAM (FIG. A-22)

SYSTEM: 90% H_2O_2 – 85% $N_2H_4 \cdot H_2O$

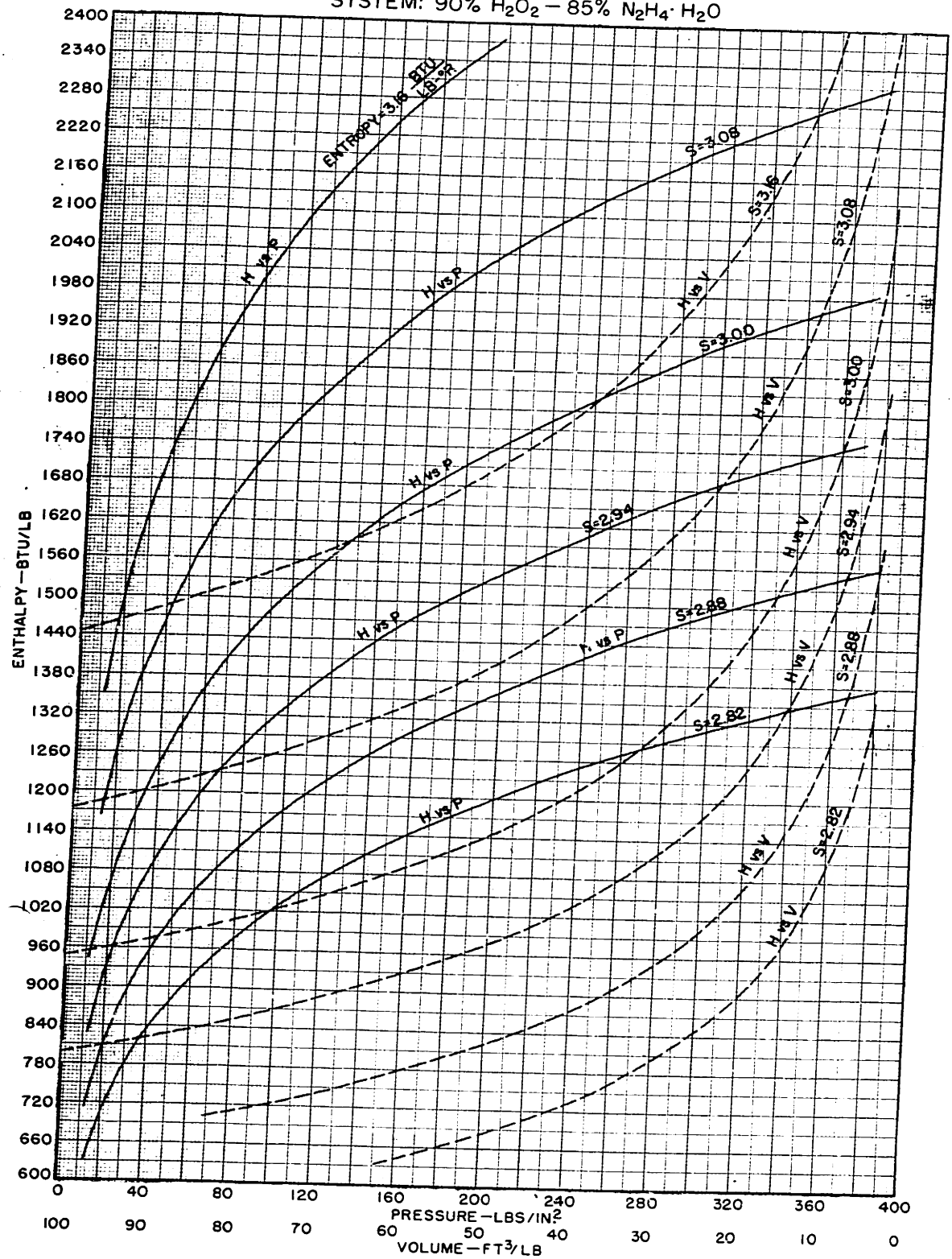

These calculations were carried out for the peroxide-hydrazine hydrate system for temperatures of 2400, 2200, 2000, 1800, 1600, 1400, 1200, and 1000°K and at pressures of 14.7, 80, 150 and 300 psia. However, equilibrium was assumed frozen at temperatures below 1600°K, so the calculations at 1400, 1200, and 1000°K consisted merely in evaluating the enthalpy, entropy and specific volume of the equilibrium gas mixture which was determined in the 1600°K calculations at these additional temperatures and pressures. Perfect gas laws were assumed in all of these calculations.

The calculations described above resulted in values at 32 different points which formed the basis for the enthalpy-entropy diagram of figure A-22. Other points for the volume and pressure lines were obtained by interpolation and extrapolation along lines of constant temperature on a log-log cross-plot of volume and pressure versus ~~pressure~~ entropy. Figures A-23 + A-24

Construction of Lines of Constant $\left(\frac{\partial p}{\partial v}\right)_s$

In order to construct lines of constant $\left(\frac{\partial p}{\partial v}\right)_s$ values on the Mollier Type diagram obtained as above, the following procedure was employed.

First, a combined plot of pressure against enthalpy and volume against enthalpy each at several values of entropy was constructed (see Figure A-25). From this

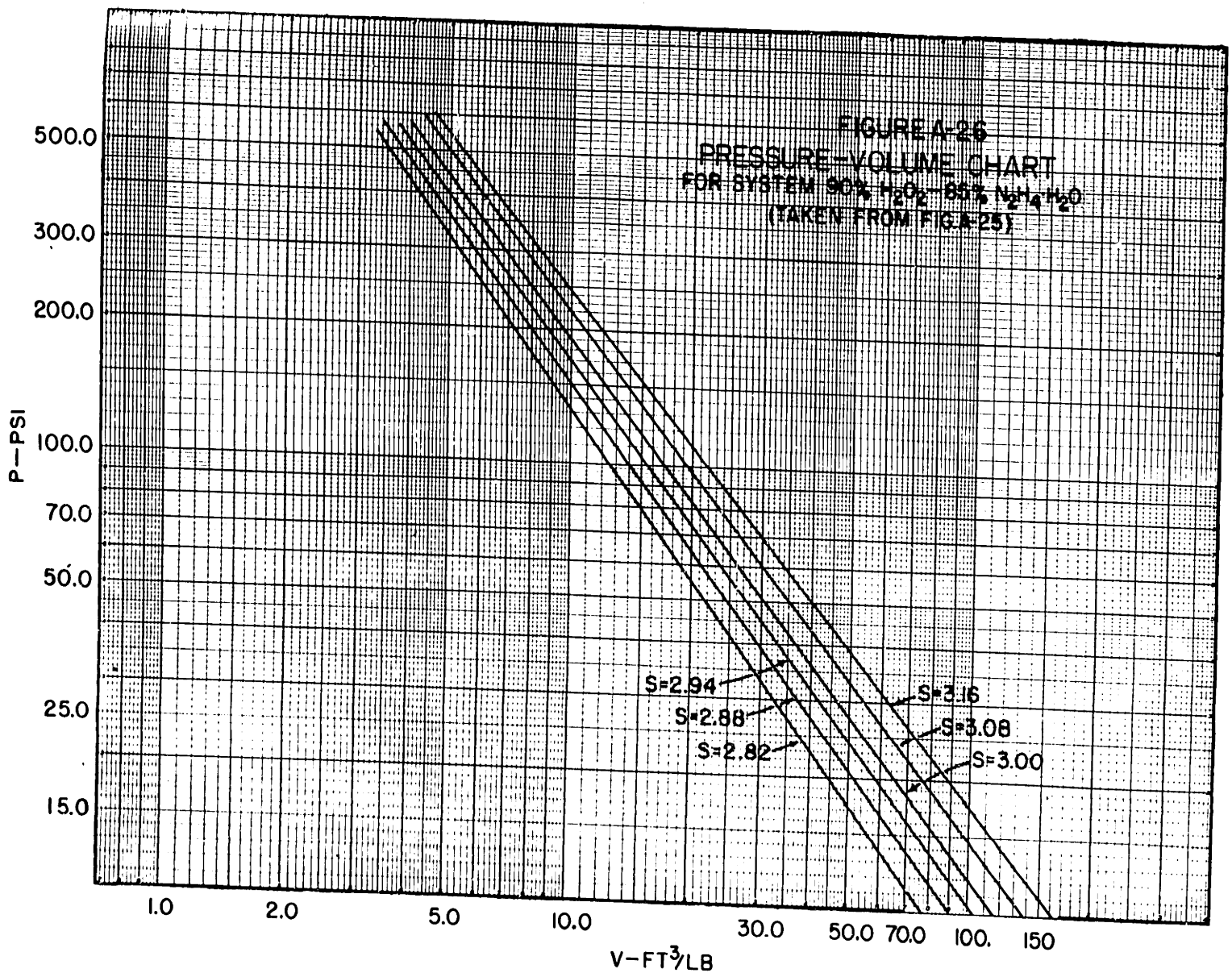
FIGURE A-26
PRESSURE-VOLUME CHART
FOR SYSTEM 90% H_2O_2-65% N_2H_4-H_2O
(TAKEN FROM FIG. A-25)
P-PSI
500.0
300.0
200.0
100.0
70.0
50.0
25.0
15.0
S=2.94
S=2.88
S=2.82
S=3.16
S=3.08
S=3.00
1.0
2.0
5.0
10.0
30.0
50.0
70.0
100.
150
V-FT³/LB

FIGURE A-27

PRESSURE vs $\left(\frac{\partial P}{\partial V}\right)_S$ CHART

FOR SYSTEM 90% H_2O_2 – 85% $N_2H_4 \cdot H_2O$ (TAKEN FROM FIGURE A-26)

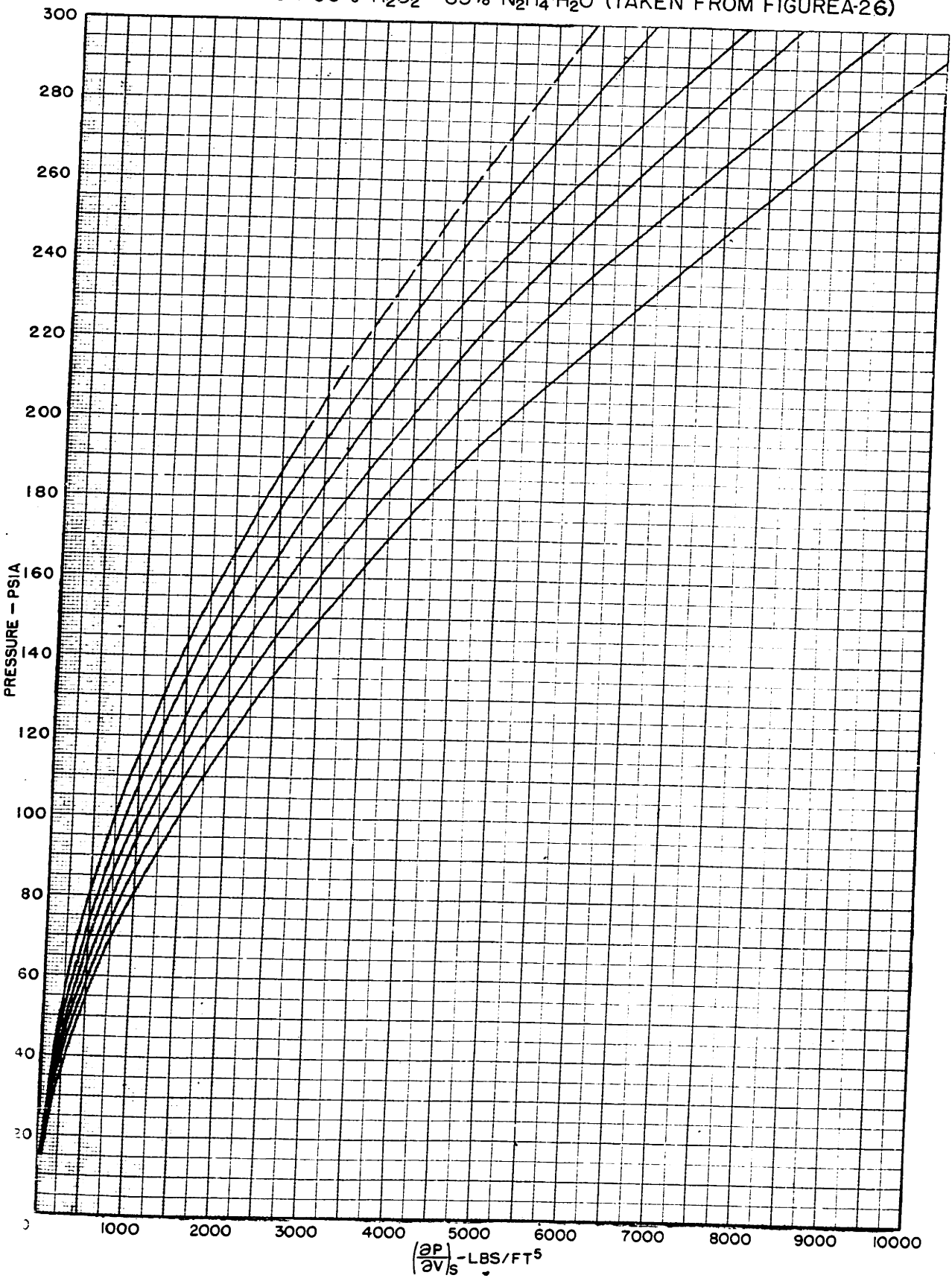

FIGURE A-28
PRESSURE vs ENTROPY CHART SHOWING LINES OF CONSTANT $(\frac{\partial P}{\partial V})_s$
FOR THE SYSTEM 90% H_2O_2 — 85% $N_2H_4 \cdot H_2O$ (TAKEN
FROM FIG. A-27)

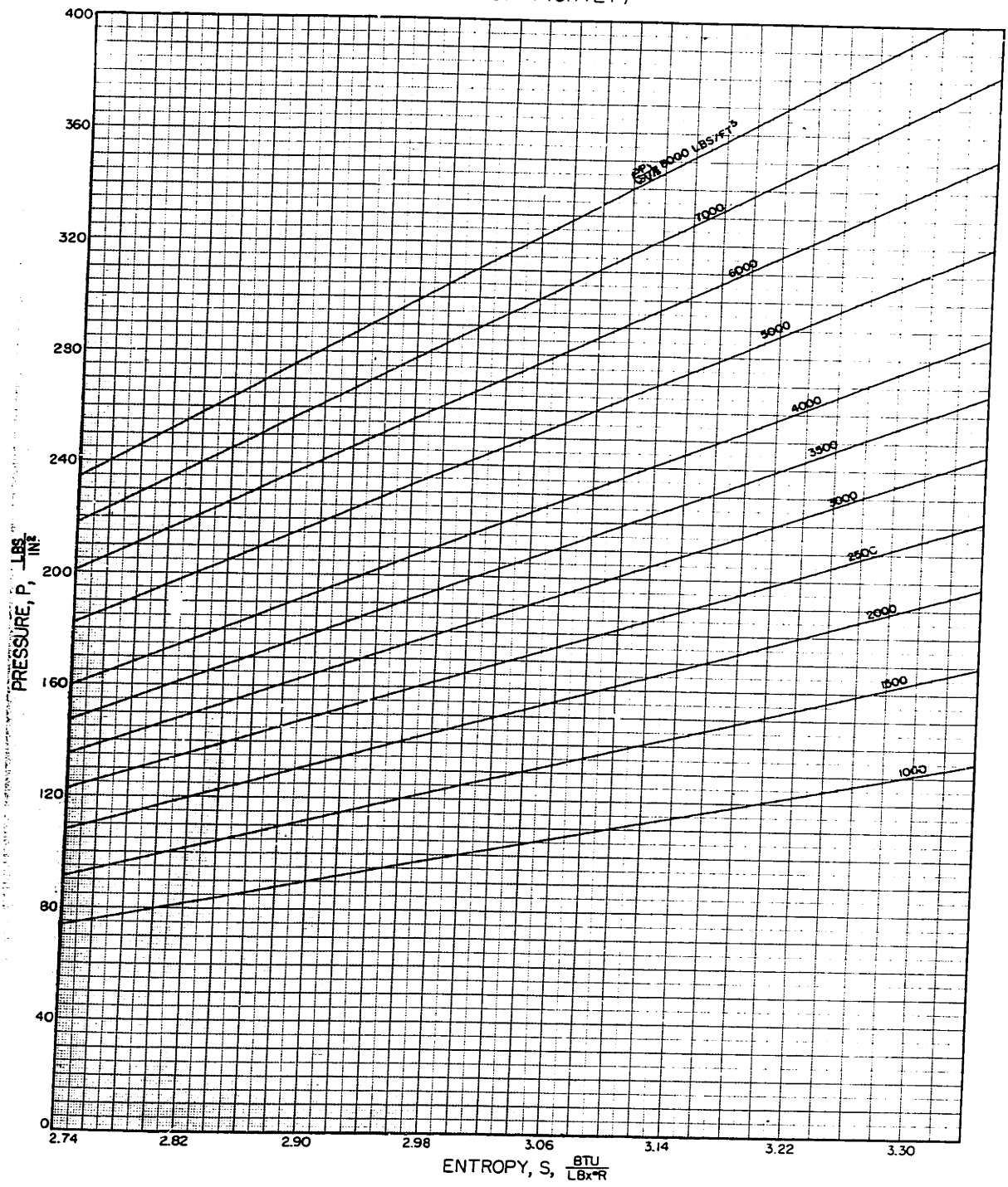

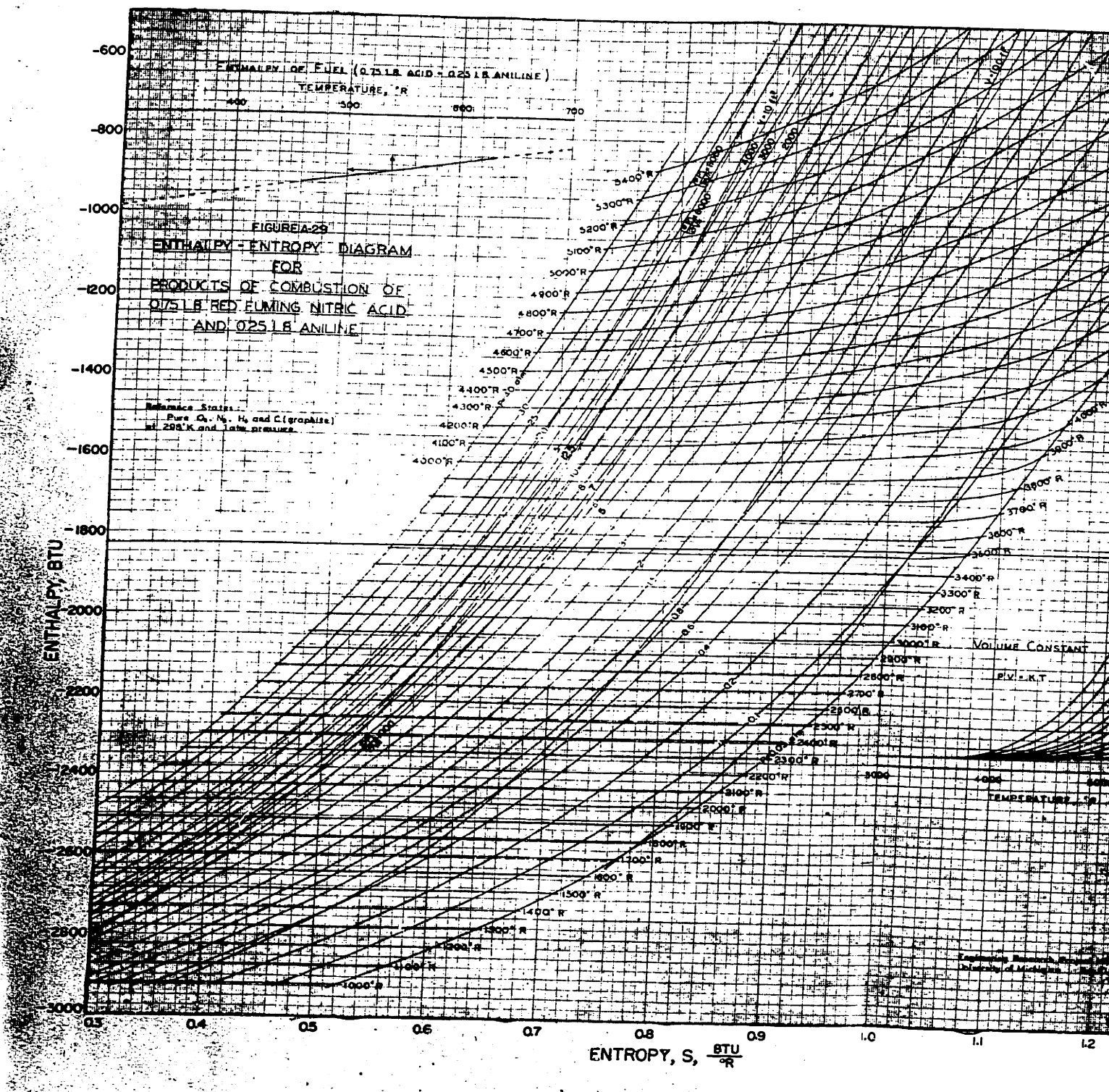
ENTHALPY OF FUEL (0.75 LB ACID + 0.25 LB ANILINE)
TEMPERATURE, °R
400
500
600
700
-600
-800
-1000
-1200
-1400
-1600
-1800
-2000
-2200
-2400
-2600
-2800
-3000
ENTHALPY, BTU
FIGURE A-29
ENTHALPY - ENTROPY DIAGRAM
FOR
PRODUCTS OF COMBUSTION OF
0.75 LB RED FUMING NITRIC ACID
AND 0.25 LB ANILINE
Reference States:
Pure O2, N2, H2 and C (graphite)
at 298°K and 1 atm. pressure.
5400°R
5300°R
5200°R
5100°R
5000°R
4900°R
4800°R
4700°R
4600°R
4500°R
4400°R
4300°R
4200°R
4100°R
4000°R
3900°R
3800°R
3700°R
3600°R
3500°R
3400°R
3300°R
3200°R
3100°R
3000°R
2900°R
2800°R
2700°R
2600°R
2500°R
2400°R
2300°R
2200°R
2100°R
2000°R
1900°R
1800°R
1700°R
1600°R
1500°R
1400°R
1300°R
1200°R
1100°R
1000°R
VOLUME CONSTANT
PV = RT
TEMPERATURE, °R
0.3
0.4
0.5
0.6
0.7
0.8
0.9
1.0
1.1
1.2
ENTROPY, S, BTU/°R

chart corresponding values of pressure and
read for several points along each constan
and plotted against each other on a log-l
in Figure A-26. From the slopes of these l

the values of $\left(\frac{\partial P}{\partial v}\right)_s$ were obtained by the f

$$\left(\frac{\partial \ln P}{\partial \ln v}\right)_s = \left(\frac{\partial P}{\partial v}\right)_s \left(\frac{v}{P}\right)$$

at several pressures along each constant en
These resulting points were plotted as show
From this figure A-27, a final cross plot of
pressure at constant values of $\left(\frac{\partial P}{\partial v}\right)_s$ was
see Figure A-28. And, from this final chart
the lines of constant $\left(\frac{\partial P}{\partial v}\right)_s$ were construc
original Mollier Type diagram by obtaining v
along each $\left(\frac{\partial P}{\partial v}\right)_s$ line on figure A-28 at ea
pressure for which there was a line on the o
diagram.

Nitric Acid-Aniline Chart

In constructing lines of constant $\left(\frac{\partial}{}\right.$
Mollier type diagram of the system Red fuming
aniline (obtained from a report by R. H. Boli
procedure to that outlined above was used. H
this case corresponding values of pressure an
several points along constant entropy lines c
be obtained from the original chart. These w
volume against pressure on a log-log plot sim
Figure A-26. The remaining procedure followed
as that described previously for the peroxide-
system.

APPENDIX N

NOMENCLATURE

The following is a list of the symbols used in this thesis with the definitions and explanations of each. Not included in this list are those symbols used in Appendix B which have conflicting meanings in some cases and have already been defined separately at the time of their use. In addition to the symbols defined below, the standard chemical symbols were used throughout the thesis to designate the various chemical elements and compounds.

A - Cross-Sectional Area in sq. in. or sq. ft.

a - a constant

b - a constant

C - A correlation factor used in extrapolating and interpolating enthalpy at other pressures than 300 psia and 14.7 psia from the value at these two pressures. See Figure A-20.

$$C = \frac{H_{red\ p} - H_{red\ 14.7}}{H_{red\ 300} - H_{red\ 14.7}}$$

^{o}C - degrees Centigrade

c_p - heat capacity at constant pressure in Btu/lb.

c_v - heat capacity at constant volume in Btu/lb.

c_{eff} - the effective exhaust velocity (ft/sec.), i.e. the average velocity of the exhaust stream in

the direction of thrust which would be necessary to produce the measured thrust at the measured mass flow rate, i.e. $c_{eff} = \frac{F_{go}}{\dot{m}}$

c_F -The nozzle thrust coefficient. It is defined empirically as $c_F = \frac{F}{P_c A_t}$ (dimensionless) and is commonly used in the rocket field as a measure of the performance of the exhaust nozzle.

c^* -the characteristic exhaust velocity (ft./sec.), is defined empirically as $c^* = \frac{C_{eff}}{C_F}$ and is commonly used in the rocket field as a measure of combustion chamber performance.

D -diameter in inches or feet

d__ -the mathematical symbol for the differential of a given variable, representing an infinitisimal change in the value of the variable in question.

E -the thermodynamic function, internal energy, in Btu/lb. or Btu/lb.mol.

F -thrust force in lbs.

^oF -degrees Fahrenheit

F/O -Fuel to oxidant ratio in lbs./lb. or mols/mol.

$\frac{F}{F+F \approx O}$ -Fuel to fuel plus fuel equivalent (Stoichiometric) to oxidant ratio in lbs./lb. or mols./mol. (Generalized fuel fraction)

G -Mass flow rate per unit of cross-sectional area $\frac{\text{lbs.}}{\text{sec. x in.}}$ or $\frac{\text{lbs.}}{\text{sec. x ft.}}$

g_o -a conversion factor, as in the expression Force =

$\frac{\text{mass x acceleration.}}{g_o}$ It has the value of

32.17 $\frac{\text{ft. x lbs. mass}}{\text{sec. x lbs.force}}$

H -the thermodynamic function, enthalpy in Btu/lb. or Btu/lb. mol.

H_{system} -the enthalpy of the unburnt system (propellant combination) in Btu/lb.

$H_{f,2400}, H_{f,0}$ -the enthalpy of the simplified or fictitious gas composition at 2400°K and 0°K respectively as used in Satterfield's generalized correlation of thermodynamic properties (in Btu/lb. or Btu/lb. mol.).

H_{red} -The Satterfield reduced enthalpy function which is defined as $H_{red} = \frac{H_{system} - H_{F,0}}{H_{P,2400} - H_{F,0}}$

h -The heat transfer coefficient (convective) in Btu/sec. x sq. in. x °R.

I_{sp} -Specific Impulse - or the impulse per pound of propellants in $\frac{\text{lbs.force-sec.}}{\text{lb. mass}}$

°K -degrees Kelvin

k -thermal conductivity in Btu/sec. x in. x °R.

L -frictional energy loss in Btu/lb.

L/D -length to diameter ratio for a combustion chamber in in./in. or ft./ft.

L* -characteristic length of a combustion-chamber defined as $\frac{V_c}{A_t}$.

l -Heat loss in Btu/lb. of propellant

MW -Molecular Weight in lbs./mol.

Mc_p -Molal Heat capacity at constant pressure, $\frac{\text{Btu}}{\text{lb.mol.x}^\circ\text{R}}$.

Mc_v -Molal Heat capacity at constant volume, $\frac{\text{Btu}}{\text{lb.mol.x}^\circ\text{R}}$.

$\dot{m}$ -mass flow rate in lbs./sec.

p -pressure, lbs./in^2.

Q -the quantity of heat added to the system in Btu/lb.

q -Rate of heat transfer in $\frac{\text{Btu}}{\text{sec. x in.}^2}$.

R -the Universal Gas Constant, 1.986 $\frac{\text{Btu}}{\text{lb. mol. x }^\circ\text{R.}}$.

or 1545.5 $\frac{\text{ft. lbs.}}{\text{lb. mol. x }^\circ\text{R}}$

Re -the Reynolds Number which is defined as

$\text{Re} = \frac{DG}{u}$ (dimensionless).

S -the Thermodynamic function of Entropy in Btu/lb. x $^\circ$R or Btu/lb. mol. x $^\circ$R.

S_f -the entropy of the simplified or fictitious gas composition at 2400°K as used in Satterfield's generalized correlation of thermodynamic properties. (Also in $\frac{\text{Btu}}{\text{lb. x }^\circ\text{R}}$ or $\frac{\text{Btu}}{\text{lb.mol. x }^\circ\text{R}}$).

S_{red} -The Satterfield reduced entropy function which is defined as $S_{red} = \frac{S}{S_f}$.

$\mathcal{S}$ -The surface area in sq. in. or sq. ft.

T -temperature in $^\circ$K, $^\circ$R, $^\circ$F or $^\circ$C.

u -velocity in ft./sec.

V -total Volume in cu. ft.

v -specific volume in cu. ft./lb.

w_{sp} -specific fuel consumption or the mass of fuel consumed per unit of total impulse produced. This is the reciprocal of specific impulse and has the units of $\frac{\text{lbs. mass}}{\text{lbs.force-sec.}}$.

x -thickness or linear dimension, in inches or feet.

y -linear dimension in inches or feet in a direction perpendicular to that in which x is measured.

GREEK LETTERS

α -the half angle of divergence of the exhaust nozzle.

γ -the isentropic exponent for a gas defined as

$$\gamma = \frac{\left(\frac{\partial H}{\partial T}\right)_p}{\left(\frac{\partial H}{\partial T}\right)_p - R}$$

Δ — -change in a given quantity.

ε -the emissivity defined as the ratio of the emissive power of a surface or gas compared to that of a black surface under identical conditions.

λ -a correction factor in the expression for thrust which allows for the divergence of part of the exhaust gas stream due to the divergence angle of the nozzle. It is defined as

$$\lambda = 0.5\,(1 + \cos\alpha)$$

θ -time in seconds or minutes.

μ -the viscosity of a fluid in lbs./hr.x ft.

SUBSCRIPTS

1,2,3,--etc.- at points 1,2,3, ---etc. whose exact location is not determined but which appear in order of ascending number as the process occurs.

1-2 or c-t etc. - indicating the limits over which various average values are taken.

atm. -at atmospheric conditions.

av. -the average of the quantity in question over the range in question, usually the arithmetic average of the initial and final values.

c -at chamber conditions or more specifically at the entrance to the exhaust nozzle.

c.300 -corrected to a chamber pressure of 300 psia.

chl -corrected for heat lost.

cchl -corrected for the chamber heat loss

cahl -corrected for all heat lost in both chamber and nozzle.

cece -corrected to the experimentally measured combustion chamber efficiency.

conv.noz. or c_n -referring to the approach or converging section of the exhaust nozzle i.e. the section up to the throat.

div.noz. or d_n -referring to the divergent section of the exhaust nozzle i.e. the section from throat to exit.

e -representing conditions at the exit plane of the exhaust nozzle.

eff. -effective, i.e. the value of the variable in question which is actually effective in the prccess under consideration.

exp. -experimentally measured or determined from experiment.

F - referring to the fuel component of the propellant system.

f -fictitious

form. -of formation as H_{form} is the enthalpy of formation.

i.w. -at the inside surface of the wall.

n -in or of the nozzle or for the exhaust nozzle.

nhl -neglecting heat losses.

O -referring to the oxidizing component of the propellant system.

o.w. -at the outside surface of the wall.

P -at constant pressure, (often the numerical value of the pressure is used in place of just P).

S -at constant entropy.

T -at constant temperature, (often the numerical value of the temperature is given instead of just T).

Th -theoretically calculated or determined, or based

on a theoretical value.

t -representing conditions at the throat of the exhaust nozzle.

x -at any point x along a linear dimension in the x direction.

SUPERSCRIPTS

' (single prime) - representing arithmetic type average

''(double prime) - representing logarithmic type average.

APPENDIX P

Tables of Experimental Data and Calculated Values Derived Therefrom

The significant quantities which were measured experimentally in runs on the micro motors are tabulated in Tables 8 to 20 together with calculated values derived from or based on these experimental data. Stationary stand runs are covered in Tables 8 to 10 while thrust stand runs are presented in Tables 11 to 20.

Remarks

atalyst in fuel

atalyst in fuel

atalyst in fuel

atalyst in fuel

D
80°
fined

E
1800
open

Table 9

Experimental and Calculated Data
Motors A, A', & B - Stationary Stand
90% Hydrogen Peroxide - 85% Hydrazine Hydrate System
(2 x Catalyst unless otherwise noted)

Run No.	Injector	Time of Run (sec)	Total Oxidant Used (lbs)	Total Fuel Used (lbs)	F/O	Flow Rate (lbs/sec)	Nozzle	A_t	P_c exp	P_c th nhl	C^*_{exp}	100 x $\frac{P_c \text{ exp}}{P_c \text{ th nhl}}$	100 x $\frac{P_c \text{ exp chl}}{P_c \text{ th nhl (approx)}}$	Remarks
E-2	A	90	2.670	2.105	0.5063	0.05306	a	3.132	279	319.3	4210	87.28	90	
E-3	B	13.5	0.416	0.323	0.4986	0.05622	a	2.259	302	337.5	4301	89.39	92	
E-4	B	44	1.355	1.048	0.4967	0.05461	a	2.195	271	328.8	3972	82.33	85	
E-5	B	85	2.625	2.040	0.4991	0.05488	a	2.205	286	330.0	4173	86.58	90	5 x catalyst fuel (injector badly eroded)
E-6	B	65	2.025	1.568	0.4973	0.05528	a	2.221	304	332.5	4403	91.34	94	
E-7	C	90	2.785	2.150	0.4958	0.05483	a	2.203	316	329.8	4614	95.72	99	
E-8	C	85	2.650	2.080	0.5041	0.05565	a	2.236	322	334.8	4633	96.09	99	
E-9	D	35	1.112	0.848	0.4898	0.05600	a	2.250	234	336.7	3346	69.41	72	
E-12	D	35	1.098	0.852	0.4983	0.05571	a	2.239	295	335.0	4239	87.97	91	
E-13	D	80	2.525	1.937	0.4927	0.05578	a	2.242	244	335.6	3501	72.62	76	
E-14	D	71	2.202	1.710	0.4987	0.05510	a	2.214	294	331.5	4272	88.60	92	
E-15	C	97.5	3.000	2.285	0.4892	0.05421	a	2.178	331	325.5	4889	101.60	105	
E-16	C	94	2.919	2.260	0.4972	0.05510	a	2.214	332	331.5	4824	100.06	103	
E-17	C	97	2.979	2.310	0.4990	0.05453	a	2.191	326	325	4787	99.30	102	
E-18	C	52	1.613	1.255	0.4997	0.05515	a	2.216	333	332	4834	100.21	103	
E-19	E	60	1.858	1.443	0.4988	0.05502	a	2.211	313	331	4554	94.47	97	
E-20	E	62	1.925	1.492	0.4979	0.05511	a	2.215	313	331.5	4546	94.33	97	Injector Badly Eroded
E-21	F	80	2.499	1.923	0.4942	0.05528	a	2.221	199	332.5	2882	59.76	63	Considerable Injector Erosion
E-23	G	95	2.955	2.260	0.4912	0.05489	a	2.206	310	330.2	4521	93.79	97	
E-24	G	92	2.880	2.219	0.4948	0.05542	a	2.227	284	333.5	4103	85.07	88	
E-25	G	90	2.795	2.165	0.4975	0.05511	a	2.215	316	333.5	4589	94.66	98	5 x Catalyst Fuel
E-26	H	51	1.577	1.224	0.4985	0.05492	a	2.207	244	330.3	3557	73.78	77	5 x Catalyst Fuel
E-27	H	56	1.732	1.343	0.4980	0.05491	a	2.207	294	330.3	4285	88.92	92	5 x Catalyst Fuel
E-28	G	90	2.810	2.180	0.4982	0.05544	a	2.228	313	333.5	4519	93.76	97	
F-1	G	105	2.065	1.607	0.5000	0.03500	b	2.513	366	376.1	4685	97.20	97	
F-2	G	105	2.072	1.617	0.5012	0.03513	b	2.532	371	379.4	4714	97.70	98	
F-3	I	105	2.057	1.615	0.5042	0.03497	b	2.509	384	375.4	4938	102.20	102	
F-4	I	104	2.040	1.598	0.5031	0.03498	b	2.510	381	375.6	4883	101.40	101	

/O ta

Calcul ted Data
Stationary Stand
– Naphferrol System

c th nhl	C*exp	100 x $\frac{P_{c\ exp}}{P_{c\ th\ nhl}}$	100 x $\frac{P_{exp\ chl}}{P_{c\ th\ nhl}}$ (approx)	Remarks
399.0	3889	72.75	75	
350.4	3632	72.20	74	
352.7	3852	76.58	79	
347.7	3824	84.14	88	Plugging in injector
350.5	4131	92.17	84	Plugging in nozzle
282.0	-	81.30	83	
282.0	4252	84.73	87	
352.0	3989	78.98	82	
282.0	4333	86.17	89	
275.3	4291	85.32	87	
279.0	4521	89.96	92	
282.5	4377	87.09	89	
326.5	3879	77.18	79	
328.5	4179	83.11	85	
307.9	3962	78.95	81	
56.0	3922	78.09	80	

Injector	A	B	C	D	E
Angle of Impingement	60°	60°	90°	74°	60°
Type of Mixing	open	confined	confined	confined	open
Equal Area Orifices	X	X	X		
Unequal Area Orifices				X	X

11

Calculated Data
hrust Stand
Hydrazine Hydrate System
(1 x catalyst)

W/A_t	P_c exp	C^* exp	q (Av.) (chamber) Btu/in²·sec	q (Av.) (nozzle) Btu/in²·sec	$l_{chamber}$ (Btu/lb.)	l_{nozzle} (Btu/lb.)	Remarks
3.265	270	3835	-	-	-	-	
3.333	261	3599	-	-	-	-	
3.265	276	3820	-	-	-	-	
3.297	259	3627	0.571	3.00	111.1	56.2	
3.294	277	3885	0.454	3.06	91.8	57.6	
3.286	273	3842	0.490	3.27	98.0	61.7	
3.294	273	3829	0.471	2.89	94.6	54.5	

System

$I_{sp\ th\ nhl}$	$I_{sp\ th\ cchl}$	I_{dn}	$I_{sp\ th\ cahl}$	$I_{sp\ th\ cece}$	$I_{sp\ exp\ chl}$	$\frac{100 \times I_{sp\ exp\ chl}}{I_{sp\ th\ nhl}}$	$\frac{100 \times I_{sp\ exp\ c\cdot3}}{I_{sp\ th\ cece}}$
198	192.3	-	191.3	-	-	-	-
198	192.3	-	191.3	155.0	161.7	81.67	100.06
198	192.3	-	191.3	169.0	169.6	85.66	96.45
19[illegible]	191.3	39.9	190.3	155.9	173.7	87.73	105.26
19[illegible]	192.8	40.9	191.8	162.8	168.0	84.85	99.69
198	192.3	43.8	191.3	165.7	170.3	86.01	98.55
19[illegible]	192.4	39.7	191.4	164.9	166.8	84.24	97.21

e System

P_c exp	C^*exp	q(Av.) (Btu/in²·sec) (chamber)	q(Av.) (Btu/in²·sec) (nozzle)	$l_{chamber}$ (Btu/lb)	l_{nozzle} (Btu/lb)	Remarks
314	4322	--	--	--	--	
291	4129	0.708	3.98	136.0	74.6	
294	4181	0.540	4.17	107.6	78.7	
326	4602	0.580	3.33	113.8	63.1	5 x catalyst in fuel
323	4571	0.599	3.64	116.9	69.3	" " " "
280	3970	0.500	3.87	100.6	73.4	
302	4224	0.602	4.05	116.2	76.1	
302	4224	0.577	4.17	112.2	78.3	
309	4345	0.606	4.11	117.7	77.6	5 x catalyst in fuel
323	4571	0.520	4.60	103.8	88.2	" " " "

confined mixing
Page .

System

th nhl	$I_{sp\ th\ cchl}$	I_{dn}	$I_{sp\ th\ cahl}$	$I_{sp\ th\ cece}$	$I_{sp\ exp\ chl}$	$\frac{100 \times I_{sp\ exp\ chl}}{I_{sp\ th\ nhl}}$	$\frac{100 \times I_{sp\ exp\ c30}}{I_{sp\ th\ cece}}$
09.7	203.1	-	201.9	188.5	195.0	92.99	99.68
09.7	201.9	52.9	200.7	178.8	181.3	86.46	95.75
09.7	203.4	56.8	202.2	180.3	196.9	93.90	103.88
09.7	203.2	44.8	202.2	201.5	205.1	97.81	98.06
09.7	203.0	49.2	202.0	200.0	201.5	96.09	96.95
09.7	203.8	52.1	202.6	169.7	174.5	83.21	97.70
9.7	202.7	53.9	201.5	183.8	194.1	92.56	100.87
9.7	203.4	55.8	202.2	183.8	190.0	90.61	98.64
9.7	202.8	55.1	201.6	188.7	195.9	93.42	99.31
9.7	203.5	61.9	202.1	199.6	202.6	96.61	97.85

stem

nhl	$I_{sp\ th\ cchl}$	I_{dn}	$I_{sp\ th\ cahl}$	$I_{sp\ th\ cece}$	$I_{sp\ exp\ chl}$	$100 \times \frac{I_{sp\ exp\ chl}}{I_{sp\ th\ nhl}}$	$100 \times \frac{I_{sp\ exp\ c300}}{I_{sp\ th\ cece}}$
.7	201.0	81	199.2	185.9	192.5	91.80	98.17
7	198.9	84.5	196.9	197.3	202.0	96.33	97.06
7	201.0	80.5	199.2	191.6	192.0	91.56	95.22
1	192.7	82.0	190.6	194.8	206.6	101.22	100.00
1	192.8	79.0	190.7	191.3	201.0	98.48	98.59
1	193.7	94.0	191.2	194.0	195.1	95.59	95.47
1	195.1	79.5	193.1	185.6	189.9	93.04	96.72
7	201.7	75.5	199.9	191.2	194.8	92.89	97.02
0	197.7	70.5	195.9	184.6	193.3	93.83	99.13
4	192.2	69.0	190.5	190.9	197.1	97.86	98.22
4	191.7	80.0	189.8	196.1	200.6	99.60	96.89
4	191.5	68.0	189.2	192.9	202.5	100.55	99.79
0	189.0	67.5	187.1	190.9	203.1	102.57	101.41
9	189.5	78.0	187.4	197.7	208.9	104.50	100.72
9	191.3	68.5	189.4	198.5	199.4	99.75	97.08
7	198.2	32.0	198.4	205.3	212.7	101.43	99.32
7	197.4	42.0	196.4	192.6	209.4	99.86	102.38
7	196.2	42.5	195.2	192.6	202.0	96.33	98.44
7	197.4	42.0	196.4	192.2	199.6	95.18	97.61

Table 17

Data

Motor M – Pumpkin Blend

Oxidizer Peroxide – 90% Hydrazine Hydrate

2 x Catalyst

(calc)	I_{sp} exp	F/F* F=0 (mol/mol)	A_t	P_c exp	C* exp	q (Av.) (chamber) (Btu/in²·sec)	q (Av.) (nozzle) (Btu/in²·sec)	$l_{chamber}$ (Btu/lb)	l_{nozzle} (Btu/lb)	Remarks
.395	186.6	0.5005	2.165	289	4294	1.095	2.54	65.8	44.0	
.395	179.0	0.4990	2.175	289	4274	1.07	2.48	63.8	42.4	
.37	171.8	0.5038	2.200	268	3919	0.910	2.11	53.8	35.7	
.36	173.7	0.5475	2.050	260	4080	0.867	2.01	54.2	36.3	
.36	174.3	0.5483	2.065	260	4051	0.860	1.99	54.0	35.8	
.36	165.3	0.5487	2.160	263	3917	0.833	1.94	50.1	33.2	
.35	150.2	0.6003	2.215	253	3674	0.819	1.90	48.0	32.1	
.35	157.0	0.6013	2.215	253	3674	0.841	1.95	48.5	32.2	
--	--	0.5483	2.075	243	3767	0.779	1.80	48.6	32.2	
.35	154.7	0.5483	2.065	245	3817	0.842	1.955	52.7	34.9	
.36	157.6	0.4975	2.150	247	3696	0.793	1.84	48.0	32.1	
.365	163.2	0.4995	2.145	257	3854	0.829	1.92	50.3	33.2	5 x catalyst in fuel
.37	165.9	0.5000	2.150	270	4039	0.892	2.07	52.9	34.9	" " " "
.36	168.6	0.5487	2.065	257	4004	0.960	2.23	60.4	40.5	" " " "
.39	176.0	0.5005	2.145	283	4244	0.941	2.19	57.1	38.1	
.36	164.8	0.5487	2.060	261	4076	0.992	2.30	62.7	41.6	
.365	172.2	0.5467	2.050	270	4237	0.902	2.10	56.5	37.4	5 x catalyst in fuel
.385	171.1	0.4995	2.145	278	4169	0.970	2.25	56.7	38.0	" " " "
.39	174.4	0.5483	2.065	278	4331	0.822	1.905	49.8	33.1	" " " "
.395	177.6	0.4980	2.160	290	4319	1.056	2.445	61.0	40.7	" " " "
.37	166.4	0.4369	2.130	272	4108	0.890	2.06	52.1	34.8	
.36	164.8	0.4383	2.145	263	3944	0.979	2.26	56.9	38.1	
.36	165.5	0.4382	2.145	261	3914	0.917	2.12	53.2	35.6	
--	--	--	2.205	259	3779	0.667	1.545	37.8	25.3	
.37	169.7	0.5054	2.100	267	4090	0.800	1.855	47.5	31.5	Small gas leak in motor
.375	169.2	0.5079	2.200	272	3977	0.775	1.80	43.9	29.5	Small gas leak in motor
.385	170.4	0.4995	2.145	280	4199	0.900	2.09	52.3	34.8	
.355	163.8	0.5483	2.065	251	3910	0.743	1.725	45.0	29.8	
.36	164.8	0.4382	2.145	259	3884	0.669	1.55	39.0	26.2	
.33	143.9	0.6047	2.215	240	3486	0.569	1.32	32.0	21.3	Slight gas leak

P

confined Mixing
2, Page .

open mixing
2. Page .

ystem

nhl	$I_{sp\ th\ cchl}$	I_{dn}	$I_{sp\ th\ cahl}$	$I_{sp\ th\ cece}$	$I_{sp\ exp\ chl}$	100 x $\frac{I_{sp\ exp\ chl}}{I_{sp\ th\ nhl}}$	100 x $\frac{I_{sp\ exp\ c300}}{I_{sp\ th\ cece}}$
7	205.8	26.0	186.3	187.1	191.6	91.37	100.16
9	208.1	25.0	185.5	186.4	184.3	86.97	96.51
	206.5	21.0	167.2	169.4	178.9	85.31	102.72
	200.6	21.5	172.5	175.5	181.0	88.68	100.63
	200.6	21.0	173.7	176.8	179.3	87.85	100.17
	200.7	19.5	166.1	168.7	171.9	84.22	99.47
	194.7	19.0	153.8	156.6	156.9	79.24	97.57
	194.6	19.0	153.8	156.6	164.2	82.93	101.98
	200.8	19.0	158.3	162.2	-	-	-
	200.6	20.5	160.6	164.4	162.5	79.62	96.23
	206.7	19.0	156.2	159.7	164.5	78.45	100.81
	206.6	19.5	163.4	166.4	170.3	81.21	99.82
	206.5	20.5	173.4	175.5	171.5	81.78	95.61
	200.1	24.0	169.5	172.6	176.2	86.33	99.36
	208.1	22.5	183.9	185.2	181.8	85.92	95.68
	200.0	24.5	173.3	176.1	172.7	84.62	95.00
	200.4	22.0	180.7	183.0	178.1	87.26	95.25
	208.1	22.5	181.3	183.0	177.6	83.93	94.32
	200.8	19.5	185.3	187.0	179.4	87.90	94.06
	208.0	24.0	187.3	188.0	182.6	86.21	94.79
	198.3	20.5	175.9	178.0	172.2	85.29	94.49
	197.5	22.5	168.3	170.9	171.7	85.25	97.83
	197.8	21.0	166.6	169.3	172.3	85.55	99.23
	195.4	15.0	159.2	161.8	-	-	-
	208.0	18.5	175.6	178.1	175.8	83.32	96.57
	206.4	17.5	170.5	172.4	174.9	83.40	99.19
	206.5	20.5	182.0	183.0	184.8	88.13	93.61
	201.0	17.5	165.4	168.9	170.5	83.54	98.93
	198.8	15.5	163.2	165.0	172.8	85.80	101.52
	195.7	12.5	144.9	148.3	149.6	75.56	99.26

culated Data
st Stand
Aerojet-General Corporation

A_t	P_c exp	C^* exp	$\dot{q}_{(Av)}$ (chamber) Btu/in²·sec	$\dot{q}_{(Av)}$ (nozzle) Btu/in²·sec	$l_{chamber}$ Btu/lb.	l_{nozzle} Btu/lb	Remarks
75	258	3816	0.278	3.30	71.1	85.4	
54	279	4167	0.693	4.10	179.5	107.4	
75	288	4260	0.377	4.37	96.6	112.7	
65	256	3804	0.305	3.32	78.1	86.3	
54	242	3614	0.300	3.18	77.6	83.2	
54	244	3644	0.295	3.58	76.3	93.8	
65	262	3893	0.286	3.80	73.7	98.9	Low C_F = possible plugging ∴area correction
75	267	3949	0.286	3.54	73.2	91.8	
60	294	4008	0.347	4.25	82.0	101.5	
63	295	4033	0.383	4.42	90.6	106.3	
53	314	4293	0.354	3.73	83.9	89.6	Low C_F = possible plugging ∴area correction
88	287	3899	0.297	3.75	69.8	89.2	Low C_F = possible plugging ∴area corrected
0	25.	3482	0.274	3.54	64.7	84.3	
8	24	3858	0.350	4.45	82.3	105.8	
8	306	4157	0.327	4.50	77.0	107.5	Low C_F = possible plugging ∴area correction
5	283	4205	0.290	4.52	74.5	117.5	Low C_F = possible plugging ∴area corrected

ector

impingement, confined mixing

Fig. 22, page

BIOGRAPHICAL NOTE

Arthur Spragens Collins was born on October 31, 1921 in Lebanon, Kentucky. He attended the Public Schools in Lebanon and the University of Kentucky at Lexington, Kentucky, from which institution he was graduated in May, 1942, with the degree of Bachelor of Science in Industrial Chemistry. Since that time he has been connected with the Massachusetts Institute of Technology in various capacities; first as a research assistant in the Division of Industrial Cooperation, then as half-time graduate student and half-time teaching assistant in the Department of Chemical Engineering, next as a research associate in the Division of Industrial Cooperation, and finally as a research associate and graduate student in the Department of Chemical Engineering. During this last appointment, the present thesis was carried out.

He is a member of Alpha Chi Sigma, Phi Beta Kappa, Sigma Pi Sigma, Sigma Xi, and the American Chemical Society.

Table 20

Calculated and Theoretica
Motor No. W - Thrust S
90% Hydrogen Peroxide - Naphferr

Run No.	F/F + F=0 (mol/mol)	$(\dot{W}/A_t)_{eff}$	P_c th nhl	I_{eff} Btu/lb	P_c th chl psia	P_c exp psia	P_c exp chl psia	100 x P_c exp chl / P_c th nhl	I_{sp} exp	I_{sp} exp c3
Y-1	0.503	2.175	340.0	83.5	336.4	258	266	78.24	155.7	158.5
Y-2	0.497	2.203	344.5	195.1	335.1	279	288.5	83.74	168.4	169.8
Y-3	0.502	2.175	340.0	112.9	335.0	288	296	87.06	177.0	177.8
Y-4	0.503	2.165	338.5	90.6	334.7	256	265	78.29	155.5	158.4
Y-5	0.503	2.154	336.8	89.7	332.9	242	251	74.52	146.4	149.9
Y-6	0.501	2.154	336.8	89.9	332.9	244	252	74.82	157.6	161.2
Y-7	0.503	2.236	349.7	84.0	345.7	262	259	74.06	154.6	156.9
Y-8	0.509	2.175	340.0	86.5	336.2	267	275	80.88	168.3	170.6
Y-9	0.399	2.408	347.7	96.7	341.5	294	297.5	85.56	162.5	162.9
Y-10	0.399	2.353	339.8	106	333.1	295	305	89.76	166.6	167.0
Y-11	0.399	2.600	375.6	96.9	368.9	314	296	78.81	160.0	160.9
Y-12	0.623	2.554	380.2	82.7	374.1	287	277	72.86	149.4	150.1
Y-13	0.622	2.360	350.6	76.9	345.3	254	263	75.01	142.6	145.2
Y-14	0.621	2.404	357.0	97.6	350.1	284	290.5	81.37	156.3	157.2
Y-15	0.621	2.451	363.9	92.6	354.1	306	307	84.36	166.7	166.3
Y-16	0.503	2.321	363.0	91.5	358.6	289	272	74.93	161.3	162.3

l Data
tand
ol System

)0 $I_{sp\ th\ nhl}$	$I_{sp\ th\ cchl}$	l_{dn}	$I_{sp\ th\ cahl}$	$I_{sp\ th\ cece}$	$I_{sp\ exp\ chl}$	100 x $\frac{I_{sp\ exp\ chl}}{I_{sp\ th\ nhl}}$	100 x $\frac{I_{sp\ exp\ c300}}{I_{sp\ th\ cece}}$
220.1	217.3	60.6	216.4	167.6	165.2	75.05	94.57
220.1	212.7	76.2	211.4	178.7	180.2	81.87	95.02
220.1	216.3	80.0	215.0	185.9	184.2	83.69	95.64
220.1	217.1	61.3	216.2	166.9	162.6	73.88	94.91
220.1	217.1	59.0	216.2	160.1	156.8	71.24	93.63
220.1	217.1	66.6	216.0	158.3	170.9	77.65	101.83
220.1	217.1	70.2	216.0	166.0	163.8	74.42	94.52
220.1	217.1	65.2	216.0	174.8	176.8	80.33	97.60
204.7	200.2	72.1	198.6	170.4	171.5	83.78	95.60
204.7	200.0	75.5	198.4	176.3	174.5	85.25	94.72
204.7	200.2	63.6	198.8	170.9	168.2	82.17	94.15
208.9	205.4	63.3	204.1	155.1	158.5	75.87	96.78
208.9	205.7	59.9	204.4	146.3	155.4	74.39	99.25
208.9	204.6	75.2	202.9	163.9	165.3	79.13	95.91
208.9	204.9	76.3	203.2	173.6	173.7	83.15	95.79
220.1	217.0	83.5	215.7	172.8	169.1	76.83	93.92

APPENDIX R

Tables of Theoretical Calculations and Working Plots Derived Therefrom

The significant quantities which were calculated from theory on the propellant systems studied experimentally in this thesis are presented in Tables 21 to 44. These theoretically calculated results were translated into the form of working plots for simplicity of use in application to given experimental data. These working plots are shown in Figures A-30 to A41 presented here as well as in Figures 5 to 8 presented earlier in the section on Thermodynamics.

Table 21

Calculated Values of Chamber Pressure for System
85% Hydrazine Hydrate - 80% Hydrogen Peroxide (Equal Volumes)
F/O = 0.550 mols/mol

H_{system} Btu/lb	Total $l_{c\ eff}$ Btu/lb	H_c Btu/lb	$H_{f,o}$ Btu/lb	$H_{f,2400}$ Btu/lb	H_{red}	T_c °K	γ_{Av}	MW_{Av}	$\dot{w}/A_t$ (lb/sec-in²)	P_c psia	$P_c/P_{c\,nhl}$
	0	1860			0.767	1895	1.2221			335.5	1.0
	100	1760			0.723	1810	1.2242			327.5	0.9760
	200	1660			0.678	1720	1.2282			319.1	0.9510
1860	300	1560	124.2	2388	0.634	1625	1.2323	19.08	2.361	310.1	0.9240
	400	1460			0.589	1530	1.2377			299.9	0.8939
	600	1260			0.501	1330	1.2491			279.2	0.8320
	800	1060			0.413	1125	1.2654			255.1	0.7604

Simplified Gas Composition:

H_2O	83.7
H_2	2.3
N_2	14.0

Table 22

Calculated Values of Specific Impulse for System
85% Hydrazine Hydrate - 80% Hydrogen Peroxide
(Equal Volume Mixture) F/O = 0.550 mols/mol [P_e = 14.7 psia]

P_c psia	Total $l_{c\ eff}$ Btu/lb	$P_c/P_{c\ nhl}$	T_c °K	T_e °K	γ_{Av}	I_{sp} lbs-sec/lb	$P_{c\ nhl}$ psia	$\dot{m}/A_t$ lbs/sec x in^2
270	↑	↑	↑	1150	1.238	195.4	270	1.901
300	0	1.0	1895	1130	1.239	198.1	300	2.112
340	↓	↓	↓	1100	1.240	201.1	340	2.393
270	↑	↑	↑	1108	1.242	190.2	276.4	1.951
300	100	0.9760	1810	1089	1.243	192.7	307.5	2.165
340	↓	↓	↓	1061	1.244	195.9	348.2	2.455
270	↑	↑	↑	1073	1.246	185.3	284.0	2.000
300	200	0.9510	1720	1052	1.247	187.9	315.7	2.222
340	↓	↓	↓	1029	1.248	191.1	357.7	2.518
270	↑	↑	↑	1034	1.250	180.6	292.0	2.057
300	300	0.9240	1625	1014	1.251	183.1	324.4	2.285
340	↓	↓	↓	992	1.252	186.3	368.0	2.593
270	↑	↑	↑	748	1.261	162.0	324.4	2.285
300	600	0.8320	1330	728	1.262	164.9	360.4	2.541
340	↓	↓	↓	707	1.263	168.2	408.9	2.876

Table 23

Calculation of the Effect of Diverging Nozzle Heat Loss on Specific Impulse for System: 85% $N_2H_4 \cdot H_2O$ - 80% H_2O_2 (Equal Volume Mixture)
F/O = 0.550 mols/mol; P_c = 300 psia; P_e = 14.7 psia

H_{system} Btu/lb	Total l_c eff Btu/lb	H_c Btu/lb	l_{dn} Btu/lb	H_c' Btu/lb	T_c' °K	T_e' °K	γ'_{Av}	$I_{sp}'_{cahl}$ lbs-sec/lb	$I_{sp}{}_{cchl}$ lbs-sec/lb	I_{spcahl}/I_{spcchl}
			0	1860	1895	1130	1.239	198.1		1.0
			50	1835	1870	1117	1.239	196.9		0.994
	0	1860							198.1	
			100	1810	1846	1104	1.239	195.7		0.988
			150	1785	1821	1092	1.240	194.3		0.981
			0	1660	1720	1052	1.247	187.9		1.0
			50	1635	1695	1038	1.247	186.6		0.993
1860	200	1660							187.9	
			100	1610	1671	1026	1.247	185.3		0.986
			150	1585	1647	1014	1.248	184.0		0.979
			0	1260	1330	728	1.262	164.9		1.0
			50	1235	1306	716	1.263	163.3		0.990
	600	1260							164.9	
			100	1210	1281	705	1.264	161.6		0.980
			150	1185	1256	693	1.264	160.0		0.970

Table 24

Calculated Values of Chamber Pressure for System
85% Hydrazine Hydrate - 90% Hydrogen Peroxide (Fuel Rich Mixture)
F/O = 0.752 mols/mol

H_{system} Btu/lb	Total l_c eff Btu/lb	H_c Btu/lb	$H_{f,o}$ Btu/lb	$H_{f,2400}$ Btu/lb	H_{red}	T_c °K	γ_{Av}	MW_{Av}	$\dot{m}/A_t$ lbs/sec x in^2	P_c psia	P_c/P_{cnhl}
	0	2280			0.7179	1800	1.2400			315.8	1.0
	20	2260			0.7092	1783	1.2407			314.2	0.995
	60	2220			0.6918	1750	1.2420			311.2	0.986
	80	2200			0.6832	1730	1.2428			309.3	0.980
	100	2180			0.6745	1710	1.2435			307.5	0.974
	120	2160			0.6658	1692	1.2444			305.8	0.968
2280	160	2120	626	2930	0.6484	1655	1.2463	17.90	2.222	302.3	0.957
	180	2100			0.6398	1636	1.2472			300.4	0.951
	200	2080			0.6311	1618	1.2480			298.7	0.946
	220	2060			0.6224	1600	1.2488			297.0	0.941
	260	2020			0.6050	1562	1.2507			293.3	0.929
	280	2000			0.5964	1543	1.2516			291.4	0.923
	400	1880			0.5430	1433	1.2580			280.4	0.888
	700	1580			0.4140	1148	1.2781			249.3	0.790

Simplified Gas Composition

H_2O	72.90
H_2	10.90
N_2	16.20

Table 25

Calculated Values of Chamber Pressure for System
85% Hydrazine Hydrate - 90% Hydrogen Peroxide (Fuel Rich Mixture)
F/O = 0.607 mols/mol

H_{system} Btu/lb	Total l_c eff Btu/lb	H_c Btu/lb	$H_{f,o}$ Btu/lb	$H_{f,2400}$ Btu/lb	H_{red}	T_c °K	γ_{Av}	MW_{Av}	$\dot{m}/A_t$ lbs/sec x in^2	P_c psia	P_c/P_{cnhl}
	0	2111			0.7967	1960	1.2232			324.1	1.0
	20	2091			0.7876	1940	1.2238			322.4	0.995
	60	2051			0.7695	1900	1.2250			318.7	0.984
	80	2031			0.7604	1885	1.2255			317.6	0.980
	100	2011			0.7514	1869	1.2259			316.3	0.976
	120	1991			0.7423	1852	1.2266			314.8	0.971
2111	160	1951	352	2560	0.7242	1817	1.2278	18.70	2.222	311.7	0.962
	180	1931			0.7151	1798	1.2287			309.9	0.956
	200	1911			0.7061	1777	1.2296			308.1	0.951
	220	1891			0.6970	1759	1.2302			306.4	0.945
	260	1851			0.6789	1720	1.2318			302.9	0.934
	280	1831			0.6698	1700	1.2325			301.1	0.929
	400	1711			0.6150	1587	1.2379			290.6	0.896
	700	1411			0.4790	1292	1.2557			260.6	0.804

Simplified Gas Composition

H_2O	79.30
H_2	5.40
N_2	15.30

Table 26

Calculated Values of Chamber Pressure for System
85% Hydrazine Hydrate - 90% Hydrogen Peroxide (Stoichiometric Mixture)
F/O = 0.500 mols/mol

H_{system} Btu/lb	Total $l_{c\ eff}$ Btu/lb	H_c Btu/lb	$H_{f,o}$ Btu/lb	$H_{f,2400}$ Btu/lb	H_{red}	T_c °K	γ_{Av}	MW_{Av}	$\dot{m}/A_t$ lbs/sec x in^2	P_c psia	P_c/P_{cnhl}
	0	1968			0.8865	2135	1.2111			332.7	1.0
	20	1948			0.8775	2118	1.2116			331.3	0.996
	60	1908			0.8595	2082	1.2126			328.4	0.987
	80	1888			0.8505	2065	1.2129			327.0	0.983
	100	1868			0.8414	2048	1.2134			325.7	0.978
	120	1848			0.8324	2030	1.2140			324.1	0.974
1968	160	1808	0	2220	0.8144	1996	1.2148	19.44	2.222	321.3	0.966
	180	1788			0.8054	1977	1.2153			319.7	0.961
	200	1768			0.7964	1960	1.2161			318.3	0.957
	220	1748			0.7874	1940	1.2166			316.6	0.952
	260	1708			0.7694	1900	1.2178			313.2	0.941
	280	1688			0.7604	1885	1.2183			312.0	0.938
	500	1468			0.6610	1681	1.2262			294.2	0.884
	800	1168			0.5260	1393	1.2414			266.4	0.800

Simplified Gas Composition

H_2O	85.60
N_2	14.40

Table 27

Calculated Values of Chamber Pressure for System
85% Hydrazine Hydrate - 90% Hydrogen Peroxide (Oxidant Rich Mixture)
F/O = 0.390 mols/mol

H_{system} Btu/lb	Total l_c eff Btu/lb	H_c Btu/lb	$H_{f,o}$ Btu/lb	$H_{f,2400}$ Btu/lb	H_{red}	T_c °K	γ_{Av}	MW_{Av}	$\dot{w}/A_t$ lbs/sec x in^2	P_c psia	P_c/P_{cnhl}
	0	1790			0.8565	2078	1.2189			319.7	1.0
	20	1770			0.8469	2060	1.2193			318.3	0.996
	60	1730			0.8278	2020	1.2206			315.0	0.985
	80	1710			0.8182	2000	1.2209			313.5	0.981
	100	1690			0.8086	1980	1.2214			311.8	0.975
	120	1670			0.7990	1962	1.2220			310.4	0.971
1790	160	1630	0	2090	0.7799	1922	1.2231	20.42	2.222	307.1	0.961
	180	1610			0.7703	1904	1.2238			305.6	0.956
	200	1590			0.7608	1887	1.2243			304.2	0.951
	220	1570			0.7512	1869	1.2249			302.6	0.947
	260	1530			0.7321	1832	1.2263			299.5	0.937
	280	1510			0.7225	1815	1.2266			298.1	0.932
	400	1390			0.6653	1685	1.2335			287.9	0.901
	700	1090			0.5214	1380	1.2502			259.3	0.811

Simplified Gas Composition

H_2O	79.50
O_2	7.40
N_2	13.10

Table 28

Calculated Values of Specific Impulse for System
85% Hydrazine Hydrate - 90% Hydrogen Peroxide
(Fuel Rich Mixture) F/O = 0.752 mols/mol [P_e = 14.7]

P_c psia	Total l_c eff Btu/lb	P_c/P_c nhl	T_c °K	T_e °K	γ_{Av}	I_{sp} lbs-sec / lb	P_c nhl psia	$\dot{m}/A_t$ lbs / sec x in^2
240.0	↑	↑	↑	1044	1.253	192.7	240.0	1.690
296.0				988	1.255	197.7	296.0	2.083
315.8	0	1.0	1800	975	1.256	199.1	315.8	2.222
335.5	↓	↓	↓	963	1.256	200.5	335.5	2.361
380.0				942	1.257	203.1	380.0	2.676
240.0	↑	↑	↑	978	1.258	187.5	246.4	1.737
288.3				943	1.259	191.8	296.0	2.083
307.5	100	0.974	1710	931	1.260	193.2	315.8	2.222
326.7	↓	↓	↓	920	1.260	194.5	335.5	2.361
380.0				897	1.262	197.5	390.2	2.745
240.0	↑	↑	↑	917	1.264	181.0	253.8	1.788
280.0				881	1.265	185.5	296.0	2.083
298.7	200	0.946	1618	869	1.265	186.9	315.8	2.222
317.4	↓	↓	↓	858	1.266	188.2	335.5	2.361
380.0				830	1.268	191.8	401.3	2.827
240.0	↑	↑	↑	833	1.274	169.5	270.2	1.902
270.0				812	1.275	172.4	304.0	2.140
300.0	400	0.888	1433	793	1.276	174.9	337.9	2.378
340.0	↓	↓	↓	773	1.277	177.8	382.6	2.696
380.0				754	1.278	180.5	428.1	3.013
240.0	↑	↑	↑	652	1.296	149.2	303.9	2.140
270.0				633	1.297	152.0	342.0	2.406
300.0	700	0.790	1148	616	1.298	154.5	379.9	2.676
340.0	↓	↓	↓	597	1.299	157.3	430.4	3.032
380.0				569	1.300	160.1	480.9	3.385

Table 29

Calculated Value of Specific Impulse for System
85% Hydrazine Hydrate - 90% Hydrogen Peroxide
(Fuel Rich Mixture F/O = 0.607 mols/mol [P_e = 14.7 psia]

P_c psia	Total lc eff Btu/lb	P_c/P_c nhl	T_c °K	T_e °K	γ_{Av}	I_{sp} lbs-sec/lb	P_c nhl psia	$\dot{m}/A_t$ lbs/sec x in^2
240.0	↑	↑	↑	1136	1.235	198.8	240.0	1.648
303.8				1090	1.237	204.3	303.8	2.083
324.1	0	1.0	1960	1077	1.237	207.3	344.4	2.222
344.4	↓	↓	↓	1063	1.237	207.3	344.4	2.361
380.0				1042	1.238	209.6	380.0	2.605
240.0	↑	↑		1080	1.239	193.7	245.9	1.688
296.5			↑	1045	1.240	198.5	303.8	2.083
316.3	100	0.976	1869	1032	1.241	200.1	324.1	2.222
336.1	↓	↓	↓	1020	1.241	201.4	344.3	2.361
380.0				996	1.243	204.1	389.4	2.669
240.0	↑	↑	↑	1030	1.243	188.6	252.2	1.731
288.8				999	1.244	192.6	303.9	2.083
308.1	200	0.951	1777	987	1.245	194.1	324.1	2.222
327.4	↓	↓	↓	975	1.245	195.7	344.4	2.361
380.0				951	1.247	199.1	399.8	2.741
240	↑	↑		1018	1.251	176.7	267.9	1.838
270			↑	999	1.253	179.4	301.4	2.067
300	400	0.896	1587	883	1.254	181.7	334.6	2.295
340	↓	↓	↓	863	1.255	184.5	379.6	2.602
380				850	1.256	186.2	424.0	2.803
240	↑	↑		736	1.272	158.2	298.4	2.045
270			↑	717	1.273	161.1	336.0	2.304
300	700	0.804	1292	699	1.274	163.7	373.5	2.559
340	↓	↓	↓	678	1.275	166.9	423.0	2.900
380				659	1.276	169.7	472.8	3.242

Table 30

Calculated Values of Specific Impulse for System
85% Hydrazine Hydrate - 90% Hydrogen Peroxide
(Stoichiometric Mixture) F/O = 0.5 mols/mol [P_e = 14.7 psia]

P_c psia	Total l_{c^*} eff Btu/lb	P_c/P_c nhl	T_c °K	T_e °K	γ_{Av}	I_{sp} lbs-sec / lb	P_c nhl psia	$\dot{m}/A_t$ lbs / sec x in^2
240.0	↑	↑	↑	1284	1.222	204.3	240.0	1.609
311.9				1230	1.223	210.8	311.9	2.083
330.7	0	1.0	2135	1215	1.223	212.5	330.7	2.222
353.5	↓	↓	↓	1202	1.223	213.9	353.5	2.361
380.0				1184	1.224	215.8	380.0	2.544
240.0	↑	↑	↑	1226	1.224	199.9	245.4	1.642
305.7				1182	1.225	205.7	312.1	2.083
325.7	100	0.978	2048	1169	1.226	207.2	332.3	2.222
346.0	↓	↓	↓	1156	1.226	208.7	353.7	2.361
380.0				1136	1.227	211.1	388.2	2.600
240.0	↑	↑	↑	1159	1.228	195.3	250.5	1.679
298.4				1118	1.229	200.4	311.9	2.083
318.3	200	0.957	1960	1105	1.229	202.0	332.4	2.222
338.2	↓	↓	↓	1093	1.230	203.4	353.5	2.361
380.0				1069	1.231	206.2	396.5	2.662
240.0	↑	↑	↑	1113	1.230	190.8	255.9	1.716
292.4				1074	1.232	195.8	312.0	2.083
312.0	280	0.938	1885	1062	1.232	197.3	332.4	2.222
331.5	↓	↓	↓	1050	1.232	198.7	353.5	2.361
380.0				1024	1.233	201.9	405.0	2.715
240.0	↑	↑	↑	1004	1.240	180.7	271.7	1.810
270.0				982	1.241	183.6	305.7	2.037
300.0	500	0.884	1681	961	1.242	186.3	339.7	2.256
340.0	↓	↓	↓	939	1.243	189.2	384.4	3.563
380.0				920	1.244	191.7	430.0	2.861
240.0	↑	↑	↑	821	1.257	161.5	300.0	2.011
270.0				799	1.258	164.7	337.8	2.277
300.0	800	0.800	1393	780	1.259	167.3	375.0	2.524
340.0	↓	↓	↓	759	1.260	170.2	425.0	2.863
380.0				739	1.261	173.0	475.0	3.207

Table 32

Calculation of the Effect of Diverging Nozzle Heat Loss on Specific Impulse for System: 85% $N_2H_4 \cdot H_2O$ - 90% H_2O_2 (Fuel Rich Mixture)
F/O = 0.752 mols/mol; P_c = 300 psia; P_e = 14.7 psia

H_{system} Btu/lb	Total l_c eff Btu/lb	H_c Btu/lb	l_{dn} Btu/lb	H_c' Btu/lb	T_c' °K	T_e' °K	γ'_{Av}	$I_{sp}'_{cahl}$ lbs-sec/lb	$I_{sp}{}_{cchl}$ lbs-sec/lb	$\frac{I_{sp}{}_{cahl}}{I_{sp}{}_{cchl}}$
			0	2280	1800	985	1.255	198.0		1.0
			50	2255	1778	972	1.255	196.8		0.994
	0	2280							198.0	
			100	2230	1756	960	1.256	195.4		0.987
			150	2205	1734	947	1.256	194.2		0.981
			0	2080	1618	868	1.265	187.0		1.0
			50	2055	1595	857	1.265	185.5		0.992
2280	200	2080							187.0	
			100	2030	1572	844	1.266	184.3		0.985
			150	2005	1549	833	1.266	182.7		0.977
			0	1580	1148	616	1.298	154.5		1.0
			50	1555	1123	626	1.298	152.8		0.989
	700	1580							154.5	
			100	1530	1098	615	1.299	151.3		0.979
			150	1505	1073	605	1.299	149.6		0.968

Table 33

Calculation of the Effect of Diverging Nozzle Heat Loss on Specific Impulse for System: 85% $N_2H_4 \cdot H_2O$ - 90% H_2O_2 (Fuel Rich Mixture)
F/O = 0.607 mols/mol; P_c = 300 psia; P_e = 14.7 psia

H_{system} Btu/lb	Total l_c eff Btu/lb	H_c Btu/lb	l_{dn} Btu/lb	H_c' Btu/lb	T_c' °K	T_e' °K	γ'_{Av}	$I_{sp}'_{cahl}$ lbs-sec/lb	$I_{sp_{cchl}}$ lbs-sec/lb	$\frac{I_{sp_{cahl}}}{I_{sp_{cchl}}}$
			0	2111	1960	1093	1.237	204.1		1.0
			50	2086	1936	1080	1.237	202.9		0.994
	0	2111							204.1	
			100	2061	1910	1067	1.237	201.7		0.988
			150	2036	1885	1055	1.238	200.4		0.982
			0	1911	1777	992	1.245	193.5		1.0
			50	1886	1753	981	1.245	191.2		0.993
2111	200	1911							193.5	
			100	1861	1728	969	1.245	190.8		0.986
			150	1836	1703	956	1.246	189.4		0.979
			0	1411	1292	699	1.274	163.7		1.0
			50	1386	1266	686	1.274	162.1		0.990
	700	1411							163.7	
			100	1361	1240	673	1.275	160.5		0.980
			150	1336	1215	660	1.275	159.0		0.971

Table 34

Calculation of the Effect of Diverging Nozzle Heat Loss on Specific Impulse
for System: 85% $N_2H_4 \cdot H_2O$ - 90% H_2O_2 (Stoichiometric)
F/O = 0.5 mols/mol; P_c = 300 psia; P_e = 14.7 psia

H_{system} Btu/lb	Total l_c eff Btu/lb	H_c Btu/lb	l_{dn} Btu/lb	H_c' Btu/lb	T_c' °K	T_e' °K	γ'_{Av}	$I_{sp}'_{cahl}$ lbs-sec/lb	$I_{sp_{cchl}}$ lbs-sec/lb	$\frac{I_{sp_{cahl}}}{I_{sp_{cchl}}}$
			0	1968	2135	1240	1.223	210.1		1.0
			50	1943	2113	1232	1.223	209.0		0.995
	0	1968							210.1	
			100	1918	2091	1221	1.223	208.0		0.990
			150	1893	2069	1210	1.223	206.9		0.985
			0	1768	1960	1120	1.229	200.5		1.0
			50	1743	1937	1104	1.229	199.3		0.994
1969	200	1768							200.5	
			100	1718	1913	1090	1.229	198.1		0.988
			150	1693	1889	1076	1.229	196.9		0.982
			0	1168	1393	780	1.259	167.3		1.0
			50	1143	1369	771	1.259	165.9		0.991
	800	1168							167.3	
			100	1118	1345	757	1.259	164.5		0.983
			150	1093	1321	742	1.259	163.1		0.974

Table 35

Calculation of the Effect of Diverging Nozzle Heat Loss on Specific Impulse
for System: 85% $N_2H_4 \cdot H_2O$ - 90% H_2O_2 (Oxidant Rich Mixture)
F/O = 0.390 mols/mol; P_c = 300 psia; P_e = 14.7 psia

H_{system} Btu/lb	Total l_c eff Btu/lb	H_c Btu/lb	l_{dn} Btu/lb	H_c' Btu/lb	T_c' °K	T_e' °K	γ'_{Av}	$I_{sp}'_{cahl}$ lbs-sec/lb	$I_{sp_{cchl}}$ lbs-sec/lb	$I_{sp_{cahl}}/I_{sp_{cchl}}$
			0	1790	2078	1167	1.231	201.4		1.0
			50	1765	2055	1154	1.231	200.2		0.994
	0	1790							201.4	
			100	1740	2032	1143	1.231	199.2		0.989
			150	1715	2009	1129	1.232	198.0		0.983
			0	1590	1887	1073	1.238	191.2		1.0
			50	1565	1864	1062	1.238	190.1		0.994
1790	200	1590							191.2	
			100	1540	1841	1051	1.238	188.7		0.987
			150	1515	1818	1040	1.239	187.4		0.980
			0	1090	1380	765	1.268	163.0		1.0
			50	1065	1355	755	1.269	161.5		0.991
	700	1090							163.0	
			100	1040	1330	745	1.269	160.1		0.982
			150	1015	1305	735	1.269	158.6		0.973

Table 36

Calculated Values of Chamber Pressure for System
Naphferrol - 90% Hydrogen Peroxide (Fuel Rich Mixture)
F/O = 0.441 mols/mol

H_{system} Btu/lb	Total $l_{c\ eff}$ Btu/lb	H_c Btu/lb	$H_{f,o}$ Btu/lb	$H_{f,2400}$ Btu/lb	H_{red}	T_c °K	γ_{Av}	MW_{Av}	$\dot{w}/A_t$ lbs/sec x in^2	P_c psia	P_c/P_{cnhl}
↑	0	3174	↑	↑	0.899	2167	1.211	↑	↑	330.2	1.000
	20	3154			0.889	2145	1.212			328.8	0.998
	75	3099			0.864	2095	1.213			325.2	0.985
	95	3079			0.854	2076	1.213			323.4	0.983
	150	3024			0.829	2022	1.214			319.0	0.967
3174	160	3014	1227	3392	0.824	2013	1.214	20.00	3.2222	318.5	0.965
	170	3004			0.819	2004	1.215			317.7	0.963
	225	2949			0.795	1954	1.216			313.0	0.948
	245	2929			0.786	1936	1.216			312.0	0.946
	500	2674			0.667	1693	1.232			290.2	0.878
↓	800	2374	↓	↓	0.529	1392	1.248	↓	↓	257.5	0.780

Simplified Gas Composition

H_2O	65.07
H_2	13.48
CO	9.55
CO_2	11.90 (SO_2 = 0.52)

Table 37

Calculated Values of Chamber Pressure for System
Naphferrol - 90% Hydrogen Peroxide (Stoichiometric Mixture)
F/O = 0.270 mols/mol

H_{system} Btu/lb	Total $l_{c\ eff}$ Btu/lb	H_c Btu/lb	$H_{f,o}$ Btu/lb	$H_{f,2400}$ Btu/lb	H_{red}	T_c °K	γ_{Av}	MW_{Av}	$\frac{\dot{w}_{in}/A_t}{\frac{lbs}{sec \times in^2}}$	P_c psia	P_c/P_{cnhl}
	0	2403			1.169	2568	1.159			347.5	1.000
	20	2383			1.159	2556	1.159			346.3	0.998
	75	2328			1.130	2517	1.160			344.0	0.990
	95	2308			1.121	2504	1.160			343.2	0.988
	150	2253			1.094	2467	1.161			340.3	0.980
2403	160	2243	0	2060	1.088	2457	1.161	22.15	2.222	339.9	0.978
	170	2233			1.082	2447	1.161			339.5	0.977
	225	2178			1.057	2412	1.162			336.6	0.968
	245	2158			1.048	2399	1.162			335.8	0.967
	600	1803			0.875	2108	1.195			311.7	0.898
	1000	1403			0.680	1723	1.207			280.8	0.810

Simplified Gas Composition

H_2O 83.21

CO_2 16.79 (SO_2 = 0.4)

Table 38

Calculated Values of Chamber Pressure for System
Naphferrol - 90% Hydrogen Peroxide (Oxidant Rich Mixture)
F/O = 0.179 mols/mol

H_{system} Btu/lb	Total $l_{c\ eff}$ Btu/lb	H_c Btu/lb	$H_{f,o}$ Btu/lb	$H_{f,2400}$ Btu/lb	H_{red}	T_c °K	γ_{Av}	MW_{Av}	$\dot{m}/A_t$ lbs/sec x in^2	P_c psia	P_c/P_{chi}
	0	1908			0.946	2243	1.192			320.9	1.0
	20	1888			0.936	2224	1.192			319.5	0.998
	75	1833			0.910	2178	1.193			316.4	0.986
	95	1813			0.900	2160	1.193			315.2	0.984
	150	1758			0.872	2105	1.194			310.9	0.969
1908	160	1748	0	2017	0.867	2096	1.195	22.25	2.2222	310.2	0.967
	170	1738			0.862	2087	1.195			309.6	0.964
	225	1683			0.835	2036	1.196			305.1	0.900
	245	1663			0.825	2017	1.198			303.9	0.949
	500	1408			0.699	1760	1.214			283.0	0.882
	800	1108			0.500	1444	1.233			253.3	0.790

Simplified Gas Composition

H_2O 79.57

CO_2 11.78 (0.28 = SO_2)

O_2 8.65

Table 39

Calculated Values of Specific Impulse for System
Naphferrol - 90% Hydrogen Peroxide
(Fuel Rich Mixture) F/O = 0.441 mol H_2O_2/CH_3OH (P_e = 14.7 psia)

P_c psia	Total l_c eff Btu/lb	P_c/P_c nhl	T_c °K	T_e °K	I_{sp} lbs-sec/lb	P_c nhl psia	w_p/A_t lbs/sec x in^2
240	↑	↑	↑	1334	203.3	240	1.622
270	↑	↑	↑	1304	206.1	270	1.822
300	0	1.0	2167	1280	208.8	300	2.022
340	↓	↓	↓	1251	212.0	340	2.288
380	↓	↓	↓	1225	214.5	380	2.552
240	↑	↑	↑	1288	199.4	244	1.648
270	↑	↑	↑	1261	202.8	274	1.848
300	75	0.985	2095	1238	205.9	304	2.040
340	↓	↓	↓	1202	208.8	346	2.328
380	↓	↓	↓	1175	211.7	386	2.592
240	↑	↑	↑	1268	197.6	246	1.662
270	↑	↑	↑	1242	200.8	276	1.862
300	110	0.977	2062	1218	203.3	307	2.068
340	↓	↓	↓	1183	206.5	348	2.342
380	↓	↓	↓	1155	210.0	389	2.612
240	↑	↑	↑	1248	195.5	248	1.676
270	↑	↑	↑	1222	198.8	279	1.882
300	150	0.967	2022	1199	202.1	310	2.088
340	↓	↓	↓	1165	204.7	352	2.368
380	↓	↓	↓	1135	207.7	393	2.628
240	↑	↑	↑	1199	191.6	253	1.708
270	225	0.948	1954	1162	195.0	285	1.924
300	↓	↓	↓	1139	198.3	317	2.134

340	225	0.948	1954	1110	201.7	359	2.414
380	225	0.948	1954	1090	204.7	401	2.692
240	↑	↑	↑	1142	188.9	258	1.742
270				1115	191.9	290	1.956
300	300	0.9295	1884	1090	194.5	323	2.176
340	↓	↓	↓	1065	197.5	366	2.460
380				1045	200.2	408	2.738
240	↑	↑	↑	1013	177.7	273	1.823
270				992	180.4	308	2.066
300	500	0.878	1688	970	183.1	342	2.300
340	↓	↓	↓	979	185.8	387	2.601
380				945	188.4	433	2.917
240	↑	↑	↑	693	145.9	340	2.285
270				677	147.6	382	2.564
300	1000	0.707	1186	664	149.5	425	2.859
340	↓	↓	↓	647	151.2	481	3.240
380				632	153.1	537	3.622

Table 40

Calculated Values of Specific Impulse for System Naphferrol - 90% Hydrogen Peroxide (Stoichiometric Mixture) F/O = 0.270 mol H_2O_2/mol CH_3OH [P_e = 14.7 psia]

P_c psia	Total l_c eff Btu/lb	P_c/P_c nhl	T_c °K	T_e °K	I_{sp} lbs-sec/lb	P_c nhl psia	$\dot{m}/A_t$ lbs/sec x in^2
240	↑	↑	2558	1767	213.5	240	1.538
270			2564	1743	217.2	270	1.728
300	0	1.0	2567	1717	220.3	300	1.920
340	↓	↓	2572	1686	223.4	340	2.176
380			2576	1660	226.2	380	2.430
240	↑	↑	2510	1715	212.1	242	1.548
270			2514	1688	214.9	273	1.740
300	75	0.9905	2517	1663	217.9	303	1.940
340	↓	↓	2521	1633	221.3	343	2.196
380			2525	1609	224.0	384	2.458
240	↑	↑	2485	1691	210.7	243	1.554
270			2489	1664	213.7	274	1.752
300	110	0.9855	2492	1638	217.2	305	1.952
340	↓	↓	2496	1608	220.2	345	2.301
380			2500	1582	223.2	386	2.470
240	↑	↑	2458	1667	208.9	245	1.568
270			2462	1637	212.1	275	1.760
300	150	0.9795	2464	1612	215.3	306	1.960
340	↓	↓	2468	1580	219.2	347	2.222
380			2471	1555	221.8	388	2.484
240	↑	↑	2408	1619	205.7	248	1.588
270	225	0.9680	2412	1592	208.9	279	1.786
300	↓	↓	2414	1568	212.0	310	1.984

300	225	0.9500	2036	1212	194.5	316	2.184
340	↓	↓	↓	1184	197.6	358	2.480
380	↓	↓	↓	1159	200.2	400	2.768
240	↑	↑	↑	1207	185.7	258	1.784
270	↑	↑	↑	1181	188.7	290	2.008
300	300	0.9310	1960	1158	191.2	322	2.228
340	↓	↓	↓	1129	194.0	365	2.528
380	↓	↓	↓	1106	196.4	408	2.824
240	↑	↑	↑	1066	175.9	272	1.882
270	↑	↑	↑	1041	178.7	306	2.117
300	500	0.882	1762	1018	181.3	340	2.353
340	↓	↓	↓	995	183.9	385	2.665
380	↓	↓	↓	974	186.7	431	2.983
240	↑	↑	↑	700	146.0	333	2.305
270	↑	↑	↑	685	147.6	375	2.595
300	1000	0.721	1228	671	149.6	416	2.883
340	↓	↓	↓	654	151.5	471	3.268
380	↓	↓	↓	636	153.8	527	3.660

Table 42

Calculation of the Effect of Diverging Nozzle Heat Loss on Specific Impulse for System: Naphferrol - 90% H_2O_2 (Fuel Rich Mixture)
F/O = 0.441 mols CH_3OH/mol H_2O_2; P_c = 300 psia; P_e = 14.7 psia

H_{system} Btu/lb	Total l_c eff Btu/lb	H_c Btu/lb	l_{dn} Btu/lb	H_c' Btu/lb	T_c' °K	T_e' °K	$I_{sp_c'ahl}$ lbs-sec/lb	I_{sp_cchl} lbs-sec/lb	$\frac{I_{sp_cahl}}{I_{sp_cchl}}$
			0	3174	2167	1280	208.8		1.0
			50	3149	2143	1266	207.8		0.995
	0	3174						208.8	
			100	3124	2119	1252	206.9		0.991
			150	3099	2095	1238	205.9		0.986
			0	2674	1688	970	183.1		1.0
			50	2649	1663	957	181.8		0.993
3174	500	2674						183.1	
			100	2624	1638	944	180.5		0.986
			150	2599	1612	930	179.1		0.978
			0	2174	1186	664	149.5		1.0
			50	2149	1160	650	148.0		0.990
	1000	2174						149.5	
			100	2124	1135	637	146.4		0.979
			150	2099	1110	624	144.7		0.968

Table 43

Calculation of the Effect of Diverging Nozzle Heat Loss on Specific Impulse for System: Naphferrol - 90% H_2O_2 (Stoichiometric Mixture)
F/O = 0.270 mols CH_3OH/mol H_2O_2; P_c = 300 psia; P_e = 14.7 psia

H_{system} Btu/lb	Total $l_{c\ eff}$ Btu/lb	H_c Btu/lb	l_{dn} Btu/lb	H_c' Btu/lb	T_c' °K	T_e' °K	$I_{sp}'_{cahl}$ lbs-sec/lb	$I_{sp_{cchl}}$ lbs-sec/lb	$I_{sp_{cahl}}/I_{sp_{cchl}}$
			0	2403	2567	1717	220.3		1.0
			50	2378	2542	1703	219.6		0.997
	0	2403						220.3	
			100	2353	2518	1690	218.8		0.993
			150	2328	2493	1676	218.1		0.990
			0	1903	2194	1361	201.0		1.0
			50	1978	2169	1348	200.0		0.995
2403	500	1903						201.0	
			100	1953	2144	1335	199.0		0.990
			150	1928	2120	1321	198.0		0.985
			0	1403	1734	1012	180.8		1.0
			50	1378	1709	1000	179.5		0.993
	1000	1403						180.8	
			100	1353	1684	987	178.3		0.986
			150	1328	1660	975	177.0		0.979

Table 44

Calculation of the Effect of Diverging Nozzle Heat Loss on Specific Impulse for System: Naphferrol - 90% H_2O_2 (Oxidant Rich Mixture) F/O = 0.179 mols CH_3OH/mol H_2O_2; P_c = 300 psia; P_e = 14.7 psia

H_{system} Btu/lb	Total $l_{c\ eff}$ Btu/lb	H_c Btu/lb	l_{dn} Btu/lb	H_c' Btu/lb	T_c' °K	T_e' °K	$I_{sp'cahl}$ $\frac{lbs\text{-}sec}{lb}$	I_{spcohl} $\frac{lbs\text{-}sec}{lb}$	$\frac{I_{spcahl}}{I_{spcohl}}$
			0	1908	2243	1373	204.8		1.0
			50	1873	2219	1359	203.8		0.995
	0	1908						204.8	
			100	1848	2196	1345	202.7		0.990
			150	1823	2172	1332	201.5		0.984
			0	1408	1762	1018	181.3		1.0
			50	1373	1748	1005	180.0		0.993
1908	500	1408						181.3	
			100	1348	1724	991	178.8		0.986
			150	1323	1700	978	177.3		0.978
			0	908	1228	671	149.6		1.0
			50	873	1203	659	148.1		0.990
	1000	908						149.6	
			100	848	1178	647	146.6		0.980
			150	823	1152	635	145.1		0.970

FIG. A-30 THEORETICAL SPECIFIC IMPULSE FOR ADIABATIC NOZZLE EXPANSION AS A FUNCTION OF $\frac{\dot{m}}{A_t}$ AND $\frac{P_c}{P_{c\ nhl}}$

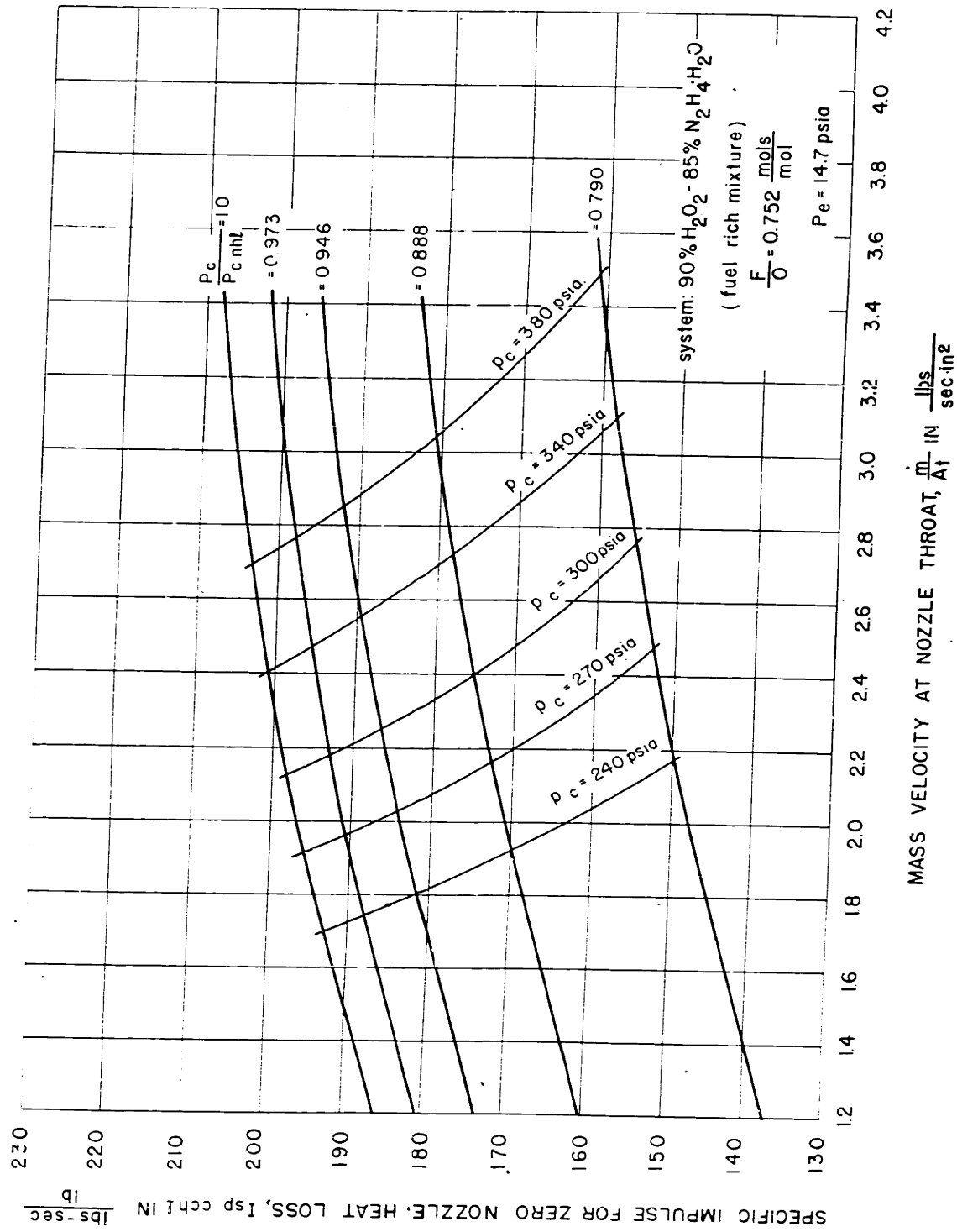

FIG. A-31 THEORETICAL SPECIFIC IMPULSE FOR ADIABATIC NOZZLE EXPANSION AS A FUNCTION OF $\frac{\dot{m}}{A_t}$ AND $\frac{P_c}{P_c \text{ nhl}}$

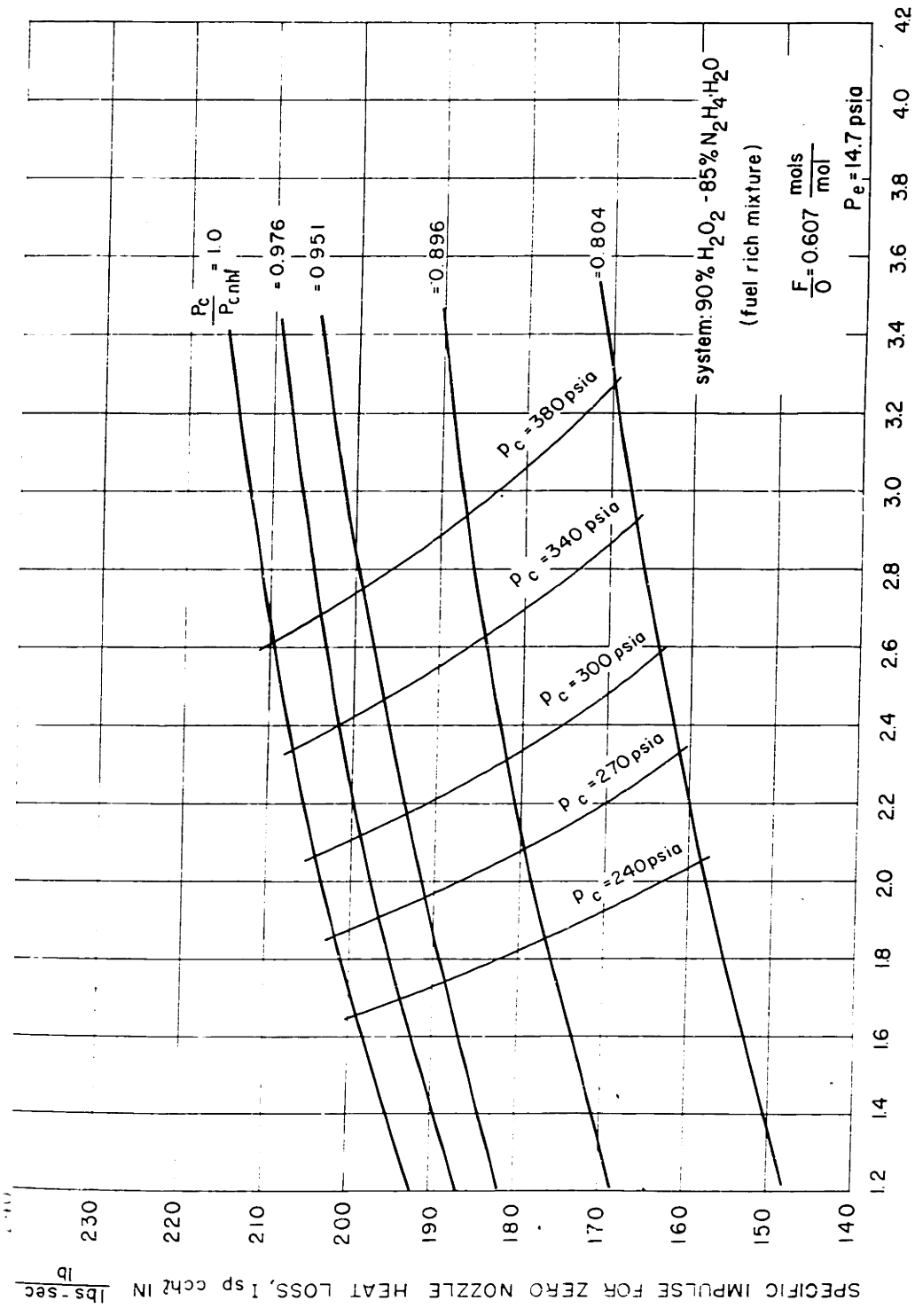

FIG. A-32 THEORETICAL SPECIFIC IMPULSE FOR ADIABATIC NOZZLE EXPANSION AS A FUNCTION OF $\frac{\dot{m}}{A_t}$ AND $\frac{P_c}{P_{c\,nhl}}$

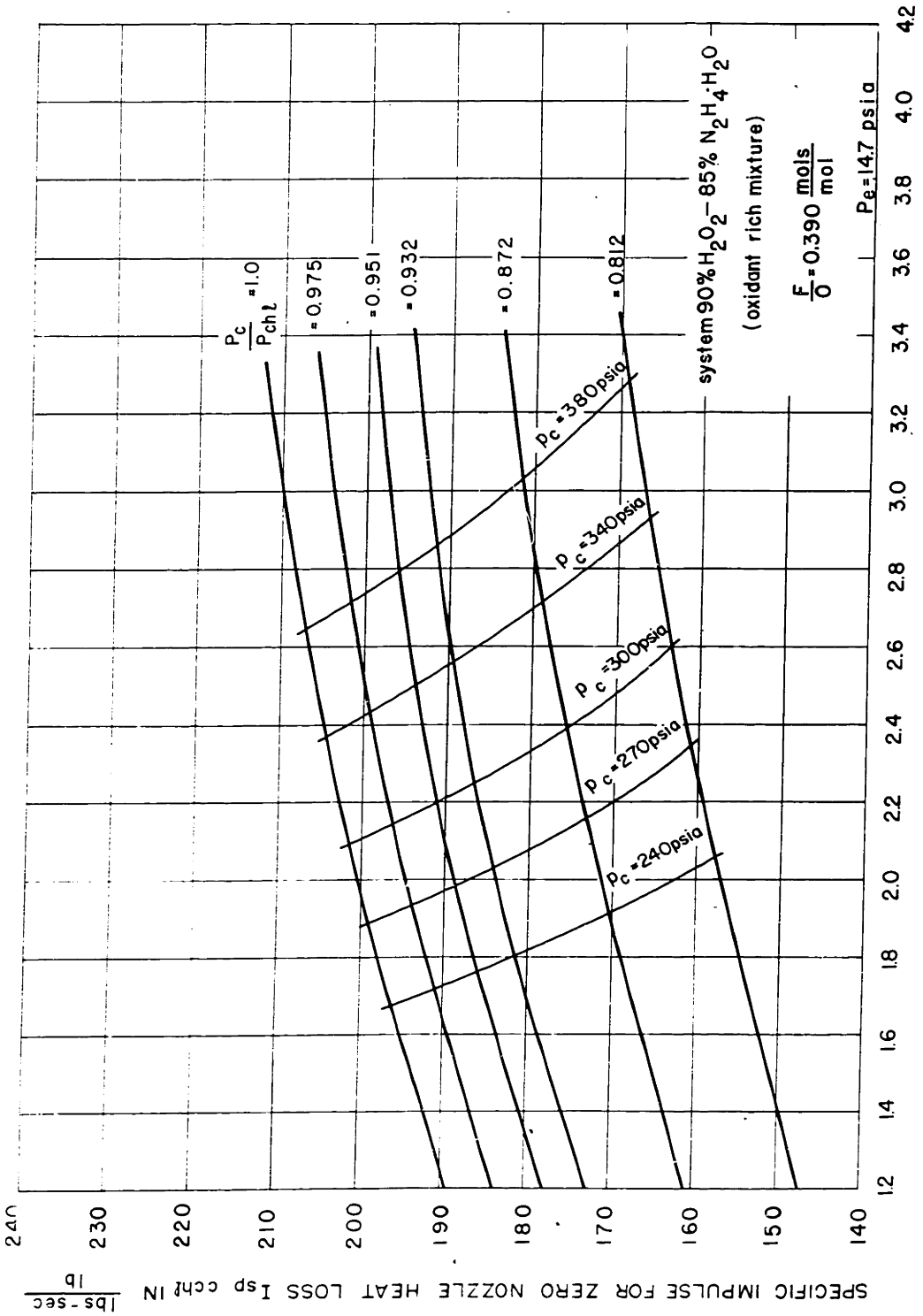

FIGURE A-33 THEORETICAL CHAMBER PRESSURE
(ADIABATIC CASE)
AS A FUNCTION OF MASS FLOW RATE

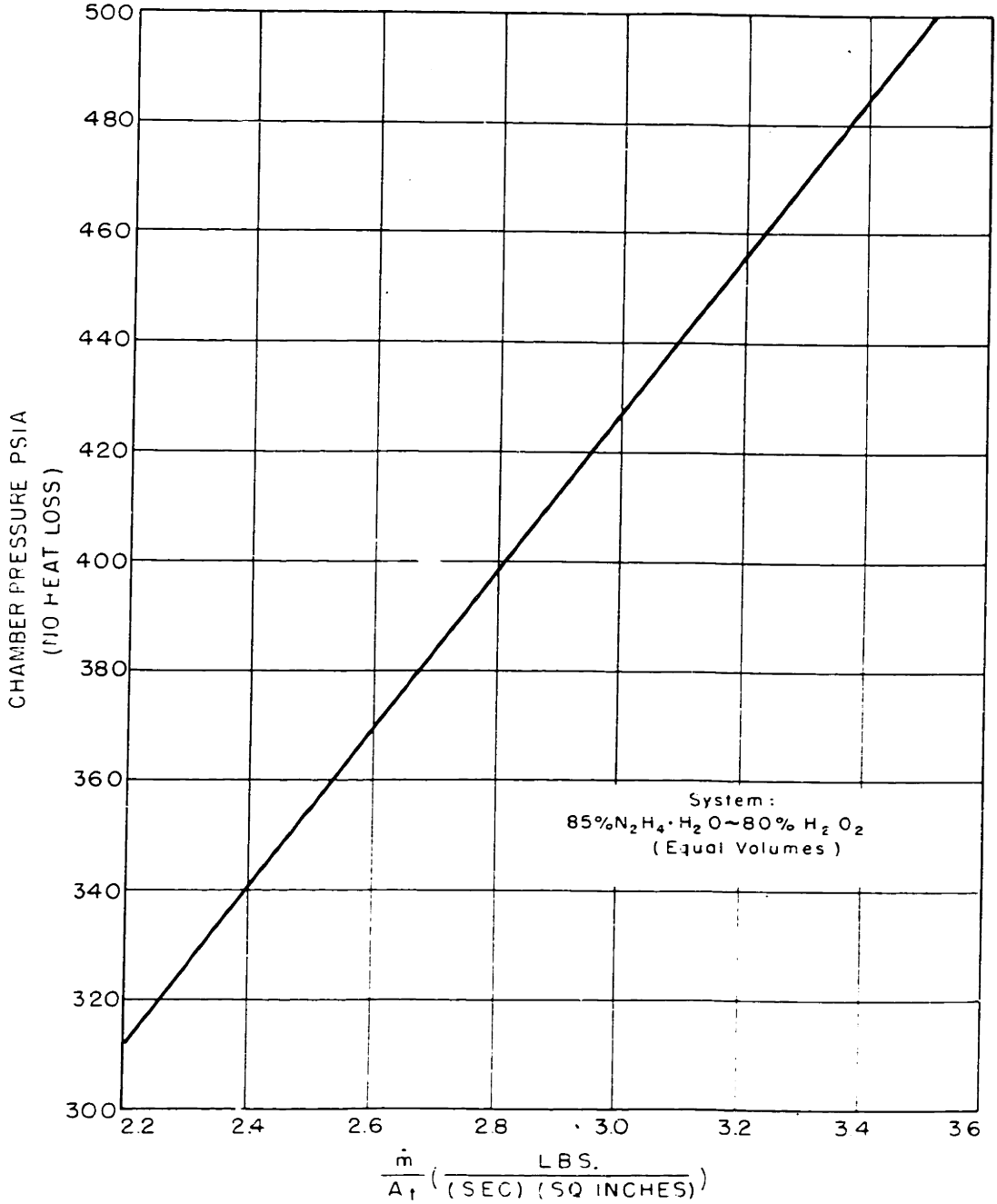

FIGURE A-34 EFFECT OF HEAT LOSS ON CHAMBER PRESSURE FOR A GIVEN MASS FLOW RATE

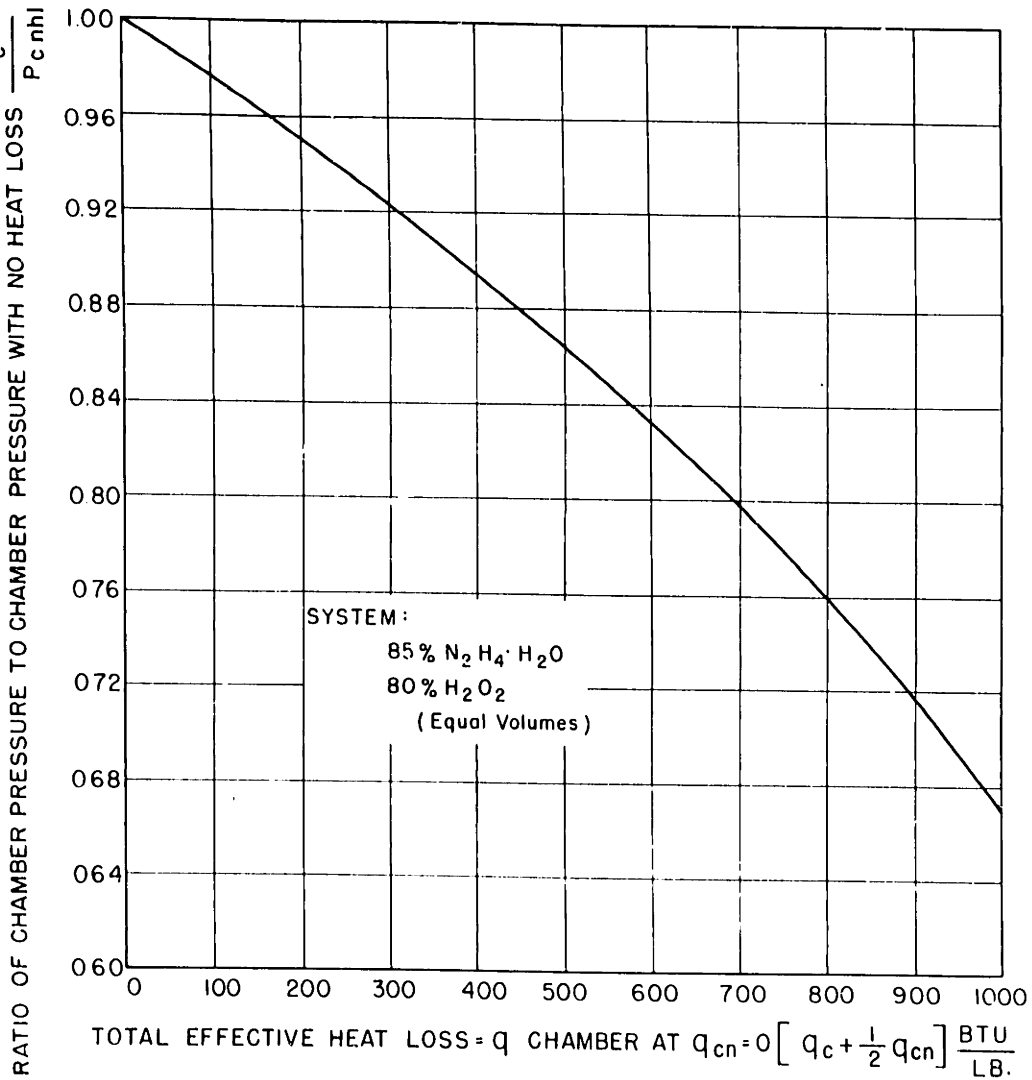

FIGURE A-35 THEORETICAL SPECIFIC IMPULSE FOR ADIABATIC ISENTROPIC NOZZLE EXPANSION AS A FUNCTION OF EXPANSION PRESSURE RATIO (ACTUALLY $\frac{\dot{m}}{A_t}$ AND $\frac{P_c}{P_{c\ nhl}}$)

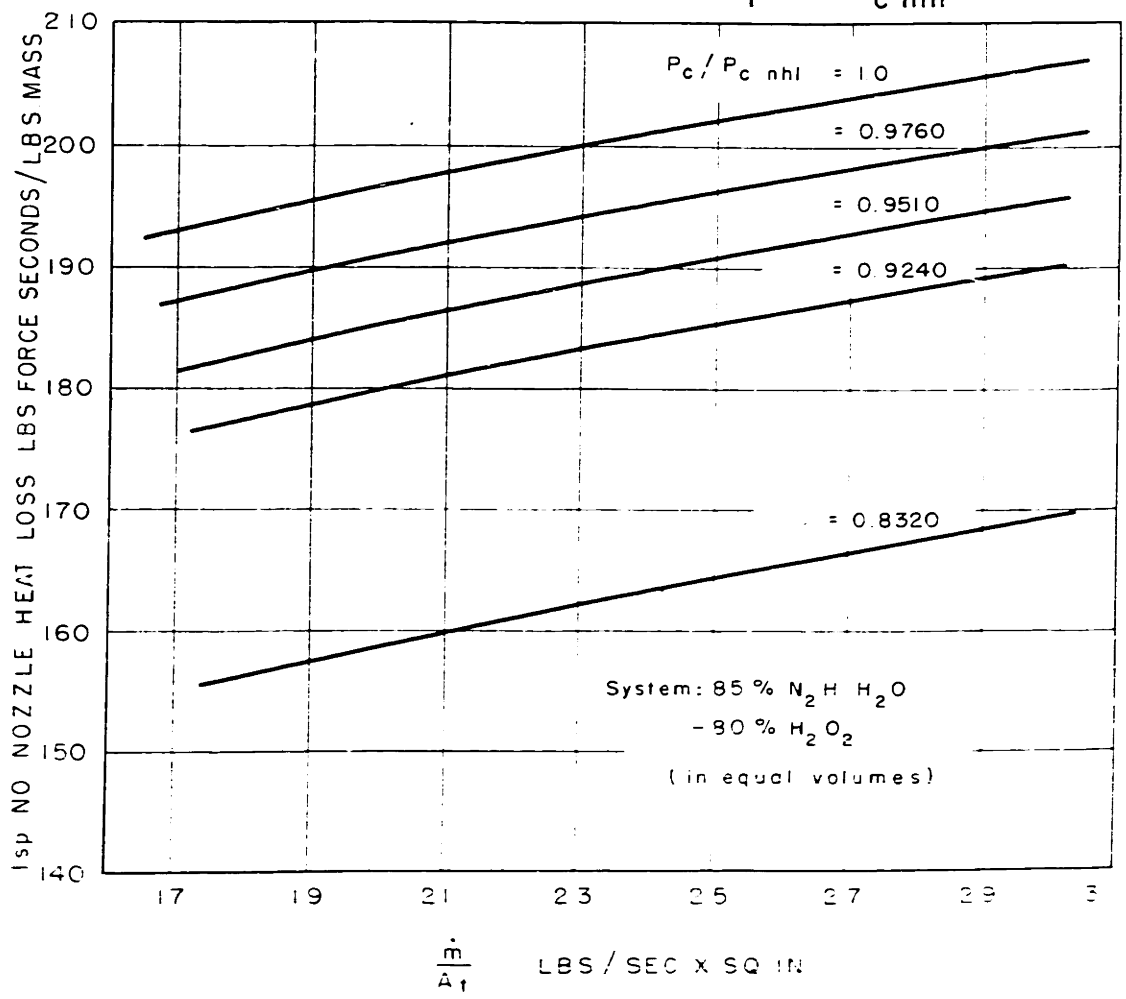

FIG. A-36 EFFECT OF DIVERGING NOZZLE HEAT LOSS ON SPECIFIC IMPULSE
(THEORETICAL CALCULATIONS)

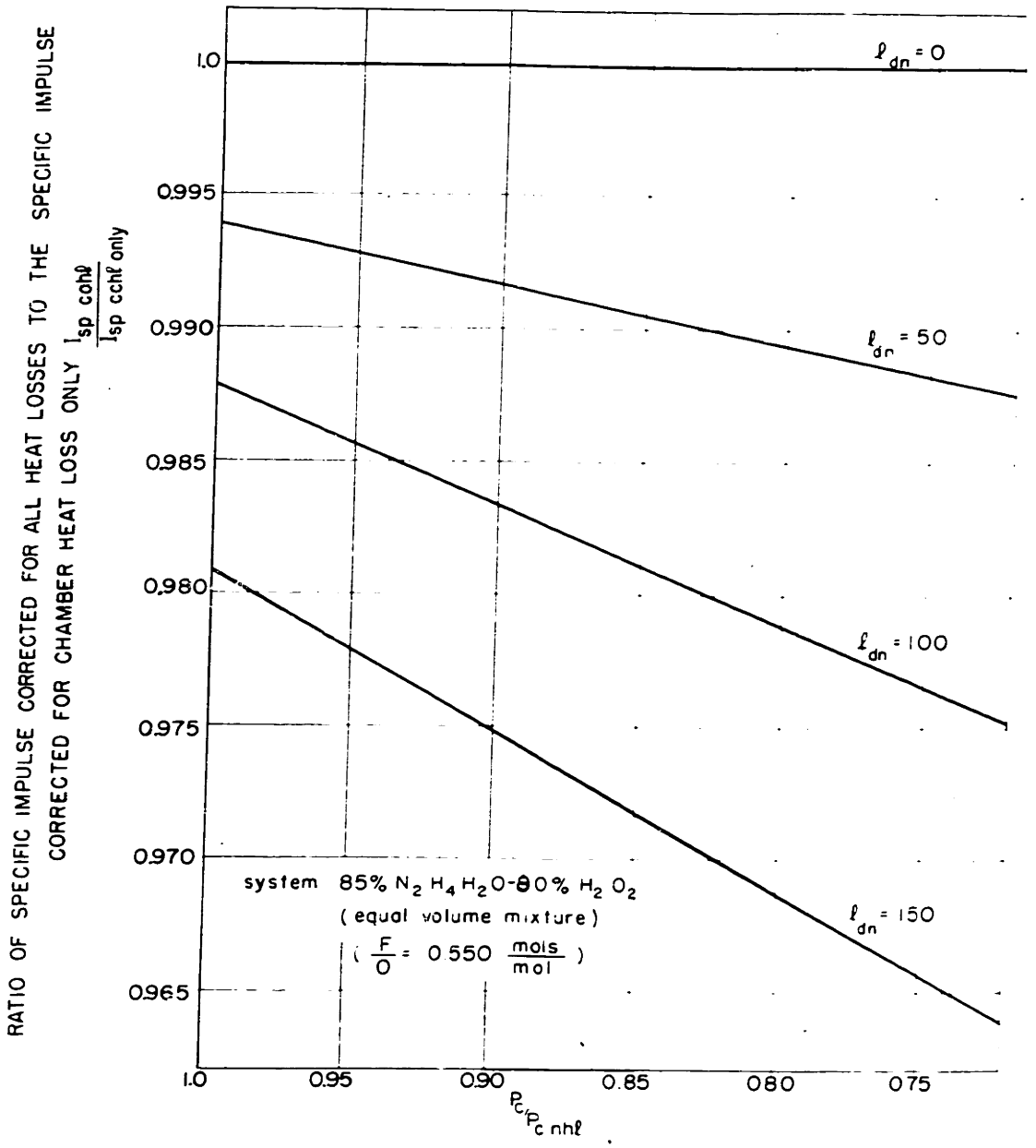

FIGURE A-37 THEORETICAL CHAMBER PRESSURE
(ADIABATIC CASE)
AS A FUNCTION OF MASS FLOW RATE

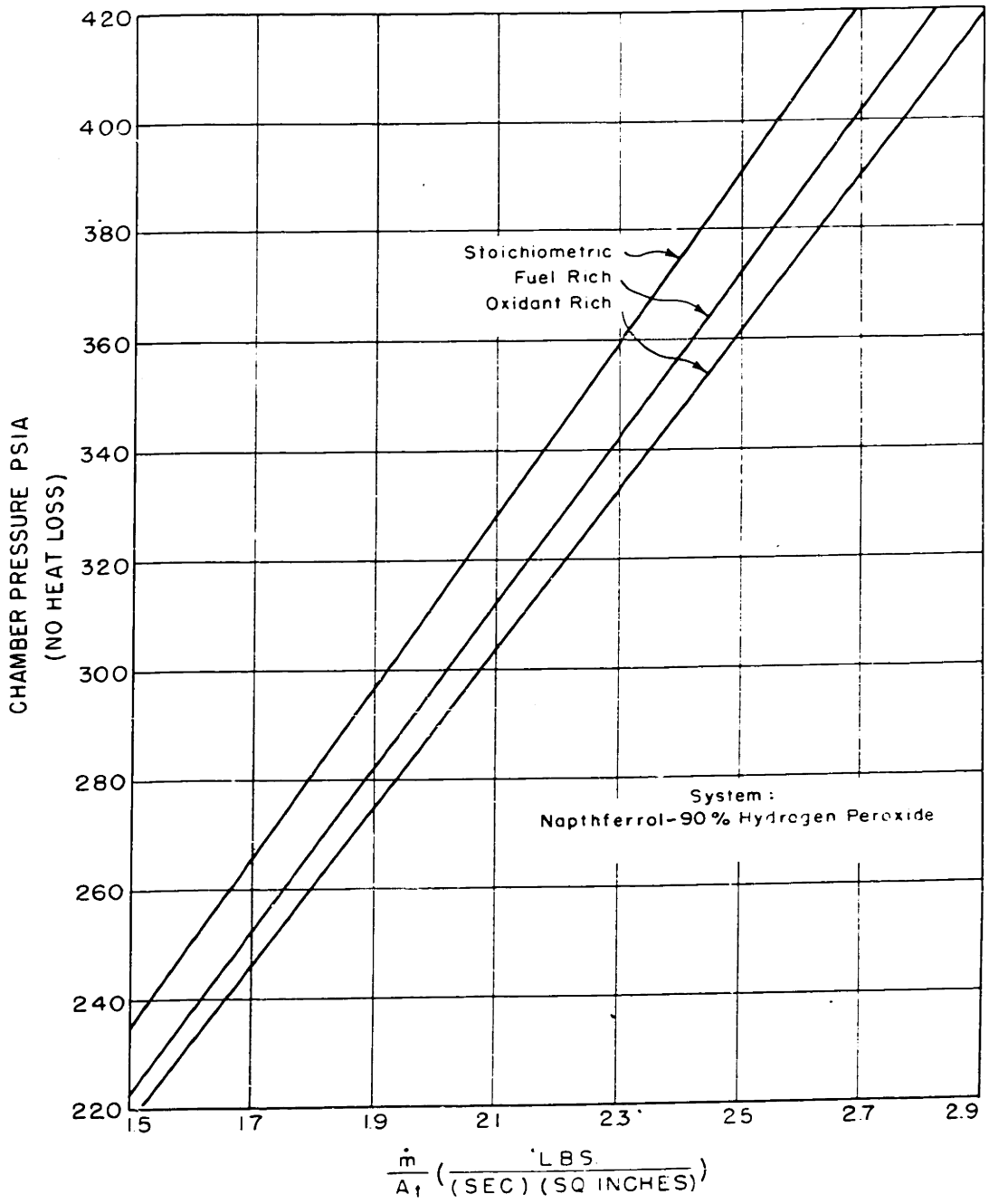

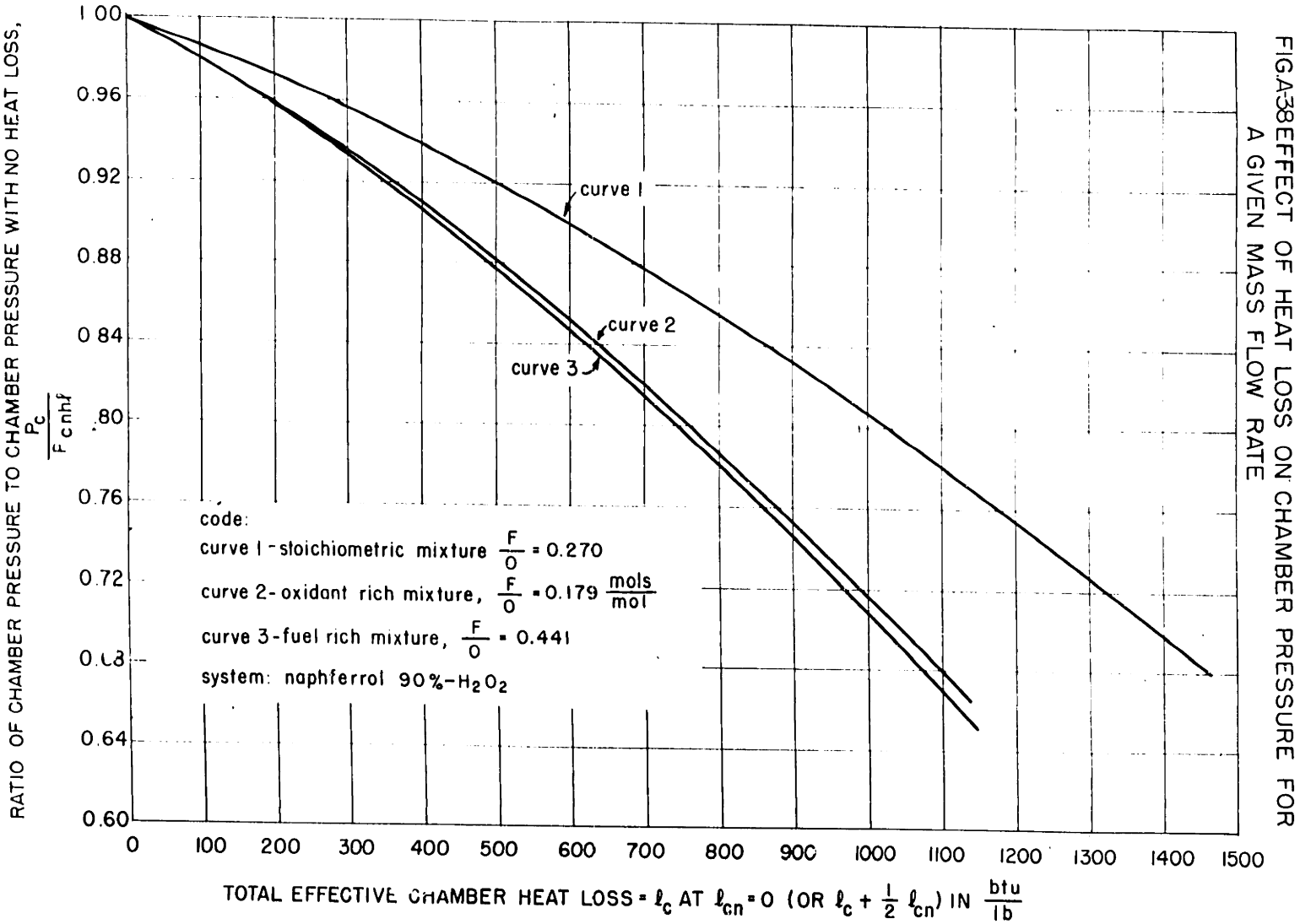

FIG. 38 EFFECT OF HEAT LOSS ON CHAMBER PRESSURE FOR A GIVEN MASS FLOW RATE

FIG.A-39 THEORETICAL SPECIFIC IMPULSE FOR ADIABATIC NOZZLE EXPANSION AS A FUNCTION OF $\frac{\dot{m}}{A_t}$ AND $\frac{P_c}{P_{c\,nhl}}$

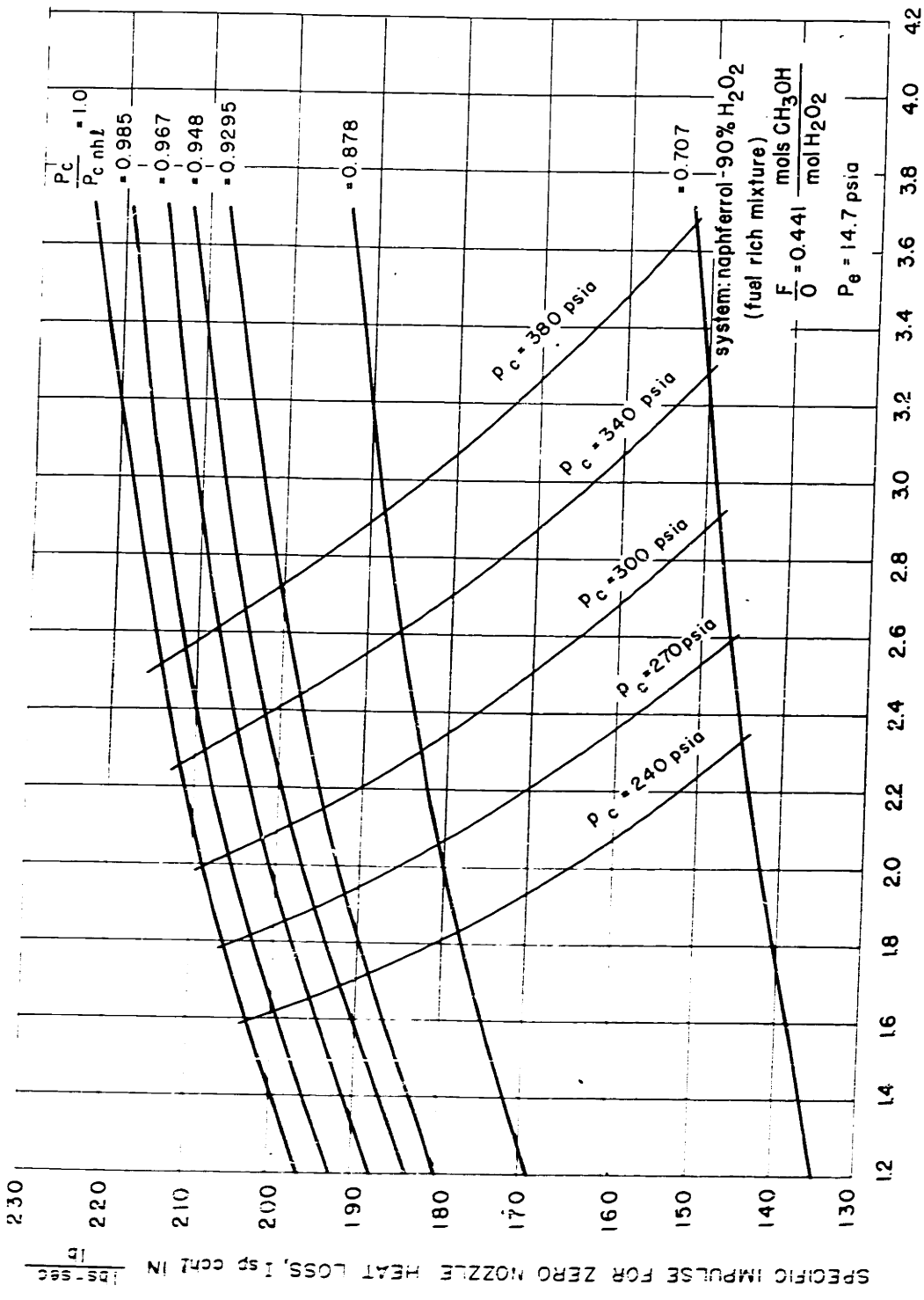

FIG. A-40 THEORETICAL SPECIFIC IMPULSE FOR ADIABATIC NOZZLE EXPANSION AS A FUNCTION OF $\frac{\dot{m}}{A_t}$ AND $\frac{P_c}{P_{c\,nhl}}$

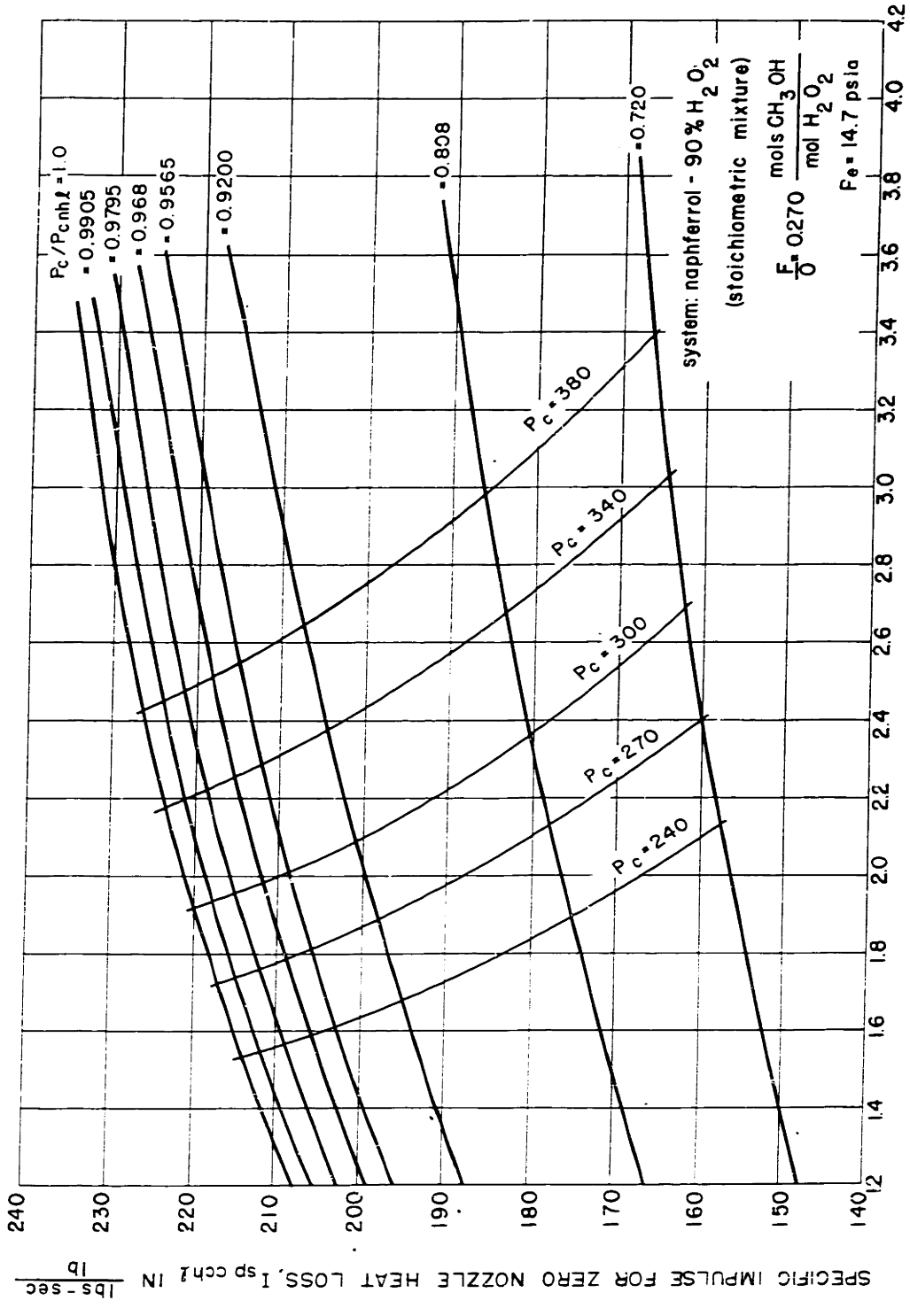

FIG. A-41 THEORETICAL SPECIFIC IMPULSE FOR ADIABATIC NOZZLE EXPANSION AS A FUNCTION OF $\frac{\dot{m}}{A_t}$ AND $\frac{P_c}{P_{c\,nhf}}$

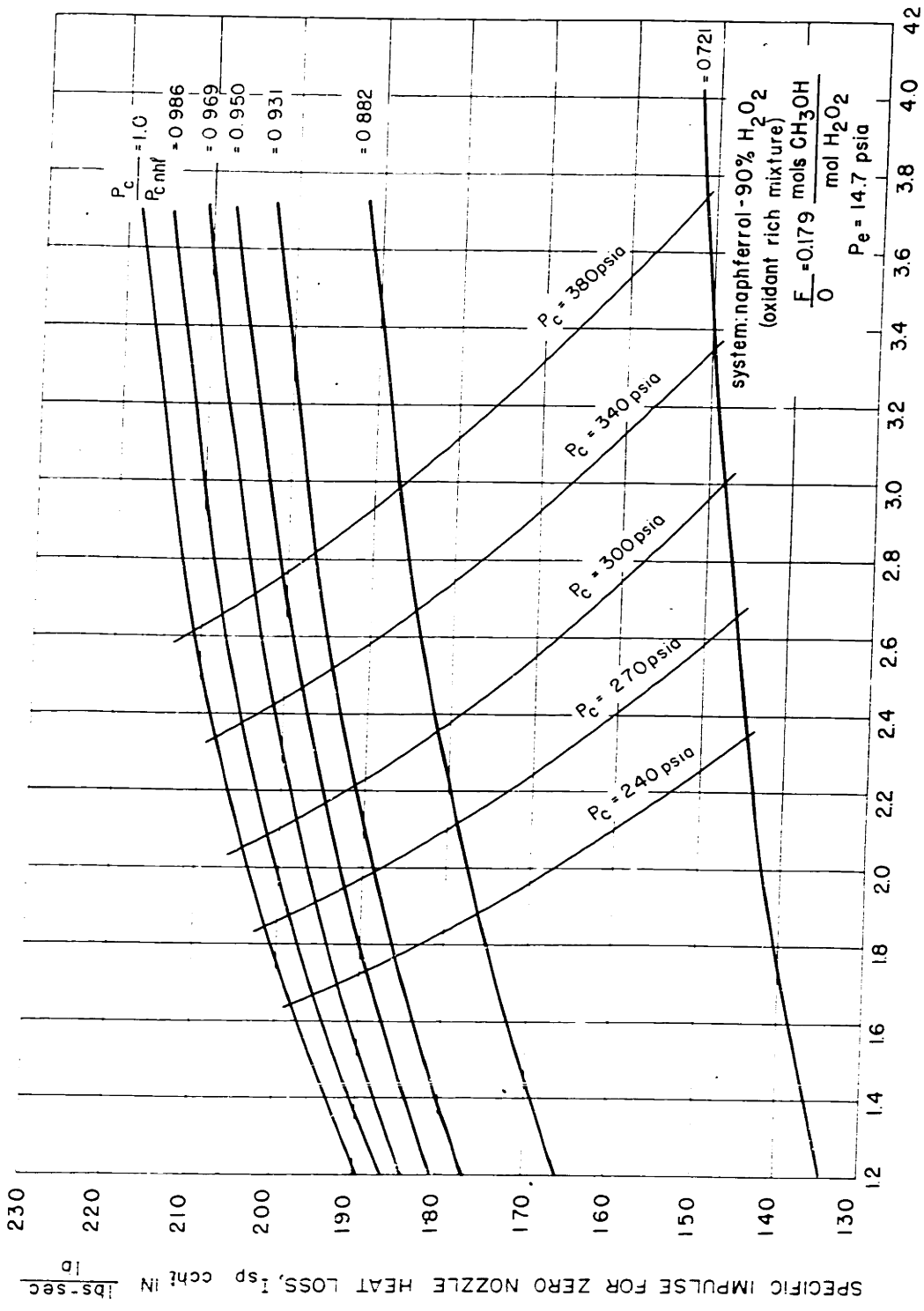

APPENDIX B

Location of Original Data

The original data for this thesis are contained in three M.I.T. Laboratory Work Books and in accompanying data sheets, as well as in the recorder charts and films from the various recording instruments used. These records are preserved in the files of M.I.T. DIC Project 6552 located in Room 4-055.

APPENDIX T

Bibliography

(1) Africano, A., Astronautics, 37, 13-16 (1937); also J. Aeron. Sc., 3, 287-290 (1936).

(2) American Rocket Society, Astronautics and J. Amer. Rocket Society (1937 to present).

(3) Ananoff, A., L'Ariophile, 46, 157-207 (1938).

(4) Anderson, Beyer and Watson, Natl. Petrol. News, 36, R476-484 (1944).

(5) Bodoche, M., Chem. Abstracts, 40, 5988[7] (1946) from Bull. Soc. Chim., 37-43 (1946).

(6) Bichowsky and Rossini, "Thermochemistry of Chemical Substances," New York, Reinhold Publishing Co.,1936.

(7) Bone, Newitt and Townsend, "Gaseous Combustion at High Pressures," p. 296, London, Longmans Green and Co, 1927.

(8) Bone and Townsend, "Flame and Combustion in Gases," p. 323, London, Longmans Green and Co., 1927.

(9) Borden, W. E., "Heat Flux Through a Small Rocket Motor," M.S. Thesis, Chem. Eng., M.I.T. (1947).

(10) Brinsmade, A. F., "Thermodynamic Properties of the Working Fluid in Rockets," M.S. Thesis, Chem. Eng., M.I.T. (1942).

(11) Bryant, W. M. D., Ind. Eng. Chem., 25, 820-823 (1933).

(12) Buckingham, E., "Jet Propulsion for Airplanes," NACA Report 159, Cleveland, 1923.

(13) Egbert, R.B., "Radiation from Gases," Sc.D. Thesis, Chem. Eng., M.I.T. (1941).

(14) Esnault-Pelterie, R., "L'Astronautique," pp. 109-151, Paris, A. Lahure (1930).

(15) Goddard, R. H., "Liquid-Propellant Rocket Development," Smithsonian Miscellaneous Collections, 95, No. 3 (1936) and 71, No. 2 (1919).

(16) Grinstead, Frawley, Chapman and Schultz, SAE Journal (Transactions), 52, No. 11, 534-556 (1944).

(17) Hausenstein, A., Zeit. fur das Gesamte Schiess. u. Springstoffwesen, 34, No. 12, 331-333 (1939) and 35, No. 1 and 2 (1940).

(18) Hershey, Eberhard and Hottel, SAE Journal (Transactions), 39, No. 4, 409-424 (1936).

(19) Huckaba, C. E. and Keyes, F. G., M.I.T. DIC Project 6552, Report No. 20, "The Density of Aqueous Hydrogen Peroxide Solutions, Cambridge, Mass., Sept. 30, 1947.

(20) International Critical Tables, 1st Edition, Vol. 5, p. 163, New York, McGraw Hill Book Co. (1929).

(21) Johnston, H. L. and Walker M. K., J. Am. Chem. Soc., 55, 179 (1933).

(22) Kassel, L. S., J. Am. Chem. Soc., 56, 1838 (1934).

(23) Kelley, K. K., Bur. of Mines Bull., 350, p. 54 (1936).

(24) Lewis, B. and von Elbe, G., J. Am. Chem. Soc., 57, 612-14 (1935).

(25) Malina, F. J., J. of the Franklin Inst., pp. 433-454, Oct. 1940.

(26) Marks, L. S., "Mechanical Engineers' Handbook," 4th Edition, pp. 416-424, New York, McGraw Hill Book Co., 1941.

(27) McAdams, W. H., "Heat Transmission," 2nd Edition, p. 174, New York, McGraw Hill Book Co., 1942.

(28) McAdams, W. H., ibid., pp. 410-11.

(29) McAdams, W. H., ibid., pp. 64-69.

(30) Oberth, H., "Wege zur Raumschiffahrt," pp. 23-38, München, R Aldenbourg, 1933.

(31) Osann and Schroder, Archiv. Eisenhuttenwesen, 7 89-94, (1933)

(32) Pauling, L., "Nature of the Chemical Bond," Second Edition, Ithaca, N.Y., Cornell University Press, 1945.

(33) Rinin, N. A., "Propulsione a Reazione Senza Utilizzatione dell' Aria," pp. 628-636, Roma, Qunto Convegno Volta.

(34) Rogge, E., Zeit fur das Gesamte Schiess. u. Sprinstoffwesen, 35, No. 7, 150-152 (1940).

(35) Sänger, E., "Raketen-Flugtichnik," p. 4-57, Munchen, R. Aldenbourg (1933).

(36) Satterfield, Hottel and Williams, M.I.T. DIC Project 6552, Report No. 17, "Generalized Thermodynamics of High Temperature Combustion," Cambridge, Mass., May 15, 1947.

(37) Satterfield, C. N., Personal Communication, April 30, 1948.

(38) Satterfield, C. N., Personal Communication, March 19, 1948.

(39) Schwartz, A., "A Study of the Storage Stability of Hydrazine-Based Fuels," B.S. Thesis, Chem. Eng. M.I.T. (1947).

(40) Stemmer, J., Schweizer Areo, Revue, 16, No. 6 (1941).

(41) U.S. Naval Technical Mission to Japan, Japanese Fuels and Lubricants, Article 5, "Research on Hydrogen Peroxide and Hydrazine Hydrate," reporting on work of Chem. Eng. Lieut. M. Shimo (1946).

(42) Vogelpohl, G., Forschung auf dem Gebute des Ingenieurwesens, 8, 35-41 (1937).

(43) Wagner, C., "Explanation of Diagrams for Determination of Exhaust Speed of Fuel Gases", Washington Documents Center Translation from Office of Naval Intelligence (1946)

(44) Kinkev, M.S., NACA Technical Memo. No. 1066. "Comparative Results of Several Different Types of Nozzles", Cleveland, 1945.

(45) Keenan, J., "Thermodynamics" p. 143-144, New York, John Wiley & Sons Co., 1942

Bond," Second
iversity Press,

e Senza Utiliz-
Roma, Qunto

ess. u. Sprin-
940).

4-57, Munchen,

I.T. DIC Project
Thermodynamics
Cambridge, Mass.,

cation,

cation,

Stability of
s, Chem. Eng.

6, No. 6 (1941).

, Japanese Fuels
ch on Hydrogen
eporting on
(1946).

te des Ingenieur-

. Determination of
ington Documents
al Intelligence (1946)
Memo. No. 1066.
fferent Types of

" p. 143-144,
, 1942

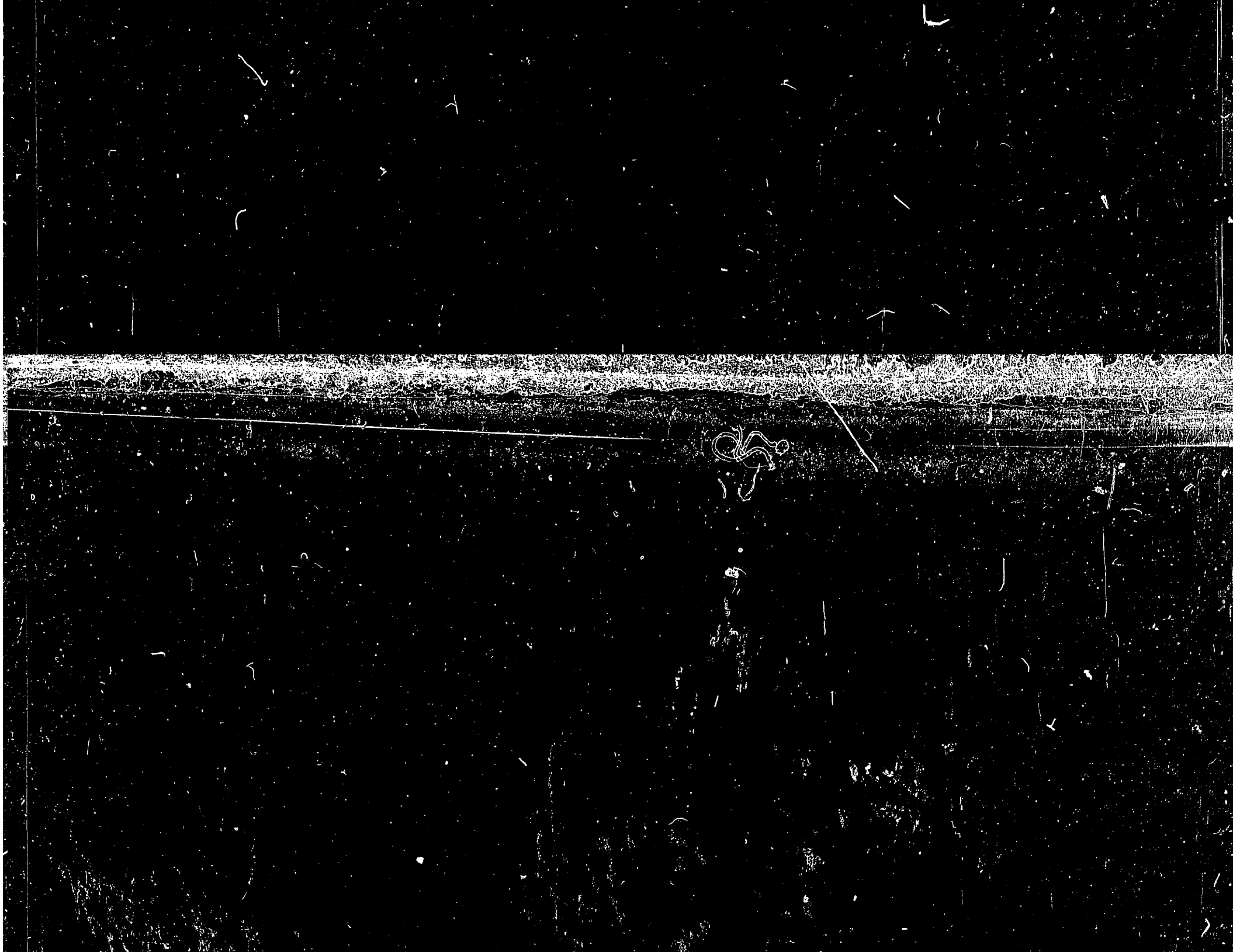

ON THE USE OF COORDINATE PERTURBATIONS IN THE SOLUTION OF PHYSICAL PROBLEMS

by

PHYLLIS ANN FOX

A.B., Wellesley College
(1944)

S.M., Massachusetts Institute of Technology
(1949)

SUBMITTED IN PARTIAL FULFILLMENT OF THE
REQUIREMENTS FOR THE DEGREE OF
DOCTOR OF SCIENCE
at the
MASSACHUSETTS INSTITUTE OF TECHNOLOGY
1953

Signature of Author.....
Department of Mathematics,
November 10, 1953

Certified by.....
Thesis Supervisor

Accepted by.....
Chairman, Departmental Committee
on Graduate Students

TABLE OF CONTENTS

ABSTRACT

Perturbation solutions to physical problems expressed in the form

$$f(x,y) = f^{(0)}(x,y) + f^{(1)}(x,y) + \varepsilon^2 f^{(2)}(x,y) + \ldots$$

(where ε is the perturbation parameter and $f^{(i)}$ are the successive perturbation functions of the problem) often prove unsatisfactory in certain regions of the (x,y)-plane. A method is discussed for improving these solutions by submitting the independent variables x and y to similar perturbation expansions in terms of new independent quantities. For the case of elliptic partial differential equations, discussed here with reference to the flow past a thin airfoil, no outstanding advantages appear from the attempted improvement, but the technique does seem useful for problems of a hyperbolic character. In particular, wave propagation problems were studied and both the dependent and independent physical variables of the problem were expressed as perturbation series in terms of the characteristic variables. For the case of a plane wave the convergence of the series is proved and it is shown that the solution can be made to hold even somewhat after the development of a weak shock. Extensions to the cases of cylindrical and spherical flow are discussed.

The writer wishes to express great appreciation to her supervisor Professor C. J. Lin, who suggested the problem, for valuable suggestions and assistance given throughout the development of the thesis.

INTRODUCTION

This study deals with possible improvements effected in solutions to physical problems by changes in the coordinate system of the problem. In particular, perturbation solutions to the problems are investigated with a view to improving the usual solution by allowing a perturbation of the independent variables as well as of the dependent variables. The technique has proved useful for wave propagation problems of a hyperbolic nature described in Chapter 2, but has been less successful for the elliptic problem of the flow past a thin airfoil discussed in Chapter 3.

The idea of perturbing the independent variable of a problem was used some time ago by Poincaré in finding the limit cycle of a nonlinear oscillator (20), and more recently (1949) M. J. Lighthill considered the method at some length in a most interesting paper (12). Lighthill considers various types of ordinary differential equations whose usual perturbation solutions are unsatisfactory, and also in this paper he deals briefly with nonlinear partial differential equations. In a later paper (11) he applies the technique of coordinate perturbation to correcting the usual solution to the problem of incompressible flow past a thin airfoil. In the usual solution which is based on the small slope of the airfoil profile a satisfactory answer is not obtained near the leading edge of a blunt nosed airfoil, but Lighthill found that a small constant shift of the coordinate system corrected the

first order solution, making it valid uniformly, and he implied that successive corrections could be made in the coordinates as the higher order perturbation solutions were found.

This problem was the initial impetus of our investigation and it was planned to study the problem at greater length and in particular with reference to the case of compressible flow. However, as the study progressed it became clear that the perturbation series developed for the independent variables were not satisfactory. Actually the successive perturbation functions in these series, in order to correct the increasing order of singularities in the velocity functions near the leading edge, have to carry the singularities themselves, and in the singular region each term of the perturbation series becomes of the same instead of decreasing order. The results and the failure of the series near the leading edge are discussed in more detail in Chapter 3.

Nevertheless the hope remained that at least some sort of one-state correction could be found for the case of compressible flow past a thin airfoil, since the small constant coordinate shift does effectively correct the incompressible case. Several lines of investigation were attempted and various types of coordinate correction were considered, but unfortunately none of them proved successful. For example a constant coordinate shift is no longer correct since it does not satisfy the more complicated equations for the compressible

case. Then as far as other types of functions are concerned one important aspect arising from the investigation should be remarked. Upon attempting series expansions based on a perturbation parameter, ε, in the form

$$x = x^{(0)}(X,Y) + \varepsilon x^{(1)}(X,Y) + \varepsilon^2 x^{(2)}(X,Y) + \ldots \qquad (1.1)$$

where X and Y are new coordinates, it was found that functions of the type, $x^{(i)}$, appearing in (1.1) could not be obtained, but rather that due both to boundary conditions and to changes of order in the derivatives of the perturbation functions that the functions were of the form

$$x^{(i)}(X,Y,\varepsilon) \qquad (1.2)$$

In other words the functions, $x^{(i)}$, did not fit the usual type of perturbation solution (1.1).

Actually such functions might be acceptable in a new frame of perturbation solutions of the type

$$x = x^{(0)}(X,Y,\varepsilon) + \varepsilon x^{(1)}(X,Y,\varepsilon) + \varepsilon^2 x^{(2)}(X,Y,\varepsilon) + \ldots \qquad (1.3)$$

where the ε necessary to fulfill the requirements of the problem is allowed to appear in the perturbation functions. This line of investigation has not been pursued, but might lead to new methods of problem solution and is perhaps worthy of some study.

Next, since it had not been possible to find real solution improvement for the elliptic case, the investigation turned to problems of a hyperbolic character. In particular

The nonlinear hyperbolic partial differential equations governing wave propagation dependent on one space variable and one time variable were considered. Problems of this sort for the cases of spherical and cylindrical waves have been discussed by Whitham [23], [24], in papers where a correction to one set of characteristics is advocated. That is in lieu of being the usual functions of a linearized characteristic variable in the form

$$f(x - c_0 t) \quad , \qquad c_0 = \text{speed of sound at infinity} \tag{1.4}$$

where the characteristics are straight and parallel in the (x,t)-plane, Whitham suggests a correction in the form of a new variable, z, which is to be constant along the true characteristics of the problem now to be solved by functions of the type $f(z)$. He has obtained interesting results from this approach, but a drawback of the method is its failure to deal with both sets of characteristics at the same time.

The question arose as to whether it might not be possible to devise a method correcting the solution along both characteristic directions, and thus allow for waves propagating in either direction. It seemed natural to consider solutions expanded in terms of characteristic variables both for the dependent and independent variables, since in this way both the physical quantities and the correct characteristic curves might be found in the physical (x,t)-plane by a mapping from the characteristic plane. Attention was restricted mainly to the case of plane wave propagation where the equations are

simpler than for higher dimensional cases, and a solution was attempted in terms of characteristic variables α and β for velocity, u, and speed of sound, c, and for the originally independent space and time variables x and t. For a perturbation parameter, ε, the solutions were assumed in the form

$$\begin{aligned} u &= u^{(0)}(\alpha,\beta) + \varepsilon u^{(1)}(\alpha,\beta) + \varepsilon^2 u^{(2)}(\alpha,\beta) + \dots \\ c &= c^{(0)}(\alpha,\beta) + \varepsilon c^{(1)}(\alpha,\beta) + \varepsilon^2 c^{(2)}(\alpha,\beta) + \dots \\ x &= x^{(0)}(\alpha,\beta) + \varepsilon x^{(1)}(\alpha,\beta) + \varepsilon^2 x^{(2)}(\alpha,\beta) + \dots \\ t &= t^{(0)}(\alpha,\beta) + \varepsilon t^{(1)}(\alpha,\beta) + \varepsilon^2 t^{(2)}(\alpha,\beta) + \dots \end{aligned} \tag{1.5}$$

Such a type of solution proved to be most satisfactory. In the case of a plane wave the series for u and c terminate, and a general expression can be found for the nth perturbation function in the series for x and for t. Furthermore, and of some importance, one finds that the convergence of these latter two series can be demonstrated for sufficiently small initial disturbances so that the correctness of the solution is assured. More precisely, the convergence is dependent on the size of the initial disturbance u' and c' to the base quantities u_0 and c_0 only to the extent of requiring that

$$\frac{u'}{u_0} < \frac{2}{\gamma+1} \qquad \frac{c'}{c_0} < \frac{\gamma-1}{\gamma+1} \tag{1.6}$$

where γ is the adiabatic exponent so that for example if $\gamma = 1.4$

$$\frac{u'}{u_0} < 0.833 \qquad \frac{c'}{c_0} < 0.166 \ .$$

In terms of density, ρ, this becomes

$$\frac{\rho'}{\rho_0} < 1.161$$

which is of the order of the requirement on velocity disturbance. In other words the series is a convergent one even for an initial density ratio as high as 2.16.

The convergence of the series in the ordinary regions of the flow is useful, but the outstanding fact is that convergence persists into the region where the mapping from the characteristic plane onto the physical plane becomes multiple-valued and where a shock would develop. In such a region the characteristics in the physical plane form an envelope, and one can show from the solutions (1.5) that the envelope develops for t of the order of $1/\varepsilon$. Then by digressing to state that the usual type of perturbation solution takes the form (see Chapter 2)

$$u = f^{(0)}(x,t) + \varepsilon f^{(1)}(x,t) + \varepsilon^2 t f^{(2)}(x,t) + \varepsilon^3 t\, f^{(3)}(x,t) + \ldots$$

or

$$u = f^{(0)}(x,t) + \varepsilon\left[f^{(1)}(x,t) + \varepsilon t f^{(2)}(x,t) + (\varepsilon t)^2 f^{(3)}(x,t) + \ldots\right] \tag{1.7}$$

the great improvement introduced by solution (1.5) becomes clear. Equation (1.5) converges in a perturbation sense of decreasing order of terms even as t becomes $O(1/\varepsilon)$, but the terms in (1.7) become all of the same order for this size t and no longer represent a satisfactory perturbation solution. The solution (1.7) fails in the same way as that for the ordinary case in 1.1, but (1.5) remains satisfactory.

In extending (1.5) into the region where the solution becomes multiple-valued, a shock wave is introduced to allow a jump in the physical quantities. Its location can be satisfactorily demonstrated, and one can show that the shock speed is the average of the slopes of the characteristics on either side. The distance, x, which the solution may be continued beyond the point of shock development depends on the degree of accuracy desired. It is shown that an error of the order of $\varepsilon x^{3/2}$ is introduced into the solution at a distance x along the shock.

The theory developed in Chapter 2 is illustrated there by a particular example of an initial value problem involving a periodic distribution of density in a fluid initially at rest. The solution to the problem is found both for the usual type of perturbation theory and for the improved type, and the advantages of the second type are demonstrated.

One would hope that the same advantages arising from coordinate perturbation in the plane wave case would carry over to the higher dimensional cases of cylindrical and spherical flow. Of course one can carry out the same steps of the process, but for these cases where the equations are more complicated the series for u and c no longer terminate, and as yet no convergence proof for the series has been obtained. There is thus no guarantee of the solutions, but as is after all usually the case with perturbation solutions one can assume validity for "small enough" epsilon. It seems appropriate to extend the coordinate per-

turbation technique to these problems, justifying the procedure by the improvement the technique brought to the plane wave case, and hoping that in time a convergence proof will be developed outlining the regions of validity of a solution.

In summary then coordinate perturbation is a very useful technique for improving the perturbation solutions to problems of a hyperbolic nature. The characteristic variables are the "natural" variables of the problem and it now seems clear that all the quantities of a problem including the physical coordinates should be expanded in terms of the characteristic variables if the best type of perturbation scheme is to be used. For the elliptic case on the other hand no set of natural variables is available. Problem solution in terms of the imaginary characteristics is of no advantage, and so when a solution becomes unsatisfactory and singularities arise one's only recourse is to modify their effect in some way. In the case of the airfoil the singularity could be partially hidden inside the profile but its presence was still felt in the region of the leading edge and the singular behavior of the solution in the region persisted.

It is concluded that coordinate perturbation as discussed in this thesis does not yet offer a real improvement to elliptic problems, but rather finds great usefulness in its application to hyperbolic problems where the technique allows the solution to hold even somewhat after the development of a shock.

THE HYPERBOLIC CASE

1. Plane Wave Propagation

Introduction:

The solution to the problem of one-dimensional isentropic wave propagation may always be given in the form of an integral involving the Riemann function and the initial conditions and boundary conditions of the problem [14], [1]. However, except in certain special cases, such a representation of the solution is not very tractable, and some other form would be more useful.

One of the alternative forms of solution often appropriate, and in fact one of the favorite approaches of applied mathematicians, is that of a perturbation solution where the problem is linearized by expanding the solution in terms of a small parameter of the problem. The resultant solution is satisfactory as long as the series behaves properly, but there may be regions where the solution fails. In particular, as will be shown later, for the problem of plane wave propagation the series will diverge in regions where a shock starts to form and in these regions the series solution is no longer satisfactory.

In the attempt to overcome such drawbacks of the perturbation type of solution, and in line with the general aims of this investigation, a solution to the plane wave problem has been found in terms of a perturbation not only of the dependent quantities, velocity and density, but also of the space and time variables, x and t. The new independent variables

used are the characteristic parameters, and the four perturbation series for x, t, velocity, and density are expanded in terms of functions of the characteristics. The solution seems most promising in that the convergence of the series can be proved for an appropriately chosen perturbation parameter, and also in the fact that the region of shock development can be studied. That is, even though the mapping of the characteristic plane onto the physical plane becomes multiple-valued indicating the appearance of a shock, the solution series does not break down, and may be used to describe the phenomenon even somewhat after the formation of a weak shock.

In the first section of this part the four perturbation series are found for the initial value problem with general initial conditions, and a proof of the convergence of the series is given. An example of a simple physical problem is then given to illustrate such aspects as the inadequacies of the usual type of perturbation solution and the improvement effected by the improved perturbation solution. A further simplification of the example problem is then made so that the solution may be found easily from the Riemann function, expanded in terms of the small perturbation parameter ε, and compared with the perturbation solution. The solutions are found to agree and in fact the order of ε required to allow the expansion of this latter solution is that expected from the general theory.

The second section is concerned with the incidence of a shock wave. The geometry of the mapping of the characteristic plane onto the physical plane is discussed, and the ability of

the solution to penetrate slightly into the region where the mapping starts to "fold over" is demonstrated. In the discussion entropy changes are neglected so that accuracy only through second order in shock strength is maintained. The same physical example used above is described near the regions of shock development.

Section 2: Perturbation solution and proof of convergence.

When the equations governing the propagation of a plane wave are cast into the form of differential equations along the characteristic directions of the problem, they become, for the case of a polytropic gas,

$$\begin{aligned} x_\alpha &= (u + c)t_\alpha & \frac{u_\alpha}{2} + \frac{c_\alpha}{\gamma - 1} &= 0 \\ x_\beta &= (u - c)t_\beta & \frac{u_\beta}{2} - \frac{c_\beta}{\gamma - 1} &= 0 \end{aligned} \tag{2.1}$$

where γ is the adiabatic exponent, α and β, the characteristic variables, and u and c the local velocity and speed of sound respectively [4].

Since a perturbation form of the solution to the initial value problem is to be obtained, the initial conditions must be given as disturbances superimposed on some prior uniform state. The choice of values to be assigned to α and β on the initial line is governed only by the requirement that a correct parametric (for example single-valued) representation of the initial state is achieved. Since the equations (2.1) are homogeneous in α or β. For simplicity the initial line $t = 0$, in the characteristic plane will be chosen as $\alpha = \beta$.

Then for a perturbation parameter ε, and initial perturbations $c_0 g(x)$ and $c_0 f(x)$ to c and u, the initial conditions become

$$\text{on } \alpha = \beta \begin{cases} x = \alpha = \beta \\ t = 0 \\ c = c_0(1 + \varepsilon g(\alpha)) = c_0(1 + \varepsilon g(\beta)) \\ u = \varepsilon c_0 f(\alpha) = \varepsilon c_0 f(\beta). \end{cases} \tag{2.2}$$

where the unperturbed gas was assumed at rest with uniform density.

A solution to equations (2.1) under the conditions of (2.2) is to be attempted in the form of the perturbation series,

$$\begin{aligned} x &= x^{(0)} + \varepsilon x^{(1)}(\alpha,\beta) + \varepsilon^2 x^{(2)}(\alpha,\beta) + \ldots \\ t &= t^{(0)} + \varepsilon t^{(1)}(\alpha,\beta) + \varepsilon^2 t^{(2)}(\alpha,\beta) + \ldots \\ u &= u^{(0)} + \varepsilon u^{(1)}(\alpha,\beta) + \varepsilon^2 u^{(2)}(\alpha,\beta) + \ldots \\ c &= c^{(0)} + \varepsilon c^{(1)}(\alpha,\beta) + \varepsilon^2 c^{(2)}(\alpha,\beta) + \ldots \end{aligned} \tag{2.3}$$

This form of solution will linearize the problem and give sets of equations from which the higher order perturbation functions may be successively determined.

The terms free from ε in the equations and initial conditions yield the initial approximation

$$r^{(0)} = \frac{\alpha+\beta}{2}$$

$$s,t^{(0)} = \frac{\alpha-\beta}{2} \qquad (2.4)$$

$$u^{(0)} = 0$$

$$v^{(0)} = c_0.$$

For the functions u and v, the boundary conditions together with the two equations of (2.1) homogeneous in u and v, show that in (2.3) one will obtain

$$u^{(k)} = 0 \quad \text{and} \quad v^{(k)} = 0 \quad \text{for } k > 1, \qquad (2.5)$$

whereas for $u^{(1)}$ and $v^{(1)}$ one finds

$$\frac{u^{(1)}}{2} + \frac{v^{(1)}}{\gamma-1} = r(\beta)$$

$$\frac{u^{(1)}}{2} - \frac{v^{(1)}}{\gamma-1} = -s(\alpha) \qquad (2.6a)$$

where the initial conditions require

$$r(\beta) = c_0\left(\frac{f(\beta)}{2} + \frac{g(\beta)}{\gamma-1}\right)$$

$$-s(\alpha) = c_0\left(\frac{f(\alpha)}{2} - \frac{g(\alpha)}{\gamma-1}\right) \qquad (2.6b)$$

From these expressions and from equations (2.1), any perturbation function $x^{(k)}$ or $t^{(k)}$ is found from,

$$x^{(k)} = \frac{1}{2}\int_{\beta}^{\alpha} (u^{(1)}+c^{(1)}) \frac{\partial t^{(k-1)}}{\partial \alpha} d\alpha - \frac{1}{2}\int_{\beta}^{\alpha} (u^{(1)}-c^{(1)}) \frac{\partial t^{(k-1)}}{\partial \beta} d\beta$$

$$t^{(k)} = -\frac{1}{2c_0}\int_{\beta}^{\alpha} (u^{(1)}+c^{(1)}) \frac{\partial t^{(k-1)}}{\partial \alpha} d\alpha - \frac{1}{2c_0}\int_{\beta}^{\alpha} (u^{(1)}-c^{(1)}) \frac{\partial t^{(k-1)}}{\partial \beta} d\beta \quad . \qquad (2.7)$$

In equations (2.7) using equations (2.6) the integrands contain.

$$\frac{u^{(1)} + c^{(1)}}{2c_0} = Ar(\beta) - Bs(\alpha)$$

$$\frac{u^{(1)} - c^{(1)}}{2c_0} = Br(\beta) - As(\alpha) \qquad (2.8)$$

where $A = \frac{\gamma + 1}{4c_0}$, $B = \frac{3 - \gamma}{4c_0}$.

Now since the functions $x^{(k)}$ and $t^{(k)}$ are analogous, only the functions $t^{(k)}$ will be treated, and it will be shown that these functions may be expressed in a certain general form. Then from this expression, the convergence of the perturbation series for t may be proved.

The form assumed by the functions will be shown to be,

$$c_0 t^{(n+1)} = \sum_{i+\mu+\rho+\nu = n+1} R^{(n+1)\ \lambda,\mu}_{\rho,\nu}\ r^{\rho}(\beta) s^{\nu}(\alpha) \int_{\beta}^{\alpha} r^{\lambda}(\xi) s^{\mu}(\xi) d\xi \qquad (2.9)$$

where

$R^{(n+1)\,\lambda,\mu}_{i,\nu} = R^{(n+1)\,\mu,\lambda}_{\nu,i}$ = constants such that:

$$R^{(n+1)\,\lambda,\mu}_{i,\nu} = R^{(n)\,\lambda,\mu}_{i-1,\nu}\left(B\frac{i-1}{i}-A\right) + R^{(n)\,\lambda,\mu}_{i,\nu-1}\left(B\frac{\nu-1}{\nu}-A\right) + B\sum_{j=0}^{\mu-1}\frac{1}{j+1}R^{(n)\,\lambda,\mu-1-j}_{i,j}\,\delta_{\nu 0} + B\sum_{j=0}^{\lambda-1}\frac{1}{j+1}R^{(n)\,\lambda-1-j,\mu}_{j,\nu}\,\delta_{i0} \quad (2.10)$$

$\delta_{\nu 0}$ = Kronecker delta

(all indices in (2.10) non-negative)

Proof of the validity of (2.9) is carried out by mathematical induction from equations (2.7) and (2.8).

At the first stage for $i+\mu+\rho+\nu = 1$ evidently (2.9) holds since

$$c_0 t^{(0)} = \frac{\alpha-\beta}{2}$$

From (2.9):

$$\frac{\partial}{\partial\alpha}(c_0 t^{(n)}) = \sum_{j+\kappa+\rho+q=n} R^{(n)\,j,\kappa}_{\rho,q}\, r^{\rho}(\beta)\left[q\,s^{q-1}(\alpha)\frac{\partial s}{\partial\alpha}\int_\beta^\alpha r^q(\mu)s^\kappa(\mu)d\mu + s^{j+\kappa}(\alpha)r^q(\alpha)\right]$$

$$\frac{\partial}{\partial\beta}(c_0 t^{(n)}) = \sum_{j+\kappa+\rho+q=n} R^{(n)\,j,\kappa}_{\rho,q}\, s^{q}(\alpha)\left[\rho\,r^{\rho-1}(\beta)\frac{\partial r}{\partial\beta}\int_\beta^\alpha r^q(\mu)s^\kappa(\mu)d\mu - r^{\rho+q}(\beta)s^\kappa(\beta)\right] \quad (2.11)$$

so that equation (2.7) for $t^{(n+2)}$ becomes

$$\zeta_0 \tau^{(n+1)} = \int_\beta^\alpha \sum_{\substack{j+K+p+q=n \\ p,q}} R^{(n)}_{j,K} r^p(\beta) \Big[B q s^q(\xi) \frac{\partial s}{\partial \xi} \int_\beta^\xi r^j s^K d\mu + B s^{j+K+1}(\xi) r^j(\xi) - A q r(\beta) s^{q-1}(\xi) \frac{\partial s}{\partial \xi} \int_\beta^\xi r^j s^K d\mu - A r(\beta) s^{j+K}(\xi) r^j(\xi) \Big] d\xi +$$

$$+ \int_\beta^\alpha \sum_{\substack{j+K+p+q=n \\ p,q}} R^{(n)}_{j,K} s^q(\alpha) \Big[A p s(\alpha) r^{p-1}(\xi) \frac{\partial r}{\partial \xi} \int_\xi^\alpha r^j s^K d\mu - A s(\alpha) r^{p+1}(\xi) s^K(\xi) - B p r^p(\xi) \frac{\partial r}{\partial \xi} \int_\xi^\alpha r^j s^K d\mu + B r^{p+1}(\xi) s^K(\xi) \Big] d\xi \quad (2.12)$$

Then use is made of the formula,

$$\int_\beta^\alpha \frac{\partial s^n(\xi)}{\partial \xi} \Big[\int_\beta^\xi r^m(\mu) s^n(\mu) d\mu \Big] d\xi = s^n(\alpha) \int_\beta^\alpha r^m(\mu) s^n(\mu) d\mu - \int_\beta^\alpha r^m(\mu) s^{n+n}(\mu) d\mu \quad (2.13)$$

and equation (2.12) may be interpreted using (2.13) to give

$$\zeta_0 \tau^{(n+1)} = \sum_{\substack{j+K+p+q=n \\ p,q}} R^{(n)}_{j,K} r^p(\beta) \Big[\frac{Bq}{q+1} s^{q+1}(\alpha) \int_\beta^\alpha r^j s^K d\mu - \frac{Bq}{q+1} \int_\beta^\alpha r^j s^{K+q+1} d\mu - A r(\beta) s^q(\alpha) \int_\beta^\alpha r^j s^K d\mu +$$

$$+ A r(\beta) \int_\beta^\alpha r^j s^{K+q} d\mu + B \int_\beta^\alpha s^{q+K+1} r^j d\mu - A r(\beta) \int_\beta^\alpha s^{q+K} r^j d\mu \Big] +$$

$$+ \sum_{\substack{j+K+p+q=n \\ p,q}} R^{(n)}_{j,K} s^q(\alpha) \Big[\frac{Bp}{p+1} r^{p+1}(\beta) \int_\beta^\alpha r^j s^K d\mu - \frac{Bp}{p+1} \int_\beta^\alpha r^{j+p+1} s^K d\mu - A s(\alpha) r^p(\beta) \int_\beta^\alpha r^j s^K d\mu +$$

$$- A s(\alpha) \int_\beta^\alpha r^{p+j} s^K d\mu + B \int_\beta^\alpha r^{p+j} s^q d\mu - A s(\alpha) \int_\beta^\alpha r^{p+j} s^K d\mu \Big] . \quad (2.14)$$

This expression is of the form (2.9) and upon proper treatment of indices yields the recurrence formula, (2.10). From (2.10) of course one finds that the rule for symmetry in the indices (by pairs $-(\lambda,\rho)$ and (μ,ν)) holds at the $(n+1)^{st}$ stage if it holds at the n^{th}.

The next step in the investigation is the proof of the convergence of the series for τ,

$$\tau = \tau^{(0)} + \varepsilon\tau^{(1)} + \varepsilon^2\tau^{(2)} + \ldots \tag{2.15}$$

from the expression (2.9) for the functions $\tau^{(k)}$.

It will be shown that if the functions r and s are bounded for the entire range of their argument by, say, a constant, M,

$$\begin{aligned} |r| &\leq M \\ |s| &\leq M, \end{aligned} \tag{2.16}$$

(which means of course from (2.6b) that the original perturbation functions f and g must be bounded), then the following geometric series may be shown to dominate (2.15),

$$\tfrac{1}{2}(\alpha-\beta)\sum_{j=0}^{\infty}\varepsilon^j\cdot(4A)^j\cdot M^j. \tag{2.17}$$

This series converges if ε is chosen such that

$$\varepsilon < \frac{1}{4AM}. \tag{2.18}$$

For proof, the terms in the series for $\delta_0\tau$ are evaluated from (2.9):

$$\left| c_0 t^{(n+1)} \varepsilon^{n+1} \right| \leq \varepsilon^{n+1} \left| \sum_{\lambda+\mu+\rho+\nu=n+1} R^{(n+1)\,\lambda,\mu}_{\rho,\nu} \; M^{\rho+\nu+\lambda+\mu} \; (\alpha-\beta) \right|$$

or

$$\left| c_0 t^{(n+1)} \varepsilon^{n+1} \right| \leq \varepsilon^{n+1} \; M^{n+1} \; (\alpha-\beta) \sum_{\lambda+\mu+\rho+\nu=n+1} \left| R^{(n+1)\,\lambda,\mu}_{\rho,\nu} \right| . \tag{2.19}$$

The problem then resolves itself into estimating the expression

$$\sum_{\lambda+\mu+\rho+\nu} \left| R^{(n+1)\,\lambda,\mu}_{\rho,\nu} \right| . \tag{2.20}$$

The estimation is made by summing the recurrence formula (2.10) in terms of absolute values. Furthermore of course only three of the four indices λ, μ, ρ, ν are independent so one may set

$$\lambda = n+1-\mu-\rho-\nu . \tag{2.21}$$

Finally, to make use of the delta functions, the sum is broken up into the form

$$\sum_{n=0}^{n+1} \; \sum_{\rho+\nu=m} \; \sum_{\mu=0}^{n+1-n} \equiv \sum_{n=0}^{n+1} \; \sum_{\nu=0}^{m} \; \sum_{\mu=0}^{n+1-n} \tag{2.22}$$

where $\rho = m - \nu$,

which represents correctly the requirement

$0 \leq \mu + \rho + \nu \leq n+1$, where no arrangement is

repeated. *

Ther from (2.10)

$$\sum_{n=0}^{n+1}\sum_{\nu=0}^{m}\sum_{\mu=0}^{n+1-m}\left|R^{(n+1)}_{n+1-\mu-m,\,\mu;\;m-\nu,\,\nu}\right| \le \sum_{m=0}^{n+1}\sum_{\nu=0}^{m}\sum_{\mu=0}^{m+1-m}\left(\left|R^{(n)}_{n+1-\mu-m,\,\mu;\;m-\nu-1,\,\nu}\left(B\tfrac{m-\nu+1}{m-\nu}-A\right)\right|+\left|R^{(n)}_{n+1-m-\mu,\,\mu;\;m-\nu,\,\nu+1}\left(B\tfrac{\nu+1}{\nu}-A\right)\right|+\right.$$

$$\left.+\sum_{m=0}^{n+1}\sum_{\mu=0}^{n+1-m}\left(\sum_{q=0}^{\mu-1}\left|B\tfrac{1}{q+1}\,R^{(n)}_{n+1-\mu-m,\,\mu-1-q;\;m,\,q}\right|+\sum_{\zeta=0}^{n-m-\mu}\left|B\tfrac{1}{\zeta+1}\,R^{(n)}_{n-\mu-m-\zeta,\,\mu;\;\zeta,\,m}\right|\right)\right. . \qquad (2.23)$$

In this expression, from (2.8)

$$A = \frac{\gamma+1}{2\omega_0}$$

$$B = \frac{1-\gamma}{2\omega_0}$$

so that for $\gamma > 1$, $A > B$ and

$$B\tfrac{\rho-1}{\rho} - A \le A\,. \qquad (2.24)$$

---

* To prove that $\sum_{m=0}^{n+1}\sum_{\rho+\nu=m}\sum_{\mu=0}^{n+1-m} R^{(n+1)\;\;n+1-\mu-m,\;\mu}_{\rho,\;\nu}$ does include every type of R, it suffices to show that a particular $R^{(n+1)\;i,j}_{k,\ell}$ (i,j,k,ℓ = definite values such that $i+j+k+\ell = n+1$) can appear in one and only one way. In other words

m can only equal k $\Rightarrow \nu \le m$ as required,

and " " " ℓ $\Rightarrow \mu \le n+1-m$ as required.

Then, by replacing $\frac{1}{1+1}$ by 1 in (2.23), and by showing that in each of the form sums, expressions of the type,

$$\sum_{\lambda+\mu+\rho+\nu=n} \left| R^{(n)}{}^{\lambda,\mu}_{\rho,\nu} \right| \qquad \text{hold,}$$

the proof in each case is the same as that for the bottom of page 19), one achieves an evaluation of (2.10)

$$\sum_{\lambda+\mu+\rho+\nu=n+1} \left| R^{(n+1)}{}^{\lambda,\mu}_{\rho,\nu} \right| \leq \frac{1}{4}A \sum_{\lambda+\mu+\rho+\nu=n} \left| R^{(n)}{}^{\lambda,\mu}_{\rho,\nu} \right| . \qquad (2.25)$$

So that if $T^{(n)}$ is an upper bound at the n^{th} stage,

$$\sum_{\lambda+\mu+\rho+\nu=n+1} \left| R^{(n+1)}{}^{\lambda,\mu}_{\rho,\nu} \right| \leq T^{(n+1)} \leq \frac{1}{4}AT^{(n)} \leq \cdots \leq (4A)^{n+1} R^{(0)}{}^{0,0}_{0,0} = (4A)^{n+1} \frac{1}{2}$$

Finally then, from (2.19),

$$\left| c_0 t^{(n+1)} \xi^{n-1} \right| \leq \xi^{n+1} M^{n+1} (\alpha - \beta)(4A)^{n+1} . \; 1/2 \qquad (2.26)$$

so that (2.17) does represent a dominant series for (2.15), requiring a restriction of ξ of the form (2.18) for convergence, and the proof is completed.

Illustrative example

The points discussed so far in this section will be illustrated with reference to a particular simple example where the function f(x) of equation (2.2) is taken to be zero, and the function g(x) to be cosx.

Thus at $t = 0$ $\begin{cases} x = 0 \\ v = v_0(1 + \varepsilon \cos x) \end{cases}$ (2.27)

The general behavior of an initial periodic disturbance of this sort such as, for example, the development of the higher order harmonics and later the tendency of shocks to appear is of course of some interest in itself.

2. Usual perturbation solution

In the introduction it was mentioned that the usual type of perturbation solution in which only the dependent quantities u and c are expressed as perturbation series often is unsatisfactory. The particular way in which the solution is inadequate for this example problem will be demonstrated below.

The equations for plane wave propagation referred to x and t as independent variables are

$$c_t + uc_x + \frac{\gamma - 1}{2} cu_x = 0$$
$$cc_x + \frac{\gamma - 1}{2}(u_t + uu_x) = 0. \qquad (2.28)$$

In the usual perturbation scheme a solution to (2.28) subject to the initial conditions of (2.27) is attempted in the form

$$c = c^{(0)}(x,t) + \varepsilon c^{(1)}(x,t) + \varepsilon^2 c^{(2)}(x,t) + \ldots$$
$$u = u^{(0)}(x,t) + \varepsilon u^{(1)}(x,t) + \varepsilon^2 u^{(2)}(x,t) + \ldots \qquad (2.29)$$

After the details have been worked out, the resulting perturbation functions become

$$c^{(0)} = c_0$$
$$u^{(0)} = 0 \qquad (2.30)$$

$$u^{(1)} = \frac{c_0}{2}\left[\cos(x + c_0 t) + \cos(x - c_0 t)\right]$$

$$v^{(1)} = \frac{c_0}{\gamma - 1}\left[-\cos(x + c_0 t) + \cos(x - c_0 t)\right]$$

$$u^{(2)} = \frac{M}{2c_0}\left[\cos 2x - \cos 2c_0 t + 1 - \frac{1}{2}\cos 2(x + c_0 t) + \frac{1}{2}\cos 2(x - c_0 t)\right] +$$

$$Mt\left[\sin 2(x + c_0 t) - \sin 2(x - c_0 t)\right]$$

$$v^{(2)} = \frac{M}{2c_0(\gamma - 1)}\left[\cos 2(x + c_0 t) - \cos 2(x - c_0 t)\right]$$

$$- \frac{2N}{\gamma - 1}\, t\left[\sin 2(x + c_0 t) + \sin 2(x - c_0 t)\right]$$

where $M = -\frac{c_0^2}{4}\left(\frac{\gamma + 1}{2(\gamma - 1)}\right)$

$$N = -\frac{c_0^2}{2}\left(\frac{\gamma - 3}{2(\gamma - 1)}\right)$$

$$u^{(3)} = a_1\cos 3(x + c_0 t) + a_2\cos 3(x - c_0 t) + a_3\cos(x + c_0 t) +$$

$$a_4\cos(x - c_0 t) + a_5\cos(3x + c_0 t) +$$

$$a_6\cos(3x - c_0 t) + a_7\cos(x + 3c_0 t) + a_8\cos(x - 3c_0 t) +$$

$$+ t\left[b_1\sin 3(x + c_0 t) + b_2\sin 3(x - c_0 t) + b_3\sin(x + c_0 t) + \right.$$

$$b_4\sin(x - c_0 t) + b_5\sin(3x + c_0 t) + b_6\sin(3x - c_0 t) +$$

$$\left. b_7\sin(x + 3c_0 t) + b_8\sin(x - 3c_0 t)\right] +$$

$$+ t^2\left[c_1\cos 3(x + c_0 t) + c_2\cos 3(x - c_0 t) + c_3\cos(x + c_0 t) + \right.$$

$$c_4\cos(x - c_0 t) + c_5\cos(3x + c_0 t) + c_6\cos(3x - c_0 t) +$$

$$\left. c_7\cos(x + 3c_0 t) + c_8\sin(x - 3c_0 t)\right] .$$

where a_1, b_1, c_1 are constants determinable from the equations and initial conditions, and where the function $u^{(2)}$ has the same form with different constants.

$u^{(4)}$ has terms of the form:

constant, cos2x, cos4x, $\cos(2x \pm 2c_0 t)$, $\cos(2x \pm 4c_0 t)$, $\cos(4x \pm 2c_0 t)$, $\cos(4x \pm 4c_0 t)$, $\cos 4c_0 t$, $\cos 2c_0 t$,

t times sines of the same arguments,

t^2 " " " " " "

t^3 " " " " " " .

The inadequacy of such a solution appears as t becomes large, when the dominant terms in (2.29) become for example

$$u = u_0 + \varepsilon\left[u^{(1)} + \varepsilon t(\ ) + \varepsilon^2 t^2(\ ) + \ldots\right]. \qquad (2.31)$$

For $t = O(\frac{1}{\varepsilon})$ series (2.31) no longer converges in the perturbation sense, and in this sense the solution fails since every term in the bracketed expression becomes $O(1)$. The critical fact is that exactly this order of t holds at the region of shock development (see for example page 37) and thus the usual perturbation solution cannot hold into the region of shock development.

2. Perturbation solution in characteristic coordinates

If the same problem (initial conditions (2.27)) is solved by the method described earlier in this section, the perturbation functions are found as,

$$
\begin{aligned}
u^{(0)} &= 0 \\
c^{(0)} &= c_0 \\
u^{(1)} &= \frac{c_0}{\gamma-1}(\cos\beta - \cos\alpha) \\
c^{(1)} &= \frac{c_0}{2}(\cos\beta + \cos\alpha) \\
u^{(j)} &= 0 \\
c^{(j)} &= 0
\end{aligned}
\quad \text{for } j > 1. \tag{2.32}
$$

Thus $u^{(1)} + c^{(1)} = 2c_0(\bar{A}\cos\beta - \bar{B}\cos\alpha)$

$u^{(1)} - c^{(1)} = 2c_0(\bar{B}\cos\beta - \bar{A}\cos\alpha)$, where $\bar{A} = \frac{\gamma+1}{4(\gamma-1)}$ $\bar{B} = \frac{3-\gamma}{4(\gamma-1)}$

are to be used in finding

$$x = x^{(0)} + \varepsilon x^{(1)} + \varepsilon^2 x^{(2)} + \ldots$$

$$t = t^{(0)} + \varepsilon t^{(1)} + \varepsilon^2 t^{(2)} + \ldots \tag{2.33}$$

from the equations

$$x_\alpha = (u + c)t_\alpha$$

with $t = 0$ on $x = \alpha = \beta$.

$$x_\beta = (u - c)t_\beta$$

The resultant solutions are

$$
\begin{aligned}
x^{(0)} &= \frac{\alpha+\beta}{2} \\
c_0 t^{(0)} &= \frac{\alpha-\beta}{2} \\
x^{(1)} &= \frac{\alpha-\beta}{2}(\cos\beta - \cos\alpha)\bar{A} \\
c_0 t^{(1)} &= \frac{\alpha-\beta}{2}(-\cos\beta - \cos\alpha)\bar{A} + (\sin\alpha - \sin\beta)\bar{B} \\
x^{(2)} &= \frac{\alpha-\beta}{2}(\cos 2\alpha - \cos 2\beta)\left(\frac{\bar{A}^2}{2} + \frac{\bar{A}\bar{B}}{4}\right) + \\
&\qquad \frac{\alpha-\beta}{4}\bar{A}\bar{B}(2\cos\alpha\sin\beta + 2\cos\beta\sin\alpha - \sin 2\beta - \sin 2\alpha)
\end{aligned}
\tag{2.34}
$$

$$\epsilon_0 t^{(2)} = \frac{\alpha-\beta}{2}(\cos 2\alpha + \cos 2\beta)\left(\frac{\bar{A}^2}{2} - \frac{\overline{AB}}{2}\right) + \frac{\alpha-\beta}{2}(\cos\alpha\cos\beta)2\bar{A}^2 +$$

$$\frac{\alpha-\beta}{2}(\bar{A}^2 + 2\bar{B}^2 - \overline{AB}) + \text{terms not multiplied by } (\alpha-\beta).$$

$$\epsilon^{(3)} = \frac{\alpha-\beta}{2}(\cos 3\beta - \cos 3\alpha)(\quad) \text{ etc....}$$

$$\epsilon^{(4)} = \frac{\alpha-\beta}{2}(\cos 4\beta - \cos 4\alpha)(\quad) \text{ etc...}$$

The form assumed by successive terms is apparent. In particular only the first power of $(\alpha-\beta)$ appears, and $\frac{\alpha-\beta}{2}$ is the initial approximation to t. It thus seems possible to continue the solution beyond the point where t becomes $O(\frac{1}{\epsilon})$. That this is indeed possible is shown in section 3 where the details of the process are explored.

At this point it is of some interest to remark that since (2.32) and (2.34) constitute a correct solution to the problem, they must agree with the usual perturbation solution of (2.30) and also with the solution achieved using Bieberbach's function in all cases where the latter two solutions are obtainable and valid.

For the case of the usual perturbation solution the agreement may be demonstrated simply by introducing the coordinate perturbations of (2.33) and (2.34) into the solution (2.36) and showing that this causes the higher order perturbations ($j > 1$) in u and v to become zero in agreement with (2.32). This has been checked for the cases of $u^{(2)}$ and $v^{(2)}$.

For the case where the solution is given in terms of Riemann's function, the solution may be shown to be (cf. section 62 of [4])

$$\tau(\alpha,\beta) = \tau(\xi(\alpha), \eta(\beta)) = \int_{\alpha=\beta}^{\xi(\beta)} \frac{V(\lambda)}{2C(\lambda)}\, d\lambda,$$

where

and where the point $\tilde{r} = \eta(\beta)$, $\tilde{s} = \xi(\alpha)$ is the point P_1 in the $(\tilde{r},\tilde{s})$-plane of the figure corresponding to the point (α,β) in the (α,β)-plane. The functions $\tilde{r}$ and $\tilde{s}$ on the curve Γ are

$$\tilde{r}(\alpha) = \frac{c_0}{\gamma-1} + \varepsilon r(\alpha)$$

$$\tilde{s}(\alpha) = \frac{c_0}{\gamma-1} + \varepsilon s(\alpha)$$

so that $\tilde{r}$ and $\tilde{s}$ represent the result of restoring the terms of order one to the perturbation functions r and s of equations 2.6b.

In the expression for $\tau(\alpha,\beta)$ the function $V(\lambda)$ is Riemann's function, and for this problem

$$V = \left(\frac{\xi-\eta}{\tilde{r}+\tilde{s}}\right)^{-1/2\mu^2} F\left(1-\frac{1}{2\mu^2}, \frac{1}{2\mu^2}; 1; z\right)$$

where F is the hypergeometric function and where

$$\mu^2 = \frac{\gamma-1}{\gamma+1}$$

$$z = \frac{(\tilde{s}-\xi)(\tilde{r}-\eta)}{(\tilde{s}+\tilde{r})(\xi+\eta)}.$$

Now if, at this stage, the problem is further simplified by assuming that $\frac{\gamma}{2(\gamma-1)}$ is an integer, the hypergeometric function, F, becomes a finite series. For example by choosing $\gamma = 1.4$ $\frac{\gamma}{2(\gamma-1)}$ becomes equal to 3, and gives

$$F = 1 - 6z + 6z^2.$$

Then using this F in the expression for $t(\alpha,\beta)$ and expanding the result in powers of ε such that

$$c_0 t = c_0 t^{(0)} + \varepsilon c_0 t^{(1)} + \ldots,$$

one obtains

$$c_0 t^{(0)} = \frac{\alpha-\beta}{2}$$

$$c_0 t^{(1)} = -3/2(\alpha-\beta)(\cos\alpha + \cos\beta) + (\sin\alpha - \sin\beta)$$

in agreement with the previous solution of (2.34) since for $\gamma = 1.4$

$$\bar{A} = \frac{\gamma+1}{2(\gamma-1)} = 3/2$$

$$\bar{B} = \frac{3-\gamma}{2(\gamma-1)} = 1.$$

Actually, so far as the details are concerned the expansion in powers of ε as a perturbation series which arises out of terms of the sort

$$\frac{1}{\tilde{s}(\alpha)+\tilde{r}(\alpha)} = \frac{1}{\frac{2c_0}{\gamma-1} + \varepsilon[r(\alpha)+s(\alpha)]}$$

is valid only so long as

$$|\varepsilon(r(\alpha) + s(\alpha)| \leq 2\varepsilon M < \frac{2c_0}{\gamma-1},$$

where M is an upper bound on the functions r and s.

For $A = \frac{\gamma+1}{4}c_0$ (see (2.8)) this means

$$\frac{\cdot}{\cdot u^2 AM} .$$

Comparison of this inequality with the criterion of (2.18)

$$\frac{1}{4AM}$$

shows that (2.18) does give a safe bound on $\cdot$ since for $\cdot$

$$\frac{\cdot}{\cdot^2} \cdot$$

What this requirement on $\cdot$ really means in terms of the allowed initial departure of c from uniformity may be found by solving equations (2.6b) to find

$$c_0 F(x) = \frac{\gamma-1}{2}(v(x) - s(x))$$

or

$$\cdot c_0(\cdot) \leq (\gamma-1)\cdot M < \frac{\gamma-1}{4A} = \left(\frac{\gamma-1}{\gamma+1}\right)c_0 .$$

Thus the initial perturbation ratio for $\gamma = 1.4$ may be

$$\frac{\cdot c_0(\cdot)}{c_0} < \frac{\gamma-1}{\gamma+1} = \frac{1}{6} ,$$

or, in terms of the disturbance, ρ', to the density ρ_0,

$$\frac{\rho'}{\rho_0} < 1.16 ,$$

as may be found from the relation

$$\left(1 + \frac{\rho'}{\rho_0}\right) = \left(1 + \frac{c'}{c_0}\right)^{\frac{2}{\gamma-1}} .$$